

General Disclaimer

One or more of the Following Statements may affect this Document

- This document has been reproduced from the best copy furnished by the organizational source. It is being released in the interest of making available as much information as possible.
- This document may contain data, which exceeds the sheet parameters. It was furnished in this condition by the organizational source and is the best copy available.
- This document may contain tone-on-tone or color graphs, charts and/or pictures, which have been reproduced in black and white.
- This document is paginated as submitted by the original source.
- Portions of this document are not fully legible due to the historical nature of some of the material. However, it is the best reproduction available from the original submission.

(NASA-CR-159536) LEAN STABILITY
AUGMENTATION STUDY Final Report (United
Technologies Research Center) 185 p
HC A09/MF A01

CSCL 21B

N79-22244

Unclassified
G3/25 23982
NASA CR-159536
UTRC-914104-18



LEAN STABILITY AUGMENTATION STUDY

FINAL REPORT

By

J. B. McVey and J. B. Kennedy

UNITED TECHNOLOGIES RESEARCH CENTER

May 1979

prepared for

NATIONAL AERONAUTICS AND SPACE ADMINISTRATION

NASA Lewis Research Center

Contract NAS3-20804



Lean Stability Augmentation Study

TABLE OF CONTENTS

	<u>Page</u>
LIST OF TABLES	i
LIST OF FIGURES	ii
SUMMARY	1
INTRODUCTION	2
CONCEPTUAL DESIGN ANALYSIS	6
Engine and Aircraft Performance Characteristics	7
Combustor Emissions and Performance	8
Description of Augmented Combustor Concepts	10
Concept Assessment and Selection	23
FLAMEHOLDER TEST CONFIGURATIONS	25
Baseline Design	25
Self-Piloting Recessed Perforated Plate Designs	25
Catalyzed Tube Flameholder Designs	27
Piloted Flameholder Designs	28
TEST FACILITIES AND EQUIPMENT	31
Test Apparatus	31
Facility Services	33
Instrumentation	35
EXPERIMENTAL PROCEDURES	39
Test Methods	39
Data Reduction Procedure	41
TEST RESULTS	47
Fuel Preparation Section Tests	47
Concept Tests	48

R79-914104-18

Lean Stability Augmentation Study

TABLE OF CONTENTS (Cont'd)

	<u>Page</u>
DISCUSSION OF TEST RESULTS	53
CONCLUSIONS	58
APPENDIX I - CHARACTERISTICS OF STABILITY LIMIT AUGMENTATION CONCEPTS	59
APPENDIX II - INSTRUMENTATION LIST	69
LIST OF SYMBOLS	74
REFERENCES	76
TABLES	78
FIGURES	88

LIST OF TABLES

1. Lean Stability Augmentation Study Program Goals
2. Lean Stability Augmentation Concepts
3. Turbofan Engine Combustor Operating Parameters
4. Influence of Performance and Cost on Airline Direct Operating Cost
5. Cost Levels Employed in Concept Evaluation
6. Catalytic Bed Experimental Data
7. Lean Stability Augmentation Concept Rankings
8. Emissions Analysis Instrumentation
9. Matrix of Test Conditions
10. Lean Stability Blowout Limit Data Summary

LIST OF FIGURES

1. Bluff Body Flame Stabilization Process
2. Advanced Gas Turbine Engine Combustor Envelope
3. Gaseous-fuel Injector/Mixer
4. Typical E³-powered Trijet Mission Profile
5. NO_x Emission Data
6. Predicted CO Emissions
7. Piloted Combustor Concepts
8. Pilot Fuel Metering Orifice Size
9. Fuel-injected Flame Stabilizer Using Bleed-air-cooled, Fuel-rich Combustion Products
10. Characterization of Fuel-Rich Pilot Stabilization Systems
11. Supercharged, Fan-air-cooled, Fuel-rich Pilot Flame Stabilizer
12. Pilot Quench-water Requirements
13. Pilot-fuel Injected Flame Stabilizer
14. Effect of Recessing on Perforated Plate Stability Limits
15. Catalytic Augmentation Concepts
16. Effect of Inlet Temperature - Temperature Rise Tradeoff on Stability Limits
17. Fraction of Flow Contacting Surface of Catalyzed Tube Combustor
18. Catalytic Preheat Bed Characteristics
19. Heat Recirculation Stability Augmentation Concepts
20. Effect of Pumping of Recirculated Flow on Engine Fuel Consumption
21. Effect of Flow Recirculation on Mixed Gas Temperature
22. Pressure Loss for Ejector-Recirculated Primary Gas
23. Performance Characteristic of a Compact Regenerative Heat Exchanger
24. Baseline Flameholder Configuration
25. Baseline Flameholder and Retaining Ring
26. Self-Piloting Recessed Perforated Plate Flameholders
27. Photograph of Recessed Self-Piloting Perforated Plate Flameholder, SPRPP-1
28. Counterbored Perforated Plate, SPRPP-4
29. Self-Piloting Recessed Perforated Plate Final Design, SPRPP-F
30. Catalyzed Tube Flameholder Configurations
31. Catalyzed Tube Flameholder Plate-Tube Assembly
32. Catalyzed Tube Flameholder Final Design, CTF-F
33. Piloted V-Gutter Flameholder Configurations
34. Uncooled Piloted V-Gutter Flameholder
35. Piloted Perforated Plate Flameholder
36. Piloted Flameholder Final Design
37. Lean Stability Augmentation Study Test Facility
38. Lean-Premixing/Prevaporizing Combustor Test Apparatus
39. Instrumentation Section - Fuel Injector Entrance Station
40. Fuel Injector - Airflow Nozzle
41. Fuel Injector Assembly
42. Combustor Liner Configurations

LIST OF FIGURES (Cont'd)

43. Combustor Assembly Components
44. Instrumentation Section - Combustor Exit Section
45. Schematic Diagram of Fuel Supply System
46. Emission Probe Tip Construction
47. Six-probe Emission Rake Sample Transfer System
48. Emission Sampling and Analysis System
49. Smoke and Phase-Discriminating Sampling Probe
50. Phase-Discriminating Probe Sampling System
51. Fuel Profile Uniformity Test Results
52. Fuel Vaporization Test Results - Survey 1
53. Fuel Vaporization Test Results - Survey 2
54. NO_x Emissions - Baseline Configuration
55. CO Emissions - Baseline Configuration
56. UHC Emissions - Baseline Configuration
57. Combustor Performance - Baseline Configuration
58. Baseline Flameholder Blowout Limits
59. Lean Stability Limits, Self-Piloting Recessed Perforated Plate Series
60. NO_x Emissions - Self-Piloting Perforated Plate Final Design
61. CO Emissions - Self-Piloting Perforated Plate Final Design
62. UHC Emissions - Self-Piloting Perforated Plate Final Design
63. Emission Distribution - Self-Piloting Perforated Plate Final Design
64. Combustor Performance - Self-Piloting Perforated Plate Final Design
65. Post-Test Condition of Self-Piloting Recessed Perforated Plate, Final Design
66. Lean Stability Limits, Catalyzed Tube Flameholder Series
67. NO_x Emissions - Piloted V-Gutter Flameholder, Configuration 1
68. CO Emissions - Piloted V-Gutter Flameholder, Configuration 1
69. UHC Emissions - Piloted V-Gutter Flameholder, Configuration 1
70. Emission Distribution - Piloted V-Gutter Flameholder, Configuration 1
71. Combustor Performance - Piloted V-Gutter Flameholder, Configuration 1
72. NO_x Emissions - Piloted Flameholder, Configuration 4
73. CO Emissions - Piloted Flameholder, Configuration 4
74. UHC Emissions - Piloted Flameholder, Configuration 4
75. Emission Distribution - Piloted Flameholder, Configuration 4
76. Combustor Performance - Piloted Flameholder, Configuration 4
77. Effect of Coolant Type on Emissions
78. Effect of Pilot Fuel Flowrate on Emissions
79. Combustor Performance - Piloted Flameholder - Final Design
80. Variation of NO_x Emissions with Flame Temperature
81. Variation of CO Emissions with Flame Temperature
82. Effect of Flameholder Characteristics on Combustor Performance
83. Variation of Blowout Flame Temperature with Inlet Temperature
84. Perforated Plate Lean Stability Limit Data Correlation

LEAN STABILITY AUGMENTATION STUDY

FINAL REPORT

SUMMARY

An analytical conceptual design study and an experimental test program were conducted to investigate techniques and develop technology for improving the lean combustion limits of premixing, prevaporizing combustors applicable to gas turbine engine main burners. In the analytical study, three concepts for improving lean stability limits were selected for experimental evaluation among twelve approaches considered. Concepts were selected on the basis of the potential for improving stability limits and achieving emission goals, the technological risks associated with development of practical burners employing the concepts, and the penalties to airline direct operating costs resulting from decreased combustor performance, increased engine cost, increased maintenance cost and increased engine weight associated with implementation of the concepts. Tests of flameholders embodying the selected concepts were conducted in an axi-symmetric flametube test rig having a nominal diameter of 10.2 cm at a pressure of 10 atm and at a range of entrance temperatures simulating conditions to be encountered during stratospheric cruise. A total of sixteen test configurations were examined in which lean blowout limits, pollutant emission characteristics, and combustor performance were documented.

The use of hot gas pilots, catalyzed flameholder elements, and heat recirculation to augment lean stability limits was considered in the conceptual design study. On the basis of the results of the study, three classes of augmented flameholders were designed and tested. The first class involved the use of cavities or recesses located on the downstream face of a perforated plate flameholder--these configurations are referred to as Self-Piloting Recessed Perforated Plates. The second class involved the use of tube bundles wherein the inner diameter of the tubes and/or the rear face of the tube array was treated with a platinum catalyst. These configurations were referred to as Catalyzed Tube Flameholders. The third class of flameholders involved the direct injection of gaseous or liquid fuel into the recirculation regions formed behind V-gutter or perforated plate flameholders. This class of flameholders was referred to as Piloted Flameholders. The primary goal of the program was to achieve stable operation of the combustors at equivalence ratios as low as 0.25. It was desired that the NO_x emission index be less than 1.0 g/kg at the design conditions ($T_o = 600K$, $\phi = 0.6$). It was also desired that the combustor operate efficiently over a range of entrance temperatures from 600 to 800K, a range of equivalence ratios from 0.3 to 0.6, and that the maximum emission of nitric oxides be less than that corresponding to an emission index of 3.0 g/kg.

The most promising configuration identified in this program involved the injection of pilot fuel into the base or recirculation region of a bluff-body flameholder. It was determined that with a pilot fuel flow equal to 4 percent of the total fuel flow at the design conditions, combustor blowout did not occur as fuel flow was decreased to levels corresponding to an overall equivalence ratio of 0.25. For this configuration, the NO_x emission index at the design point was less than the design goal and, at off-design conditions, the maximum NO_x emission index goal was exceeded only for the $T_o = 800\text{K}$, $\phi = 0.6$ case. At the lower entrance temperature conditions tested ($T_o = 700$ and 600K), the combustion efficiency measured at low equivalence ratios was unacceptably low and further effort is required to obtain the desired performance. No substantial improvement in blowout limits was achieved for the Self-Piloting Recessed Perforated Plate Flameholder configurations or the Catalyzed Tube Flameholder configurations.

INTRODUCTION

Considerable technical effort has been given to reduction of pollutant emissions from gas turbine engines. In most instances, these efforts involve modifications of the configurations and/or operation of combustors designed according to conventional concepts. However, uncertainty concerning the effects of the introduction of nitric oxides into the stratosphere has prompted efforts to reduce NO_x emissions to lower levels than are obtainable with current combustor design technology. Therefore improvements in the state-of-the-art of combustor design must be achieved through the development of novel combustor concepts. One promising concept, lean premixing/prevaporizing combustion, involves (1) the generation of a uniformly lean, gaseous fuel air mixture prior to combustion and (2) a combustion zone having a uniformly low temperature and low species residence time, thereby achieving the necessary prerequisites to low NO_x production rates. However, successful application of this concept requires the development of practical combustor systems simultaneously offering satisfactory lean-fuel-air ratio stability characteristics, while meeting stringent combustion and system efficiency, reliability and dependability, and pollutant-emission requirements.

The objective of the present program was to select and experimentally evaluate various lean-stability-augmentation concepts applicable to the lean premixing, prevaporizing gas turbine combustors. The program goals are listed in Table 1. The primary goal was to obtain a lean stability limit corresponding to an equivalence ratio of 0.25 at simulated cruise conditions. The combustors were constrained to produce NO_x emissions less than the level corresponding to an emission index of 1.0 g/kg at the design condition and 3.0 g/kg over the range of entrance temperatures from 600 to 800K at pressures of 10 atmospheres. In addition, the combustor must meet the listed emission goals

for unburned hydrocarbons and carbon monoxide at the design conditions, must operate at efficiencies of greater than 99 percent at equivalence ratios above 0.3, and must generate a pressure loss of less than 5 percent. In addition to these quantitative goals, it is required that the augmented combustors be of a practical design and that their use result in no more than a moderate increase to airline direct operating cost.

Techniques employed in achieving improved stability limits in this program involved the use of hot gas pilots, catalyzed flameholder elements, and heat recirculation schemes. For those schemes in which hot gas pilots were employed, it was specified that no more than 10 percent of the fuel which was consumed at the design condition could be used to generate pilot gases at any condition. Within the pilot combustor, the fuel was permitted to be injected in a liquid form without the necessity of premixing and prevaporizing. Use of a catalytic combustor in which all the fuel was reacted to completion was not to be considered as part of this program; however, complete reaction of a portion of the mixture or partial reaction of the entire mixture was permitted. The use of fuel additives, including the injection of water, was not permitted. Finally the use of variable geometry and/or staged combustion systems was not permitted. The emphasis of the program was, therefore, placed on modification of the combustion process occurring in the primary zone of the combustor in order to achieve stability limit improvements.

A total of twelve different augmentation concepts were to be evaluated in an analytical design study from which three concepts were to be selected for experimental evaluation. In order to establish the twelve concepts, appeal was made to one of the generally accepted models (Ref. 1) of the flame stabilization process which occurs in the wake of a bluff body (Fig. 1). According to this model flow within the boundary layer of the incoming mixture detaches from the trailing edge of the bluff body and merges with the recirculating combustion products to form a shear layer through which significant amounts of heat, mass, and momentum transfer occur. Immediately downstream of the separation point heat is transferred from the recirculation region to the free stream and reactants are transferred into the recirculation zone. The non-exothermic induction reactions proceed until a point is reached on some streamline where the optimum temperature and concentration history exists such that ignition (onset of exothermic reaction) occurs. This ignition point always lies within the recirculation region where temperatures are high and reactant concentrations are low because of the greater sensitivity of the Arrhenius-type induction zone reactions to temperature level than to concentration level. Flame fronts are established which cause the reaction to propagate, by virtue of transport processes, into the incoming mixture as well as deeper into the recirculation region where small quantities of entrained reactants exist. Downstream of the point where the flame crosses the separation line dividing the recirculating and primary streams, heat is transferred from the combustion products existing in the primary stream to the recirculation zone which is at a lower temperature due to the heat loss incurred by virtue of heat transfer to the cold incoming

stream and to the bluff body. For this process to be stable, a balance must exist between the energy that is gained by the recirculation zone by virtue of mass and heat transfer from the incoming mixture and heat that is lost to the bluff body and the incoming stream. As the fuel-air ratio of the incoming mixture is decreased, the recirculation zone temperature decreases and the ignition point moves farther downstream and deeper into the recirculation zone. As the ignition point moves downstream, the effective surface area through which heat is transferred from the incoming mixture combustion products diminishes to the point where an energy balance cannot exist and blowout occurs. Clearly, blowout can be inhibited by direct injection of energy into the recirculation zone, and it was deemed probable that the amount of fuel required to achieve a significant change is quite small.

This idealized two-dimensional steady-state view of the flame stabilization processes is modified by three-dimensional and transient behavior in real flows. Secondary flow (drafting) patterns can exist which can cause the introduction of cold reactants into the otherwise recirculating flow with a resulting adverse effect. Conversely, drafting can cause the introduction of hot products from a more stable region with beneficial effects on overall stability. In real flows transient flow excursions occur which cause the combustion stability to be altered. An excess margin of stability is therefore always required such that recovery from a transient (which results in a less favorable flow condition) can occur. It was considered probable that improvement in blowout limits can be achieved by causing the flow patterns to be less susceptible to the effects of flow transients and by providing energy sources to promote re-ignition of flow in marginally stable configurations.

Based on means of augmenting flame stability limits suggested by the above, methods of enhancing the flame stability in a gas turbine engine main combustor were selected and combustor designs applicable to an advanced turbine engine were evaluated. A list of the concepts and designs selected for evaluation is shown in Table II. Seven of the thirteen designs involve a form of piloting. The piloting designs were characterized as those involving direct injection into the recirculation zone, enrichment of the approach flow, drafting of hot gases from stable to less stable flameholding regions, and provision of a re-ignition source by physical containment of a small fraction of the recirculation zone combustion products. Three of these schemes involved employing catalytic elements to promote local combustion. Included are concepts in which catalysts are used to further reactions in the aforementioned containment cavity, partial reaction of the mixture in a catalytic bed located upstream of the flame stabilizer, and the promotion of reactions in the boundary layer of the approaching fuel-air mixture. Three heat recirculation schemes in which energy is exchanged between the primary zone combustion products and the incoming gas mixture were considered. In two of the schemes, primary zone gases would be recirculated and mixed directly with compressor discharge gas;

in one case, the compressor would be used to provide the driving potential for recirculating the gases whereas, in the second case, ejector action would be employed. The third concept employed a heat exchanger to transfer heat between the primary zone gases and compressor discharge. Results of the evaluations of these concepts are contained in the following section entitled, Conceptual Design Studies.

On the basis of the results of the analytical design studies, three of the concepts were selected for verification in the experimental phases of the program. Five variations of each of the three concepts plus an unaugmented baseline flameholder were designed, fabricated and tested. Descriptions of the flameholders, the test apparatus, instrumentation, test procedures and graphical representations of the test results are presented in the following sections.

CONCEPTUAL DESIGN ANALYSIS

The merits of each of the augmented combustor concepts selected were evaluated in terms of the impact of the utilization of the technique on the performance of a gas turbine engine applicable to commercial aircraft. Because a developed lean premixing/prevaporizing combustor represents an advanced combustion concept, it is unlikely that this technology can be utilized on engines currently in use (JT9D class engines). It was therefore appropriate to employ characteristics of advanced engines proposed for future development in the evaluation process. The Energy Efficient Engine (E^3) being investigated by P&WA/CPD for NASA was selected as a baseline engine design by virtue of the advanced state of technology represented by the design and because of the availability of detailed information on engine component characteristics and predicted performance engine levels. The characteristics of this engine are presented in a following subsection.

The first step in the evaluation process was to establish combustor component sizes and flow areas which would be required in order to meet the combustor performance and emission goals. The axial distance between the compressor exit and turbine entrance guide vanes (42.4 cm) was fixed by the existing E^3 engine design (Fig. 2). It was necessary to establish that portion of the envelope which would be occupied by the fuel injector/mixer/vaporizer. Because design of the fuel preparation section was not within the scope of this effort, a compact gaseous fuel injector of a type proposed for use with gasified fuel oil was selected as being representative of the volume so occupied (Fig. 3). All of the conceptual combustor designs were assumed to employ the same fuel injector design. The performance penalty associated with such a design was not assessed because only relative rankings between combustor concepts were of interest. In fact, the practicality of a gaseous injector system vis-a-vis a liquid injection system has yet to be thoroughly assessed.

The length of the primary combustion zone was established on the basis of the residence time which could be permitted without the nitric oxide emissions exceeding the program goal level at the design conditions. Emission levels were predicted using existing empirical data and analytic procedures as discussed below. This residence time and the specified combustor reference velocity resulted in the establishment of an 18-cm primary zone length. The remaining combustor length, which represents the distance between the point at which dilution air would be introduced and the turbine engines guide vanes, was deemed sufficient to produce satisfactory turbine entrance temperature profiles.

Because all of the combustor concepts to be evaluated were required to operate at the same conditions and occupied the same volume, it was assumed

that all concepts had equal potential for achieving high combustion efficiency, and, therefore, no performance penalty associated with inefficient combustion was assigned to any concept. The performance differences produced by various concepts would therefore derive from differences in pressure loss and weight. Pressure losses were estimated using conventional aerodynamic loss calculations, and weight estimates were derived from mechanical design layouts generated for each concept. These performance factors plus others such as losses associated with the use of diffuser bleed or shaft power extraction were converted to equivalent increases in engine specific fuel consumption by use of influence coefficients developed for the E³ design. These specific fuel consumption increases were then converted to airline direct operating cost increases by a second set of influence coefficients derived for a typical E³-powered commercial transport. Increases in engine initial cost and maintenance cost also impact direct operating costs. A detailed study of combustor component costs was beyond the scope of this effort. Estimates of these costs were determined through the deliberations of a Concept Review Committee comprised of six senior level engineers responsible for the development of combustion systems at Pratt & Whitney Aircraft Commercial Products Division and United Technologies Research Center. After review of the type of combustor concepts being considered, a range of initial costs and hourly maintenance costs varying from an average cost characteristic of the E³ baseline design to a value far above these average costs was established. A consensus judgement of the Concept Review Committee was then used to establish at what point in this range each concept would best fit. The Concept Review Committee also established a relative ranking of the technological risks associated with the development of the technology which each concept required, as well as a ranking of probable operational problems (such as poor acceleration or poor engine light-off characteristics). Finally, the committee established an overall ranking on the basis of the potential for achieving flame stability improvement, performance, costs, technological risks, and operational considerations.

Engine and Aircraft Performance Characteristics

The performance characteristics of the Energy Efficiency Engine are shown in Table 3 along with the characteristics of a current-day engine. The advanced engine is a higher pressure ratio engine (32:1), and therefore, operates at higher combustor entrance temperature and pressure levels both at sea level and cruise in comparison with current engines. The higher entrance temperature and pressure levels of the advanced engine designs will pose a greater problem in the design of the fuel injection system and mixer/vaporizer in terms of the likelihood of the occurrence of autoignition or flashback than would be the case for current engines. Because the requirements for high performance, low cost, and low pollutant emissions are in conflict, a compromised engine whose characteristics differ from those of the advanced engine

shown in the table may, in fact, be more representative of engines employing lean, premixing combustors. Evaluation of the characteristics of such an engine was beyond the scope of this program, and it was considered that the advanced engine characteristics would be more representative of future engines than the current engine characteristics; the advanced engine characteristics were therefore used in the current study.

To determine the effects of engine performance changes on airline operating costs, it was assumed that the engine was used on a trijet transport operating on a route having a nominal length of 700 nautical miles (Fig. 4). Shown in the figure are the amounts of fuel consumed during the different mission legs, and it is obvious that performance penalties incurred during climb and cruise dominate the economics of the engine operation. The influence coefficients showing the effect of a one percent change in various engine performance parameters on the specific fuel consumption at cruise are given in Table 4. Effects of changes in combustion efficiency and combustor pressure loss are shown as well as losses associated with the use of diffuser bleed used to power an auxilliary turbocompressor in one of the concepts, and fan duct pressure loss (incurred by placement of a heat exchanger in the fan stream). The loss associated with the extraction of shaft power on a per horsepower basis is also shown. Influence coefficients showing effects of changes in the performance factors in airline direct operating costs are shown in the second column of the table. In computing these coefficients it was assumed that the performance change which would result in an engine thrust loss which would require the use of a larger engine. The cost and weight increases associated with that larger engine are reflected in each influence coefficient. The figures shown in the right-hand column of the table are derived from the direct operating cost influence coefficient and illustrate the magnitude of the performance change for each of the performance factors required to produce the same operating cost penalty as a one percent change in combustion efficiency.

The range of initial cost and maintenance cost used to assess the impact of increased combustor complexity and decrease reliability on direct operating costs is shown in Table 5. The levels labeled "average" are representative of the cost anticipated for the E³ engine. The assessment of the Concept Review Committee was that certain of the conceptual designs being considered could cost up to three times that of the baseline designs and maintenance costs could be doubled in some of the designs.

Combustor Emissions and Performance

The predicted NO_x emission index for the conceptual design was based on the experimental data reported by Semerjian and Ball (Ref. 2), who performed measurements using Jet-A Fuel; the propane and Jet-A data of Marek and Papathakos

(Ref. 3); and the propane data of Anderson (Ref. 4). These data were scaled from the inlet temperature and pressure levels and residence times employed in the respective experiments to the 600K, 10-atm design conditions applicable to this study using the pressure and temperature scaling criteria reported by Sarli et al. (Ref. 5):

$$EI_{NO_x} \sim p^{0.5} \exp(0.003T) \quad (1)$$

and assuming that the NO_x concentration varies linearly with residence time. A plot showing the predicted variation of the NO_x emission index with equivalence ratio is given in Fig. 5. On the basis of these data, it is reasonable to expect that the design goal of an emission index of 1.0 g/kg at an equivalence ratio of 0.6 can be achieved if the combustor primary zone residence time does not exceed two milliseconds.

With respect to emissions of CO, only a small amount of experimental data exists on the effect of residence time and mixture ratio on the CO levels produced by premixed combustion. Also, analytical prediction of CO emissions is not straightforward because of the dependence of CO formation rates on the complex kinetic processes responsible for the oxidation of heavy fuel molecules. The rate of oxidation of the CO produced in a flame zone depends primarily on the flame temperature; an analytical technique for approximating this process has been developed by Westenberg (Ref. 6). For this study, the anticipated CO levels are based on experimental data published by Marek and Papathakos (Ref. 3) and on the Westenberg predictions -- see Fig. 6. The experimental data were acquired at a pressure of 5.6 atm -- according to the Westenberg analysis, the CO levels produced at higher pressure should be smaller, therefore, Fig 6 provides a conservative estimate of CO levels expected at 10 atm in a combustor having a two millisecond residence time. The experimental data indicate that the CO emission index will exceed the goal of 10.0 g/kg for equivalence ratios of less than 0.5 for entrance temperatures of 600K; the analytical data indicate that the goal will be exceeded for equivalence ratios less than 0.45. Because UHC emissions can be expected to be primarily dependent on flame temperature as well, it is likely that UHC goals as well as combustion efficiency goals will be exceeded at these lower levels of equivalence ratios. The only path open to achieving lower CO and UHC emissions is to increase the combustor residence time, however, this would jeopardize the probability of achieving the NO_x emission goal. In this study the primary objectives were the achievement of wide lean stability limits while at the same time achieving low NO_x emissions over the specified equivalence ratio range. It was therefore determined that the combustor length would be fixed at a value corresponding to a residence time of two milliseconds and that the low probability of the combustion efficiency, CO, and UHC goals being met at low equivalence ratios would be accepted.

Description of Augmented Combustor Concepts

In this section, the features of each of the augmented combustor design concepts are described and the methods of evaluating the major design parameters are given.

Piloted Combustors

Three types of combustors in which hot gas pilots were used to augment stability limits were considered (Fig. 7). In the first concept, fuel was injected directly into the wake of the flame stabilizer which is shown as a V-gutter in Fig. 7a. In the second concept (Fig. 7b) hot combustion products generated in a separate pilot combustor were caused to flow over the downstream face of a perforated plate flameholder. In the third concept (Fig. 7c), recesses or cavities are placed in the downstream face of a perforated plate flameholder where small amounts of the mainstream fuel/air mixture could reside for extended periods of time in order to create local regions of hot gases which would act to stabilize the flame. In all of the designs, the primary concern was to distribute the pilot fuel or the hot pilot gases uniformly across the entire face of the flameholder array. This was important in order to ensure that piloting occurred locally at all sites from which flamespreading was initiated. This would be particularly important if low combustion efficiencies and high emissions of CO and unburned hydrocarbon were associated with intermittent blowout at these local sites. It was believed that flamespreading rates in lean flames are so small that the existence of a single, highly stable central flame would not prove to be a useful technique for achieving a practical augmented combustor design.

Fuel-Injected Flame Stabilizer

The amount of fuel required to be injected into the recirculation region downstream of a bluff body in order to achieve maximum stability limit improvement can be determined by assuming that stoichiometric recirculation zone products are desired. The fraction of the flow approaching the bluff body which is entrained in the recirculation region is approximately 5 percent of the flow which would pass through the projected area of the body (Ref. 7). Therefore:

$$\phi_p = 0.05 \times B (1.0 - \phi_m) \quad (2)$$

For a flameholder blockage of 75 percent and a mainstream equivalence ratio of 0.25, a fuel flow rate corresponding to an equivalence ratio of approximately 0.03 would be required. Equivalently, in the case where the primary zone equivalence ratio is 0.6, the pilot fuel flow required is approximately 5 percent of the total fuel flow. The major design problem is to uniformly distribute the pilot fuel throughout the recirculation region.

From a mechanical design viewpoint, the distribution problem is made evident by the extremely small orifices which would be required to meter the pilot fuel. A simple continuity balance demonstrates that microscopically small orifices will be required at the point of injection if a large number of injection sites are employed to inject liquid fuel. The relationship between the diameter of the metering orifices and the cross-sectional area of the combustor (over which the pilot flow passing through the orifice must be distributed) is given by the following expression:

$$d^2 \sim \frac{1}{N} P \times \left(\frac{t/a}{f/a}\right)_{\text{oa}} \frac{(\rho u)_m}{(\rho u)_p} \left\{ \frac{1}{\left(\frac{1}{1 + f/a} \right)_p} \right\} A_m \quad (3)$$

where N is the number of injection sites and P is the ratio of pilot flow to total fuel flow. In the case where the pilot flow is fuel only, the bracketed term becomes unity. A plot showing the relationship between orifice size and combustor area as given by this equation is shown in Fig. 8 for cases where the pilot fuel is assumed to be liquid fuel, gaseous fuel, or the products of combustion of a fuel-rich mixture. In generating the curves shown on the figure, it was assumed that the orifice discharge coefficient was unity and that a 0.68-atm pressure drop across the orifice would be acceptable. The smaller the pressure drop, the larger the diameter; however, it was felt that pressure drops smaller than the assumed level would be unacceptable due to maldistribution of pilot fuel which would result because of the nonuniform pressure distribution which exists within any real engine. The figure shows orifice sizes for the case in which it is assumed that an amount of pilot fuel equal to 5 percent of the total fuel is required. If it is required that liquid fuel be distributed to the webs of a perforated plate having 0.68 cm diameter holes and 75 percent blockage, and one injection site per hole is assumed, then the combustor area associated with each hole would be 1.2 cm^2 and an orifice size of 6 microns is required. Clearly this is impractical because of clogging problems associated with attempting to pass fuel through a passage of that size. If it were assumed that vaporized fuel is to be injected, the orifice size increases to a value of 0.12 mm which again is too small to be practical. Based on industry experience, the orifice size should be at least 0.25 mm for the injector to be serviceable.

The volume flowrate of pilot fuel can be increased above that achieved by the use of gaseous fuel by reacting the fuel with air in a pilot combustor under fuel-rich conditions. If this system were to be employed, it would be necessary to cool the products of combustion of the reacted mixture to a manageable temperature level before the gases are delivered to the pilot fuel

distribution system. A schematic diagram showing a concept in which diffuser bleed air is used in a heat exchanger to achieve this cooling is shown in Fig. 9. The improvement in volume flow rate which can be achieved with this scheme is shown in Fig. 10a, where the ratio of the volume flowrate of products to the volume flow rate of gaseous Jet-A fuel is shown as a function of the pilot-combustor equivalence ratio. Because of the performance penalties associated with cooling the products, it is advantageous to operate at as high a value of pilot equivalence ratio as possible. According to equilibrium thermodynamic calculations, carbon formation will occur above an equivalence ratio of 2.8. At this value of equivalence ratio the volume flow rate of the pilot gases would be approximately 70 times greater than that of gaseous fuel alone. Because of the necessity of cooling the pilot gas products, the heating value of the combustion products would be less than the heating value of gaseous Jet-A fuel alone as shown in the figure. The primary problem associated with the use of this scheme is the large amount of compressor bleed flow required to cool the combustion products to a manageable level (Fig. 10b). The curves were obtained from a heat balance between the pilot combustion products which were assumed to be cooled to a temperature of 922K and the diffuser bleed flow which was assumed to increase in temperature to the levels shown on the abscissa. It can be seen that because of the high compressor exit temperature associated with the E³ design at the sea-level-takeoff condition, excessively high bleed flow is required. Also, estimates of the heat exchanger tube temperatures indicate than an advancement in heat exchanger technology would be required for a practical design. Because of the penalties to engine performance and costs associated with the use of diffuser bleed to cool the combustion products, this concept was dropped from further consideration.

Derivative concepts using fuel-rich pilots which would require smaller levels of diffuser bleed flow were also considered. By cooling the diffuser bleed in a heat exchanger buried in the fanstream duct, the cooling capacity of the bleed flow could be appreciably increased. In the case where it is assumed that the bleed flow is cooled by 200K (Fig. 11), the diffuser bleed requirements at sea level takeoff can be reduced from 18 percent to 7 percent (assuming a pilot gas temperature of 890K). Despite the reduced bleed flow requirement, the performance penalties associated with this level of bleed flow, the shaft power extraction losses, and the increased duct flow pressure loss indicated that optimization of this system was not warranted.

Injection of water into the fuel-rich pilot products in order to reduce the gas temperature to workable levels was also considered. Thermodynamic calculations of the amounts of water required (Fig. 12) indicated that levels approaching 25 to 35 percent of the fuel flow rate would be required during cruise operation. Airline costs data associated with supplying high purity water for injection into engines to boost engine thrust during takeoff indicated water costs are approximately three times the cost of fuel on a per pound

basis. Although water supply costs could be expected to decrease if large quantities were to be used, it is clear that such a system would not be competitive on a cost basis.

As a result of the above considerations, the use of a fuel-rich pilot to increase the volume flow of the pilot gas to the flameholder base was abandoned and attention was focused on the use of vaporized Jet-A fuel. In order to achieve reasonable orifice size with vapor fuel, it is necessary to minimize the number of injection sites. Because of the desire to distribute pilot fuel throughout the entire base region of the flameholder, an annular V-gutter arrangement characterized by a continuous region of low velocity recirculating flow behind the bluff body was selected for study. In the case of the perforated plate, the main air jets would act to interfere with any transverse component of velocity in the recirculating flow regions and therefore it was less likely that pilot flow could be distributed throughout the base region with this configuration than in the case of the V-gutter. A method considered for distributing pilot fuel to the base of the annular V-gutter is shown in Fig. 13a. The V-gutter stabilizer has a base dimension of 1.2 cm; it is envisioned that such a flame stabilizer would be incorporated within a 75 percent blockage array in the E³ design. The leading edge of the stabilizer would be a fuel plenum from which fuel would be metered across 0.064-cm diameter orifices located 13.3 cm apart. The fuel would then be distributed throughout the 13.3-cm sector by distribution orifices across which a small pressure drop occurs. Potential problems associated with this scheme are poor pilot fuel distribution and the possibility of back flow of combustion gases into the distribution manifold by virtue of a nonuniform circumferential pressure distribution in the engine. Alternative means of distributing the pilot fuel are also shown in Fig. 13. In Fig 13b a deflection plate is used to impart a tangential velocity component to the pilot fuel jet. Cooling of the deflection plate would be accomplished by conduction of heat to the sides of the V-gutter which are cooled by the approach flow mixture. In Fig. 13c a canted orifice is employed to impart tangential component velocity to the pilot fuel. The actual degree of mixing achievable by any of these designs can only be assessed by experiments.

A summary of the assessment of the penalties associated with the use of the injection of gaseous pilot fuel is given in Table AI-1 of Appendix I. The principal difficulty with this concept is the expected increase in maintenance costs associated with the use of a fuel vaporizer. Information currently available on the characteristics of fuel vaporizers indicates that a periodic maintenance program would be required in order to remove carbonaceous deposits from the heat exchanger surfaces. Other factors adversely affecting this system are the initial costs of the control system and the complexity of the manifolding system which would contribute to the initial cost of this system being slightly above average. The penalties associated with the estimated weight of the vaporizer and manifolding is negligible. Finally, there is a significant technological risk associated with the achievement of a workable

system--the transient response of the fuel vaporizer may be a problem as well as the occurrence of fuel flow instabilities which would result from the low pressure drop across the metering orifices.

Hot Gas Drafting

The second pilot concept considered is based on the drafting of hot pilot combustion products along the downstream surface of a perforated plate flame stabilizer. Drafting refers to the establishment of a secondary flow pattern in the wake of the bluff body such that a portion of the recirculating flow is distributed throughout the bluff-body base region. Tests conducted to evaluate the designs of such flameholders used in turbofan augmentors indicate that, if a secondary flow pattern can be established such that base region flow is transported from a highly stable region to a less stable region, the stability limits of the less stable region can be significantly improved. In a turbofan application, the highly stable region is that portion of the flow at which engine exhaust is directed, whereas the less stable region is that portion of the flow associated with the low temperature duct gas. In the current application this effect could be utilized by combusting an amount of pilot flow in an isolated, conventional, highly stable combustor and injecting the products along the base of the perforated plate flame stabilizer (Fig. 7b). By canting the perforated plate and by generating a favorable pressure gradient, a secondary flow pattern could be established which would act to distribute the pilot gas along the downstream faces of the flameholder.

The primary advantage of this design is that only conventional technology is required - no improvement in the state of the art of materials or combustor technology is required. The chief disadvantages are that the amount of stability improvement cannot be estimated *a priori*; extensive tests of various pilot and combustor configurations would have to be conducted. Because of the complexity of the flow, fluid mechanic analyses are not available to optimize the geometric configurations and therefore cut and try experimental procedures would necessarily be required. An additional disadvantage is that the NO_x emissions generated within the pilot would be high and the overall NO_x emissions index could be expected to be approximately 1.9 g/kg (assuming a 10 percent pilot flow and a value of emission index 10 g/kg for the pilot fuel). The initial cost of this system would be expected to be somewhat higher than average because of the increased numbers of fuel injectors and the need for separate fuel control systems. Also, experience with the design of small combustors indicates that relatively large amounts of cooling air are required for these small designs, and therefore, there is a certain risk that the total amount of coolant available for the pilot/combustor will be insufficient. A summary of the rankings assigned to this device is given in Table AI-2.

Self-Piloting Recessed Perforated Plate

The possibility that stability limits can be augmented by providing a pocket of hot combustion products at the rear face of the perforated plate is supported by work recently conducted at UTRC (Ref. 8). The data indicate that the lean blowout limit of high blockage flameholders could be decreased from an equivalence ratio of approximately 0.5 to 0.3 by counterboring the exit of the perforations (Fig. 14). The data shown in the figure are the only known experimental data on this effect.

The chief attraction of this concept is that there would be virtually no engine performance, cost, or risk associated with the use of this concept. The major disadvantage is that because of the meager data available, the potential for improved lean stability limits must be regarded as low. Rankings assigned to this concept are given in Table AI-3.

Catalytic Augmentation Concepts

The catalytic flame stabilization augmentation schemes considered in this study were concerned with (1) techniques for pre-reacting a portion of the fuel-air mixture prior to the mixture entering the flame stabilization region and (2) providing a catalyzed surface on the downstream face of the flameholder to re-ignite the the mixture in the event that blowout is related to an intermittent blowoff/re-ignition process. Under the terms of the contract work statement, catalytic combustors in which all of the fuel is reacted to completion were not to be considered in this program. The catalytic augmentation concepts selected for study include two concepts corresponding to the first type cited above--the catalyzed perforated plate and the catalyzed bed pre-heater--and a third concept that represents a combination of the first and second types--the catalyzed, recessed, perforated plate (see Fig. 15).

Catalyzed Tube Flameholder

Analysis of the processes controlling flame stability (Ref. 1) indicates that the dominant factor in determining whether ignition will occur on a streamline in the mixing layer formed between the freestream and the recirculating flow (see Fig. 1) is the temperature history along the streamline. This temperature is controlled by both the temperature of the entering mixture and the temperature of the recirculating flow (which is close to the adiabatic flame temperature). The adiabatic flame temperature alone does not determine the flameholder stability characteristics. This is supported by the classical DeZubay blowout correlation. A plot derived from a DeZubay-type correlation for a perforated plate flameholder showing the variation in stability parameter for a constant adiabatic flame temperature shows that significant improvement in blowout limit (lower values of stabilization parameter) can be achieved by increasing the entrance temperature (Fig. 16). One method of increasing the

temperature of that portion of the approach mixture which is entrained in the mixing layer is to react a portion of the fuel in the gases in the boundary layer which forms on the surface of the bluff-body. It should be noted that when partially reacting the fuel, the fuel and oxygen concentration in the approach flow will be diminished and thus the gas state will be somewhat less favorable to ignition than would be the case if the flow were thermally heated (which, is the case for the data used to generate the conventional stability plot from which Fig. 16 was derived). However, the pre-ignition reactions can be expected to be much more sensitive to temperature level than to concentration level and therefore, it is reasonable to expect an improvement in stability limits will be achieved by pre-reaction.

Gases in the boundary layer formed on the bluff body can, in theory, be pre-reacted by catalyzing the surface of the body. Experience with catalytic combustors indicates that reaction can be expected to occur if surface temperatures approach a level of approximately 800K (Ref. 9). Extremely high surface temperatures are to be avoided because of the desirability of avoiding the use of unconventional materials as the catalyst substrate. A configuration lending itself to achievement of surface temperatures in the desired range is a flame-holder composed of a tube bundle retained by fore and aft headers. The internal surfaces of the tubes would be catalyzed and coolant would be circulated over the external surface of tubes in order to provide tube temperature control. The tubes would be heated by the reaction occurring in the boundary layer and by conduction of heat from the recirculation zone through the aft bulk head and along the tube wall.

The major design problem to be addressed is the determination of the length of the tube which would be required in order to generate significant reaction in the boundary layer flow. To accomplish this it was assumed that the flow process occurring within a single tube of the tube bundle would be similar to the processes occurring in the monolithic catalytic beds studied by Anderson (Ref. 9). Calculations were undertaken to determine the fraction of reactants which, when having diffused to the wall in the high performance bed tested by Anderson, did in fact react. The fraction diffusing to the wall can be expressed as:

$$\frac{w_{f,s}/A_s}{\mathcal{D}\Delta C_f} \frac{d}{= NUm} \quad (4)$$

where the Nusselt number for mass transfer, Nu_m is 4.0 in the laminar flow case studied by Anderson. The area, A_s , in the above equation is the surface area of the catalyst bed which is proportional to the length of the bed and the cross-sectional area of the bed:

$$A_s = k \ell A_c \quad (5)$$

The fuel flow entering the bed is given by:

$$W_f = \rho_0 U_0 A_c \times f/a \quad (6)$$

Thus,

$$\frac{W_{f,s}}{W_f} = NUm \frac{\Delta C}{d} kL \frac{l}{\rho_0 U_0 f/a} \quad (7)$$

Evaluating this expression for a representative set of data acquired by Anderson (Table 6a) indicated that $W_{f,s}/W_f = 1.13$ at the distance downstream of the bed entrance where the measured temperature rise was equal to the adiabatic temperature rise; that is, when all the fuel was reacted. In other words, under pressure, temperature, and fuel-air ratio conditions of the same magnitude as those of interest in this program, an appropriate design criterion is that the percentage of fuel reacted in the catalytic bed can be equated to the percentage of fuel which diffuses to the wall.

To extend this result to the catalyzed tube flameholder, it was assumed that approximately 5 percent of the flow which would pass through the projected area of the flameholder body would be entrained in the recirculation zone behind the body and that it was desired to pre-react all of the approach flow mixture that is entrained in the recirculation zone. Thus it was desired that 5 percent of the flow in the tubes diffuse to the wall. Using the mass transfer correlation for turbulent flow (which is appropriate for the high flow velocity configuration), it was determined that a tube length of approximately 6 cm would yield the desired performance (Fig. 17).

An assessment of the penalties to engine performance and cost resulting from the use of this concept (Table AI-4) indicated that weight, pressure loss, and initial cost penalties associated with the catalyzed tube flameholder would be minimal. However, in view of the possibility that catalyst activity will degrade with time and that refurbishment, which would require removal of the catalyzed elements, will be required on a periodic basis, a maintenance

cost ranking of far-above-average was assessed. Also, the lack of experience with the use of catalyzed elements in conjunction with Jet-A means that there is a moderate technological risk associated with the successful development of this technique. An above-average ranking in terms of the potential for achieving significant stability enhancement was assigned in view of the existing data base which indicate pre-heating of reactants can result in a significant stability improvement.

Catalytic Bed Preheater

The catalytic bed preheater concept is a more conventional use of catalysis wherein the entire fuel-air mixture is passed through a short length of bed with the objective of increasing the mixture temperature by several hundred degrees in order to achieve wider stability limits. The primary design problems to be addressed are the determination of the length of bed required and determination of the pressure loss associated with transport through the bed.

A map of temperature rise as a function of bed pressure loss was generated using Anderson's measurements as a data base. The pressure loss through the catalytic bed can be estimated by accounting for the friction and entrance/exit losses:

$$\Delta p = 4f \frac{L}{D} + C \frac{\rho V_0^2}{2g} \frac{1}{(1-B)^2} \quad (8)$$

where B is a blockage of the bed. Assuming that for a fixed bed cross-sectional area the hydraulic diameter of the bed cell passage is related to the number of cells per unit frontal area:

$$N \sim \frac{1}{d^2} \quad (9)$$

and the flow is laminar in a high cell density bed such that the friction coefficient is inversely proportional to the Reynolds number, the pressure loss can be expressed as:

$$\frac{\Delta p}{p} = C_1 \left[\frac{T(1-B)}{\rho V_0} N + C_2 \right] \left(\frac{1}{1-B} \right)^2 \left(\frac{V_0^2}{T} \right) \left(\frac{T}{T_0} \right)^2 \quad (10)$$

The temperature rise as a function of bed length was estimated by extrapolating data obtained at equivalence ratios of 0.2 to 0.24 (Table 6b) to the value of 0.3 established as the blowout design point. In the experiments, temperature data were acquired at a bed length of 2.54 cm; for the purpose of these estimates it was assumed that the temperature rise was linear with bed length. Also, in order to obtain high conversion rates (necessitated by the limited overall combustor length available), characteristics for a bed having a cell density of 87 cells per cm^2 (Thermacomb 12/6) were used, and it was assumed that the conversion efficiency could be linearly extrapolated from the data available for the lower cell densities (30 and 45 cells/ cm^2 --See Table 6c). The pressure loss and temperature rise estimates were then combined to yield the estimated bed performance shown in Fig. 18.

It was assumed that at least 200 deg of preheat would be required in order to widen the blowout limits to the desired level. According to the data shown in Fig. 18, a pressure loss of at least 0.5 percent would be realized and the bed thickness would be approximately 0.7 cm.

The assessment of penalties associated with the use of this concept in the E³ design is given in Table AI-5. Because of the small volume of the bed, no significant weight penalty resulted. However, because the bed can be expected to generate high temperatures during operation at high equivalence ratios, a cooled bed support structure probably would be required, and therefore, the cost of the system was specified as slightly above average (Rank 2).

Catalyzed Recessed Perforated Plate

This concept would combine the characteristics of the catalyzed tube flameholder and the recessed perforated plate. The downstream face of the aft bulkhead of the catalyzed tube configuration would be recessed and catalyzed. The concept would provide increased stability margin if blowout is associated with the capability to re-ignite the flow during an intermittent blowout/re-ignition sequence. The penalty characteristics associated with this design (Table AI-6) would be similar to that of the catalyzed tube flameholder plate except there would be a somewhat higher technological risk associated with developing a catalyst and a substrate which could withstand the harsh environment associated with contact with the recirculation zone gases.

Heat-Recirculation Stability Augmentation Concepts

As has previously been discussed, stability limits can be enhanced by increasing the temperature of the fuel-air mixture prior to the mixture entering the flame stabilization region. Increased temperature can be achieved by (1) recirculating a portion of the combustion gases and mixing with the entrance air and by (2) exchanging heat between the combustor exit gases and

the entrance air by means of a heat exchanger. The three concepts selected for evaluation in this study comprise a scheme whereby combustor primary zone gas is pumped by use of the last stage of the engine compressor (Fig. 19a), a scheme whereby ejector action is used to recirculate combustor flow (Fig. 19b), and a scheme employing a regenerative heat exchange (Fig. 19c).

Compressor-Recirculated Primary Gas

In order to recirculate a portion of the combustor discharge flow, some means of overcoming the combustor liner pressure loss must be provided. One means of accomplishing this is by injecting the recirculated flow ahead of the last stage of the high compressor (Fig. 19a). The pressure rise across this last stage is estimated to be approximately 1.15 whereas the pressure ratio across the diffuser and liner is approximately 0.94, and thus sufficient pumping potential exists. Estimates of the increase in specific fuel consumption which would result by loading the high compressor in this fashion (Fig. 20) indicate that substantial penalties would occur and, therefore, it would be beneficial to incorporate shut-off valves to provide for recirculation only during low power operation where stability limitations enhancement is required.

An energy balance was performed in order to determine the amount of flow required to be recirculated in order to raise the entrance air temperature level. Three recirculation schemes were considered (see Fig. 21). The energy balance equations are:

- (1) Primary combustion products are mixed with primary air

$$T_{\text{mix}} = \frac{(1-S)C_{p,\text{pri}} T_0 + P_R C_{p,r} T_r}{(1-S)C_{p,\text{pri}} + P_R C_{p,r}} \quad (11)$$

where T_r is the primary zone gas temperature.

- (2) Secondary combustion products mixed with primary air. Equation (11) is applicable where T_r is the secondary gas zone temperature.

- (3) Primary combustion products mixed with combustor (primary plus secondary) air

$$T_{\text{mix}} = \frac{C_{p,\text{pri}} + P_R C_{p,r} T_r}{C_{p,\text{pri}} + P_R C_{p,r}} \quad (12)$$

where T_r is the primary zone gas temperature.

As can be seen in Fig. 21, in order to achieve a 100K rise in primary zone inlet temperature, a flow rate equal to between 8.5 and 16 percent of the engine flow rate will be required depending upon the applicable scheme. Of the two schemes employing recirculation of primary zone gas, Scheme (1) requires significantly less flow rate than Scheme (3), however, a method of preventing the mixing of the primary and dilution air downstream of the gas injection point would be required. Techniques for accomplishing this by the inclusion of shrouds in the diffuser were rejected as being impractical from the standpoint of maintaining flow passage area tolerances and because heat exchange would occur across the shrouds. Therefore Scheme (1) was not considered applicable to this concept; Scheme (2) must be rejected on the same grounds. Thus, as indicated by the curve for Scheme (3), a flowrate of primary zone gas equivalent to 15 percent of the engine flow is required to be recirculated in order to achieve even the moderate stability limit afforded by a 100K mixture temperature increase.

Results of an evaluation of the sizes of the passages required to recirculate this amount of flow indicated that four 4.5-cm diam ducts would be suitable. Gases would be extracted from the annular combustor through 80 0.64-cm dia tubes manifolded to these transport ducts. A similar number of tubes would be used to deliver the gases to the last stage stator array. The total estimated weight increment for this design would be moderate (92 kg). However, the initial cost and maintenance costs associated with this system were estimated to be far above average because of the high temperature environment, the complexity of the shut-off valve system, and the hot section access problems associated with the existence of the manifolds and the transfer ducts. A high technological risk would be associated with this concept due to the necessity of developing reliable high temperature valves and methods of joining the other high temperature components. A summary of these assessments is given in Table AI-7.

Ejector-Recirculated Primary Gas Flow

An alternative means of pumping the primary products is by the use of an ejector effect obtained by routing the primary air to the station immediately upstream of the secondary air injection holes and accelerating the primary air in a converging section in order to reduce the local pressure such that combustion gases are entrained in this air stream (Fig. 19b). Note that in this case, primary zone gases are used to heat primary air only, and therefore the curve corresponding to Scheme (1) in Fig. 21 is applicable. The chief penalty incurred by use of this concept is additional pressure loss associated with the ejector action and the turning losses occurring in the ducts.

The magnitude of the ejector loss was estimated by performing one-dimensional ejector calculations assuming constant area mixing of the motive and driven flows. An iterative calculation procedure was employed in which for any

given amount of flow recirculation, different levels of motive flow Mach numbers were assumed and the mixture stagnation pressure calculated by application of the conservation equations for heat, mass, and momentum. When the calculated mixed total pressure less the turning losses and the flameholder pressure loss was found to be equal to the specified burner pressure (the ejected flow total pressure) a solution was obtained. In general, the solution was double valued, corresponding to a high and a low level of motive flow Mach number. The low Mach number solution ($0.2 < M < 0.4$) was selected. The calculated pressure loss for different levels of recirculated flow are given in Fig. 22. The pressure losses are almost entirely attributable to the mixing losses; the turning losses, which were estimated to be equal to twice the dynamic head, were found to be negligible because of the large flow area and hence low duct Mach numbers which would be achievable with reasonable duct geometry. The diffusion losses associated with decelerating the mixed flow were neglected.

An assessment of the penalties associated with a design employing 10 percent recirculation (1.5 percent additional pressure rise and 120 K mixture temperature increase) was performed. In terms of direct operating costs penalties, it was concluded that only the additional pressure loss was of significance; the weight of the additional shrouds (25 kg) was of little significance. The additional initial costs would not be significant and no maintenance problems are anticipated. A moderate technological risk was assessed in view of the problems of maintaining flow passage tolerances required in the ejector passages, and the uncertainty regarding the achievement of the pressure recovery calculated by the ideal flow analysis. A summary of this assessment is given in Table AI-8.

Regenerative Heat Exchange

In the regenerative heat exchange concept, (Fig 19c) only heat (not mass) is recirculated from the primary zone exhaust to the entrance air. As a result, increases in flame stability limits resulting from increased entrance temperature but also from increased adiabatic flame temperature can be expected. As in the case of any regenerative engine concept, the design of the heat exchanger is the major engineering problem.

Calculations were carried out using available data on compact heat exchanger design (Ref. 10) in order to determine the temperature rise and pressure loss characteristics of a typical unit applicable to this scheme. A cross-flow shell and tube design in which the primary air is passed through the interior of the tubes was assumed. Tubes having a 1.2 cm ID with a center-to-center spacing of 2.5 cm were arrayed with 100 tubes per row at the exit of the primary zone annulus. The calculation showed that at the low power condition ($\phi = 0.3$) approximately eight rows of tubes would be required to raise the

entrance temperature by 100K, (Fig. 23). The pressure loss associated with this design would be approximately 3 percent. Another problem associated with this design is the high tube wall temperature which will exist during high power operation. Calculated tube temperatures for operation at primary zone equivalence ratios of 0.6 are shown in Fig. 23. Clearly, advances in heat exchanger material and fabrication techniques will be required for this concept to be practical.

An assessment of the penalties associated with this concept is given in Table AI-9. Penalties associated with the weight of the heat exchanger and manifolds are small, however, both the initial cost and maintenance costs are estimated to be high. High initial costs will result from the technology required to reliably join the many pieces which will be subjected to severe thermal loads; high maintenance costs will result from the necessity to periodically clean the exchanger tubes of carbon deposits in order to maintain high effectiveness and also to repair leaks which can be expected to occur. Another problem associated with this design is that, because of the adiabatic flame temperature, nitric oxides produced at high equivalence ratios will exceed the design goal. Finally, a high technological risk exists in view of the advanced state-of-the-art of heat exchanger technology which was assumed.

Concept Assessment and Selection

A summary of the performance characteristics of each concept and the overall ranking assigned to each concept by the Concept Review Committee is presented in Table 7. In assessing the relative importance of each performance category, major emphasis was placed on the stability augmentation rating, the direct operating cost penalty, and the ability to achieve the NO_x emission goals. Technological risk and operational problems were given lesser emphasis.

The fuel-injected flame stabilizer was given the highest ranking because the highest probability of achieving wide stability limit exists with this concept and only a moderate cost penalty is predicted. The self-piloting perforated plate stabilizer received the second highest ranking because no adverse impact on aircraft performance would result from the use of this concept; the only major drawback of this concept is that only a moderate probability of achieving significant stability limit improvement is foreseen. The catalytic concepts, the ejector-recirculated primary gas concept, and the remaining piloting concept were candidates to receive the third highest ranking; the compressor-recirculated-primary-gas and the regeneratively-heated-primary-air concepts received the lowest rankings because of their high cost and low stability improvement ratings. The hot gas drafting concept was not given a high ranking because the principal NO_x goal would be exceeded with this device. The ejector-recirculation concept was also not selected because of the high risk associated with developing an efficient ejector on a full-

scale engine. Of the catalytic concepts, the catalytic bed preheater was assigned lower ratings than the catalyzed tube or catalyzed recessed perforated plate. Because the catalyzed recesses could be incorporated within the catalyzed tube concept, the catalyzed tube concept was assigned the third highest ranking.

In summary, the concepts selected for rig testing were the fuel-injected flame stabilizer, the self-piloting recessed perforated plate, and the catalyzed tube flameholder.

FLAMEHOLDER TEST CONFIGURATIONS

For each of the three augmented stability concepts selected, five design variations were tested in the flame tube test program. In addition, a baseline perforated plate design was tested. The characteristics of these 16 designs are described hereunder.

Baseline Design

The baseline flameholder was a 0.64-cm thick plate perforated with 55 holes of 0.691-cm diameter. The flameholder blockage is 75 percent. The holes, which were arranged in a hexagonal array (Fig. 24) had rounded leading edges which have previously been shown to suppress the likelihood of the occurrence of flashback. The flameholder material was Type 316 stainless steel.

Heat transfer calculations were conducted to determine the metal temperature distribution which could be expected under the most severe operating conditions ($T_o = 800K$; $\phi = 0.6$) to be employed in the tests using this uncooled design. A finite element, steady-state, two-dimensional heat conduction calculation procedure was applied to a segment of the plate. Heat transfer coefficients between the upstream surface and within the tube-like passages were calculated from a boundary layer analysis; the heat transfer coefficient on the hot downstream side was assumed to be $175 \text{ watt/m}^2 \text{ sec K}$. Metal temperatures were calculated to range from 870 to 960K (1100 to 1260F) which is satisfactory from a material allowable stress standpoint.

A particular concern in the design of the flameholder was fatigue failure of the webs due to differential expansion of the inner and outer segments of the plate during start-up and shutdown. To minimize the temperature difference between the outer rim and center of the plate, the diameter of the flameholder was made only slightly larger than the diameter of the flow passage. In this manner, only a very thin outer section (required for retention purposes) was not subjected to the combustor flow and hence combustor heat loads. A photograph of the flameholder and retaining ring is shown in Fig. 25a.

Self-Piloting Recessed Perforated Plate Designs

Three of the self-piloting recessed perforated plate (SPRPP) designs (SPRPP-1, SPRPP-2, SPRPP-3) employed the same basic air-cooled perforated plate. The fourth design and the final designs were uncooled designs.

SPRPP-1

The basic cooled SPRPP design was a 1.75-cm thick, Type 316 stainless steel plate perforated with 37 holes of 0.833-cm diameter. The flameholder blockage is 75 percent. The holes were arranged in a square array with a center-to-center spacing of 1.468 cm. The leading edge of the holes were rounded (0.4-cm R) to suppress flashback. Six coolant passages of rectangular cross section having dimensions of 0.648 cm by 0.239 cm ran between the rows of holes. The downstream face of the flameholder was recessed by drilling 32 0.792-cm diameter blind holes 0.635-cm deep between the perforations. A schematic diagram showing a typical crosssection of the plate is shown in Fig. 26; a photograph of the flameholder is presented in Fig. 27.

SPRPP-2

This configuration was a modification of SPRPP-1 in which 0.13-cm diameter passages were drilled through the webs of the plate such that a portion of the approach flow passed into each recess. These passages permitted a small amount of reactants to flow into the recesses where the reaction would release heat such that the temperature of the gas in the recesses would not be reduced due to heat transfer to the walls of the recess. The diameter of the bleed passage was determined by assuming that the amount of flow entrained in the recirculation zone behind the plate was 5 percent of the flow through the projected area of the plate and that it was desired to replenish 10 percent of that amount by bleed flow.

SPRPP-3

This configuration was a modification of SPRPP-2 in which the recesses were joined by interconnecting grooves which would act to distribute the recirculation gases. The groove depth and groove width are 0.32 cm. The grooves also serve to increase the surface area of the plate which contacts the recirculating gases such that the plate will achieve higher surface temperatures for a fixed coolant flow rate.

SPRPP-4

This configuration was an uncooled, 1.75-cm thick perforated plate having the same hole diameter and configuration as SPRPP-1. The exit of each of the holes was countersunk with a 90 deg countersink tool such that the exit diameter of the holes was 1.37 cm. Finite element heat transfer analyses indicated that this was the largest diameter countersink which could be permitted in this uncooled design without the temperature of the flameholder exceeding design limits. Increasing the countersink depth both increases the base area of the

plate which is exposed to the flame temperature and decreases the surface area of the plate which is swept by cool reactants. A countersink was selected rather than a counterbore to achieve a smaller hot side surface area for the same hole exit diameter. The hole entrance was rounded as in SPRPP-1. A photograph of the flameholder is given in Fig. 28.

SPRPP-F

The final design of this series was an 80 percent blockage flameholder having a deep counterbore in the rear face. Nineteen 1.026 cm diameter holes were arranged in an array designed to center the holes in 19 sections of equal area (Fig. 29). The maximum center-to-center dimension for the array was 3.04 cm; the characteristic center-to-center dimension is 2.4 cm. The counterbore diameter was 1.70 cm while the counterbore depth was 1.14 cm. The hole entrances were not rounded as in previous designs but were chamfered by use of a 100-deg countersink; the outer diameter of the chamfer was 1.63 cm.

Catalyzed Tube Flameholder Designs

All five of the catalyzed tube flameholder configurations were derived from the same basic design. Twenty-two 1.092 cm ID Type 321 stainless steel tubes were arrayed in a tube bundle constructed in the form of a shell and tube heat exchanger (Fig. 30). The tubes were estimated to be of sufficient length (9.53 cm) to permit more than five percent of the mixture flowing through the tubes to be transported to the tube walls by turbulent diffusion. The blockage of the flameholder was 74.6 percent.

This flameholder was actively cooled by passing air normal to the combustor flow axis and over the outer diameter of the tubes inside of which flowed the fuel-air mixture. A second coolant flow path, separated from the former by a baffle plate, exists with which the temperature of the downstream plate of the flameholder assembly was controlled. Thermocouples were attached to the outer diameter of the tubes and to the downstream surface of the rear plate. Prior to application of the catalyst, the surfaces to be activated were roughened and then an alumina coating was applied. The roughening process was carried out in order to improve the probability of the catalyst adhering to the tube surface under high temperature conditions; the aluminizing of the stainless steel tubes was carried out in order to prevent degradation of the catalyst activity due to migration of the catalyst into the substrate material. A photograph of the plate-tube assembly is given in Fig. 31.

CTF-1

The first configuration tested had catalyst applied as noted above; only the forward face of the flameholder and the initial 0.45 cm of the tube ID were uncatalyzed.

CTF-2

The second configuration was a modification of the first in which the catalyst was removed from the rear surface by wiring brushing.

CTF-3

The third configuration was a modification of the second in which catalyst was removed from the forward half of the tube ID.

CTF-4

The fourth configuration tested was identical to CTF-3 except that hot air (811K) was passed through the coolant passages at the low power conditions.

CTF-F

The final design of this series was a modification of the basic assembly in which restrictions were placed in the entrance to four of the tubes (see Fig. 32) in order to decrease the flowrate in these tubes. The diameter of the restrictions was 0.32 cm; the blockage of the flameholder was increased to 78.8 percent. The size of the restriction was based on a heat transfer calculation which indicated that tube temperatures less than the design limit (1255K) would exist if all of the flow passing through the restriction were to react to completion within the tube. Catalyst was applied to the inner diameter of the restricted tubes downstream of the restriction; catalyst was removed from the other tubes.

Piloted Flameholder Designs

Two basic types of piloted flameholders were tested: piloted V-gutters and a piloted perforated plate. Four V-gutters were tested in which gaseous Jet-A fuel was used as pilot fuel; the method of fuel injection and the flameholder blockage were varied. One piloted perforated plate configuration was tested; the pilot fuel was liquid Jet-A.

PF-1

The V-gutter flameholder consisted of two concentric annular gutters having a base characteristic dimension of 1.27 cm and a blockage of 58 percent (Fig. 33). The design was based on the considerations that a characteristic dimension of 1.27 cm should provide satisfactory stability limits (based on existing bluff-body stability limit correlations) and that the area contraction imposed on each of the three gas flow paths determined by the flameholder geometry should be equal. This latter specification was established to minimize the possibility of separation of the flow at the V-gutter apex which would lead to flameholder burnout. It was also desired to have a flameholder blockage not significantly greater than 50 percent because of experience which indicated that higher blockage devices were prone to generate high frequency combustion instabilities (screech). Pilot fuel was fed to a tubular plenum located at the flameholder apex from where it was discharged through metering orifices into a second low pressure plenum. Eight metering orifices (0.051-cm diameter) were incorporated in the outer flameholder and four 0.51 cm diameter orifices in the inner flameholder.

The initial Type 316 stainless steel flameholder (Fig. 34) was not actively cooled; cooling was provided by the approach flow gases flowing over the outer V-gutter surfaces as in conventional turbine engine afterburner designs. Results of the initial test series indicated that some distress occurred locally on the flameholder lip downstream of the 0.163-cm thick radial struts which supported the gutters. Also, there were signs of overheating in the vicinity of the pilot fuel injection orifices. To ensure that the flameholder would survive the test series, 0.32-cm OD tubing was brazed to the upstream surface of the V-gutters through which water coolant was circulated (See Fig. 33).

PF-2

This design was a modification of PF-1 in which the 12 injection orifices were plugged and re-machined such that injection occurred with a substantial tangential component in order to achieve better distribution of the pilot fuel with the recirculation zone gases. The angle formed between the centerline of the injection orifice and the exit plane of the flameholder was 25 deg compared with 90 deg for PF-1 (See Fig. 33).

PF-3

This design was a variation of the basic flameholder design in which the number of injection sites was increased from 12 to 36. The diameter of the distribution holes was 0.076 cm; the direction of the injection was parallel to the combustor flow axis (See Fig. 33).

PF-4

The fourth piloted flameholder employed a 75 percent blockage perforated plate with a single pressure atomizing fuel injector which was fitted into the central flow passage (Fig. 35). The perforated plate employed was SPRPP-3; by blocking the central flow passage, the blockage of the perforated plate was increased from 75.1 percent to 75.8 percent. The fuel injector employed is the mainburner fuel nozzle used on the PT-6 turbojet engine produced by Pratt and Whitney of Canada; the fuel injector is produced by Excello Corp and is designated as Part No. 2700-2. The nominal flowrate of Jet-A fuel at a differential pressure of 8.50 atm is 6.91 kg/hr; the nominal spray cone angle is 85 deg.

PF-F

The final flameholder configuration was a modification of PF-3 in which a portion of the three flow passages around the annular V-gutters was blocked such that the blockage was increased from 57 to 75 percent (Fig. 36). The blockage segments consisted of 4 35-deg arcs equispaced in the two annular passages plus a 1.0-cm wide bar segment placed in the center circular passage. The blockage segments were cooled by a single length of 0.32-cm dia copper tubing brazed to the upstream surfaces.

TEST FACILITIES AND EQUIPMENT

Testing was conducted in the Jet Burner Test Stand located at United Technologies Research Center. An existing facility was modified to house the test apparatus required for this effort. A schematic diagram showing the test apparatus layout is presented in Fig. 37; a photograph of the facility is given in Fig. 38. Described in this section are the test apparatus, facility services, and instrumentation employed in the test program.

Test Apparatus

Hot, high pressure air, provided by an existing facility, was discharged into a plenum which was fitted with baffles designed to break up the entrance air jet. The plenum was fitted with a burst disk to protect the apparatus from overpressure, and was insulated in order to minimize heat losses from the large diameter piping. At the exit of the plenum a contraction section reduced the flow passage diameter from 25.4 cm to 10.2 cm thereby generating a flat velocity profile at the fuel injector entrance. An instrumentation section was located at this station (Fig. 39) such that the stagnation pressure and temperature profiles could be documented.

The airflow was delivered to a multi-venturi fuel injector which was designed to provide a uniform fuel-air profile, good atomization, and a zero-area base region. The airflow passage of the fuel injector (Fig. 40) is composed of 19 converging/diverging venturi passages which were sized such that the venturis were choked under all operating conditions encountered in the test program. Choked flow was desired in order to ensure equal airflow into each of the venturi passages, and to eliminate the possibility of combustor pressure pulsations affecting the fuel delivery system. The cone angle of the divergent passages was 5 deg and was selected such that the separation region formed downstream of the shock wave would not be significant in extent. Fuel was delivered to each venturi by a 0.084-cm diameter hypodermic tube having a length of 122 cm. The tubing length was selected to provide sufficient pressure drop to minimize the effect of air-side pressure fluctuations on the flowrate of fuel delivered (Fig. 41). The hypodermic tubes entered the air passage just up-stream of the venturi throat and extended one-quarter of the distance across the passage. The hypodermic tubes were designed to be removable in the event that clogging occurred; in fact, clogging never occurred during the test program. The hypodermic tubes were flow-checked by measuring the pressure drop required to deliver four different flowrates of water. It was determined that for a fixed value of manifold pressure, the flowrates delivered by the individual tubes were within 3.5 percent of the mean.

Flow was discharged from the fuel injector into the mixer/vaporizer section which was composed of two uncooled flanged sections having an ID of 10.2 cm. The distance from the point of fuel injection to the exit of the mixer/vaporizer was 30.5 cm. The mixer/vaporizer was equipped with instrumentation (thermocouples and photo-cells) which was used to detect the occurrence of flashback.

The flameholders described in a previous section were clamped between the flanges at the mixer/vaporizer exit and combustor entrance. The downstream sections of the test apparatus were translatable such that flameholders varying in thickness from 0 to 10.2 cm could be accommodated. For those flameholders which employed air cooling, considerable emphasis was placed on attaining tight sealing such that leakage of cooling air into the flameholder base was eliminated. Combinations of Spirotallic gaskets and asbestos-graphite rope seals implanted in O-ring type grooves were employed depending on the particular flameholder configuration.

The combustor was a 27 cm length of schedule 40 carbon steel pipe inside of which was housed a 10.2-cm ID air-cooled liner. Two types of liners were designed --a ceramic liner and a metallic liner.

The ceramic liner selected was a 0.476 cm thickness sleeve of densified silicon carbide. This material was selected on the basis of its relatively favorable thermal shock characteristics as well as its ability to operate at the high surface temperatures desired. The liner was insulated from a stainless steel containment sleeve by a 0.476 cm thick layer of alumina-silica fiber (Fiberfrax) while the outer surface of the stainless steel was cooled by a flowrate (0.01 kg/sec) of air (Fig. 42). A second ceramic material considered was a fibrous alumina (Zircar Products ZAL-45) ceramic which is available at very low cost (10 percent of the cost of the densified silicon carbide) and which holds high potential in terms of thermal shock and temperature capability. Vendor fabrication problems precluded delivery of the silicon carbide liner, and failure of the fibrous alumina liner after a brief test period led to the use of an alternative metallic liner design throughout the test program.

This metallic liner design consisted of a 0.32-cm thick Hastelloy C or Type 316 stainless steel sleeve cooled by a relatively high air flowrate (0.23 kg/sec). The cooling passages (Fig. 42) were designed to pass this high amount of cooling air while creating only a small pressure differential (0.14 atm) such that liner collapse was avoided. The liner was sealed at the forward face by use of a Spirotallic gasket.

The forward flange of the combustor contained a passage through which the products of combustion of a torch ignitor flowed such that the combustor flow could be ignited immediately downstream of the flameholder.

Cooling air was introduced into the passage between the combustor housing and the liner through two 180-deg-opposed entry ports. The liner was double-walled near the forward end of the combustor and a series of holes were drilled through the outer wall such that the cooling air was distributed along the entire circumference of the inner wall of the liner. Differential thermal expansion between the liner and the housing was accommodated by fixing the liner at the forward end of the housing and allowing growth to occur in the rearward direction. A photograph showing the combustor housing, the ceramic liner assembly, the Hastelloy liner, and the igniter is given in Fig. 43.

A water-cooled instrumentation section (Fig. 44) was located immediately downstream of the combustor exit. Six emission probes, a central smoke probe, and static pressure taps were located in this instrumentation section; details of the probe designs are given in a following section. The tips of the probe extended upstream into the combustor such that the distance from the exit of the flameholder to the probe tips was 17.8 cm. With a reference velocity of 25 m/sec, this distance provides a residence time of 2 msec at the design point test condition ($T_o = 600K$, $\phi = 0.6$).

Following the instrumentation section was a transition section which caused the flow to undergo a pair of 90-deg turns and to be discharged into the section containing the backpressure valve. A window was located in the transition section such that it was possible to view the flame patterns. A purge/cooling stream of air was admitted to the transition section immediately upstream of the window. Quench water was added to the gases immediately upstream of the remotely actuated, butterfly-type backpressure valve. Larger amounts of quench water were added downstream of the backpressure valve for sound suppression purposes.

Facility Services

Compressed air was supplied to the test apparatus by two multi-stage reciprocating compressors. The moisture content of the air supplied by this system is regulated by staged drying to a dew point below 222K such that the humidity effects in the current program were negligible. During testing, the air flowrate to the test section was held constant (at flowrates up to 1.2 kg/sec) by a regulating control valve which established a fixed pressure upstream of a calibrated venturi. The air was preheated to temperatures up to 800K by means of an electrical resistance heater which was manually controlled. Secondary air at pressures up to 27 atm was delivered to the test cell where

the flow was split into both unregulated and regulated supplies. Separately regulated supplies were used to provide combustor cooling air and flameholder cooling air. Unregulated supplies were used to provide purge air to the viewing window port and a trickle stream to the cavities in the mixer/vaporizer section where the photo-cell detectors were located.

Jet-A fuel was supplied to the test cell from underground storage tanks by positive displacement pumps generating pressures up to 100 atm. For those tests in which pilot fuel was required in addition to main fuel, two separately-regulated fuel supply systems were employed. For those tests in which vaporized Jet-A fuel was required, a 64-Kw DC resistance-type fuel heater was employed to heat the fuel at supercritical pressure (27.2 atm) to temperatures of 700K. Vaporization was accomplished by flashing the fuel across an orifice. The fuel heating system was automatically controlled, and was provided with high pressure nitrogen purge flow such that fuel could be removed from the heater during cooldown thereby preventing pyrolysis of the fuel from fouling the heater lines. A schematic diagram of the fuel supply system is given in Fig. 45.

Hydrogen and oxygen were distributed to the torch igniter from high pressure storage bottles by means of remotely actuated solenoid valves. An automatic sequencing device caused the reactants to flow into the torch body, caused high voltage electrical power to be supplied to a sparkplug, and terminated the flow of reactants after a specified time interval (3-5 sec).

All the controls and instrumentation required to operate the test apparatus and monitor its performance were contained in a separate control room adjacent to the cell. Conventional pressure and temperature instrumentation readouts were provided. A window between the control room and test cell permitted observation of the test cell and test rig during operation. A television monitor permitted observation of the internal condition of the test apparatus; remote operation of the aperture, focus, and zoom was available. A system of interlocks was provided such that the test could be terminated promptly in the event of abnormal operation. Detection of high temperatures or the presence of light in the mixer/vaporizer section caused shutoff of the main fuel supply and pilot fuel supply by means of fast-acting solenoid valves in the fuel supply lines. A pressure sensor in the pilot fuel supply lines caused shutdown of the electrical power to the fuel vaporizer in the event of the loss of fuel supply pressure. The output of turbine flow meters located in the probe cooling lines and quench water cooling lines was displayed on digital voltmeters in a control room; manual shutdown procedures were employed in the event of coolant loss.

A low-speed, 25-channel data acquisition system designed to accept high-level and low-level analog signals and to convert these signals to digital forms

suitable for subsequent computer processing was used in this study. All test data were recorded upon magnetic tape and subsequently processed on a UNIVAC 1110 digital computer. A complete tabulation of the flow rates, temperature, and emission analyzer signals recorded by the data acquisition system is presented in Appendix II.

Instrumentation

The test section airflow was measured by use of an ASME standard long radius venturi located upstream of the main air heater (Fig. 37). A single venturi having a throat diameter of 2.54 cm was used for all tests. Air flows were calculated from the measured pressure upstream of the orifice, the measured temperature, and the known discharge coefficient of the venturi.

Fuel flows were measured by turbine flowmeters, calibrated prior to the initiation of the test program by time and weight methods using Jet-A fuel. Flowmeter speed was measured by an electromagnetic pickup, which produced an electronic signal with a frequency proportional to meter speed.

Temperatures were measured with metal-sheathed chromel-alumel thermocouples. For measuring gas temperatures, the sheath diameter was 3.2 mm and the sheaths were sealed over the thermocouple junctions for protection. For measuring structure temperatures, 1.6-mm diameter sheaths were employed; the sheaths were stripped back for a short distance and the thermocouple wires welded directly to the metal surface. Thermocouple signals were processed by a temperature scanner before being transmitted to the data acquisition system. The combustor entrance temperature was obtained from the average of the output of four thermocouples inserted into the airstream at the forward instrumentation system (Fig. 39). These thermocouples were located in the center of four equal area segments, each thermocouple being located at a different circumferential location.

Gas stream pressures were measured by electrical transducers connected to the test apparatus through scanning valves. The stagnation pressure probe profile approaching the fuel injector was measured by an impact tube rake locate in the forward instrumentation section (Fig. 39). The static pressure at the flameholder entrance was determined by static pressure taps located on the upper and lower surfaces of the mixer/vaporizer section approximately 6.35 cm upstream of the leading edge of the flameholder. The static pressure downstream of the flameholder was measured by a tap located in the torch igniter tube housing (Fig. 42). The stagnation pressure at the combustor exit was measured by use of the emission probe rake described below. Stagnation pressure measurements were obtained by closing the solenoid valves which controlled the sample flow and recording the pressure in the sample line immediately upstream of the solenoid valves.

Combustor exit gas composition was determined from a six-probe gas sampling rake installed in the downstream instrumentation section (Fig. 44). The six probes were located at the center of equal area segments at three circumferential locations. The probe entrance sections (Fig. 46) were designed to provide a combination of aerodynamic and thermodynamic quenching in order to freeze the chemical reaction, in particular, the CO oxidation reactions. Calculations of the heat transfer and friction losses within the supersonic flow portion of the probe indicated that the stagnation temperature would be reduced by approximately 600K in a 6-cm-long water cooled passage. At the same time, the stagnation pressure would decrease from 10 atm to 2 atm. At that point the flow could be shocked to subsonic conditions and the resulting static temperature would be sufficiently low to prevent significant CO oxidation. A notable feature of the probe design was the inclusion of a shock stabilization step which was required because boundary layer buildup in the constant area passage would otherwise force the shock to the exit of the supersonic nozzle. This would diminish the effectiveness of the aerodynamic quench.

Gas samples were routed through heated lines to an array of solenoid valves by means of which the samples could either be combined or extracted individually (Fig. 47). The pressure in the sample lines was controlled by use of a regulator and vent. The gas sample was transferred from the probe to the analytical instruments through a 0.63-cm ID stainless steel, teflon-coated line maintained at an average temperature of 450K. The sample line length is approximately 25 meters; the sample temperature was monitored at several axial locations.

The emissions sampling and analysis system is shown schematically in Fig. 48. This system is capable of continuous monitoring of emissions of carbon monoxide, oxygen, carbon dioxide, unburned hydrocarbons, and oxides of nitrogen. The signal output and attenuator position are automatically transferred to the data acquisition system for on-line recording of emission concentrations. A listing of the instrument types including ranges in accuracies is given in Table 8.

Smoke samples were collected by a single probe (Fig. 49a) located in the center of the combustor exit instrumentation section. The samples were transferred to a smoke measurement system, designed and fabricated to sample smoke according to the specifications in SAE ARP 1179. Electric timer-controlled, solenoid-actuated stainless steel gate valves permitted precise control and repeatability of sample volume through the filter paper which serves to record smoke levels. A Photovolt Model 610 reflectance meter was used for smoke filter paper reflectance measurements. A computer routine was used to compute a least squares fit of the measured reflectance values and to calculate the SAE smoke number. Calibration of the Photovolt reflectance meter was accomplished through the use of Hunter Laboratory reflectance placques.

An existing phase-discriminating probe (Fig. 49b) was used to measure the extent of vaporization of fuel at the combustor entrance station. The probe housing was installed immediately downstream of the flameholder such that the probe extended through the slotted baseline perforated plate (Fig. 25b). A schematic diagram showing the construction of the tip of the probe is given in Fig. 50a. The central passage acts as a conventional gas sampling probe and collects the total (liquid plus vapor) sample. Isokinetic flow was established within this passage by adjusting the flow rate so that the static pressure close to the probe tip is equal to the combustor static pressure. A tube oriented perpendicular to the axis of the total-sample tube is used to extract the vapor sample. A suction tube surrounding the vapor tube is used to purge any liquid which collects on the surface of the total-sample tube and which otherwise would spill over into the vapor sample tube and contaminate the vapor sample. Water jackets surround the sampling tubes so that the collected samples can be quickly cooled in order to prevent ignition of the fuel-air mixture. Provisions for introducing a flow of quench nitrogen into the sample tube were not employed in this program. Water cooling was required to ensure structural integrity of the probe since the tests were conducted with combustion occurring downstream of the flameholder.

The concentration of the fuel in the sample withdrawn by the probe was obtained from on-line determinations of the hydrocarbon content using a flame ionization detector. A schematic diagram of the sampling system is shown in Fig. 50b. The sample flows from the probe through electrically-heated stainless steel lines, through glass wool particulate filters to the gas analysis equipment. The bellows pumps shown in the figure were bypassed in this experiment because sufficient pressure differential existed to drive the flow through the analyzer. Because the flow rate in the total sample line required to ensure isokinetic sampling conditions is greater than the flow capacity of the analyzer, a throttleable bypass line is connected to the total sample line. The vapor and total samples pass to the ionization gauge via a ten-port sampling valve which permits uninterrupted flow of a carrier gas (argon) and gas samples through the ionization gauge. The valves and transfer lines are contained in an oven equipped with temperature limit switches which permits operation at the elevated temperatures required to prevent sample condensation. The sampling valve employed in this system was designed to extract a small discrete sample from either of the transfer lines and to dilute those samples with the carrier gas prior to delivery to the ionization gauge. The concentration of the sample reaching the ionization gauge is determined by the length and size of the loops on the sampling valve and the length of the line between the sampling valve and the ionization gauge.

A Gomac ionization gauge and signal conditioner (electrometer) were used to obtain measurements of the hydrocarbon concentration in the gas samples.

The probe traversing mechanism, flow control valves and sampling valves were operated remotely, and the signal from the ionization gauge was recorded by a strip chart recorder. The recorder displays the hydrocarbon concentration as a function of time and also integrates the concentration with respect to time. The system is capable of analyzing a gas sample every 30 seconds.

The flame ionization detector output is related to the number of carbon atoms released by the breaking of carbon-hydrogen bonds as the gas sample passes through the detector. By operating the analyzer at fixed temperature and pressure (400 K, 1 atm), the output can be interpreted as being proportional to the mole fraction of unburned hydrocarbons in the flame. The gas analysis system was calibrated by passing gases of known composition through the analyzer and comparing the percent carbon output to the known values. Various concentrations of methane, ethane, propane and butane were used in the calibration procedure, and the calibration of the ionization gauge was carried out over five orders of magnitude from 100 ppm to 100 percent butane.

EXPERIMENTAL PROCEDURES

Test Methods

Prior to initiation of each test sequence, standard procedures for calibrating the data acquisition system amplifiers were conducted. All emission analysis equipment including analyzers and transfer line heating tapes were operated for a minimum of two hours prior to testing in order to permit temperature levels to equilibrate. Emission analyzer zero and gain levels were set by introducing appropriate calibration gases to each instrument. Immediately prior to testing, cooling water and cooling air supplies were activated and coolant flow verified by monitoring flowmeter and pressure transducer output displays.

Testing was initiated by establishing the combustor airflow rate which would provide the required combustor reference velocity (25 m/s) when the desired entrance temperature was achieved. The main air heater was activated and the air temperature brought to a level where ignition could be achieved at a relatively low fuel flowrate. Ignition at low fuel flow levels was desired in order to minimize the magnitude of the pressure pulse created at the moment of ignition. An air temperature of 730K was used at ignition in most of the tests. Full flameholder coolant was established for the cooled flameholder designs and the back pressure valve was used to bring the combustor pressure to 6.5 atm. The fuel controller was preset to a selected value (corresponding roughly to equivalence ratio of 0.4); main fuel flow was initiated and allowed to equilibrate (approximately three seconds were required) and the torch igniter sequencer activated. Ignition was confirmed by the television monitor image; the back pressure valve was adjusted to bring the static pressure in the mixer/vaporizer section to 10 atm, and fuel flow and temperature levels desired for the first test point were established.

For the piloted V-gutter configurations, the pilot fuel was introduced after the design point test condition ($T_o = 600K$, $\phi = 0.6$) had been established. For the piloted perforated plate flameholder (PF-4), ignition was accomplished with pilot fuel only flowing, then main fuel was brought on.

The matrix of test conditions for which emission and smoke data were recorded for each of the sixteen flameholders is given in Table 9. In general, the test sequence employed was to first determine the cold flow pressure loss by stagnating the flow in the emission probes, then to acquire the emission distribution data at the design point test condition, and then to acquire the emission and smoke data at the designated equivalence ratios for each entrance temperature. Fuel flow was initially established at the $\phi = 0.6$ level and

then lowered in the desired increments until blowout was reached. Repetitive data recordings were obtained as indicated in Table 9. For those flameholders which were air cooled (SPPRP-1 to -3 and CTF-1 to -F), the coolant flowrates were reduced as equivalence ratio was reduced. The appearance of the flameholder surface radiation as displayed on the television monitor and the output of flameholder thermocouples dictated the level of coolant flow required.

Blowout fuel flows were determined in the following manner. The approach to blowout was signaled both by jitter of the Heise gauge combustor pressure readout and by a change in character of the flame image observed on the television monitor. In general, as blowout was approached, there was a diminishment of the resolution of the television image. When approach to blowout was detected, the fuel flow was slowly reduced and the back pressure valve position was adjusted to bring the combustor pressure back to the nominal value of 10 atm. The combustion efficiency degraded rapidly as blowout was approached and thus it was necessary to repeat this process of pressure readjustment several times before blowout was experienced. As indicated above, air coolant flow rates were decreased as fuel flow was decreased. For all air-cooled flameholders, the coolant flow was completely shut off at blowout except at the $T_o = 800$ case where it was necessary to bleed a small amount of flow into the cooling passages. Also, as blowout was approached, purge air was introduced into the emission and smoke sample lines to eliminate the possibility of large quantities of unburned fuel entering the probes subsequent to blowout. The actual occurrence of blowout was unmistakable because of the dramatic change in the television display, the sudden drop in combustor pressure, and the change in sound level generated by the combustion process. When blowout occurred, the fuel turbine meter output was recorded by hand, fuel flow was shut off, and the fuel lines purged.

As a rule, the zero and gain settings on the gas analysis equipment were recalibrated at the beginning of each test sequence, i.e., when entrance air temperature was changed. Also, images of the flame pattern at each condition were recorded on video tape.

At the outset of the experimental program, two special tests were performed to document the degree of fuel-air ratio uniformity and the degree of vaporization of the fuel which existed at the flameholder entrance station. Both tests were conducted at the design point test conditions. To perform the profile uniformity tests, a water-cooled spool piece was fabricated which would permit the emission probe rake to be mounted such that the probe tip station corresponded to the mixer/vaporizer exit station. The hydrocarbon analyzer was calibrated with high hydrocarbon content gases and the fuel-air ratio of the samples collected by each probe were calculated from the mixture composition.

Tests to determine the percentage of the fuel which existed in the vapor state at the flameholder station were conducted using the previously described phase-discriminating probe mounted such that the probe tip extended approximately one centimeter upstream of the forward face of the slotted baseline flameholder. The test procedure followed was to establish the design point test conditions within the test apparatus while flowing purge air through the phase-discriminating probe system. The flame ionization detector calibration was checked during this time by flowing calibration gases containing 0.1 percent methane and 4 percent methane gas mixtures through the detector. Purge gas flow and calibration gas flow were then shut off and isokinetic conditions were established for the total (liquid plus vapor) sample using a remotely operated throttling valve. Likewise, appropriate flow rates of the vapor sample and suction sample were established. The sampling valve was then actuated thereby delivering a discrete sample of either the total or the vapor sample to the ionization gauge. Approximately 30 to 60 sec were required for the samples (which were diluted by an argon carrier gas) to pass through the ionization gage. The output signal was integrated as a function of time to obtain an average value of the mole percentage of unburned hydrocarbons (taken as CH_x) in the sample. This process was repeated, alternating between total and vapor samples, until a noticeable rise in the peak magnitude of the detector output trace was noted. This rise in the magnitude of the hydrocarbons being detected by the analyzer was taken to be indicative of accumulations of sample in the water-cooled probe. The cooling capacity of the probe proved to be excessive for this application and prolonged use of the sampling system without purging the lines with nitrogen resulted in signals of doubtful validity.

Data Reduction Procedure

Data reduction was accomplished by use of two computer programs. The first program used the data stored on magnetic tape by the data acquisition system and the hand-recorded emission analyzer output to provide detailed output giving values of measured parameters (listed in Appendix II) and reduced data (emission index, combustion efficiency, pressure loss, etc.) for each test point. The reduced data was stored in computer mass storage in addition to being output by the printer. The second program permitted editing of the data output by the first program (e.g., to eliminate data generated by faulty instruments), received the hand-recorded blowout turbine meter readings, sorted the data and ordered the data, and computed average values of performance values by numerically averaging all data for specified runs obtained at the same entrance temperature and equivalence ratio levels. Report quality data tables were generated which provided detailed performance for each test configuration - these data tables are published in the Comprehensive Data Report.

The method of calculating the reported test conditions, emission levels, and performance levels are discussed below.

Test ConditionsEntrance temperature, T_o

The entrance temperature is the arithmetic average of the temperature measured by the four thermocouples located upstream of the fuel injector.

Combustor pressure, P_{so}

The combustor pressure is the arithmetic average of the two static pressure located on the upper and lower surfaces of the mixer/vaporizer.

Airflow rate, w_a

The airflow rate was determined from the equation for choked flow through a venturi

$$w_a = \frac{0.532}{2.205} \frac{\pi d^2}{4} \times 0.985 \times \frac{P}{\sqrt{T}} \quad (13)$$

where p and T are measured upstream of the venturi.

Fuel flowrate, w_f

The fuel flow rates (main and pilot) were determined from the turbine meter frequencies:

$$w_f = \rho_f \times \frac{\text{cps}}{K} \quad (14)$$

where K is the calibration constant of the flowmeter.

Fuel-air_ratio, f/a

$$(f/a)_i = \frac{w_{fi}}{w_a} \quad (15)$$

where i denotes main, pilot and total fuels.

Equivalence ratio

$$\phi_i = \frac{(f/a)_i}{0.068} \quad (16)$$

where i denotes main, pilot and total fuels.

Reference velocity, V_{ref}

$$V_{ref} = \frac{w_a (1 + f/a) \times T_{so} \times R}{P_{so} \times M_{mix} \times A_c} \quad (17)$$

where the mixture molecular weight is:

$$M_{mix} = \frac{28.962 (1 + f/a)}{1 + f/a \times \frac{28.962}{165}} \quad (18)$$

where f/a is the mainstream fuel-air ratio.

Emission levels

The concentration of NO_x , CO, UHC, CO_2 and O_2 were determined from the meter readings and the instrument calibration curves. The emission index for each gas was determined from:

$$EI_i = \frac{\text{PPM}_i}{M_{wp} \times 1000.0} \frac{1 + f/a}{f/a} M_{wi} \quad (19)$$

where f/a is the total (pilot plus main) fuel-air ratio

Performance levelsCombustion efficiency, η_c

The reported combustion efficiency is derived from the CO and UHC emission levels. For 100 percent efficiency, the CO emission level would be the equilibrium level and the UHC level would be zero. Assigning appropriate heating values to these constituents (assuming UHC can be represented by CH_4) the value of efficiency can be calculated as:

$$\eta_c = 100 \times \left[1.0 - \frac{1}{18.6 \times 10^3} (4.3 (EI_{co} - EI_{co, eq}) - 21.6 EI_{UHC}) \right] \quad (20)$$

Pressure loss

Both cold-flow and hot-flow stagnation pressure losses were reported. The entrance stagnation pressure was derived from the combustor entrance pressure and dynamic head:

$$q = \rho V_{ref}^2 \quad (21)$$

$$P_{T0} = P_{S0} + q \quad (22)$$

The cold flow loss was determined from the exit stagnation pressure which was taken as the average of the six emission sampling probe pressures with zero sample flow:

$$\left(\frac{\Delta P_T}{P_T} \right)_{cold} = \frac{1 - \frac{1}{6} \sum_{n=1}^6 P_n}{P_{T0}} \quad (23)$$

The hot flow loss was based on a calculated stagnation pressure determined from the measurement of static pressure downstream of the flameholder, P_{exit} , and a calculated dynamic head:

$$q_{exit} = \frac{1}{2g} \frac{w_0^2 (1 + f/a)^2 R T_{act}}{A_c M_w \text{mix} P_{exit}} \quad (24)$$

where T_{act} is the actual product temperature calculated in a manner described below:

$$P_{T,exit} = P_{S,exit} + q_{exit} \quad (25)$$

$$\left(\frac{\Delta P_T}{P_T} \right)_{hot} = 1 - \frac{P_{T,exit}}{P_{T0}} \quad (26)$$

Injector pressure drop

The pressure drop across the injector was the average of the four impact pressures measured at the upstream instrumentation section less the calculated mixer/vaporizer stagnation pressure

$$\Delta P_{\text{inj}} = 1/4 \sum_{i=1}^4 P_i - P_{T_0} \quad (27)$$

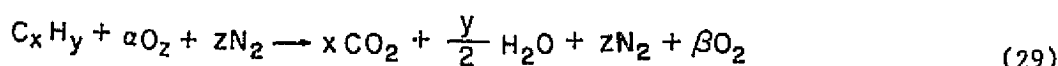
Combustion Gas Temperature, T_{act}

The combustor exit temperature is calculated from the adiabatic flame temperature and combustion efficiency.

$$T_{\text{act}} = T_0 + \eta_c (T_{ad} - T_0) \quad (28)$$

Fuel-air Ratio - Emission, f/a -EM

The fuel-air ratio is calculated from the exhaust gas composition by the Spindt method (Ref. 11). In this procedure, the combustion reaction is represented as:



Spindt has shown that the air to fuel ratio is determined by the expression:

$$(f/a)^{-1} = F_b \left[11.492 F_c \times \frac{1 + R/2 + Q}{1 + R} + \frac{120(1 - F_c)}{3.5 + R} \right] \quad (30)$$

where

$$F_b \equiv \frac{PPM_{CO} + PPM_{CO_2}}{PPM_{CO} + PPM_{CO_2} + PPM_{CH}} \quad (30a)$$

$$F_c \equiv \frac{12.011}{12.011 + 1.008(y/x)} \quad (30b)$$

$$R \equiv \frac{PPM_{CO}}{PPM_{CO_2}} \quad (30c)$$

$$Q \equiv \frac{PPM_{O_2}}{PPM_{CO_2}} \quad (30d)$$

and

$$P_{CH} = \frac{PPM_{UHC}}{1 - \frac{9.008 \times y}{M_w, p}} \quad (30e)$$

where the product molecular weight, M_w_p , is calculated from Eq. 29 and the known mixture ratio. The method thus uses the output of the O_2 , CO_2 , CO, and UHC gas analyzers, however, the major influence of composition on fuel-air ratio is due to the O_2 and CO_2 content.

In a few tests the output of the CO_2 analyzer was erratic; for these tests it was assumed that the CO_2 concentration was a function of the O_2 concentration and thus the reported fuel-air ratio determined from composition was primarily dependent on the measured oxygen levels in those tests. The equilibrium ratio of CO_2 to oxygen concentration as a function of entrance temperature and nominal (metered) fuel-air ratio was used to determine CO_2 levels to be employed in the Spindt procedure in tests where CO_2 analyzer output was questionable.

TEST RESULTS

Results of the fuel preparation section tests and concept tests are described below. A detailed tabulation of the test data is presented in the Comprehensive Data Report.

Fuel Preparation Section Tests

Tests to determine the fuel air profile uniformity and the degree of vaporization of the fuel at the exit of the mixer/vaporizer were conducted. The fuel profile uniformity goals were to achieve a fuel-air profile at the design point wherein the value of fuel-air ratio computed using the gas analyzer outputs for each probe was within ± 10 percent of the average for the profile, and to establish that the mean of the computed fuel-air ratios was within 15 percent of the fuel-air ratio determined from metered air and fuel flows. The vaporization goal was to achieve a mixture in which 90 percent of the fuel was in the vapor state at the exit of the mixer/vaporizer.

Fuel-Air Profile Uniformity

The uniformity of the fuel profile at the combustor entrance was determined by installing the six-point emission probe at an axial station four centimeters downstream of the baseline perforated plate flameholder. The combustor was operated at the design point test conditions ($T_o = 600$ K, $\phi = 0.6$). Samples were collected through each of the six probes and the gas compositions were used to compute the input fuel-air ratio. Results of these tests are shown in Fig. 51. The data points represented by the solid circular symbols correspond to data obtained with the individual probes; the triangular data points indicate measurements obtained with samples flowing through all of the probes simultaneously. In general, the derived fuel-air ratio lies above the fuel-air ratio determined from the metered values of fuel flow and air flow. Also, significant scatter exists in the data. Both of these effects are attributed to the extremely high unburned hydrocarbon content of the combustion products existing at this axial station (the mole fraction of total unburned hydrocarbons taken as CH_x was approximately 3 percent) and the insensitivity of the flame ionization detector at these high unburned hydrocarbon concentrations. The mean fuel-air ratio obtained from the individual probe measurements (with the exception of single spurious data point for Probe No. 6) was determined to be 0.045; the metered fuel air ratio was 0.040. The derived fuel air ratio profile, determined from the average of the two data points obtained for each probe is shown by the dashed line. The profile is seen to be fairly uniform with the exception of a fall off in fuel-air ratio at the combustor wall. Further evidence that the fuel-air profile is indeed close to being uniform was obtained

in subsequent tests conducted with the probe in the downstream location. These test results are presented in the Discussion of Results section.

Extent of Vaporization

Results of two surveys performed with the phase-discriminating probe are shown in Figs. 52 and 53. Shown in the figures are the magnitudes of the mole percent carbon in the total and vapor samples obtained for a series of tests. The average value of the percent vaporized noted in the figures was obtained by dividing the percent carbon observed for the vapor sample by the percent carbon in the succeeding total sample and averaging the resulting ratios. Also shown in the figures are the values of the percent of carbon based on the average of the levels measured in the total samples and the value based on the metered fuel flow rate and air flow rate. The results of these tests indicated that more than 90 percent of the fuel was vaporized at the flame stabilizer station at the baseline test condition.

Concept Tests

A brief description of the results of the tests conducted for each flameholder configuration is presented below. Data plots for selected configurations are presented; data plots for all configurations are included in the Comprehensive Data Report.

Baseline Design

Initial experience in operating the test apparatus was gained with the use of the baseline perforated plate flameholder. Entrance temperature and fuel flow were varied to determine the combustor operating characteristics and it was found that high frequency combustion instabilities existed at many conditions. The apparatus was instrumented with close-coupled pressure transducers and it was determined that the frequencies observed were in the 2000-5000 Hz range. Also, it was observed that low frequency aperiodic pressure oscillation occurred and that blow-off equivalence ratios were quite high (e.g., $\phi = 54$ at $T_o = 600K$). It was suspected that the source of pressure oscillation was the back pressure valve onto which cooling water was sprayed. This valve system was replaced with a fixed orifice and air injection system (aerodynamic choke); however, the problem was not alleviated. Operation of the apparatus at the high inlet temperature condition ($T_o = 800K$) proved significantly smoother. Examination of the television recordings of the flame pattern indicated that significant differences existed between the rough and smooth-running conditions. It was then determined that under rough-running conditions flame was being stabilized on a 2.5-cm step which existed downstream of the combustor at the junction of the diffuser and transition section (see Fig. 37). Purge air was introduced into the step region and the ignition procedure previously described (high air temperature and low

temperature and low fuel flow) was instituted and the combustor was found to operate smoothly (no evidence of low frequency pressure oscillations). The intensity and frequency of occurrence of screech was greatly diminished, however however, the combustor continued to screech under certain conditions. Flameholder overtemperature occurred frequently during high intensity screech, but was not observed subsequent to the installation of the purge air system.

Examination of the test apparatus after approximately 120 minutes of operation indicated no major hardware problems. The combustor liner indicated no evidence of degradation due to high combustion gas temperatures. Some bowing of the perforated plate flameholder occurred during testing. Also, there was evidence of crack development at a single location on the flameholder periphery adjacent to a keyway which was used to prevent flameholder rotation.

The fuel injector manifold pressure and fuel flow turbine meter output were displayed on Visicorder output during tests conducted to determine the source of the combustion instabilities. Both pressure and flow rate were found to be highly stable. Flashback of the flame into the mixer/vaporizer occurred only once during testing - shutdown initiated by flameholder thermocouples followed immediately. Visual inspection of the spikes which form the downstream contour of the fuel injector indicated no deterioration. The results of this test series indicated that the test apparatus and the instrumentation performed satisfactorily.

The emission and performance data obtained for the baseline flameholder is presented in Figs. 54 through 57. Plots of the emission index for NO_x, CO, and UHC as a function of equivalence ratio for entrance temperatures of 600, 700, and 800K are presented. Also, a plot showing combustor performance, including radial fuel-air ratio distribution, stagnation pressure loss, and combustion efficiency is presented (Fig. 57).

The blowout limits measured for the baseline design are presented in Fig. 58. In general, the blowout fuel-air ratio was found to be very repeatable. The average values of blowout fuel-air ratio at each entrance temperature are presented in Table 10 along with data acquired for other designs.

Self-Piloting Perforated Plate Series

The blowout limit tests of the five flameholders in this series indicated that there was no significant change in stability limits from those levels obtained in the baseline design (Fig. 59). Also, for all designs, there were no dramatic differences in the emissions determined for this series in comparison with the baseline series. The best performing design in this test series was the final design; emission and performance data acquired are presented in Figs. 60 through 64.

The screech problems encountered during tests of these flameholders was not severe. Screech was encountered for less than 20 percent of the test conditions and the intensity, as judged from the sound levels, was low. Flashback or autoignition was encountered when testing SPRPP-1 at the $T_o = 800K$, $\phi = 0.6$ condition. Thermocouples mounted on the forward face of the flameholder were removed and flashback was not encountered during testing of the -2 and -3 configurations. During testing of SPPRP-2, the television monitor indicated very high radiation from the rear face of the flameholder in the region close to the cooling passage outlet; testing at conditions hotter than $T_o = 800$, $\phi = 0.5$ were not conducted. Inspection of the flameholder indicated no damage had occurred. Testing of SPRPP-3 was conducted over the complete test matrix with no damage occurring.

SPRPP-4 was an uncooled design which was equipped with thermocouples attached to the upstream face; flashback or autoignition occurred at $T_o = 800K$ when the equivalence ratio was increased above $\phi = 0.55$. The final configuration was an uncooled flameholder which was designed to run hotter than the -4 uncooled flameholder. As the equivalence ratio was increased to above 0.5 at the $T_o = 800K$ condition, the video monitor indicated the occurrence of excessive radiation and, indeed, melting of the rear face had taken place (Fig. 65).

Catalyzed Tube Flameholder Series

No improvement in lean stability limit was achieved for any of the catalyzed tube configurations (Fig. 66). The behavior of the catalyzed tube flameholder configurations was expected to be dependent on the temperature of the catalyzed surfaces and, therefore, temperatures of the base of the flameholder and of a number of the tubes were monitored. The operating procedure employed in the tests was to reduce the flow of cooling air at each condition until the maximum surface temperature being monitored reached a value of 920K. For the 600 and 700K entrance temperature cases, all coolant flow was shut off at conditions approaching blowout. For the 800K case, approximately 30 percent of the coolant flow capacity was required to maintain the surface temperatures at the limit. In all cases, the highest temperature recorded was the temperature of the flameholder base (rear face). In general, at blowout the tube temperatures were somewhat lower than the entrance gas temperature for the 600K and 700K cases and slightly higher than the entrance temperature for the 800K case. It was believed that a surface temperature of at least 800K would be required before significant catalytic activity could be achieved. It was expected that surface temperatures higher than the entrance temperature could be achieved by first operating the flameholder at a high entrance temperature and then, upon initiation of reaction, lowering the entrance temperature to the desired level. However, the experimentally observed behavior was that the tube temperatures

closely followed the entrance temperature as the entrance temperature was decreased. The only positive indication that reaction was occurring on catalyzed surfaces occurred at the 800K case for values of equivalence ratio greater than 0.5. In these cases, when coolant flow was reduced, tube temperatures increased slowly at first, then abruptly increased at a rate of several hundred degrees per second necessitating shutdown of the fuel flow. Efforts to stabilize the tube temperatures at a high level as equivalence ratio was reduced were unsuccessful - the tube temperatures either plunged to the entrance gas temperature or increased at an excessive rate as described above.

In the fourth configuration tested, nitrogen was heated to 800K and circulated through the coolant system in an effort to raise the temperature of the catalyzed tube surfaces when approaching blowout. The tube temperatures were increased by approximately 80 deg K. No significant improvement in the behavior of the combustor was noted.

The final configuration of the catalyzed tube flameholder series employed four tubes having a restriction near the tube entrance which would act to reduce the flow of reactants through the tube thereby increasing the residence time and decreasing the rate of transfer of energy from the reacting boundary layer to the cooled tube surface. Measurements of the surface temperature of the tubes indicated that reaction did occur within the tubes at all equivalence ratios tested. Tube temperatures could be controlled by regulating the amount of cooling air, and runaway tube temperature conditions were not encountered in these tests. Although reaction apparently occurred within the catalyzed tubes as expected, the performance and stability limits measured showed no improvement.

Two other features of the operation of the catalyzed tube flameholder configurations are noteworthy. When the runaway tube temperature condition was encountered, the television image of the flameholder base as viewed through the downstream observation port changed character dramatically. Prior to runaway, the tubes appeared as dark circles on a moderately bright background. Surrounding each dark circle was an annular region having a brightness greater than that of the background. When runaway occurred, the dark circles immediately exhibited a brightness equal to that of the annular region. It is possible that the runaway tube temperatures were a result of flame propagating to the tube entrance. It was also noted that high frequency pressure oscillations (screech) occurred much more frequently with the use of the catalyzed tube configurations than with other flameholders.

Piloted Flameholder Series

In tests of the piloted flameholders, the pilot fuel flow rate was set equal to approximately 4 percent of the total fuel flow rate at the design point condition. The pilot flow rate was not varied, except in tests of Configuration PF-4.

Blowout was not observed in any of the tests conducted with the five flameholders included in this series. Performance levels were very low at the lowest equivalence ratios tested ($\phi = 0.25$), however, there was no evidence that blowout would occur at even lower main fuel flow levels. For the low blockage flameholders tested (PF-1, -2, and -3) the emission and performance levels recorded were typical of those presented in Figs. 67 through 71. In the PF-1 configuration in which vaporized Jet A pilot fuel was injected at a temperature of 700K in the axial direction through twelve injection sites, large amounts of carbonaceous material were formed on the downstream face of the flameholder. In tests of the PF-2 configuration in which the pilot flow was injected with a large tangential velocity component, post-test examination of the flameholder base indica indicated no carbonaceous deposits existed. Television images indicated that less luminous combustion occurred in the flameholder region as a result of the improved mixing of pilot fuel and the recirculation zone gases.

Configuration PF-3 employed axial injection of gaseous pilot fuel into the V-gutter base, but the number of injection sites was increased to 36 compared with the 12 sites used in PF-1. Carbon accumulation up was again much less than that observed for PF-1. No flashback problems were encountered despite the fact that a very low pressure drop existed across the distribution holes which separated the downstream fuel plenum from the recirculation zone gases.

High performance as well as a wide stability limit range was achieved with the piloted perforated plate flameholder (PF-4). Emission and performance data are presented in Figs. 72 through 76. In these tests, water-cooling was employed rather than air-cooling in order to guard against overheating of the perforated plate due to the high gas temperatures generated by the pilot flow. Nevertheless, during testing at the $T_o = 800K$, $\phi = 0.5$ test condition, the flameholder became highly luminous necessitating termination of the test. Inspection of the flameholder showed no significant damage had occurred. Tests were conducted at the design point conditions using air as the coolant to determine if the method of cooling influenced the recorded emission levels. The data (Fig. 77) indicate that water cooling results in somewhat lower NOx and higher UHC and CO than air-cooling. Tests were also conducted to determine the effect of pilot fuel flow rate on emissions. The data (Fig. 78) indicated that, as expected, the NOx level increased with increasing fuel flow. CO levels also increased, whereas UHC remained unchanged.

Tests of the high blockage piloted V-gutter, PF-F, also resulted in higher performance than that obtained with the low blockage V-gutters. This performance level was achieved with a significantly higher pressure loss than that associated with PF-4. The combustion efficiency and pressure loss measurements are shown in Fig. 79. The anticipated screech problems associated with high blockage V-gutters did not materialize; the device operated smoothly and quietly over most of the test matrix.

DISCUSSION OF TEST RESULTS

The most significant finding of the test program is that piloting by injection of fuel into the flameholder base region can provide wide stability limits and high performance over a limited range of test conditions, but that piloting is the only technique of those tested that had any significant influence on blowout. The results also indicated that with the piloting scheme, the wide stability limits could be achieved within the imposed NO_x emission constraints with a reasonable pressure loss. These test results are, of course, influenced by the characteristics of the test apparatus and measurement devices, and therefore, the impact of these characteristics on the results merits discussion.

In this program significant emphasis was placed on achieving fully mixed and fully-vaporized fuel-air mixtures at the combustor entrance station. The question of the impact of fuel profile uniformity and degree of vaporization on flameholder stability limits and NO_x emissions has yet to be thoroughly assessed. It is believed, however, that both non-uniformity and poor vaporization could lead to wider stability limits and higher NO_x levels than the perfectly mixed and vaporized case because of the higher local temperatures which could be generated. In the present program, as previously described, substantial efforts were applied to the design of a fuel injector which would generate a finely-atomized and well-distributed fuel spray. The results of the testing performed at the design condition to measure profile uniformity and degree of vaporization at the mixer/vaporizer exit indicate the profile and vaporization goals were met. A greater amount of data was obtained on fuel-air profile uniformity at the combustor exit; i.e., for each configuration the fuel-air ratio distribution was computed from the gas compositions acquired by the individual probes at the design point conditions. These data (e.g., Figs. 57, 64, 71, 76, 79) indicated high profile uniformity with the exception of the results obtained with PF-1 (Fig. 71). The fuel injector was dismantled and inspected after this test and no evidence of fuel distribution line (hypo tubing) clogging was found. (As indicated previously, erratic behavior of the CO_2 analyzer was believed to be responsible for the poor computed profile uniformity in this case.) The TV monitor flame patterns also indicated a high degree of uniformity was achieved by virtue of the uniform brightness of the flame radiation that was observed in the unpiloted designs. As blowout was approached, the flame intensity decreased uniformly until just prior to blowout. As fuel flow was decreased to a level corresponding to an equivalence ratio approximately 0.02 greater than blowout, some non-uniformity would generally appear, i.e., flame brighter near the center or one side.

The NO_x emission levels also give evidence that profile uniformity and degree of vaporization achieved were satisfactory by virtue of the relatively low NO_x levels measured in the unpiloted designs. Because NO_x level is exponentially dependent on temperature, a non-uniform profile would lead to a locally

very high level which would cause the average level (as collected by the ganged six-probe sampling rake) to be high. As shown in Figs. 54 and 60, the NO_x emission at the design point ($T_o = 600K$, $\phi = 0.6$) condition was substantially lower than the goal (0.4 g/kg vs. 1.0 g/kg). This may be partially attributable to the fact that the combustion efficiencies were not 100 percent (96.5% for the baseline and 99.3 percent for SPRPP-F) at this condition, however, NO_x levels lower than predicted were found even at higher flame temperature conditions where complete combustion occurred. The NO_x data for SPRPP-F plotted as a function of flame temperature is given in Fig. 80. The concentration data for the three different inlet temperatures collapses to a single data band which lies under the mean level predicted by the empirical data presented in Fig. 5. The agreement is quite good when one considers that the scaling law (Eq. 1) was not derived for premixed flames. It can be seen that the NO_x levels lie appreciably above those predicted by the extended Zeldovich kinetic mechanism (Ref. 6) (assuming instantaneous reaction and plug flow); this may be partially attributable to the NO_x produced in the recirculation regions where the residence time would be significantly higher than the two msec nominal combustor residence time.

On the basis of these data on NO_x levels, combustor exit fuel-air profile, flame luminosity observations, and the results of the probing conducted at the mixer/vaporizer exit, it is concluded that the data generated in this study represent the performance and emissions for fully premixed and prevaporized combustion systems.

One of the major instrumentation problems which has to be addressed when gas sampling of the primary zone combustion products is conducted is the method of quenching the reactions which would occur within the probe. Of the constituents being measured in this program, CO is the most difficult to measure accurately because CO oxidation occurs at relatively low temperatures levels. Evidence that the probe design employed (Fig. 46) did in fact cause the CO reactions to be quenched at the probe tip is afforded by the CO emission data plots. In Fig. 81 the CO concentrations measured in Configuration SPRPP-F are plotted as a function of adiabatic flame temperature for the three different inlet temperatures. For the 700 and 800K entrance temperatures at the higher adiabatic flame temperature the data fall along a single band which represents an equilibrium CO level. For the 600K entrance temperature case, equilibrium levels were not reached; i.e., the combustion efficiency was less than 100 percent. For any inlet temperature, as fuel-air ratio was decreased (adiabatic flame temperature decreased) a point was reached where CO levels increased due to incomplete combustion. Thermodynamic calculations were conducted to determine if the measured equilibrium levels corresponded to theoretical levels predicted for combustion at 10 atmospheres. It can be seen that the measured levels lie somewhat above the calculated levels. Calculations were also carried out to determine the theoretical equilibrium levels at the 2 atm pressure level which existed in the probe downstream of the

probe tip; agreement with the measured levels was good. If the CO reactions were not quenched immediately, the measured levels would be less than the theoretical levels; that is, CO would continue to oxidize as the gas sample was cooled until the gas temperature reached a low level where reaction rates become slow relative to gas cooling rates. The conclusion drawn from the data in Fig. 81 is that the CO reactions were quenched by the aerodynamic expansion and that sufficient cooling occurred in the supersonic flow portion of the probe to preclude further reaction when the flow shocked to subsonic conditions.

It was noted in the preceding section that screech occurred frequently during testing. The severity of this combustion instability was dependent on the flameholder type (most severe with catalyzed tube, least severe with V-gutters) and the test conditions - small changes in fuel flow changed screech intensity in an apparently random manner. The screech not only caused physical damage to the test hardware but affected the recorded emission levels. Under certain conditions, large changes in emission levels were observed when screech was particularly intense. An example of this effect is shown for the data point corresponding to $T_o = 700K$, $T_{ad} = 1650K$ in Fig. 81. Also, in the early baseline tests where very intense screech was experienced, thermocouples attached to the forward face of the flameholder indicated flameholder temperatures increased by several hundred degrees (K) when operating in the screech mode.

With respect to combustor performance, it is clear from the data acquired in this program that flameholder blockage (pressure loss) has a major impact on combustion efficiency. A comparison of the inefficiency levels associated with a 75 percent and 80 percent blockage perforated plate (Fig. 82) shows that the design point inefficiency decreased from 7.6 to 0.7 percent when the blockage was increased. Data for the high and low blockage piloted V-gutter flameholders show a decrease from 8.7 to 0.3 percent. In the case of the perforated plates, other characteristics were changed as well as blockage. The high performance configuration had fewer but larger holes and the flameholder structure temperature was higher due to the deeper counterbore. In the case of the V-gutter, the shape of the flow passages was changed from annular to an array of annular segments due to the addition of the blockage plates. The change common to both types was the increase in blockage. The fact that, of the two perforated plate flameholders, the design having fewer holes (larger required flame spreading distances) had the higher performance is worthy of note. The measured NO_x increase associated with the larger webs was minimal (0.41 g/kg for the 37 hole SPRPP-4 design and 0.46 g/kg for the 19 hole SPRPP-F design). It is clear that the expense associated with manufacturing perforated plate flameholders having a large number of small holes is not warranted.

Examination of the blowout data acquired for the unpiloted designs shows that, as in the case of conventional bluff body flameholders, increasing the

inlet temperature causes blowout to occur at equivalence ratios corresponding to lower adiabatic flame temperature (Fig. 83). Blowout is not associated with a fixed level of adiabatic flame temperatures for all entrance temperatures. Comparison of the blowout equivalence ratio levels with levels predicted on the basis of a DeZubay-type blowout correlation generated at United Technologies using data available in the literature shows that the levels are of the predicted magnitude, but that the increase in lean limit with stability parameter value is much steeper than predicted (Fig. 85). Also, in view of the fact that the SPRPP-F design had a larger hole diameter and higher loss coefficient than the baseline design yet had the same blowout limits, it must be concluded that the applicability of this type of correlation to perforated plates should be re-examined.

The principal goal of this program was to achieve a flameholder/combustor design providing wide stability limits while meeting stringent NO_x emission limits. Clearly, only the piloted designs achieved wide stability limits; in fact, it is surprising that none of the other designs produced any significant improvement. Of the five piloted schemes, two produced relatively high efficiencies in addition to wide stability limits - Configurations PF-4 (the piloted perforated plate) and PF-F (the high blockage piloted V-gutter). Of these two designs, PF-4 exhibited lower cold flow losses (2.6% vs. 5.2% for PF-F). In addition, the NO_x levels generated by PF-4 were comparable with those generated in PF-F and the concept does not require the use of a fuel vaporizer. For these reasons, Concept PF-4, is selected as the most promising concept to be used in future LPP engine designs. The tests conducted in this program indicate that by injection of an amount of pilot fuel corresponding to four percent of the cruise fuel flow, the cruise NO_x goal of 1.0g/kg can be met (Fig. 72) while at the same time high combustion efficiencies can be achieved (Fig. 76). The current test effort was conducted with the pilot fuel flow held constant at the four percent level (except for a series of test conducted at the design conditions). In an actual application, the fuel flow could be modulated such that even lower NO_x levels could be achieved. The data acquired when pilot flow was varied (Fig. 78) indicate that NO_x levels can be predicted (the dashed line) by assuming that the overall emission index is the weighted sum of the index for an unpiloted design (0.33 g/kg is the average of the EI's determined for the SPRPP series at the design conditions) and the index for conventional diffusion flames (12.6 g/kg at the design conditions). This being the case, the overall NO_x goal of 3.0 g/kg could possibly be met by reducing the pilot flow at the higher temperature conditions where piloting is not required. At the inlet temperature of 800K and equivalence ratio of 0.6, where the NO_x goal is 3.0 g/kg, the unpiloted perforated plate (SPRPP-3) produced a NO_x level of 2.4 g/kg. Thus, only a very small piloting flow could be used if the goal of 3.0 g/kg were to be met. The possibility of operating the injector at such a small flowrate without the nozzle overheating would have to be assessed by further testing.

The most surprising effect of the injection of the four percent pilot fuel was the resulting influence on combustion efficiency. The perforated plate employed in PF-4 was the SPRPP-3 configuration for which the unpiloted design point efficiency was 88.6 percent. The design point efficiency of PF-4 was greater than 99.9 percent. Thus, four percent of the fuel injected into the center of the stream downstream of the perforated plate influenced the entire combustor flow. The television monitor did in fact indicate that the highly luminous flame generated by combustion of the fuel droplets did extend through an appreciable extent of the cross section, although this flame did not reach the combustor wall. It should be recalled that injection of liquid fuel as the pilot fuel was not regarded as a practical scheme during the conceptual design study because of the impossibility of distributing the small volume flow uniformly throughout the flameholder base region. The results of this experiment indicate that it is not necessary to introduce the pilot fuel immediately at the flameholder base in order to promote high efficiency. It is possible that by optimization of the pilot injector cone angle, orifice size, and flow rate, high efficiency can be achieved over an even greater equivalence ratio range.

CONCLUSIONS

The piloted flameholder concept offers high potential for achieving a lean premixing, prevaporizing combustor design capable of providing wide blowout limits, low NO_x emissions, and high performance. The lean stability limit, design point NO_x, CO, and UHC emission levels, combustor pressure loss, and design point combustion efficiency goals (Table 1) were met by use of a pilot perforated plate flameholder (Configuration PF-4) which employed four percent of the design point fuel flow as pilot fuel. The maximum NO_x level goal could be achieved by using less pilot flow at the high entrance temperature conditions. The off-design combustion efficiency goals were met for equivalence ratios greater than 0.575 at an inlet temperature of 600K, greater than 0.45 at 700K, and greater than 0.35 at 800K. Further testing will be required to determine if increasing the pilot fuel flowrate would increase the efficiency at low equivalence ratios.

Flame stabilizer designs based on the augmentation concepts embodied by the self-piloting recessed perforated plate and catalyzed tube flameholder designs offer no improvement in lean blowout limit.

The use of perforated plates having hole diameters smaller than 1.1 cm offers no advantage in terms of combustor performance or NO_x emission levels (larger diameters were not assessed in this study). Combustion efficiency in reaction-time-limited (premixed) combustors is sensitive to flameholder pressure loss.

High frequency (several kHz) combustion instabilities are likely to occur in constant-area premixed combustors employing high blockage flameholders, and the instabilities are capable of creating physical damage to the combustor structure and will create higher burner heat loads.

APPENDIX I

CHARACTERISTICS OF STABILITY LIMIT AUGMENTATION CONCEPTS

A summary of the characteristics of each of the nine concepts for improving lean stability limits which were examined in the Conceptual Design Study is presented in Tables AI-1 through AI-9.

Table AI-1

Concept: Fuel-Injected Stabilizer - Gaseous fuel injection into V-gutter recirculation region

Class: Piloting

Factors Entering DOC (Direct Operating Cost) Calculation:

Pressure Loss: Nominal (5%)

Weight: 11 kg

Initial Cost: Slightly above average - will require a second fuel control and injection system; vaporizer development required - Rank 2

Maintenance Cost: Above average - will require cleanup of carbonaceous material deposits at regular intervals - Rank 3

Calculated DOC Increase: 0.38%

Other Considerations:

Stability: High potential for stability improvement - Rank 1

NO_x Emissions: NO_x EI at design may be slightly higher than goal but this effect can be minimized by reducing pilot flow when augmentation is not required

Operational Problems: Transient response below normal because of behavior of fuel vaporizer - Rank 2

Technological Risks: High risk associated with successful development of reliable fuel vaporization system - Rank 3

Table AI-2

Concept: Hot Gas Drafting - Drafting of hot pilot products to base of perforated plate

Class: Piloting

Factors Entering DOC (Direct Operating Cost) Calculation:

Pressure Loss: Nominal (5%)

Weight: 2kg

Initial Cost: Slightly above average - requires additional fuel control and injection system - Rank 2

Maintenance Cost: Increase above baseline expected to be insignificant - Rank 1

Calculated DOC increase: 0.12%

Other Considerations:

Stability: Minimum potential for stability improvement - Rank 3

NO_x Emissions: Pilot must be operated at high power, NO_x EI expected to be 1.9 g/kg at design

Operational Problems: None - Rank 1

Technological Risks: Possibility of high development time associated with cut-and-try approach required to achieve correct secondary flow pattern - Rank 2

Table AI-3

Concept: Self-piloting Recessed Perforated Plate - Fraction of main reactant flow bled into containment cavity

Class: Piloting

Factors Entering DOC (Direct Operating Cost) Calculation:

Pressure Loss: Nominal (5%)

Weight: No increase

Initial Cost: Average - Rank 1

Maintenance Cost: Average - Rank 1

Calculated DOC Increase: 0.0%

Other Considerations:

Stability: Large uncertainty in extent of improvement achievable - Rank 3

NO_x Emissions: No increase in NO_x above baseline design

Operational Problems: None - Rank 1

Technological Risks: None - Rank 1

Table AI-4

Concept: Catalyzed Tube Perforated Plate - Reaction in boundary layer formed on inside of tube promoted by catalysis

Class: Catalytic

Factors Entering DOC (Direct Operating Cost) Calculation:

Pressure Loss: Nominal (5%)

Weight: Average - no increase above baseline

Initial Cost: Average - Rank 1

Maintenance Cost: Average - Rank 1

Calculated DOC Increase: 0.48%

Other Considerations:

Stability: Potential not yet demonstrated - Rank 3

NO_x Emissions: No increase in NO_x above baseline design average

Operational Problems: None - Rank 1

Technological Risks: Long lifetime catalyst using metal substrate not yet demonstrated - Rank 2

Table AI-5

Concept: Catalytic Bed Preheater - Mixture is partially reacted in low pressure drop catalytic bed

Class: Catalytic

Factors Entering DOC (Direct Operating Cost) Calculation:

Pressure Loss: 5.5%

Weight: Average - no increase above baseline

Initial Cost: Slightly above average due to tube cooling system required - Rank 2

Maintenance Cost: Far above average due to requirement for periodic refurbishment of bed - Rank 5

Calculated DOC increase: 0.54%

Other Considerations:

Stability: Marginally above average - Rank 3

NOx Emissions: No increase in NOx above baseline

Operational Problems: Catalytic bed will require preheating during start-up - Rank 2

Technological Risks: Development of non-metallic catalytic bed substrate material required to avoid burnout during high power operation - Rank 3

Table AI-6

Concept: Catalyzed Recessed Perforated Plate - Catalyzed downstream surface of recessed perforated plate

Class: Catalytic

Factors Entering DOC (Direct Operating Cost) Calculation:

Pressure Loss: Nominal (5%)

Weight: No increase

Initial Cost: Average - Rank 1

Maintenance Cost: Far above average due to necessity to refurbishment of catalyzed surfaces - Rank 5

Calculated DOC increase: 0.48%

Other Considerations:

Stability: Large uncertainty in augmentation potential - Rank 3

NOx Emissions: No increase above baseline

Operational Problems: None - Rank 1

Technological Risks: Long life, high temperature catalyst technology must be developed - Rank 3

Table AI-7

Concept: Compressor-Recirculated Primary Gas ~ Combustion products recirculated through last compressor stage

Class: Heat Recirculation

Factors Entering DOC (Direct Operating Cost) Calculation:

Pressure Loss: Nominal (5%)

Weight: 40 kg

Initial Cost: Far above average due to intricate manifolding and use of high temperature gas; hot flow valves required - Rank 5

Maintenance Cost: Significantly above average due to increased number of hot section components - Rank 4

Calculated DOC increase: 0.84%

Other Considerations:

Stability: Marginal stability increase expected due to 100K increase in mixture temperature - Rank 3

NOx Emissions: Recirculation shut off at high power - no increase of NOx above baseline at design condition

Operational Problems: None - Rank 1

Technological Risks: Development of suitable methods of providing thermal barrier in recirculation tubes required; ability to design efficient compressor which can handle variable amounts of last stage injection must be demonstrated - Rank 3

Table AI-8

Concept: Ejector-Recirculated, Primary Gas - Ejector action produced using the primary air causes flow to recirculate

Class: Heat Recirculation

Factors Entering DOC (Direct Operating Cost) Calculation:

Pressure Loss 6.5%

Weight: 25kg

Initial Cost: Average - Rank 1

Maintenance Cost: Average - Rank 1

Calculated DOC increase: 0.23%

Other Considerations:

Stability: Marginally above average due to small increase in mixture temperature achievable - Rank 3

NOx Emissions: No increase in NOx above baseline design

Operation Problems: None - Rank 1

Technological Risks: Development of efficient ejector on full-scale engine must be demonstrated; will be difficult to hold flow area tolerances in Large devices - Rank 3

Table AI-9

Concept: Regenerative Heat Exchange - Heat exchanger installed at primary zone exit

Class: Heat Recirculation

Factors Entering DOC (Direct Operating Cost) Calculation:

Pressure Loss: 8%

Weight: 30kg

Initial Cost: Above average due to complexity of fabrication of heat exchanger - Rank 3

Maintenance Cost: Significantly above average - cleanup of carbon deposits required to maintain effectiveness - Rank 4

Calculated DOC increase: 0.85%

Other Considerations:

Stability: Marginally above average due to limited entrance air temperature rise achievable in practical designs - Rank 3

NOx Emissions: NOx exceeds goals due to increased adiabatic flame temperature at design point.

Operational Problems: None - transient heat exchanger response expected to be rapid Rank 1.

Technological Risks: Significant materials and fabrication problems associated with high temperature heat exchangers must be overcome - Rank 3

APPENDIX II
INSTRUMENTATION LIST

The tables included in the Appendix list the temperatures, pressures, flowrates, and emission analyzer outputs recorded in the test program.

Table AII-1
Instrumentation List-LARC System

<u>Symbol</u>	<u>Parameter</u>	<u>LARC Channel</u>	<u>Control Room Readout</u>
HC	FID output-Phase discriminating probe system	1	Strip Chart
P	Pressure scanivalve-See Table AII-2	2	
PVU	Pressure upstream of venturi	3	Gauge
PFP	Pilot fuel manifold pressure	4	DVM
DPP	Pilot fuel injector ΔP	5	DVM
PFM	Main fuel manifold pressure	6	DVM
PSMV	Mixer/vaporizer pressure	7	Gauge
DPI	Airflow pressure drop across fuel injector	8	DVM
PTI2	Main air inlet total pressure	9	DVM
CO	Carbon monoxide emissions	10	Gauge
T	Temperature scanner - No. 1 See Table AII-3	11	
T	Temperature scanner - No. 2 See Table AII-4	12	
	Open	13	
	Open	14	
CO ₂	Exhaust gas carbon dioxide content	15	Gauge
NO	Nitric oxide emissions	16	Gauge
	Open	17	
UHC	Unburned hydrocarbon emissions	18	Gauge
HCA	Hydrocarbon analyzer attenuation	19	Gauge
WFP	Pilot fuel flow meter	20	DVM
WFM	Main fuel flow meter	21	DVM
WCS	Coolant flow meter	22	DVM
WBPS	Coolant flow, back pressure valve	23	DVM
O ₂	Exhaust gas oxygen content	24	Gauge
-	Phase discriminating probe, selector switch	25	-

Table AII-2

Instrumentation List-Pressure Scanivalve

<u>Symbol</u>	<u>Parameter</u>	<u>Lead No.</u>	<u>Gauge Display</u>
PVU	Main air venturi, upstream	1	X
PVTH	Main air venturi, throat	2	X
PTI1	Main Air, inlet total pressure	3	X
PTI2	Main air, inlet total pressure	4	
PTI3	Main air, inlet total pressure	5	
PTI4	Main air, inlet total pressure	6	
PSIT	Main air, inlet static-top	7	
PSIL	Main air, inlet static-bottom	8	
PSTP-UP	Step coolant, upstream of orifice	9	
	Open	10	
	Open	11	
PCFH-UP	Flameholder cooling air upstream orifice	12	
PCFH-P	Flameholder cooling air-plenum	13	
PSMU	Main air, mixer/vaporizer-upstream	14	
PSMD	Main air, mixer/vaporizer-downstream	15	
PCAF	Combustor entrance static-flange	16	
PCAT	Combustor entrance static-torch	17	
PCCU	Combustor coolant orifice upstream	18	X
PCC	Combustor coolant	19	X
PSICT	Instrumentation section static-top	20	
PCICB	Instrumentation section static-bottom	21	
PTC1	Combustor exit total pressure-pos 1	22	
PTC2	Combustor exit total pressure-pos 2	23	
PTC3	Combustor exit total pressure-pos 3	24	
PTC4	Combustor exit total pressure-pos 4	25	
PTC5	Combustor exit total pressure-pos 5	26	
PTC6	Combustor exit total pressure-pos 6	27	
PWCU	Window cooling air, orifice upstream	28	
PWCD	Window cooling air, orifice downstream	29	
PCCD	Combustor coolant, orifice downstream	30	

Table AII-3

Instrumentation List-Temperature Scanner No. 1

<u>Symbol</u>	<u>Parameter</u>	<u>TC No.</u>	<u>LARC Scan No.</u>	<u>Display</u>
ZERO	Zero	-	1	
FULLSC	Calibration	-	2	
TV	Air temperature - venturi entrance	1	3	Drum+
THEX	Air temperature - heater exit	2	4	Drum
TTI1	Air temperature - mixer/vaporizer entrance	3	5	Drum
TTI2	Air temperature - mixer/vaporizer entrance	4	6	
TTI3	Air temperature - mixer/vaporizer entrance	5	7	
TTI4	Air temperature - mixer/vaporizer entrance	6	8	
TFP	Pilot fuel temperature (heater exit)	7	9	Drum
TFM	Main fuel temperature	8	10	
TCFH-EX	Flameholder coolant gas temperature out	9	11	
TWM1	Wall temperature, mixer/vaporizer	11	13	
TWM2	Wall temperature, mixer/vaporizer	12	14	
TA1	Flameholder temperature - No. 1	13	15	API
TA2	Flameholder temperature - No. 2	14	16	API
TA3	Flameholder temperature - No. 3	15	17	Drum
TA4	Flameholder temperature - No. 4	16	18	Drum
TCFU	Flange temperature, combustor-upper	17	19	Drum
TCFD	Flange temperature, combustor-lower	18	20	API
TWC-6-4	Wall temperature, combustor,	19	21	API
TWIT	6 o'clock, 4 inches			
TWC-1-5	Wall temperature, combustor,	20	22	API
TWIB	1 o'clock, 5 inches			
TWC-9-55	Wall temperature, combustor, 9 o'clock, 7 inches	21	23	API
TW	Wall temperature, window flange	23	25	Drum
TGBPV	Gas temperature, back pressure valve valve	24	17-2	Drum
TWEMLIN-1	Transfer line, No. 1	51	26	Drum

Table AII-4

Instrumentation List-Temperature Scanner No. 2

<u>Symbol</u>	<u>Parameter</u>	<u>TC No.</u>	<u>LARC Scan No.</u>	<u>Display</u>
TWEMLIN-2	Transfer line, NO. 2	52	3	Drum
TFHTUB-6	Flameholder, No. 6	-	4	
TFHTUB-5	Flameholder, No. 5	-	5	
TORCH	Torch body	30	6	DVM
TCONDN	Emission analyzer condensor	31	7	
TFHTUB-8	Flameholder, No. 8	32	8	
TPLUG	Combustion gas at water-coaled plug	29	9	
TSMP-1	Gas sample at probe exit, Probe 1	1	10	Drum
TSMP-2	Gas sample at probe exit, Probe 2	2	11	Drum
TSMP-3	Gas sample at probe exit, Probe 3	3	12	Drum
TSMP-4	Gas sample at probe exit, Probe 4	4	13	Drum
TSMP-5	Gas sample at probe exit, Probe 5	5	14	Drum
TSMP-6	Gas sample at probe exit, Probe 6	6	15	Drum
TWPILIN	Pilot fuel line wall	-	16	
	Open		17	
TGEP	Gas temperature, exhaust duct	24	18	
TGPPILBY	Pilot fuel by pass line wall	16	19	
TGFHC-PR	Flameholder primary coolant exit	32	20	Drum
	Analyzer attenuator signals		21-25	
TGFHC-SC	Flameholder secondary coolant exit	33	26	Drum

LIST OF SYMBOLS

A	Area (cm^2)
B	Blockage
C	Constant
c	Concentration (g/cm^3)
C_D	Discharge coefficient, perforated plate loss coefficient
c_p	Specified heat (cal/gmK)
C_1, C_2	Constants (Eq. 10)
D	Binary diffusion coefficient (m^2/sec)
d	Diameter
EI	Emission index (g/kg)
f	Friction factor
f/a	Fuel-air ratio
g	Gravitational constant
L	Length
M	Mach number
Mw	Molecular weight
N	Number
Nu_m	Nusselt number for mass transfer
P	Pressure (atm); ratio of pilot fuel flow to total fuel flow
P_R	Fraction recirculated - defined in Fig. 21
PPM	Concentration in parts per million by volume

q	Dynamic pressure (atm)
R	Universal gas constant
S	Ratio of secondary (dilution) airflow to total (primary plus secondary) air flow
T	Temperature (K)
V	Velocity (m/s)
w	Flow rate (kg/sec)
x, y, z	Stoichiometric coefficients
α , β	Stoichiometric coefficients
η_c	Combustion efficiency
ϕ	Equivalence ratio
ρ	Density (gm/cm ³)
τ	Residence time (sec)

Subscripts:

act	Actual
ad	Adiabatic flame
bo	Blowout
c	Cross section, calculated
e	Equilibrium
m	Mainstream, metered
o	Approach flow condition
p	Pilot stream
pri	Primary stream

R Recirculated
s Surface
sec Secondary
tot Total stream (primary plus secondary)

REFERENCES

1. Cheng, S. I. and A. A. Kovitz: Theory of Flame Stabilization by a Bluff Body. Seventh International Symposium on Combustion. Butterworths Scientific Publications, London, pp. 681-691, (1959).
2. Semerjian, H. G. and I. C. Ball: Potential Reduction in NO_x Emissions with Premixed Combustors, The Combustion Institute - Central States Section, March 1977.
3. Marek, C. J. and L. C. Papathakos: Exhaust Emissions from a Premixing, Prevaporizing Flame Tube Using Liquid Jet A Fuel, NASA TM X-3383, April 1976.
4. Anderson, D.: Effects of Equivalence Ratio and Dwell Time on Exhaust Emissions from an Experimental Premixing, Prevaporizing Burner, NAS TM X-71592, March 1975.
5. Sarli, V. J., D. C. Eiler, and R. L. Marshall: Effects of Operating Variables on Gaseous Emissions, Air Pollution Control Association Specialty Conference, New Orleans, LA, October 1975.
6. Westenberg, A. A.: Kinetics of NO and CO in Lean, Premixed Hydrocarbon-Air Flames, Combustion Science and Technology, Vol. 4, 1971.
7. Ozawa, R. I.: Survey of Basic Data on Flame Stabilization and Propagation for High Speed Combustion Systems, AFAPL Technical Report AFAPL-TR-70-81, January 1971.
8. Spadaccini, L. J.: Low Emission Combustors for Gas Turbine Powerplants, Combustion Science and Technology, Vol. 9, 1974, pp. 133-136.
9. Anderson, D. N.: Effect of Catalytic Reactor Length and Cell Density on Performance, Paper presented at the Second Workshop on Catalytic Combustion, Raleigh, NC, June 21-22, 1977.
10. Kays, W. M. and A. L. London: Compact Heat Exchangers, McGraw-Hill Book Co., 1958.

Table 1

LEAN STABILITY AUGMENTATION PROGRAM GOALS

Test Conditions:	$P = 10 \text{ atm}$
	$600 \leq T_o \leq 800 \text{ K}$
	$0.25 \leq \phi \leq 0.6$
	$V_{\text{ref}} = 25 \text{ m/sec}$
Design Condition	$T_o = 600\text{K}$ $\phi = 0.6$
Emissions:	$El_{\text{NOX}} < 1.0 \text{ g/kg at design; } < 3.0 \text{ g/kg overall}$
	$El_{\text{CO}} < 10.0 \text{ g/kg at design}$
	$El_{\text{UHC}} < 1.0 \text{ g/kg at design}$
Performance:	$\eta_{\text{comb}} \geq 0.99 \text{ for } 0.3 \leq \phi \leq 0.6$
	$\Delta P/P < 0.05$

Table 2
LEAN STABILITY AUGMENTATION CONCEPTS

<u>Concept</u>	<u>Class</u>	<u>Design Considered</u>
Fuel injection into recirculation zone	Pilot	(1) Pilot stream is liquid fuel
"	Pilot	(2) Pilot stream is gaseous fuel
"	Pilot	(3) Pilot stream is fuel-rich combustion products
"	Pilot	(4) Pilot stream is mixture of water and fuel-rich combustion products
Enrichment of incoming stream boundary layer flow	Pilot	(5) Pilot stream transpired through porous medium
Drafting of hot gas from stable to unstable region	Pilot	(6) Annular pilot discharging flow parallel to main combustion product flow
Physical containment of recirculating gases	Pilot	(7) Fraction of main flow is bled into containment cavity
"	Catalyst	(8) Containment cavity is coated with catalyst to promote reaction
Heating or partial reaction of incoming mixture	Catalyst	(9) Catalytic bed causes partial reaction of mixture upstream of stabilizer
"	Catalyst	(10) Catalyzed inner diameter of tube forming perforated plate flameholder promotes reaction in boundary layer
"	Heat Recirculation	(11) A portion of primary zone gas is recirculated and injected ahead of the last compressor stage
"	Heat Recirculation	(12) Heat is transferred from primary zone gas to compressor discharge air via heat exchanger
"	Heat Recirculation	(13) Ejector action is used to re-inject primary zone products into compressor discharge air

Table 3

TURBOFAN ENGINE COMBUSTOR OPERATING PARAMETERS

	Inlet Total Pressure (atm)	Inlet Total Temperature (Deg K)	Fuel Air Ratio	Combustor Airflow (kg/sec)
ADVANCED ENGINES (E³)				
Idle	4.1	506	.0103	10.9
Sea Level 30% Thrust (Approach)	12.1	629	.0136	26.7
Sea Level 85% Thrust (Climb)	27.8	783	.0217	53.0
Sea Level Takeoff	32.0	813	.0238	64.3
Cruise (35,000 ft. M = .8)	13.8	755	.0231	28.8
Flight Idle (35,000 ft. M = .8)	3.1	500	.0094	8.7
CURRENT ENGINES (JT9D)				
Bled Idle (6% Thrust)	2.9	428	.0126	16.5
Unbled Idle (8.2% Thrust)	3.9	463	.0100	23.3
Sea Level 30% Thrust (Approach)	8.5	586	.0130	45.1
Sea Level 85% Thrust (Climb)	18.5	734	.0194	85.7
Sea Level Takeoff	21.1	767	.0215	94.7
Cruise (35,000 ft. M = .9)	9.3	703	.0205	91.8
Flight Idle (25,000 ft. M = .8)	3.3	490	.0087	19.2

Table 4

INFLUENCE OF PERFORMANCE AND COST ON AIRLINE
DIRECT OPERATING COST

Factor	<u>Influence Coefficient</u>		<u>Equal DOC penalty</u>
	TSFC	DOC	
Combustor efficiency	-1.0	-0.35	1%
Combustor ΔP/P	0.36	0.13	2.7%
Diffuser bleed flow	0.2	0.07	5%
Duct ΔP/P	0.74	0.26	1.36%
Shaft power (per HP)	0.004	0.0015	230 HP
TSFC		0.35	1%
Weight		0.047	230 Kg
Cost		0.040	\$85,000
Maintenance		0.090	\$2.93/hr

Table 5

COST LEVELS EMPLOYED IN CONCEPT EVALUATION

Rank	Initial Combustor Cost		Maintenance cost
		(\$K)	(\$/hour)
Average	1	46	5
Marginally above average	2	75	6
Above Average	3	100	7
Significantly above average	4	125	8
Far above average	5	150	9

Table 6

CATALYTIC BED EXPERIMENT DATA

a) Data used to evaluate Equation (7) (Data from Ref. 9)

$$\begin{aligned} T_o &= 800K \\ V_o &= 10 \text{ m/sec} \\ P_o &= 3.0 \text{ atm} \\ \phi &= 0.2 \\ L &= 8.5 \text{ cm } (\Delta T_{8.5} = \Delta T_{ad}) \end{aligned}$$

Assumed bed characteristics (Thermacomb 8/8)

$$\begin{aligned} \text{Open area fraction} &= 0.65 \\ \text{Holes/cm}^2 &= 35 \\ \text{Area hole} &= 0.019 \text{ cm}^2 \end{aligned}$$

b) Data used to estimate bed temperature

ϕ	0.2	0.24	0.20
N (cell/cm ²)	30	30	45
T ($L = 2.54$ cm)	975	1020	1020

c) Data used to evaluate Equation (10)

$$\begin{aligned} T_o &= 800K \\ V_o &= 10 \text{ m/sec} \\ P_o &= 3.0 \text{ atm} \\ T_{ad} &= 400K \\ L &= 11 \text{ cm} \\ N \text{ (cell/cm}^2\text{)} & 45 \quad 30 \\ \Delta P/P & 0.37 \quad 1.7 \end{aligned}$$

ORIGINAL PAGE IS
OF POOR QUALITY

TABLE 7
LEAN STABILITY AUGMENTATION CONCEPT RANKINGS

	Piloting Concepts			Catalyst Concepts			Heat Recirculation Concepts		
	Fuel-Injected Stabilizer	Hot Gas Drafting	Self-Piloting Recessed PP	Catalyzed Tube PP	Catalytic Bed Preheater	Catalyzed Recessed PP	Compressor-Recirculated Primary Gas	Ejector-Recirculated Primary Gas	Regeneratively Heated Air
Pressure Loss									
△ Pressure Loss	-	-	-	-	0.5	-	-	1.5	3.0
△ Weight (kg)	11	2	-	-	-	-	40	25	30
Initial Cost Rating	2	2	1	1	1	1	5	1	3
Maintenance Cost Rating	3	1	1	5	5	5	4	1	4
△ Direct Operating Cost (Perc. t)	0.38	0.12	0.0	0.48	0.54	0.48	0.84	0.23	0.85
NO _x Emission Index (g/kg)	1.0 ⁺	1.0	1.0	1.0	1.0	1.0	1.0 ⁺	1.0	3.0
Stability Augmentation Rating	1	3	3	3	2	3	3	3	3
Operational Considerations	2	1	1	1	2	1	1	1	1
Technological Risk	3	2	1	2	3	2	3	3	3
Overall Rank	1	5	2	3	6	4	8	7	9

Note: Low numerical value of rating factors and rank indicate high merit.

TABLE 8
EMISSIONS ANALYSIS INSTRUMENTATION

<u>Component</u>	<u>Range</u>	<u>Instrument and Detection Method</u>	<u>Instrument Error %</u>
			<u>Full Scale</u>
THC	0-1 ppmv	Flame Ionization Detector	+5.0%
	Intermediate ranges		+1.0%
	0-10%		+1.0%
NO _x	0-2.5 ppmv	Chemiluminescence Detector	+1.0%
	Intermediate ranges (6)	TECO Model 10A	+1.0%
	0-10,000 ppmv		+1.0%
CO	0-100 ppmv	Nondispersive Infrared	+2.0%
	0-500, 0-1000 ppmv	Beckman Model 315B	+1.0%
	0-5%, 0-10%		+1.0%
CO ₂	0-2%	Nondispersive Infrared	+1.0%
	0-5%	Beckman Model 315B	+1.0%
	0-15%		+1.0%
O ₂	0-1%	Paramagnetic Analyzer	+1.0%
	0-5%	Scott Model 150	+1.0%
	0-10%		+1.0%
	0-25%		+1.0%

Table 9

MATRIX OF TEST CONDITIONS

Emission measurements (ganged probes) and smoke probe measurements:

T_o (K)	600	700	800
\emptyset	0.6 to 0.25	0.6 to 0.3	0.6 to 0.3
Configuration		-1 to -4	Final
Emission sample \emptyset increment		0.05	0.025
Smoke sample \emptyset increment		0.1	0.1

Emission measurements - individual probes:

T_o (K)	600
\emptyset	0.6

Cold flow stagnation pressure loss measurement:

T_o (K)	600
\emptyset	0.0

Blowout fuel-air ratios determined for $T_o = 600, 700, 800$ K

Notes:

- 1) For certain configurations at $T_o = 800$ K, $\emptyset \geq 0.5$ emission data is not available due to flameholder over temperature
- 2) A minimum of four gas analysis readings were recorded at each test point
- 3) A minimum of three blowout fuel flow readings were recorded for each entrance temperature
- 4) $P = 10$ atm for all tests

Table 10

LEAN STABILITY BLOWOUT LIMIT DATA SUMMARY

Configuration	$\Delta P/P$	Blockage	Hole Diameter (cm)	No. of Holes	ϕ_{bo}		
					$T_o = 600K$	700K	800K
Baseline	2.5	74.6	0.691	55	0.47	0.39	0.29
SPRPP-1	2.3	75.1	0.833	37	0.47	0.39	0.28
SFRPP-2	2.0	74.6	0.833	37(3)	0.50	0.40	0.30
SPRPP-3	2.1	74.6	0.833	37(3)	0.48	0.39	0.29
SPRPP-4	2.6	74.6	0.833	37(3)	0.47	0.38	0.29
SPRPP-5	3.7	80.6	1.026	19	0.47	0.38	0.29
CTF-1	2.7(1)	74.6	1.092	22	0.46	0.38	0.29
CTF-2	2.2	74.6	1.092	22	0.49	0.38	0.29
CTF-3	2.3	74.6	1.092	22	0.45	0.38	0.30
CTF-4	2.3	74.6	1.092	22	0.47	0.38	0.29
CTF-F	3.4	78.8	1.092	18(2)	0.54	0.40	0.30
PF-1	0.8(1)	56.2	(4)	(4)	(6)	(6)	(6)
PF-2	0.7	56.2	(4)	(4)	(6)	(6)	(6)
PF-3	0.7(1)	56.2	(4)	(4)	0.45(7)	(6)	(6)
PF-4	2.6	75.2	0.328	36	(6)	(6)	(6)
PF-F	5.2	75.1	(5)	(4)	(6)	(6)	(6)

NOTE: $26.3 \text{ } V_{ref} (\text{m/s}) \text{ } 28.0$

- (1) Extrapolated from hot flow data
- (2) Four additional tubes with 0.318 ID
- (3) 32 additional 0.132-cm dia bleed holes
- (4) Two 1.27-cm wide annular V-gutters
- (5) Two 1.27-cm wide annular V-gutter and four 35 deg blockage segments
- (6) Blowout did not occur
- (7) Blowout data obtained with zero pilot fuel flow

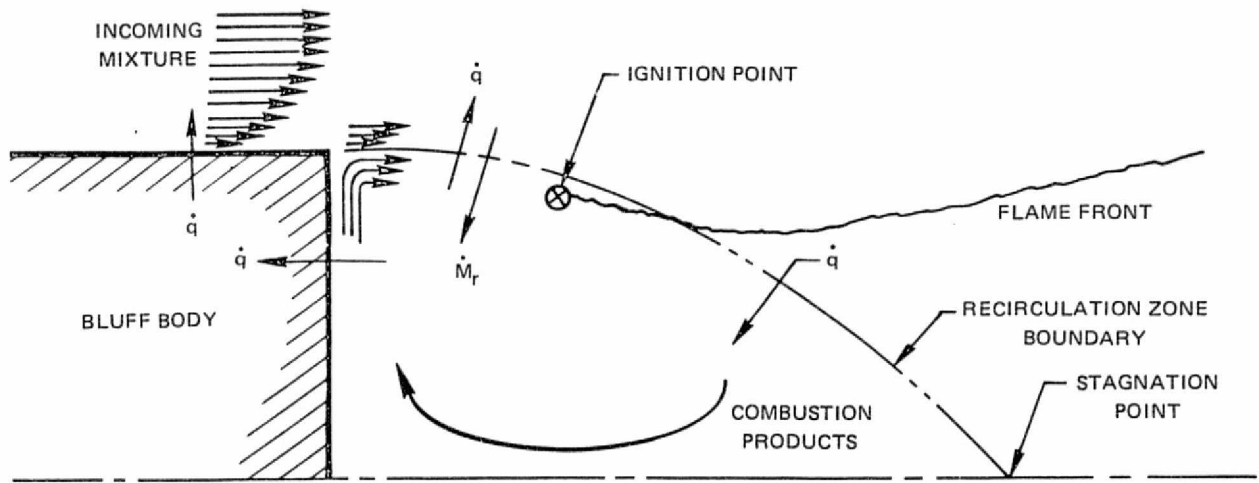


Figure 1. Bluff Body Flame Stabilization Process

ORIGINAL PAGE IS
OF POOR Q'

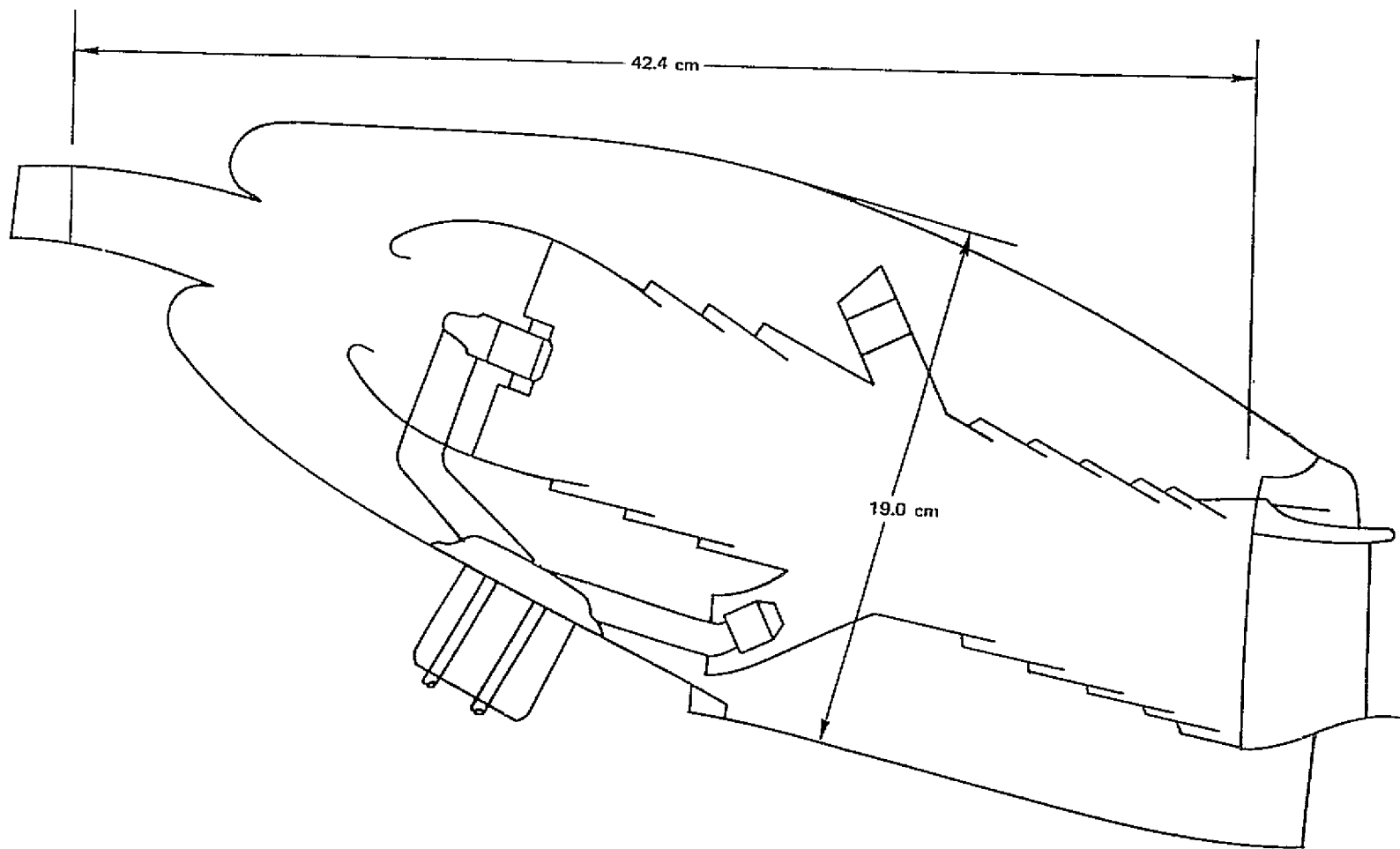


Figure 2. Advanced Gas Turbine Engine Combustor Envelope

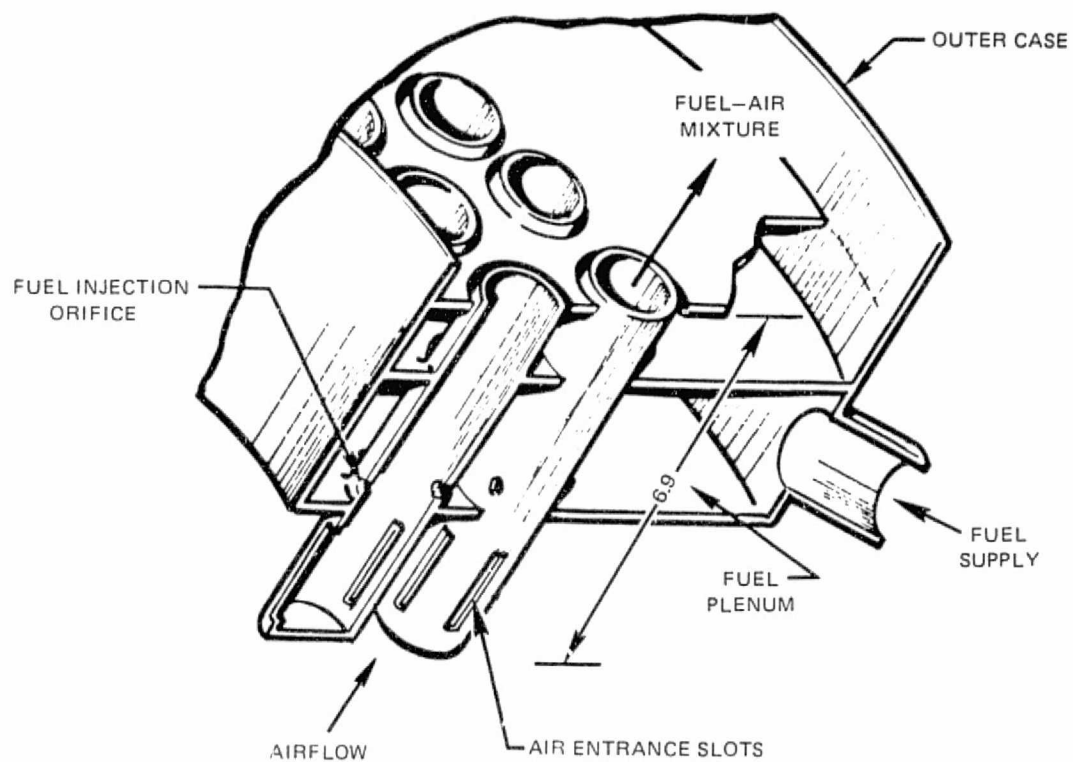
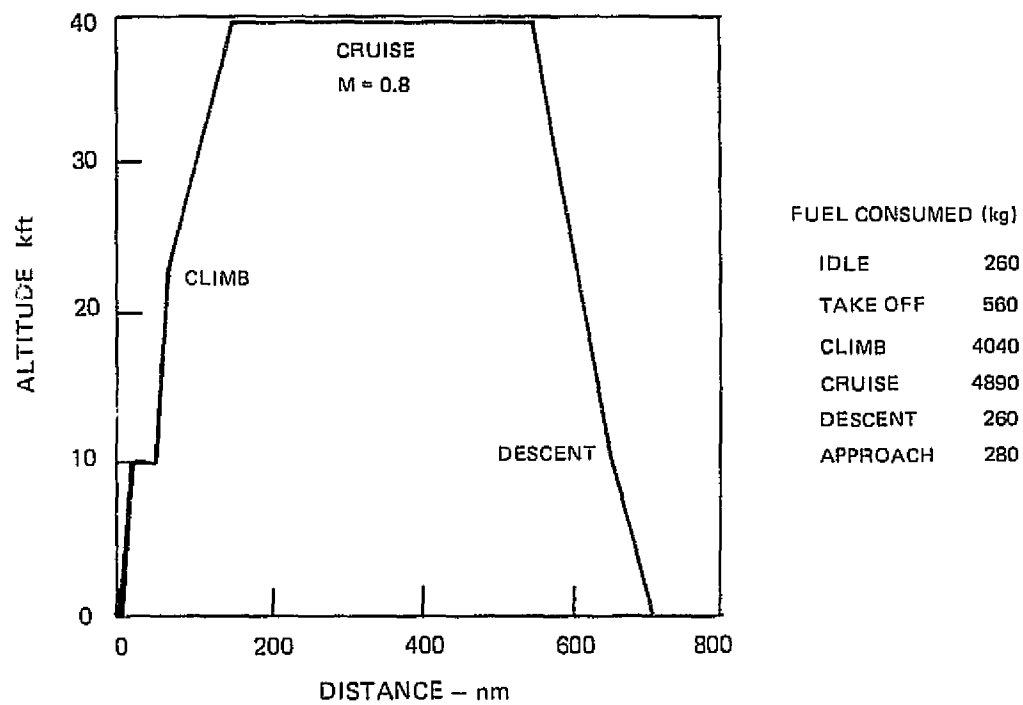
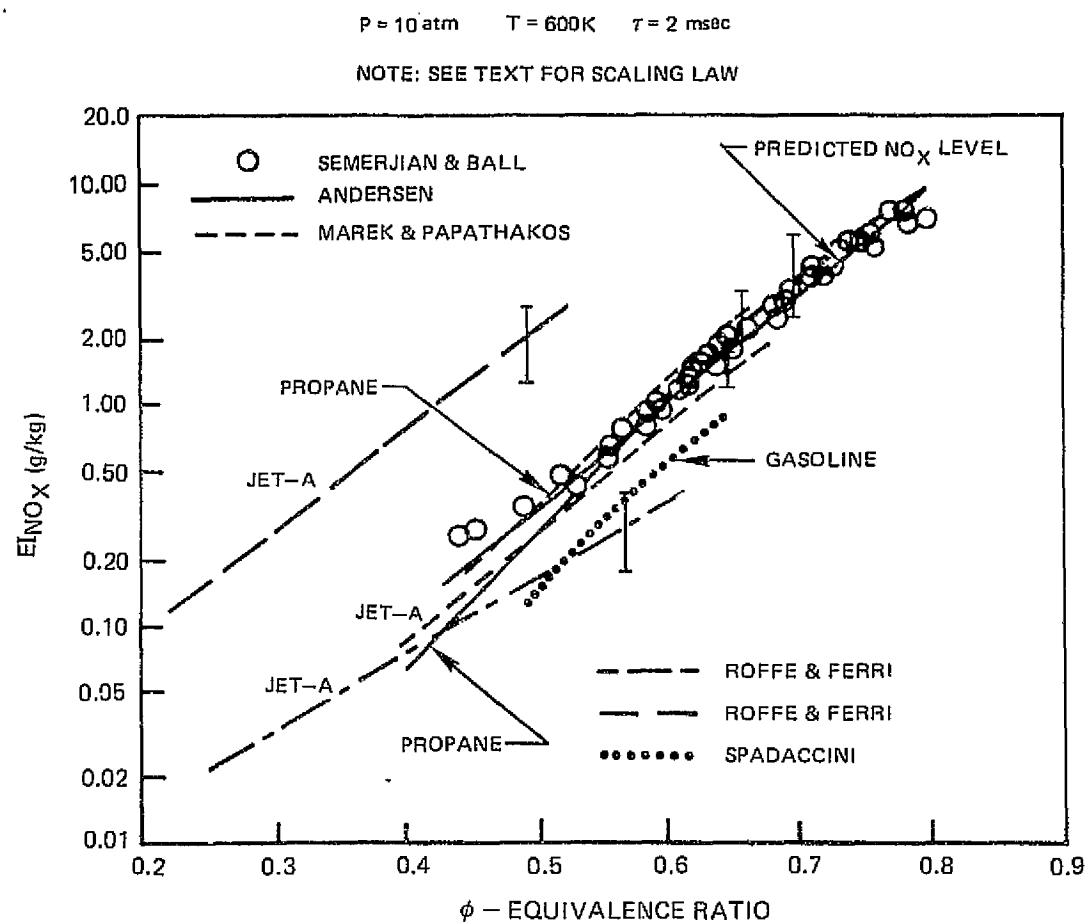


Figure 3. Gaseous-Fuel Injector/Mixer

ORIGINAL PAGE IS
OF POOR QUALITY

Figure 4. Typical E³-Powered Trijet Mission Profile

Figure 5. NO_x Emission Data

ORIGINAL PAGE IS
OF POOR QUALITY

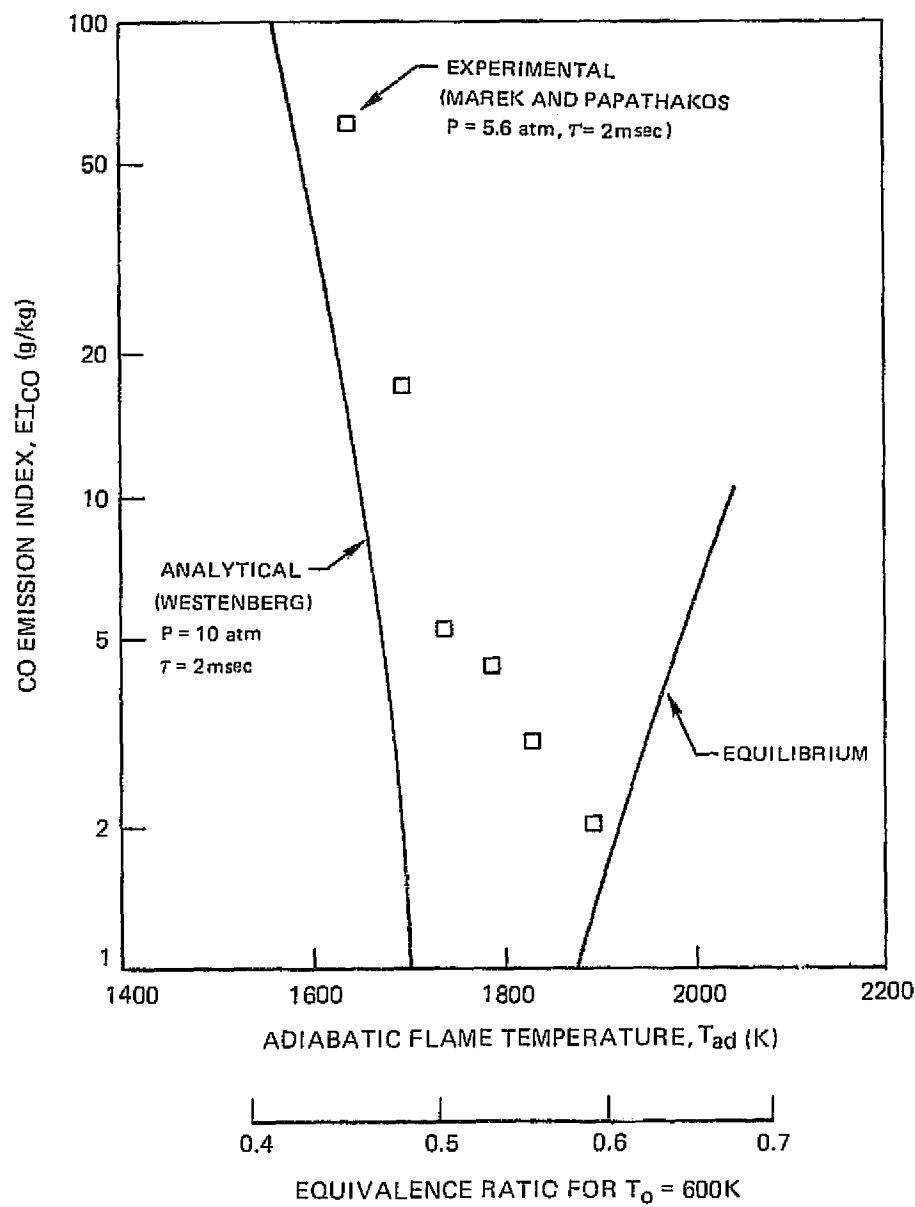
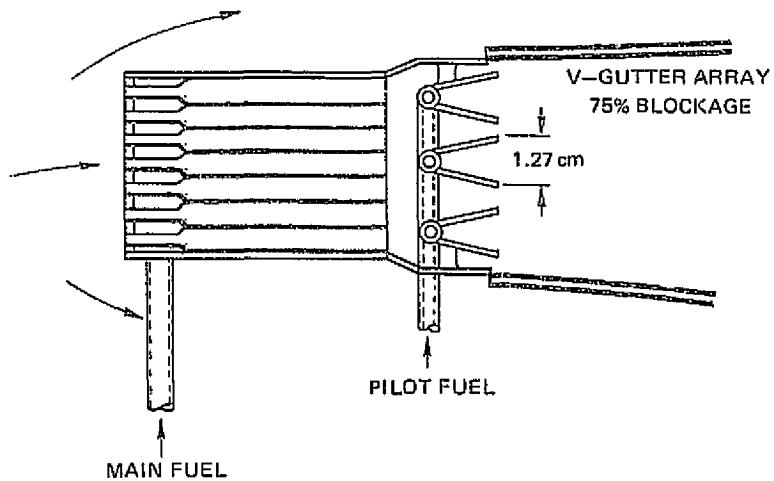
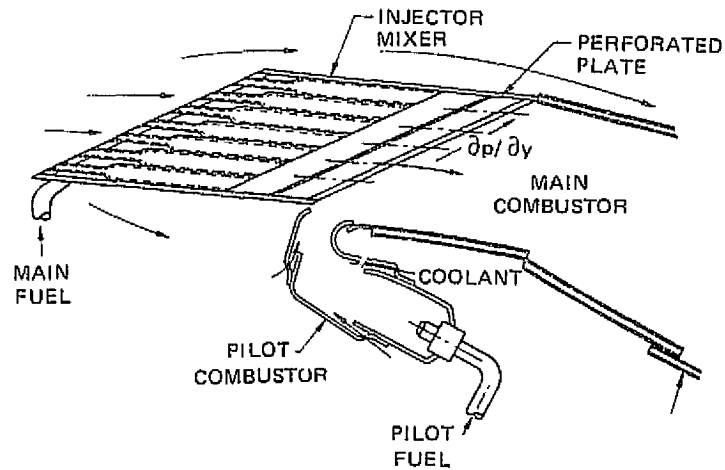


Figure 6. Predicted CO Emissions

a) WAKE-INJECTED BLUFF BODY



b) DRAFTING OF PILOT COMBUSTION PRODUCTS



c) RECESSED SELF-PILOTING PERFORATED PLATE

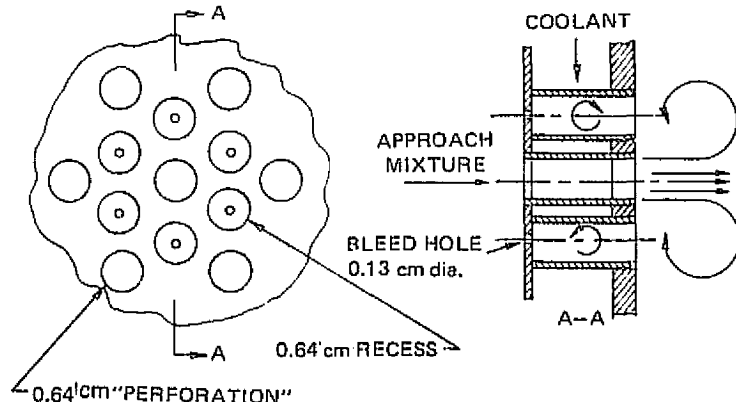


Figure 7. Piloted Combustor Concepts

**ORIGINAL PAGE IS
OF POOR QUALITY**

$$W_{f,p} = 0.05 \times W_{f,tot,des}$$

$$T_0 \approx 600\text{K}$$

$$P = 10 \text{ atm}$$

$$\phi_p = 0.6$$

$$\Delta P = 0.68 \times 10^5 \text{ N/m}^2$$

$$C_D = 1.0$$

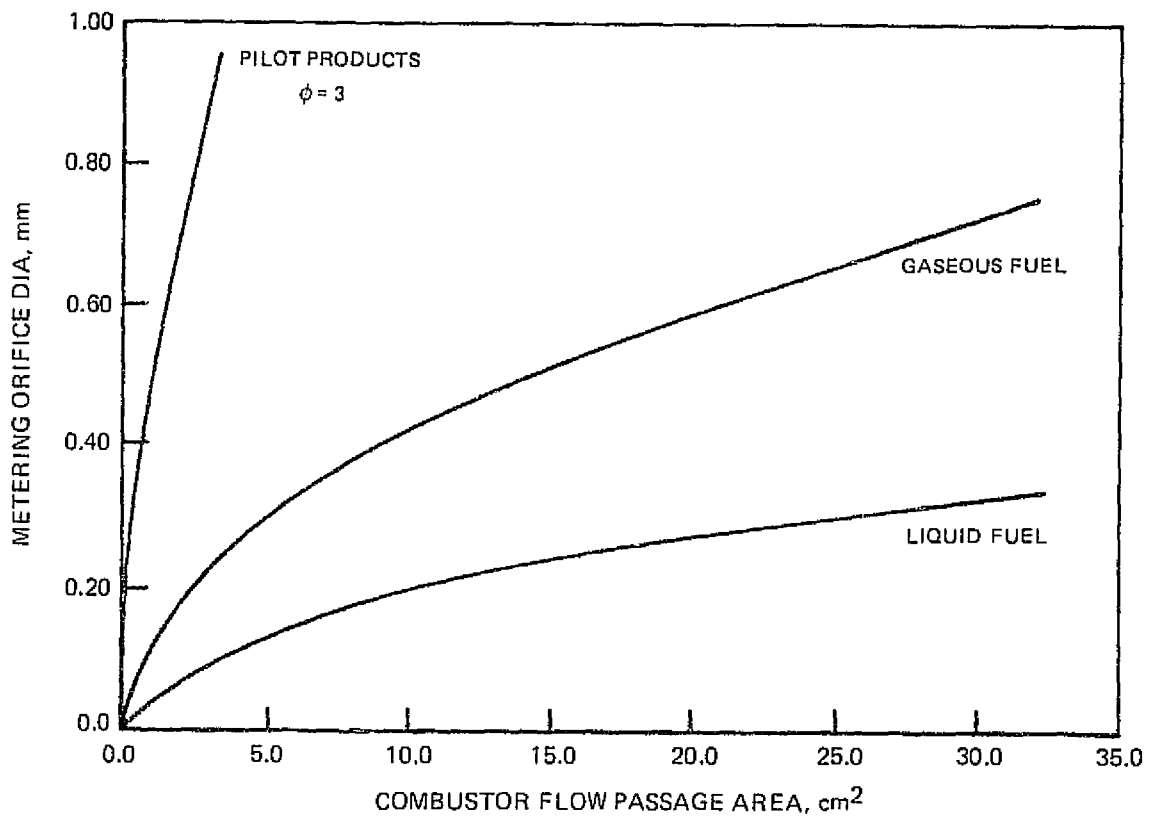


Figure 8. Pilot Fuel Metering Orifice Size

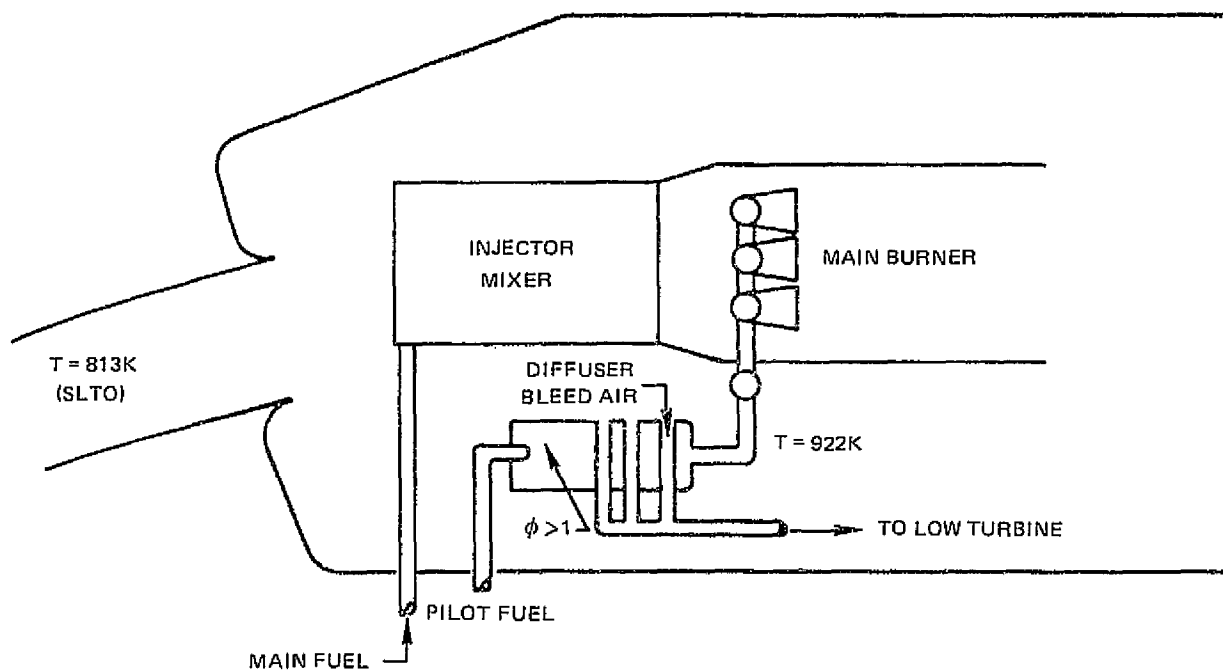
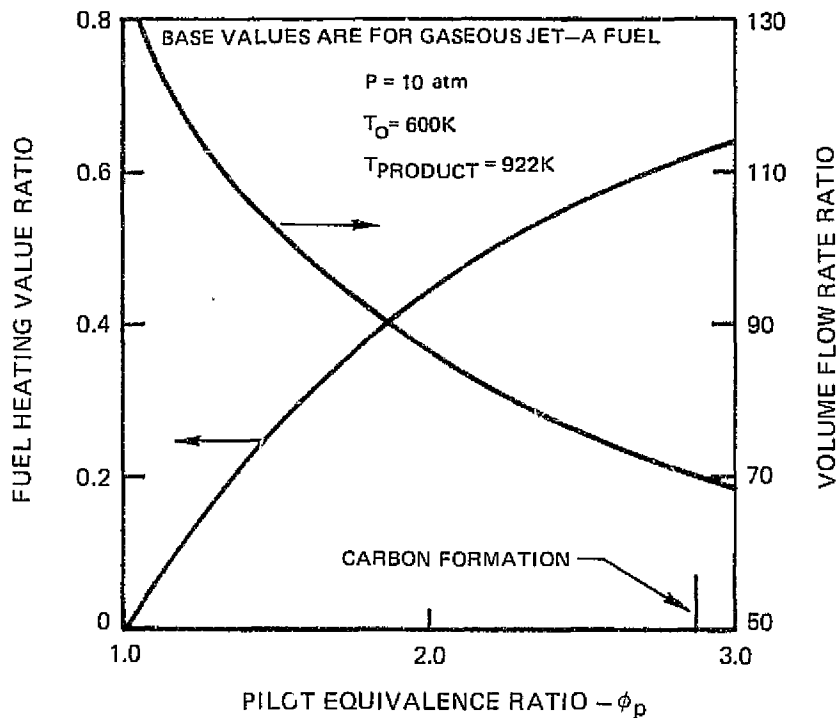


Figure 9. Fuel-Injected Flame Stabilizer using Bleed-Air-Cooled, Fuel-Rich Combustion Products

ORIGINAL PAGE IS
OF POOR QUALITY

a. COMBUSTION PRODUCT CHARACTERISTICS



b. BLEED-AIR FLOW REQUIREMENTS

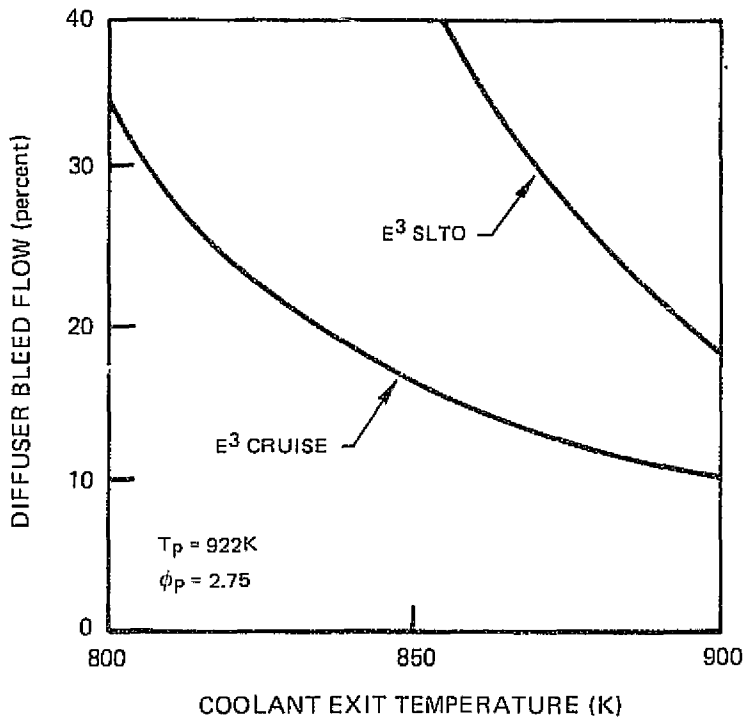


Figure 10. Characteristics of Fuel-Rich Pilot Stabilization System

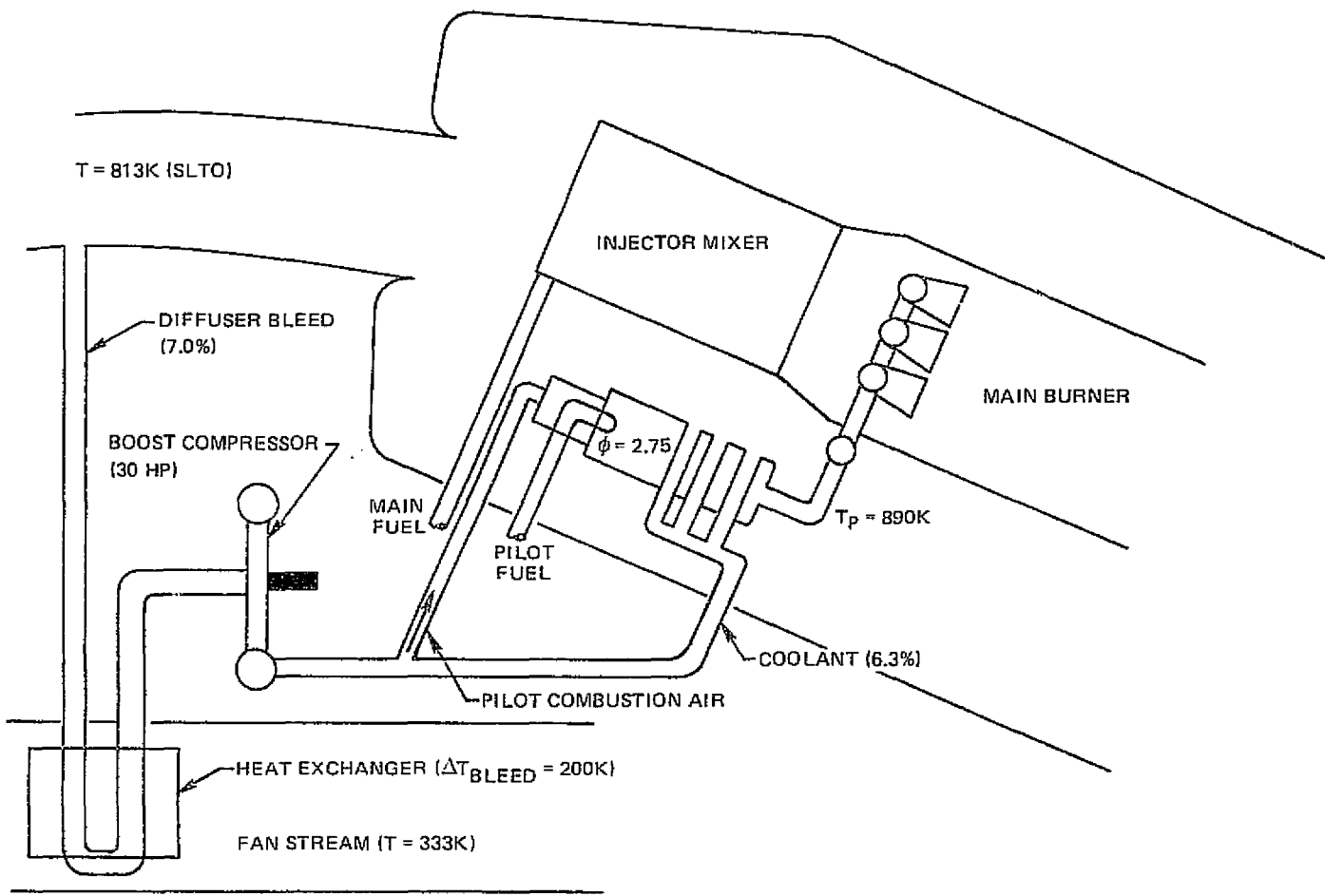


Figure 11. Supercharged, Fan-Air-Cooled, Fuel-Rich Pilot Flame Stabilizer

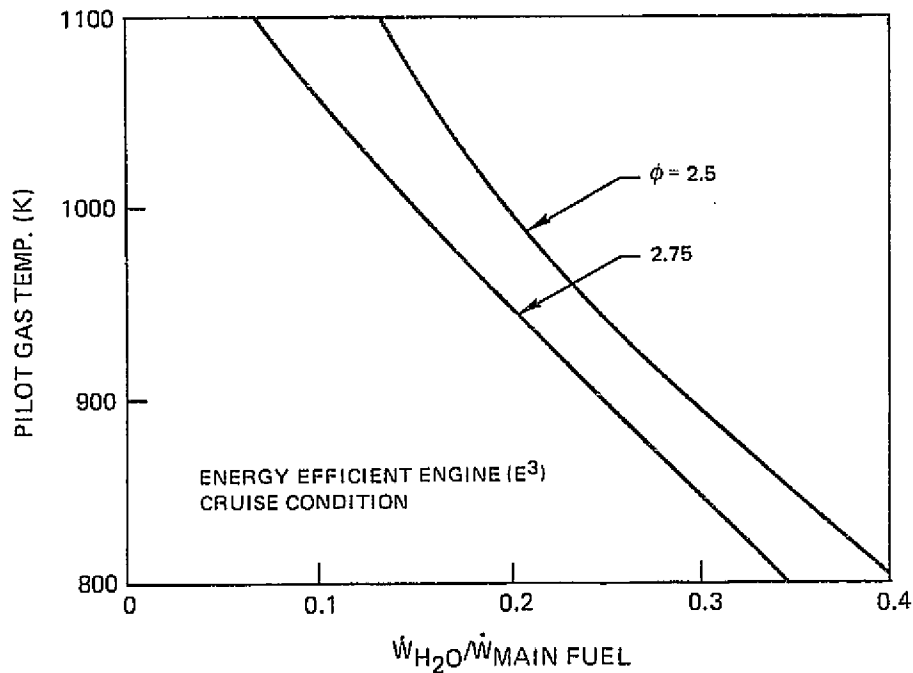
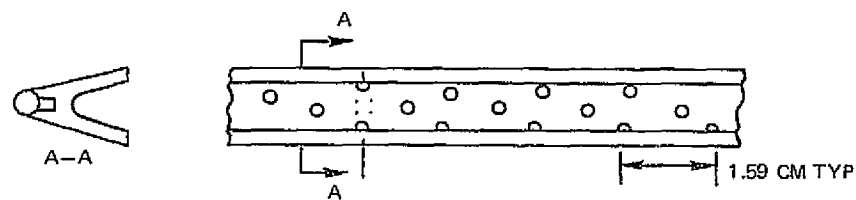
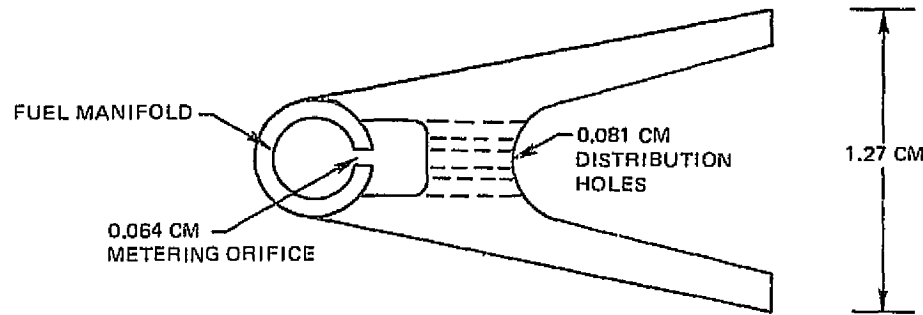


Figure 12. Pilot Quench-Water Requirements

ORIGINAL PAGE IS
OF POOR QUALITY



METERING ORIFICE SPACING = 13.3 CM

a. BAFFLE-DISTRIBUTED PILOT FUEL

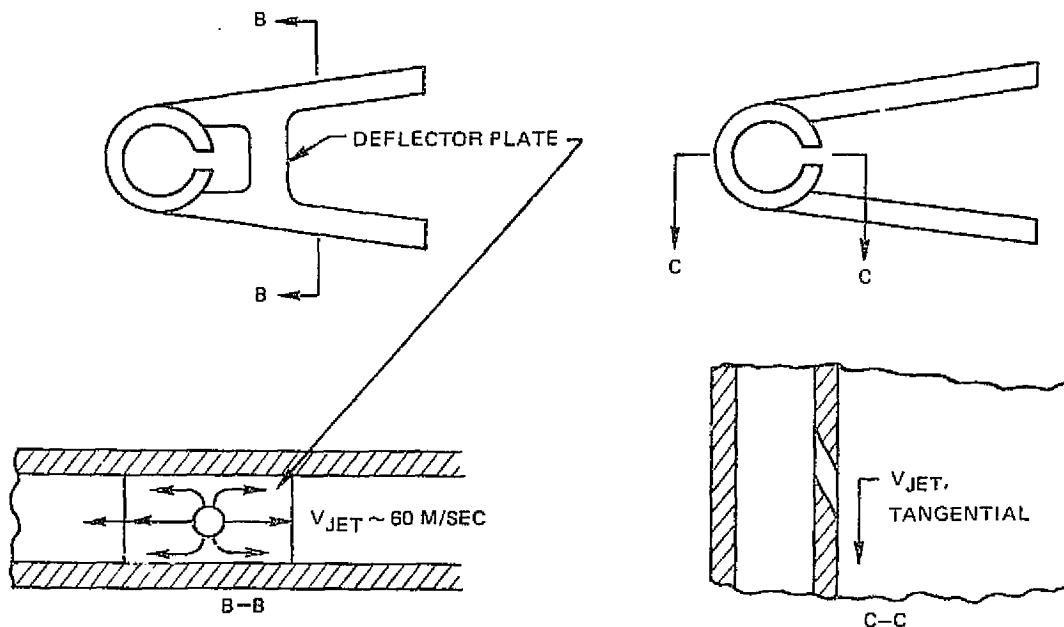


Figure 13. Pilot-Fuel Injected Flame Stabilizer

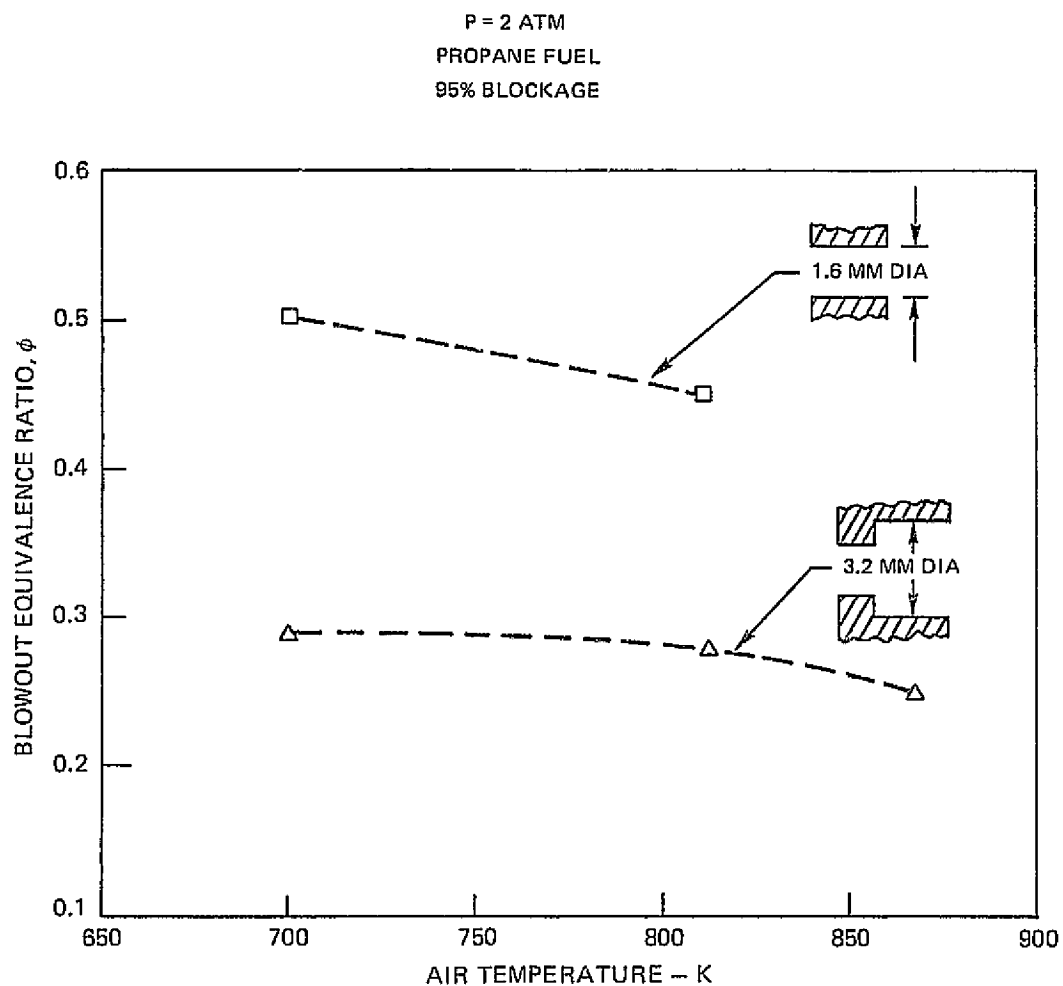


Figure 14. Effect of Recessing on Perforated Plate Stability Limits

ORIGINAL PAGE IS
OF POOR QUALITY

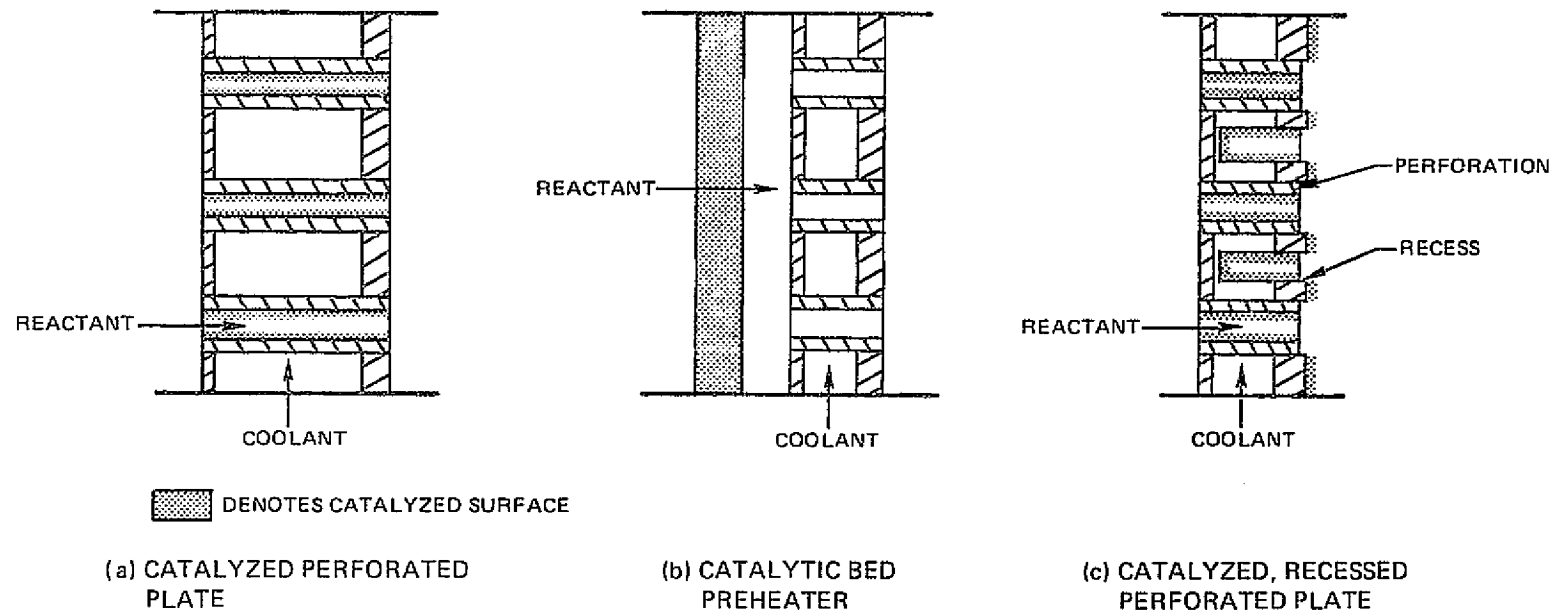


Figure 15. Catalytic Augmentation Concepts

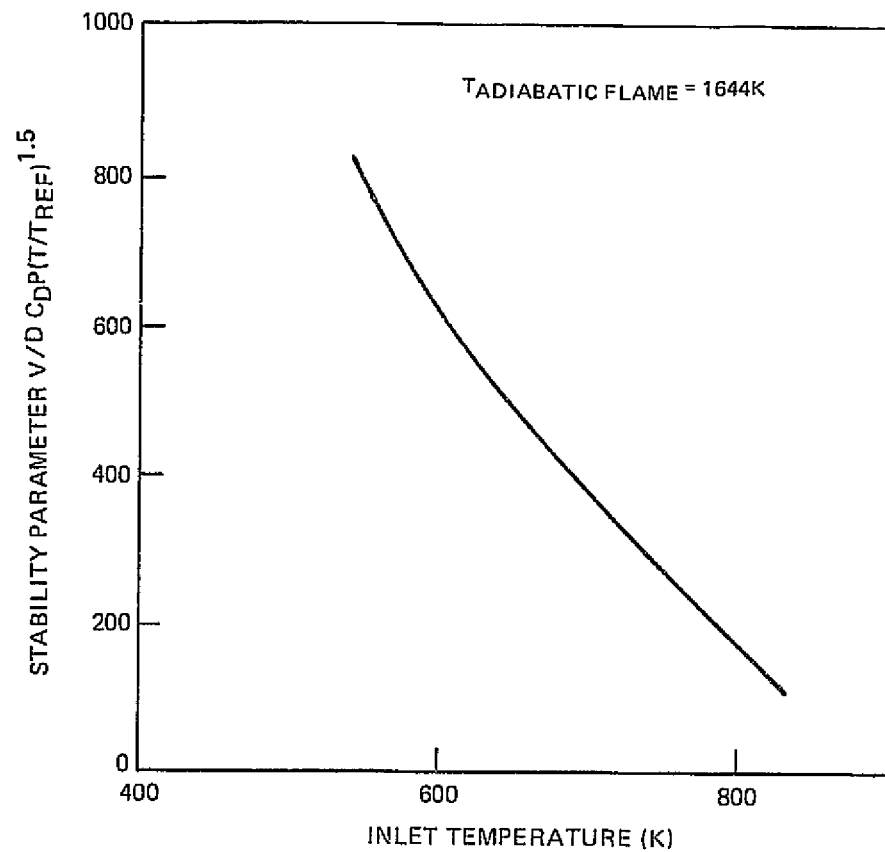


Figure 16. Effect of Inlet Temperature — Temperature Rise Tradeoff on Stability Limits

ORIGINAL PAGE IS
OF POOR QUALITY

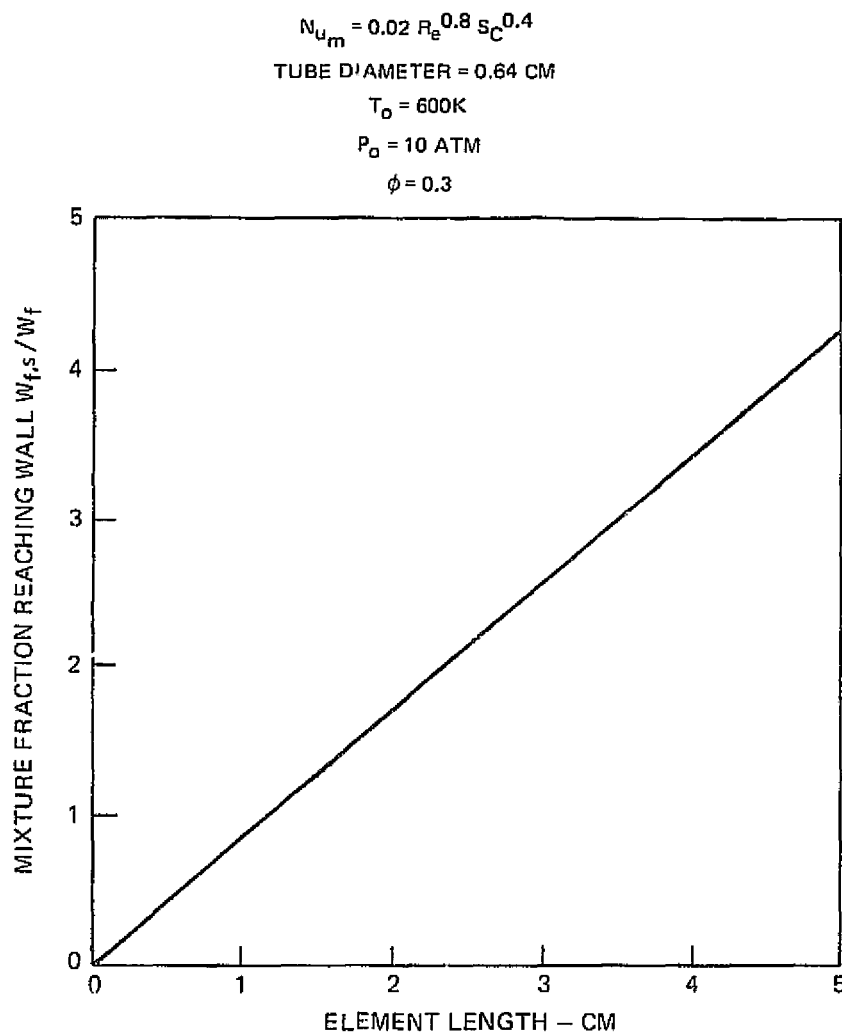


Figure 17. Fraction of Flow Contacting Surface of Catalyzed Tube Combustor

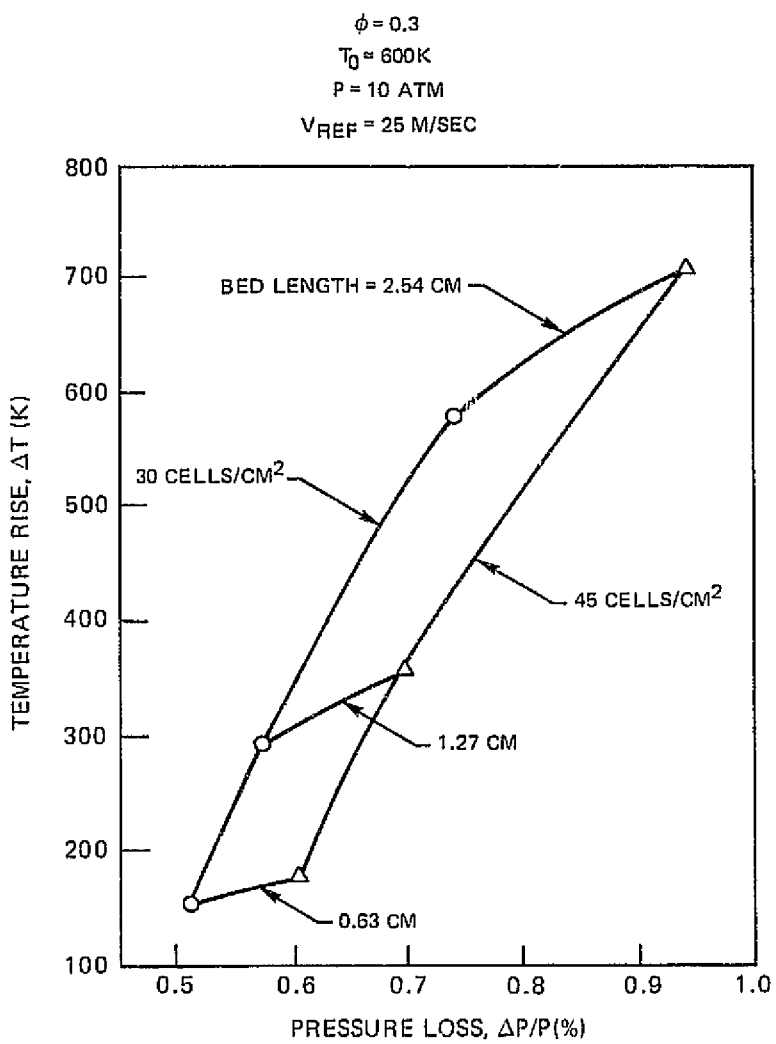
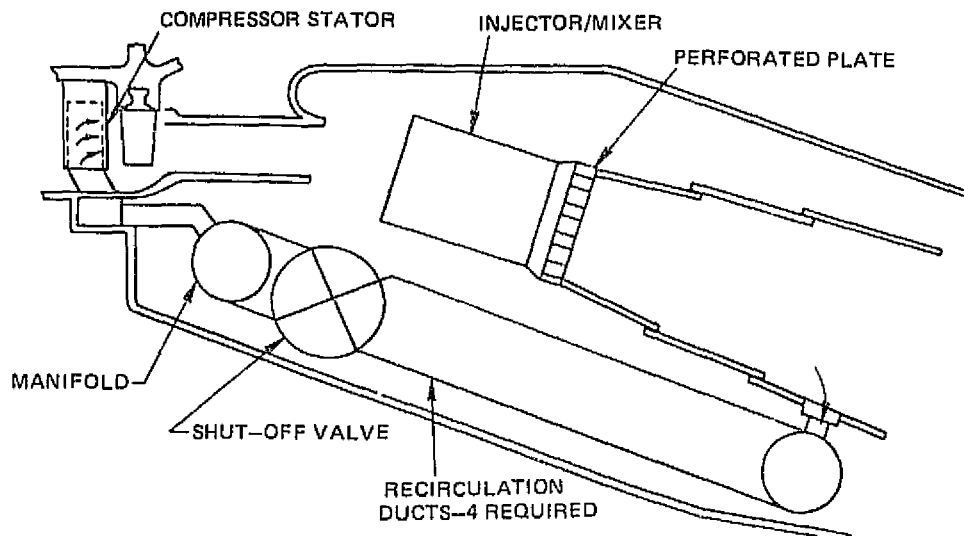


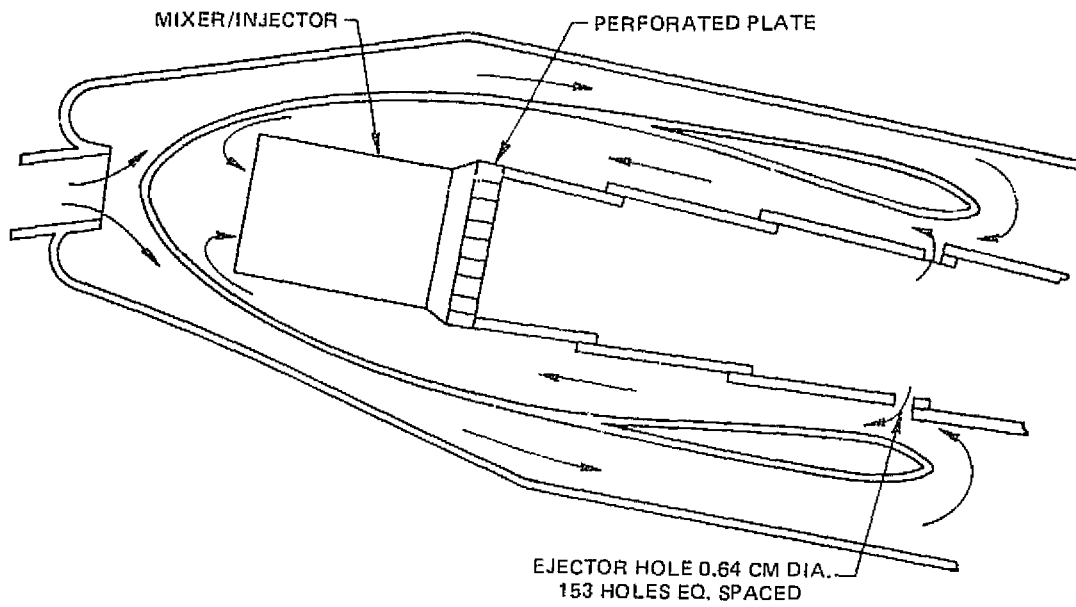
Figure 18. Catalytic Preheat Bed Characteristics

ORIGINAL PAGE IS
OF POOR QUALITY

a) COMPRESSOR-RECIRCULATED PRIMARY GAS



b) EJECTOR-RECIRCULATED PRIMARY GAS



c) REGENERATIVELY-HEATED COMBUSTOR INLET AIR

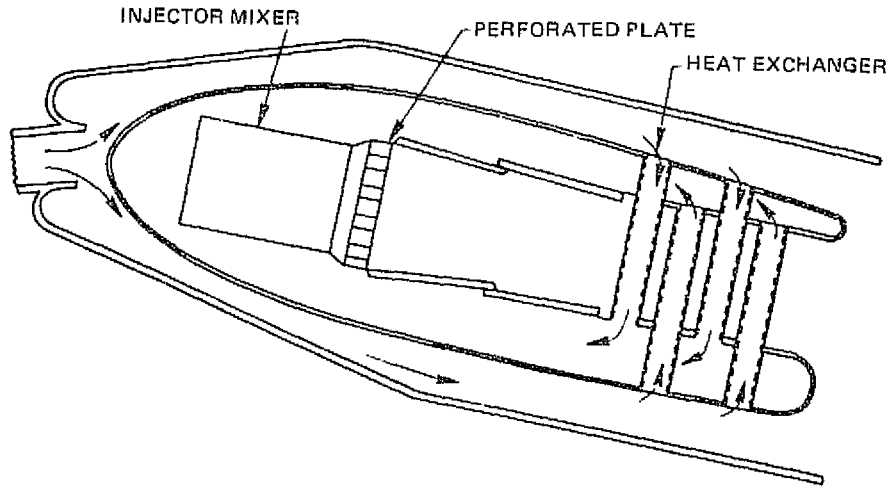


Figure 19. Heat Recirculation Stability Augmentation Concept

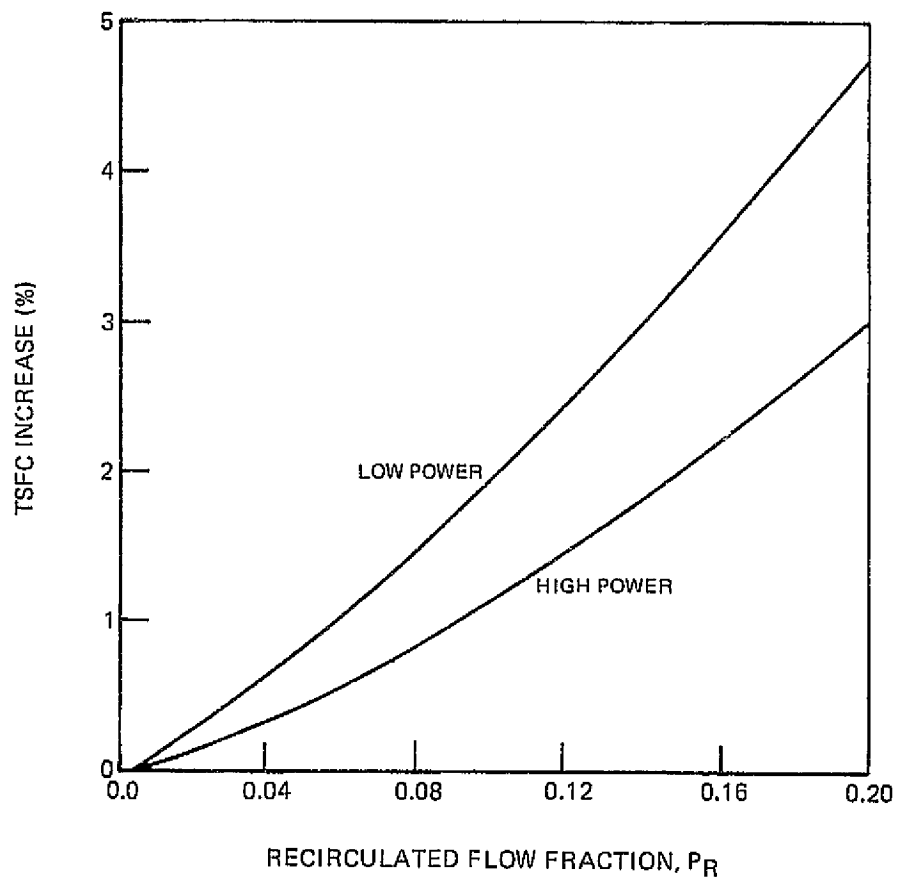


Figure 20. Effect of Pumping of Recirculated Flow on Engine Fuel Consumption

JOURNAL PAGE IS
OF POOR QUALITY

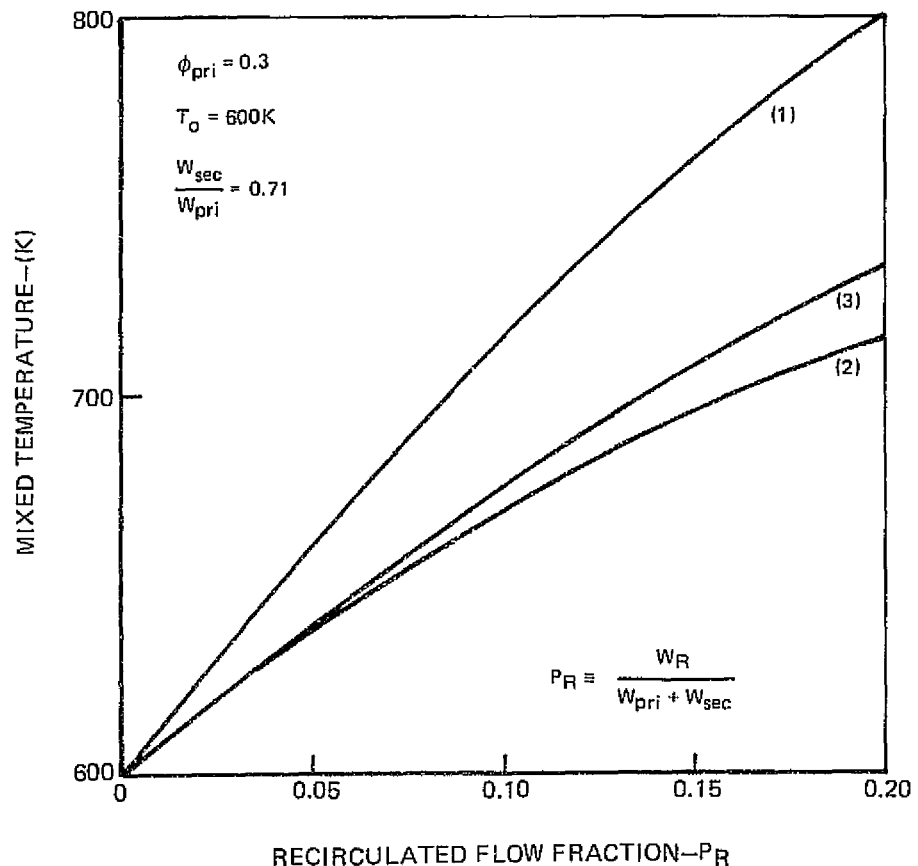
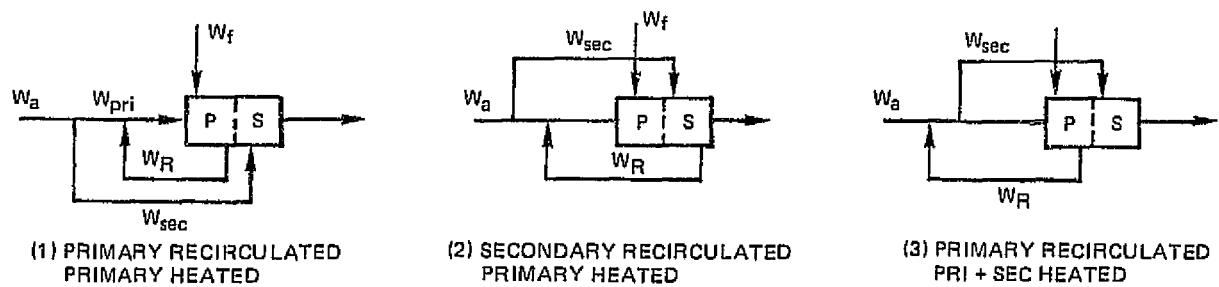


Figure 21. Effect of Flow Recirculation on Mixed Gas Temperature

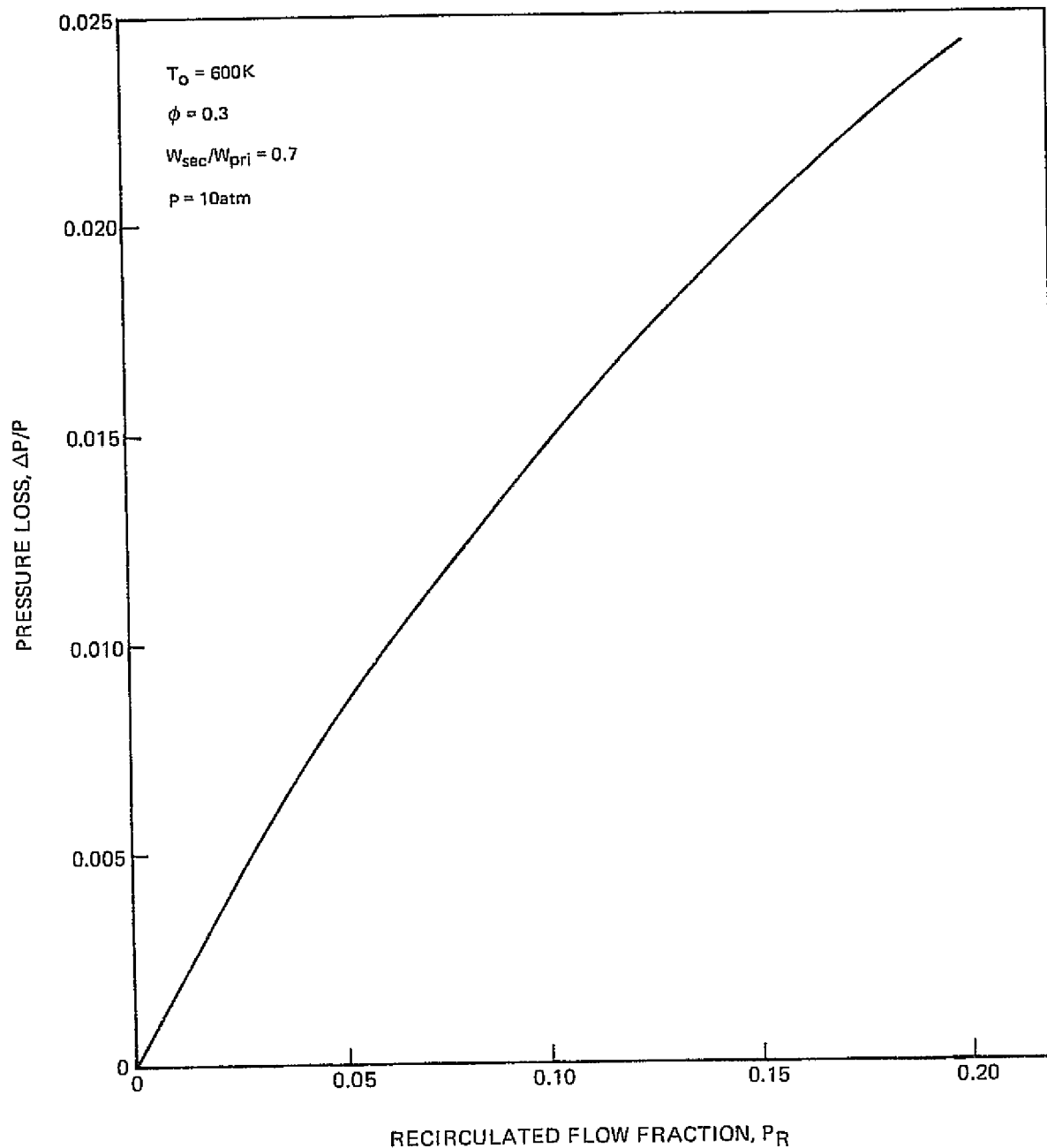


Figure 22. Pressure Loss for Ejector—Recirculated Primary Flow

ORIGINAL PAGE IS
OF POOR QUALITY

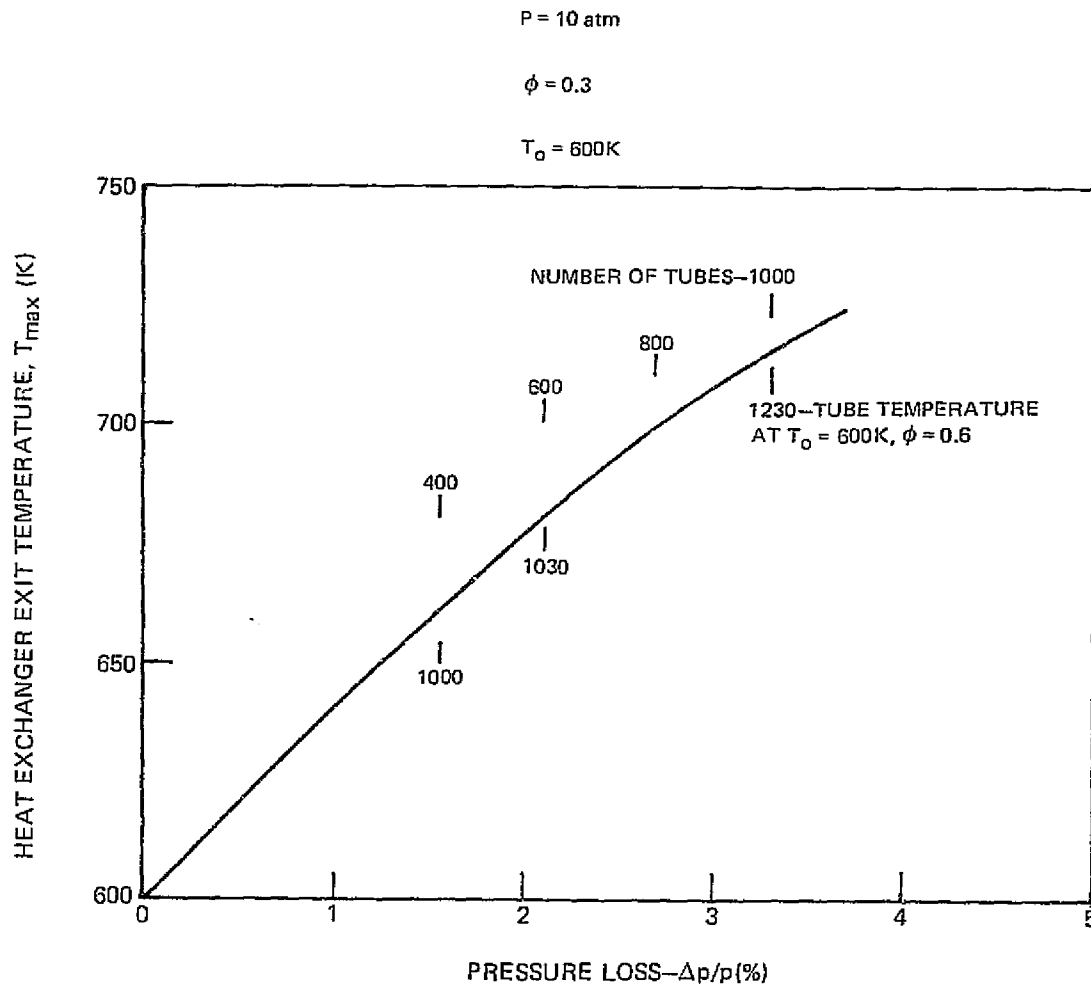


Figure 23. Performance Characteristics of a Compact Regenerative Heat Exchanger

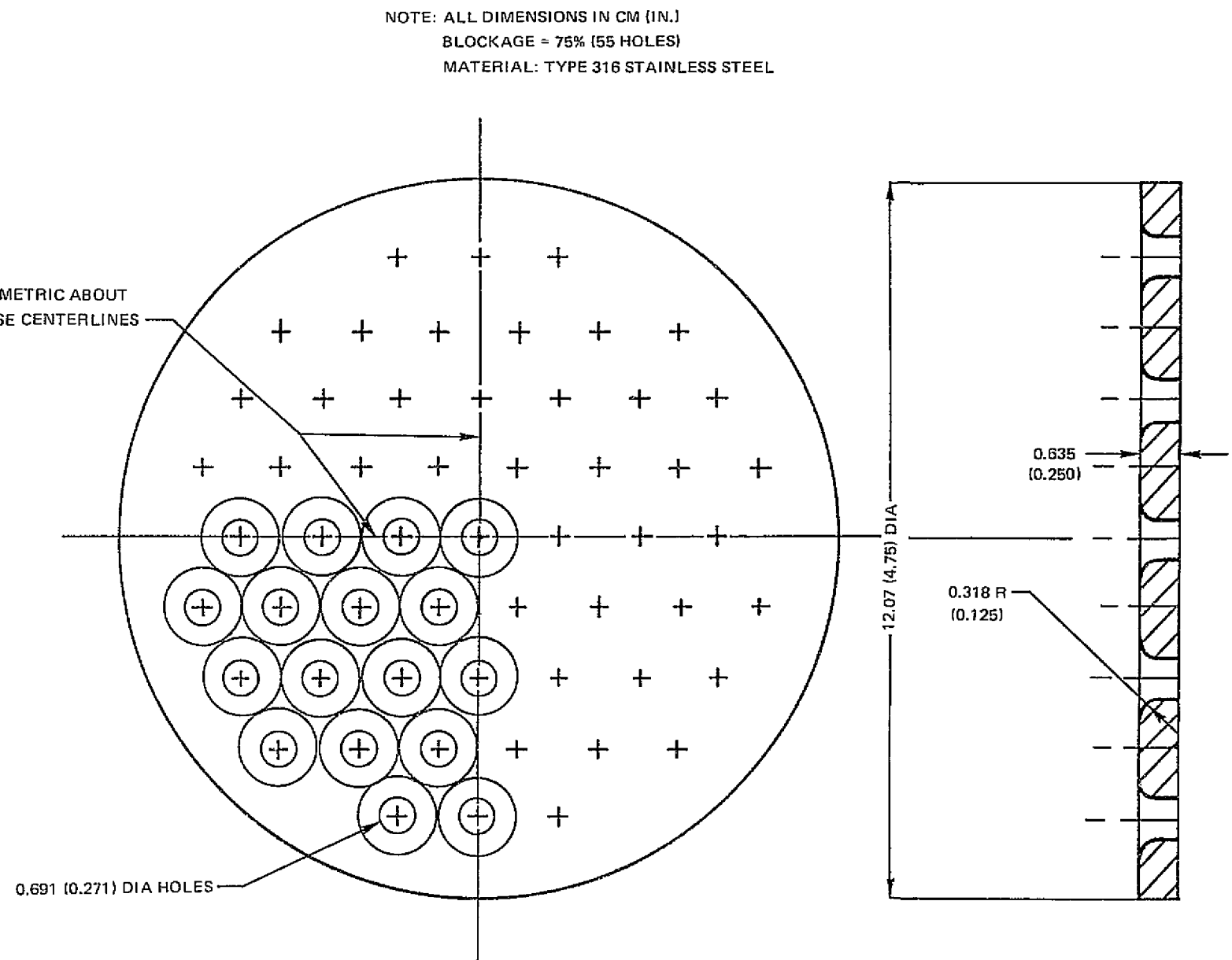


Figure 24. Baseline Flameholder Configuration

FIGURE 24
PAGE 12
OF POOR QUALITY

7B-03-286-1

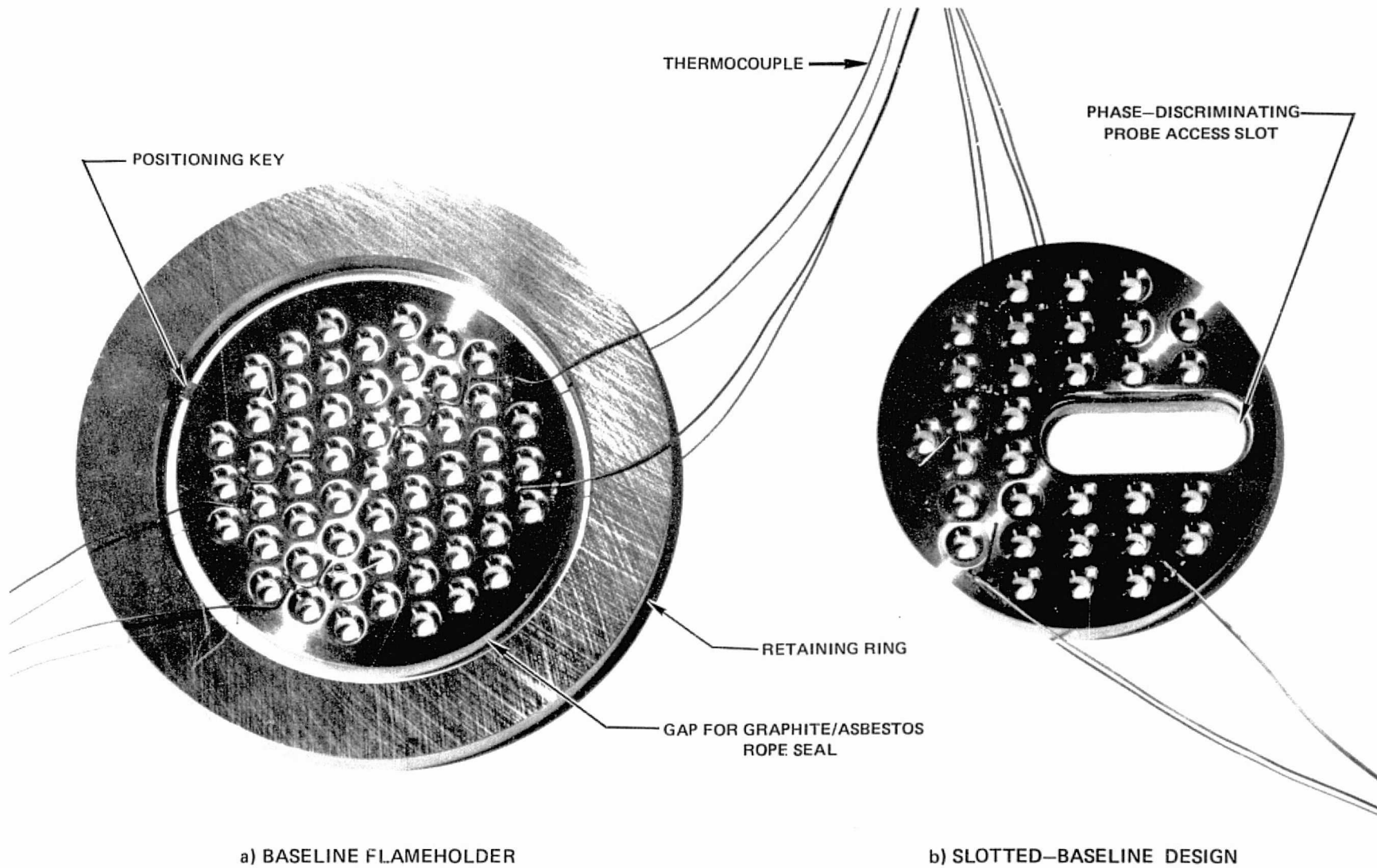
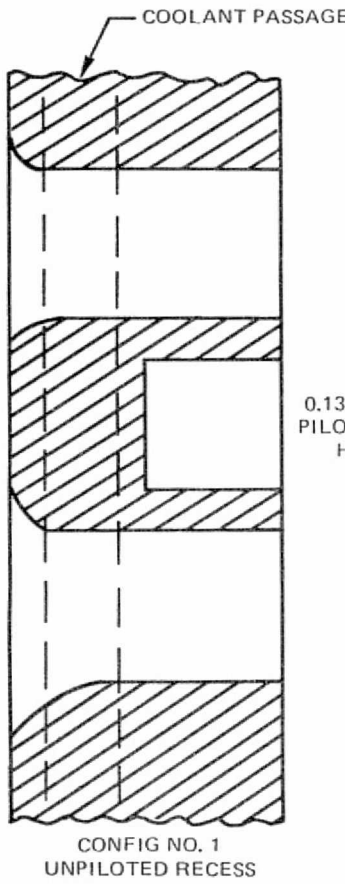
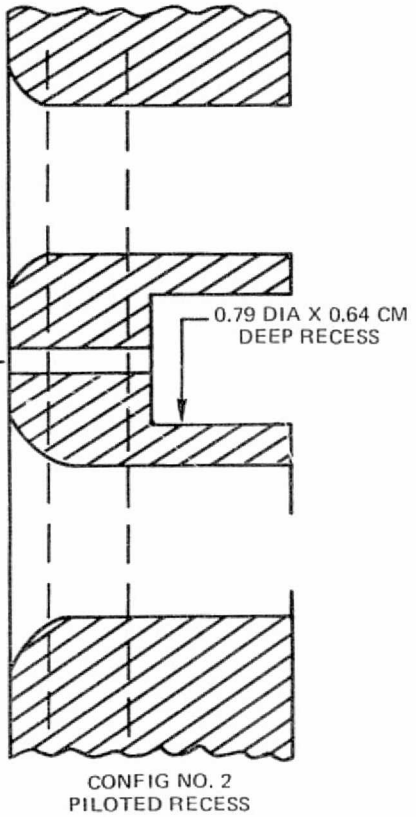


Figure 25. Baseline Flameholder and Retaining Ring

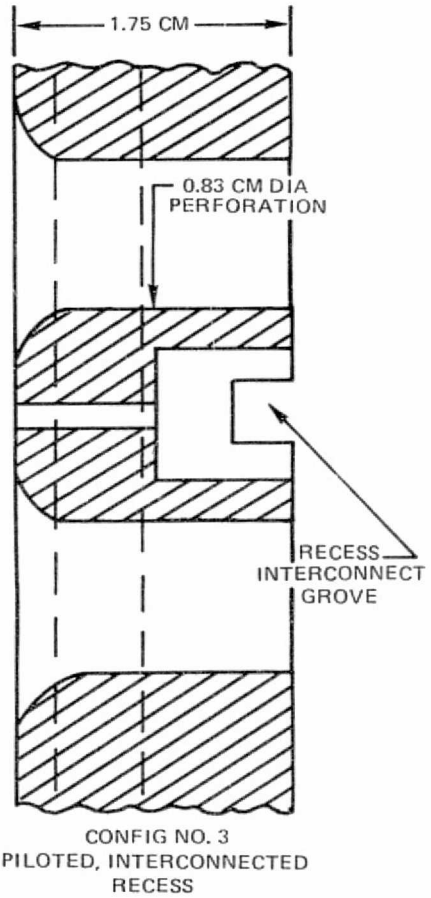
**ORIGINAL PAGE IS
OF POOR
QUALITY**



0.13 CM DIA
PILOT/BLEED
HOLE

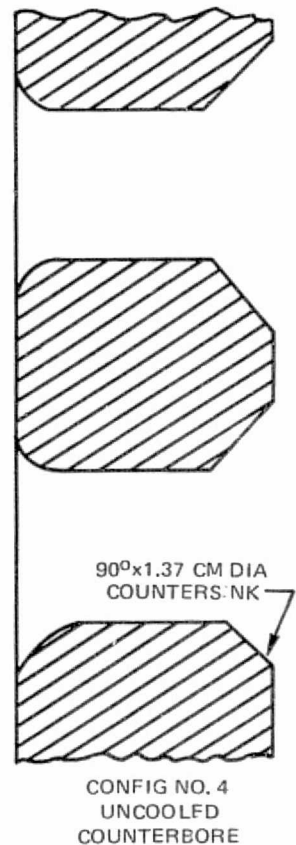


0.79 DIA X 0.64 CM
DEEP RECESS



1.75 CM

0.83 CM DIA
PERFORATION



90°x1.37 CM DIA
COUNTERBORE

Figure 26 Self-Piloting Recessed Perforated Plate Flameholders

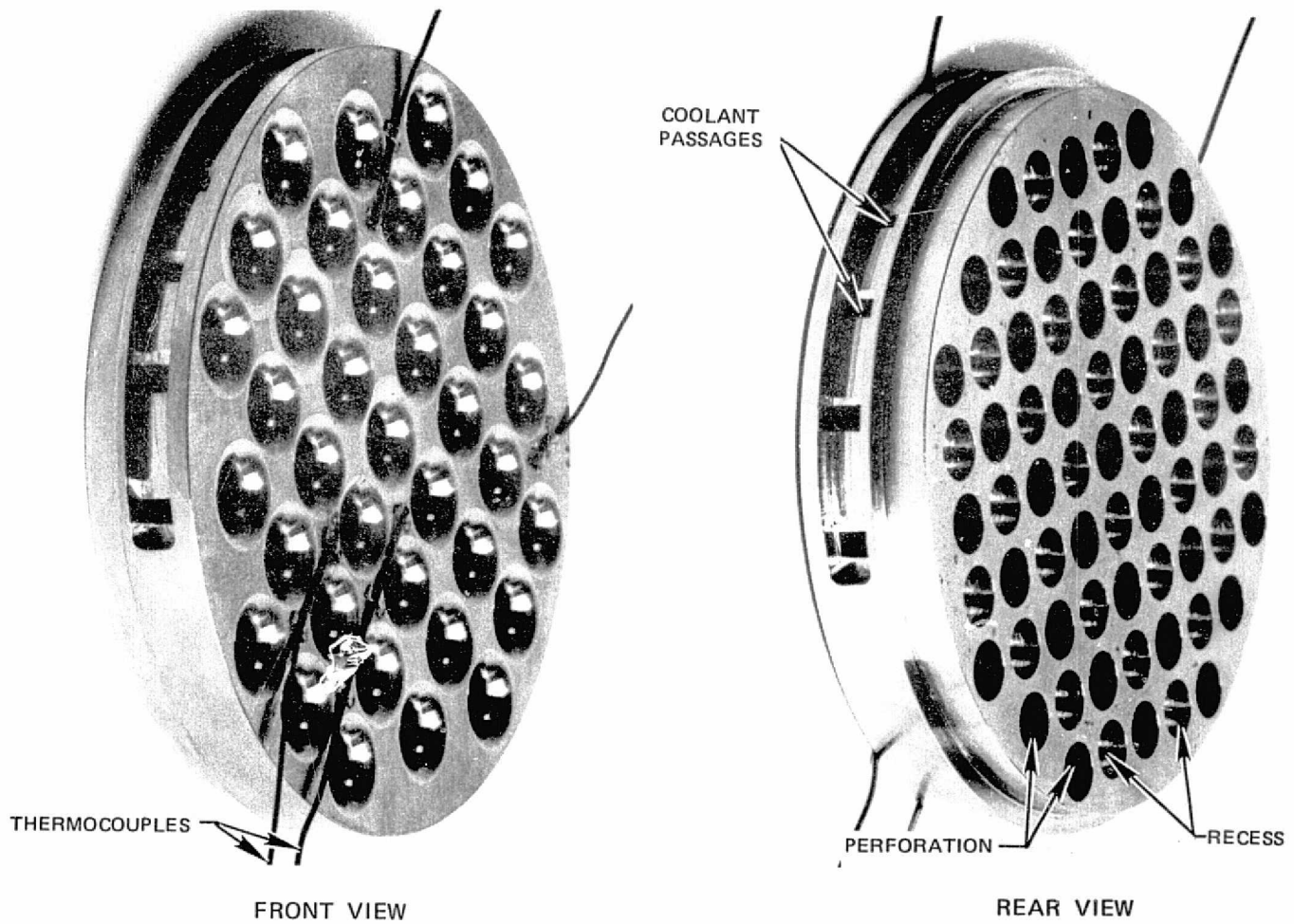


Figure 27. Photograph of Recessed Self-Piloting Perforated Plate Flameholder, SPRPP-1

ORIGINAL
PRINTED
BY
POOR
QUALITY

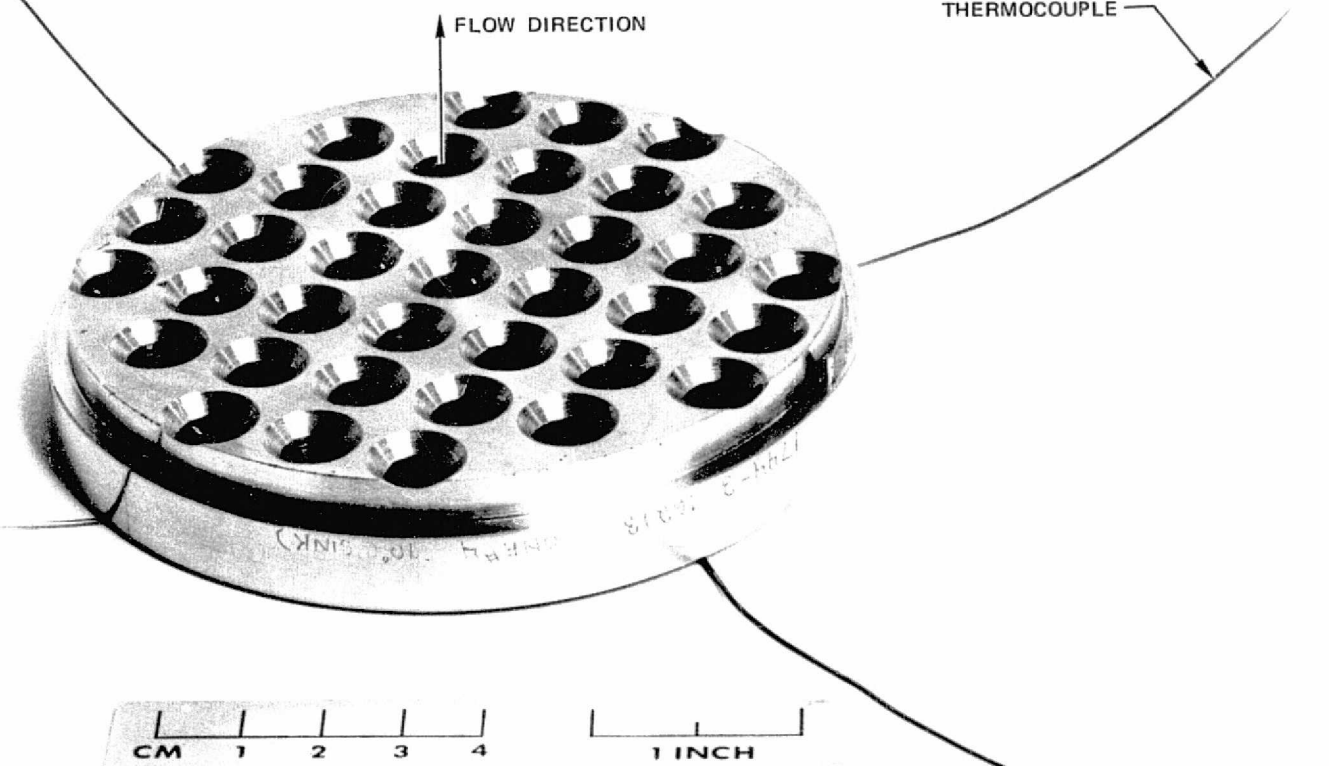


Figure 28. Counterbored Perforated Plate, SPRPP-4

NOTE: ALL DIMENSIONS IN CM

80% BLOCKAGE

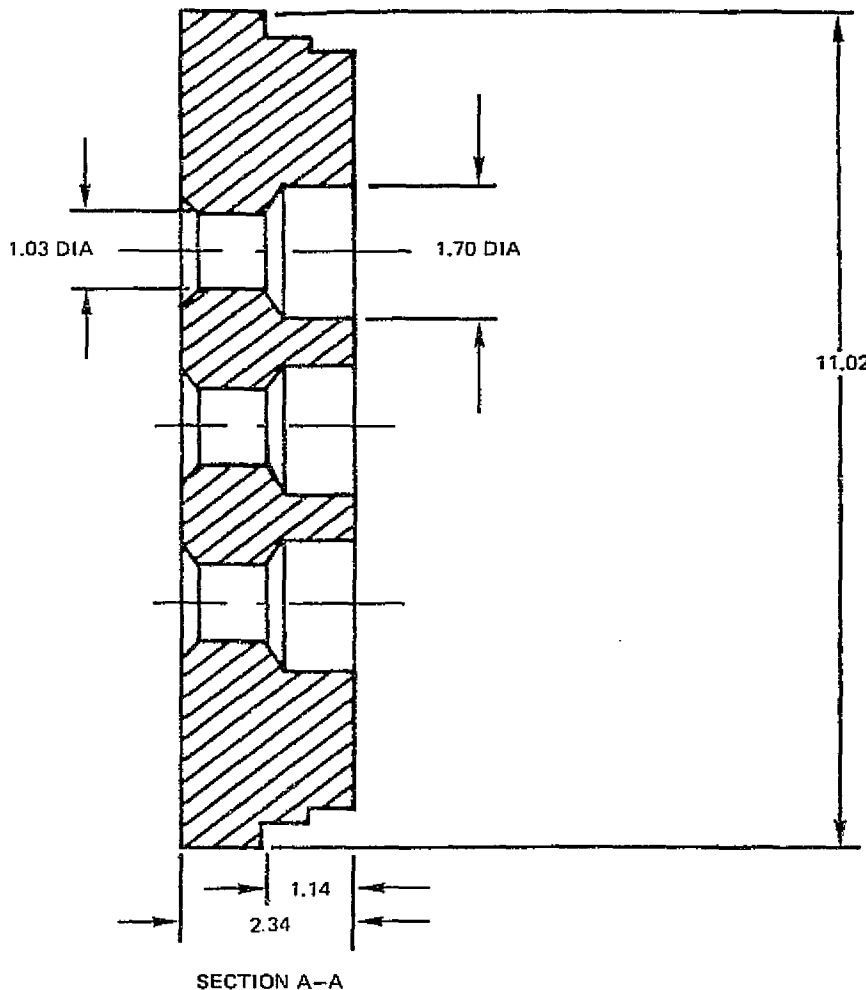
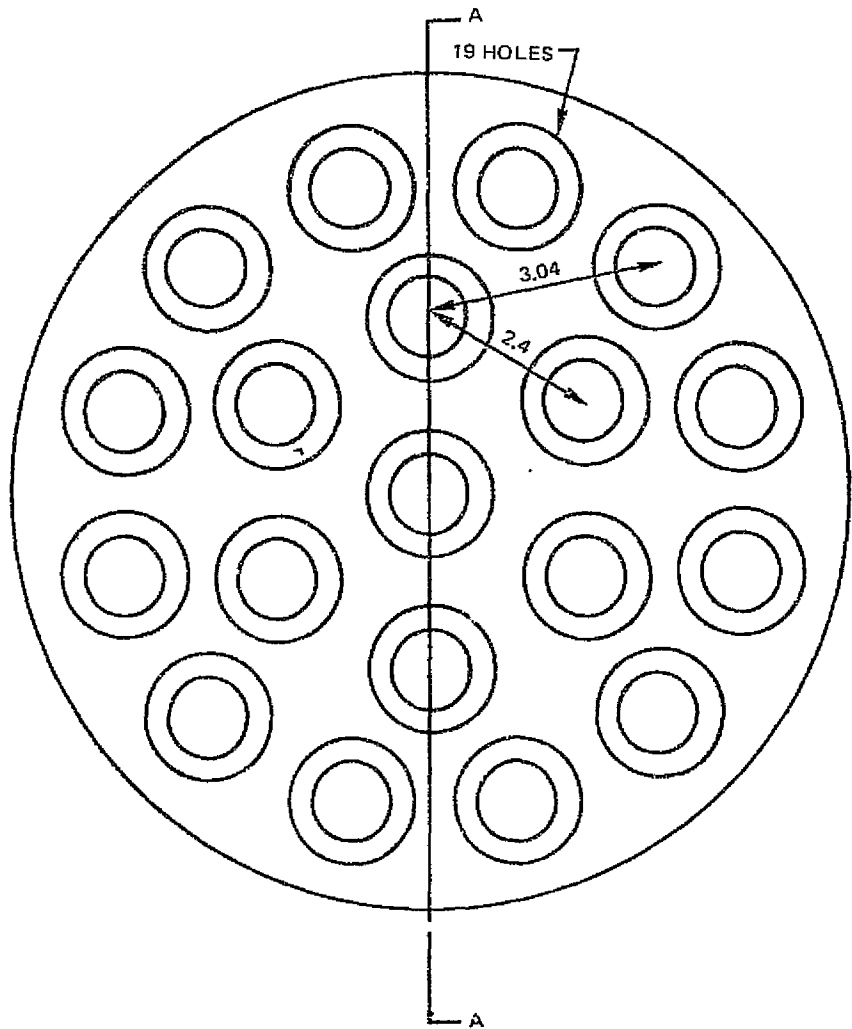
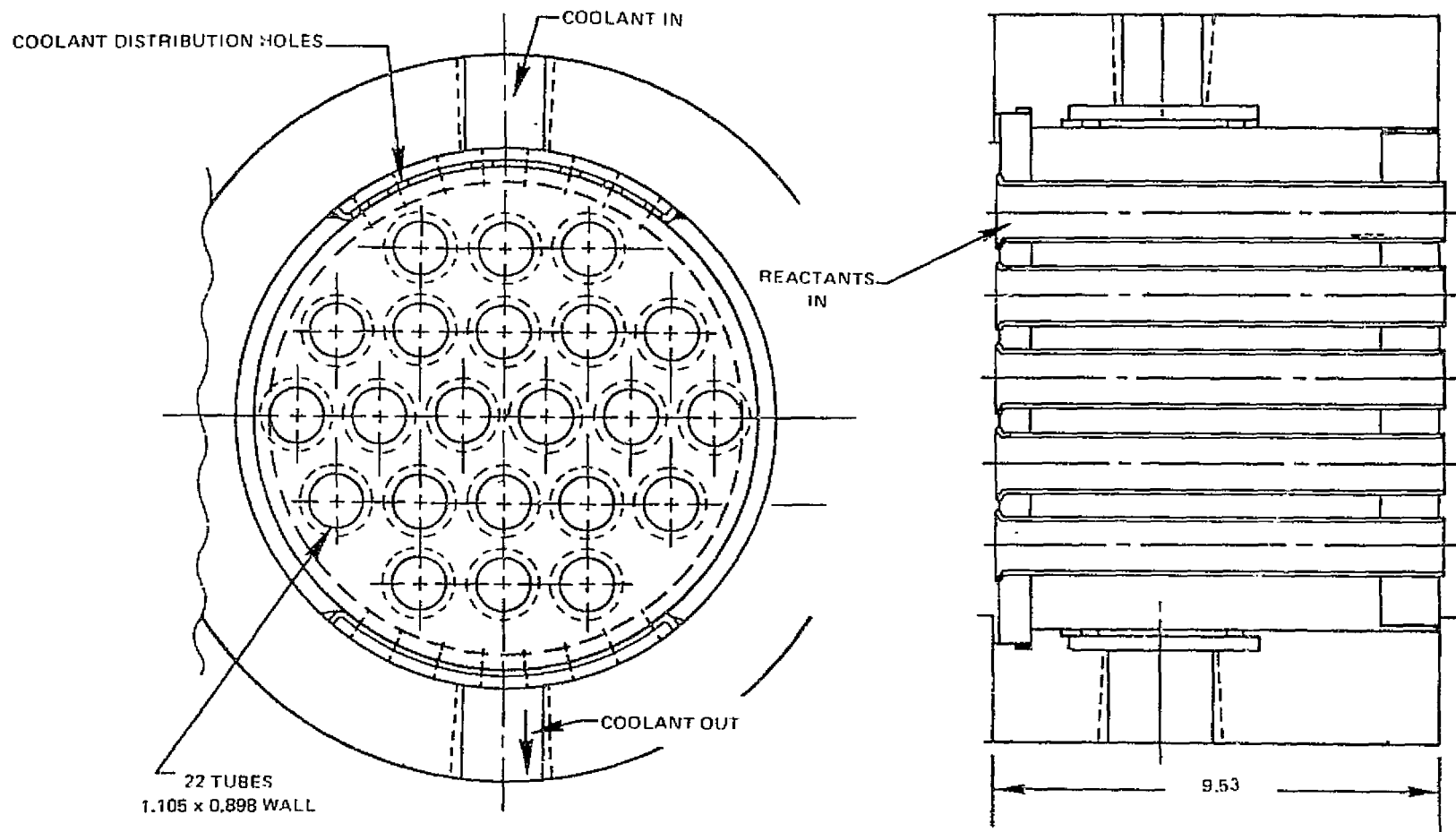


Figure 29. Self-Piloting Recessed Perforated Plate Final Design, SPRPP-F



CONFIGURATION	CATALYZED SURFACES
CTF-1	TUBE ID, 8.9 CM, REAR PLATE
CTF-2	TUBE ID, 8.9 CM
CTF-3	TUBE ID, 4.45 CM
CTF-4	TUBE ID, 4.45 CM (HEATED)

Figure 30. Catalyzed Tube Flameholder Configurations

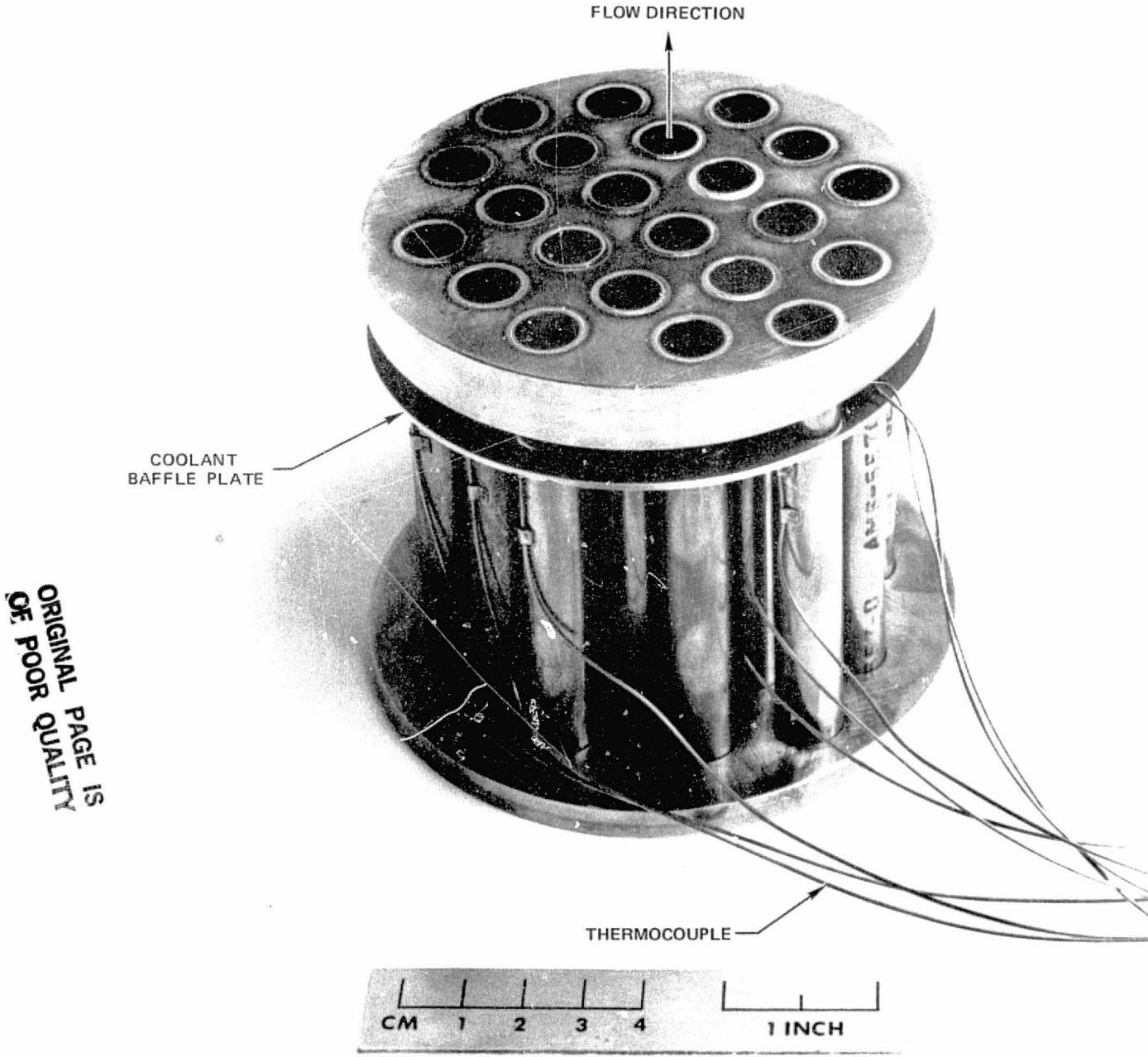


Figure 31. Catalyzed Tube Flameholder Plate — Tube Assembly

PAGE IS
ORIGINAL
OF POOR QUALITY

NOTE: ALL DIMENSIONS IN CM

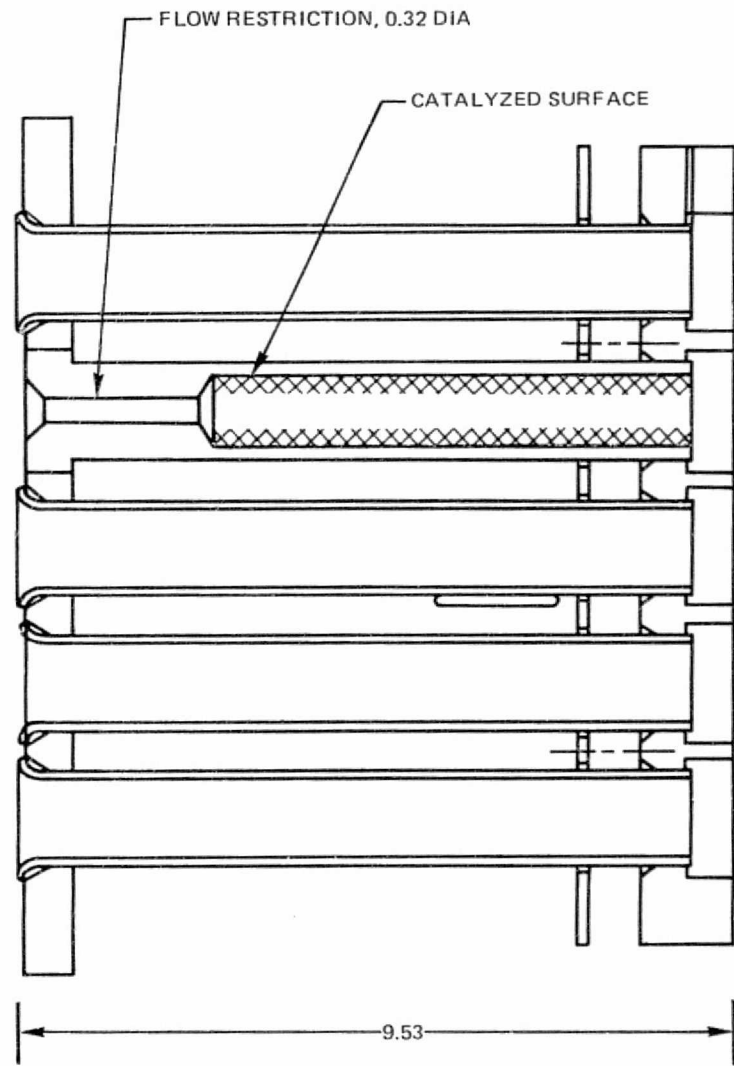
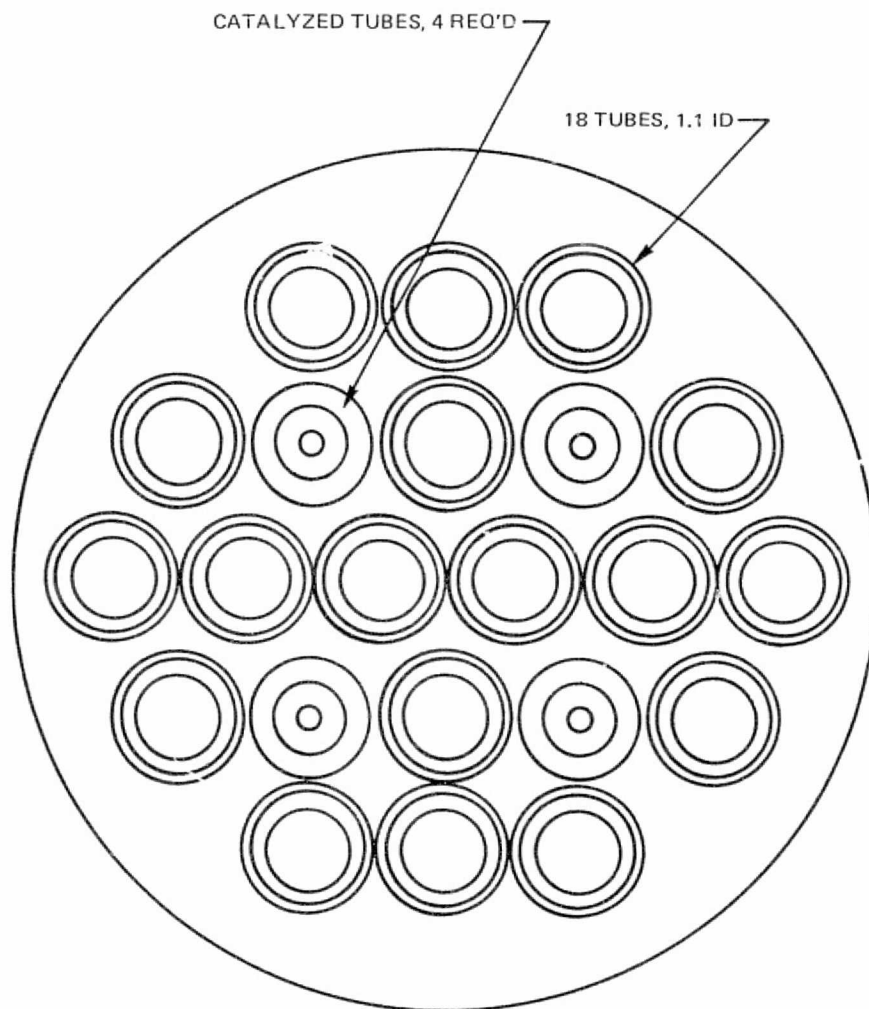
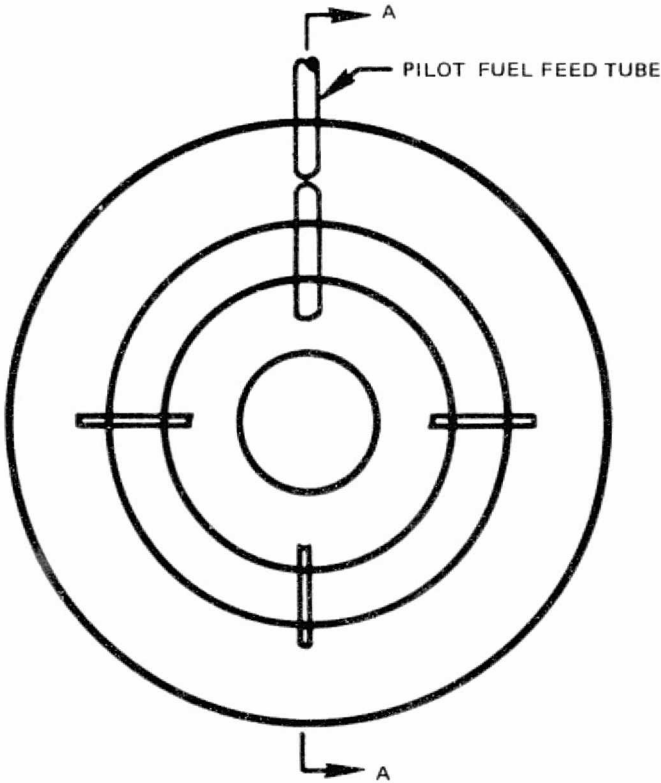


Figure 32. Catalyzed Tube Flameholder Final Design, CTF-F

ORIGINAL PAGE IS
OF POOR QUALITY



NOTE: ALL DIMENSIONS IN CM

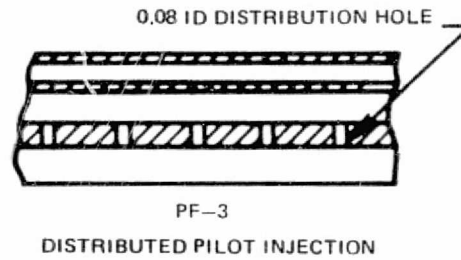
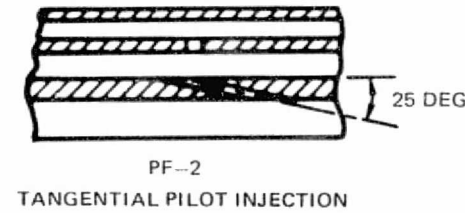
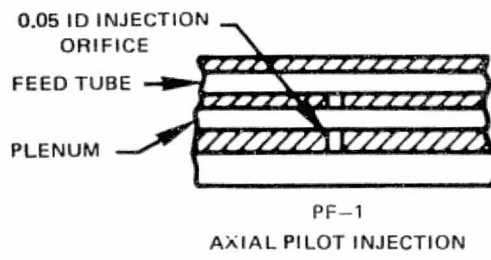
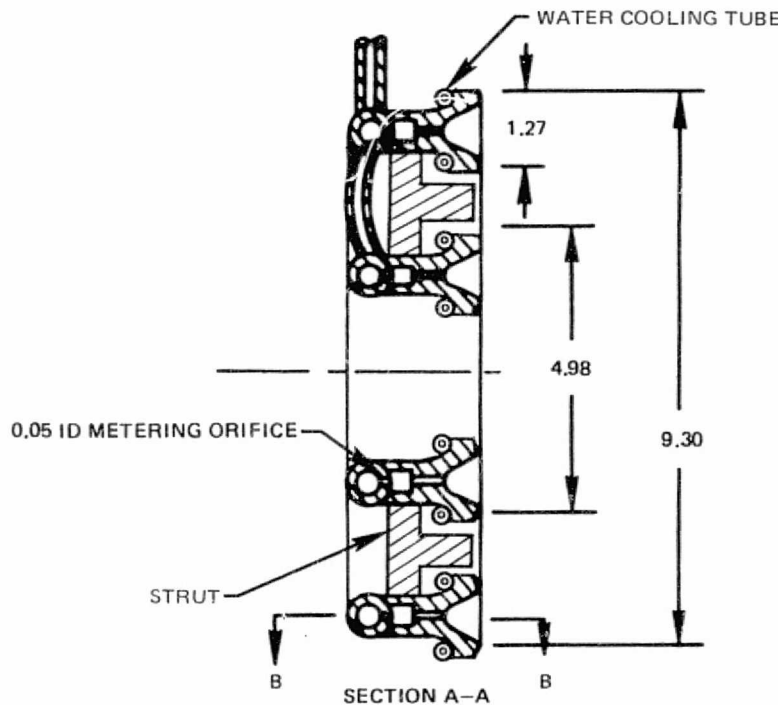
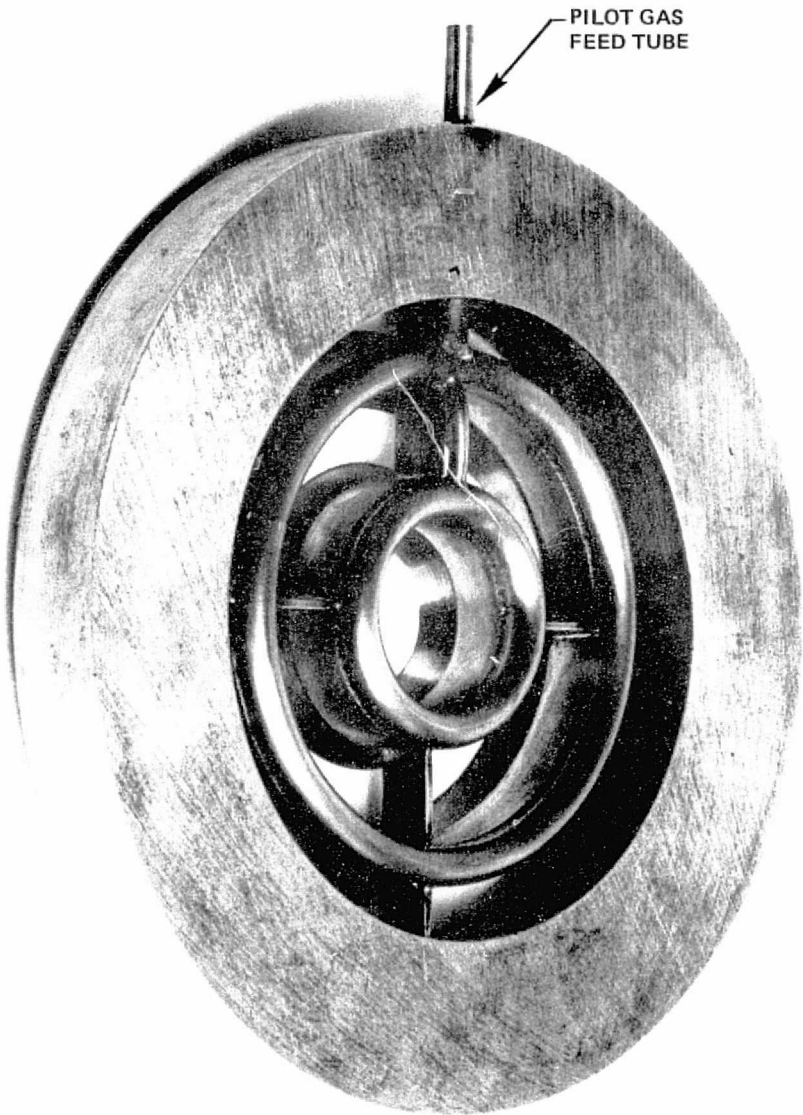
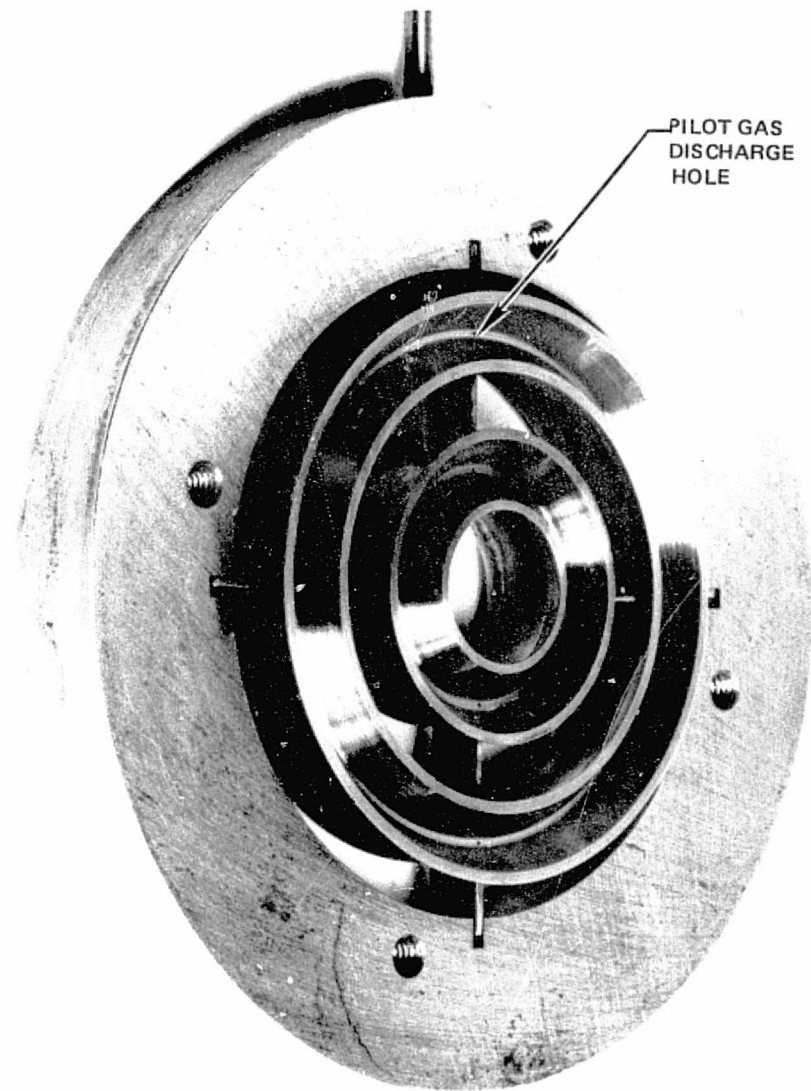


Figure 33. Piloted V-Gutter Flameholder Configurations



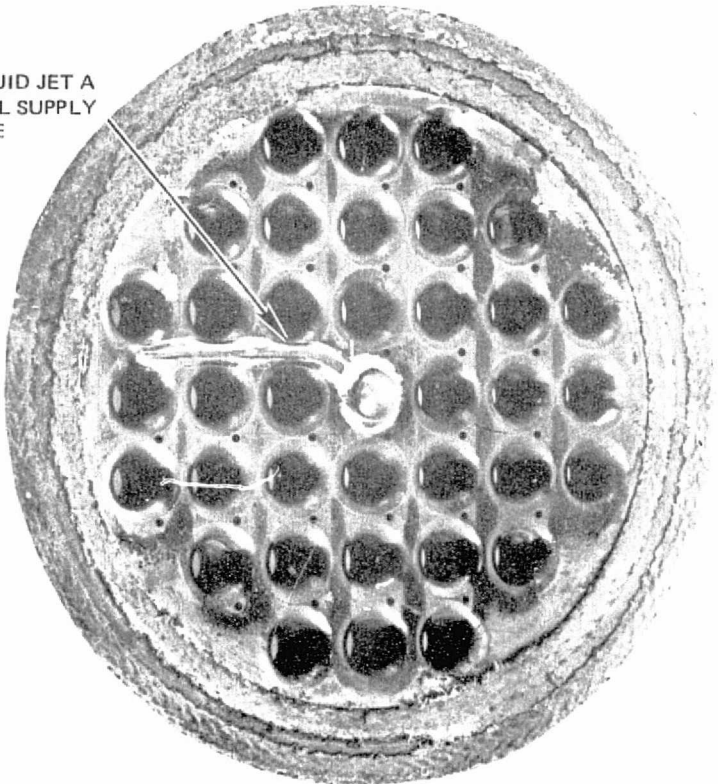
FRONT VIEW



REAR VIEW

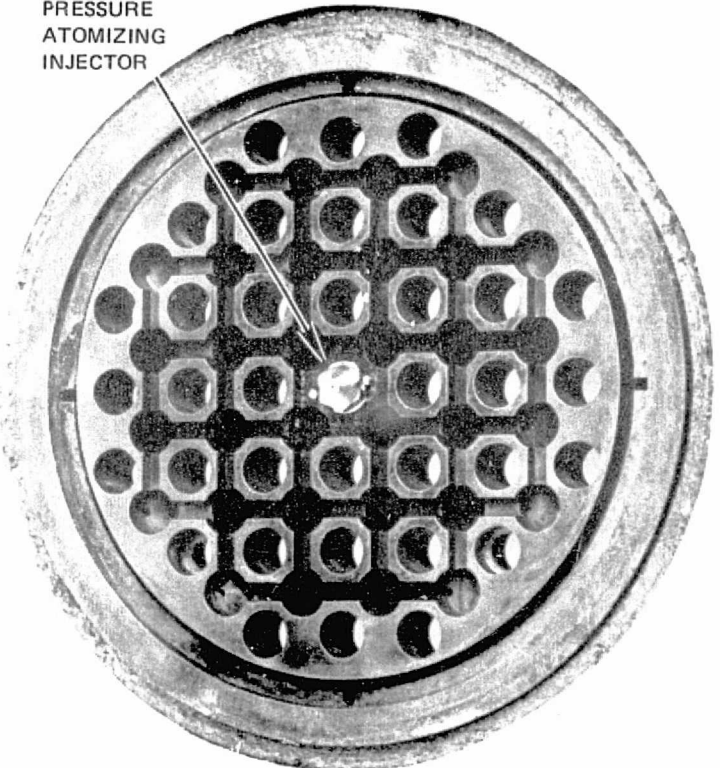
Figure 34. Uncooled Piloted V-Gutter Flameholder

LIQUID JET A
FUEL SUPPLY
LINE



FRONT VIEW

PRESSURE
ATOMIZING
INJECTOR



REAR VIEW

Figure 35. Piloted Perforated Plate Flameholder , PF-4

ORIGINAL PAGE IS
DE
POOR
QUALITY

BLOCKAGE = 75%
36 PILOT FUEL INJECTION SITES

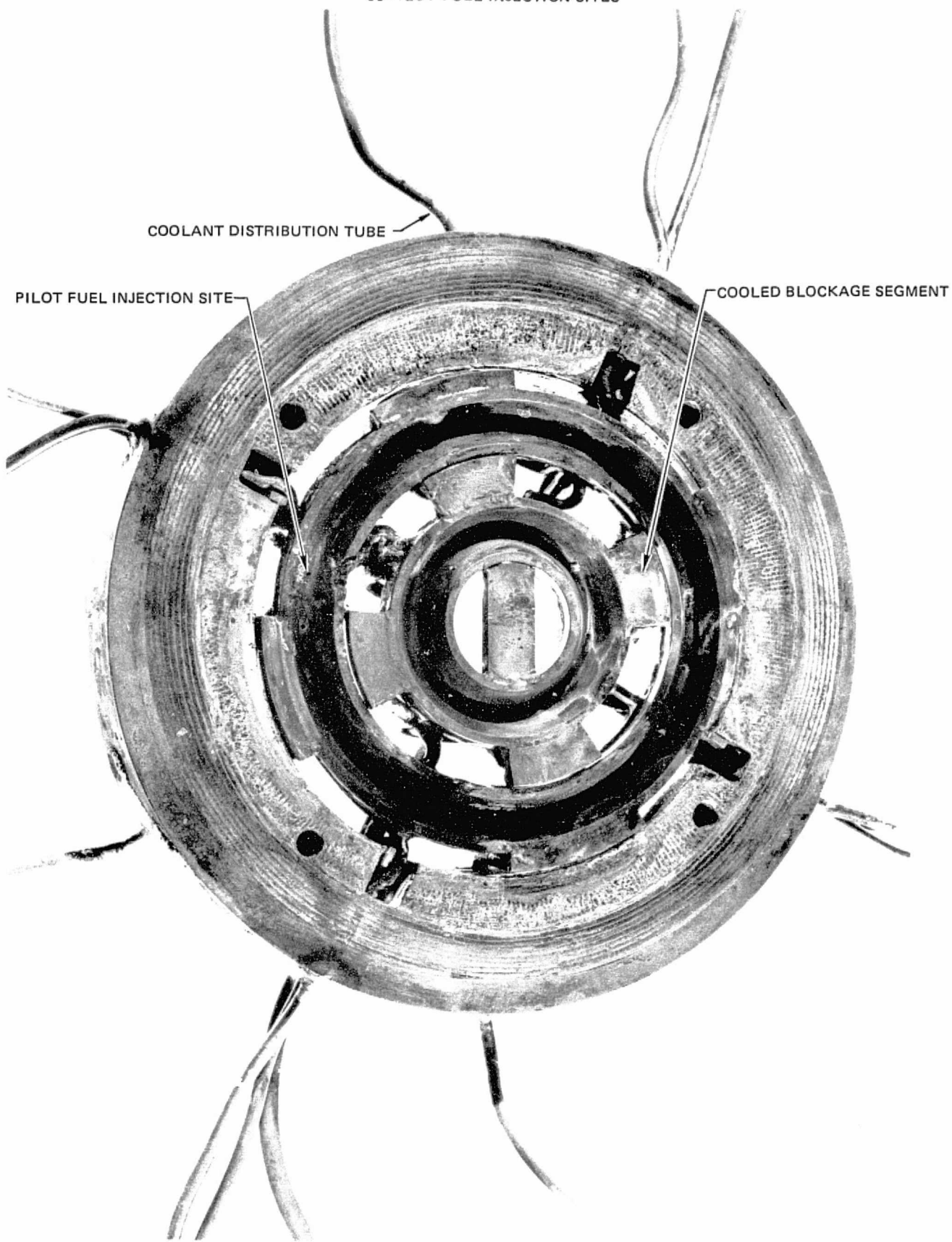
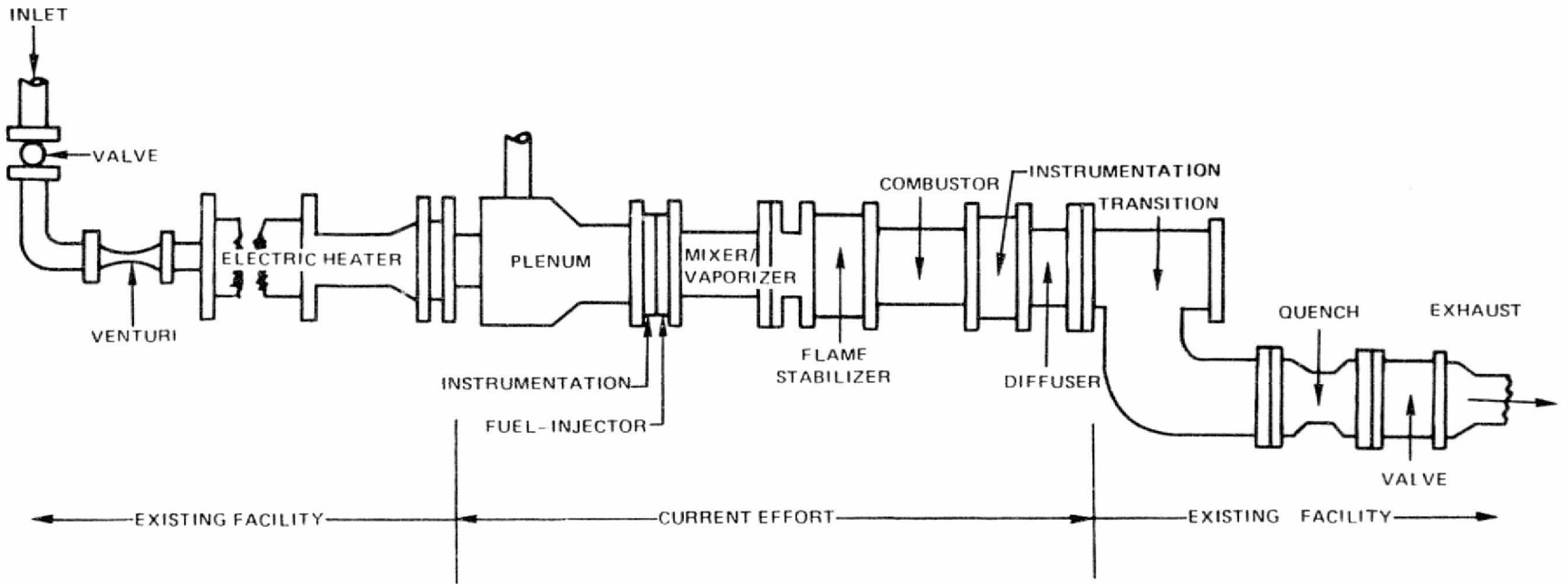


Figure 36. Piloted Flameholder Final Design PF-F

78-12-186-1
78-410-B



ORIGINAL PAGE IS
OF POOR QUALITY

Fig. 37. Lean Stability Augmentation Study Test Facility.

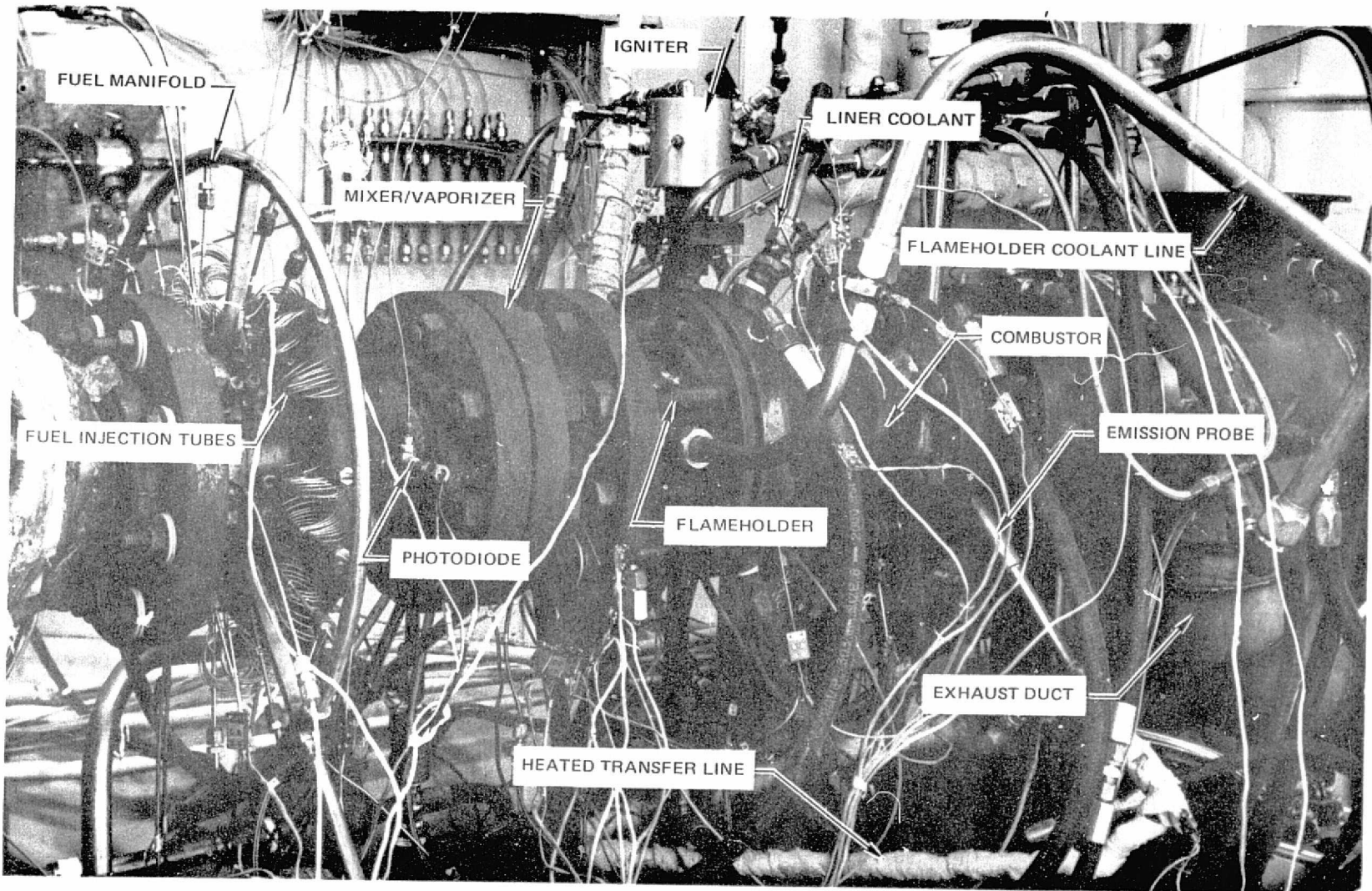


Figure 38. Lean-Premixing/Prevaporizing Combuster Test Apparatus

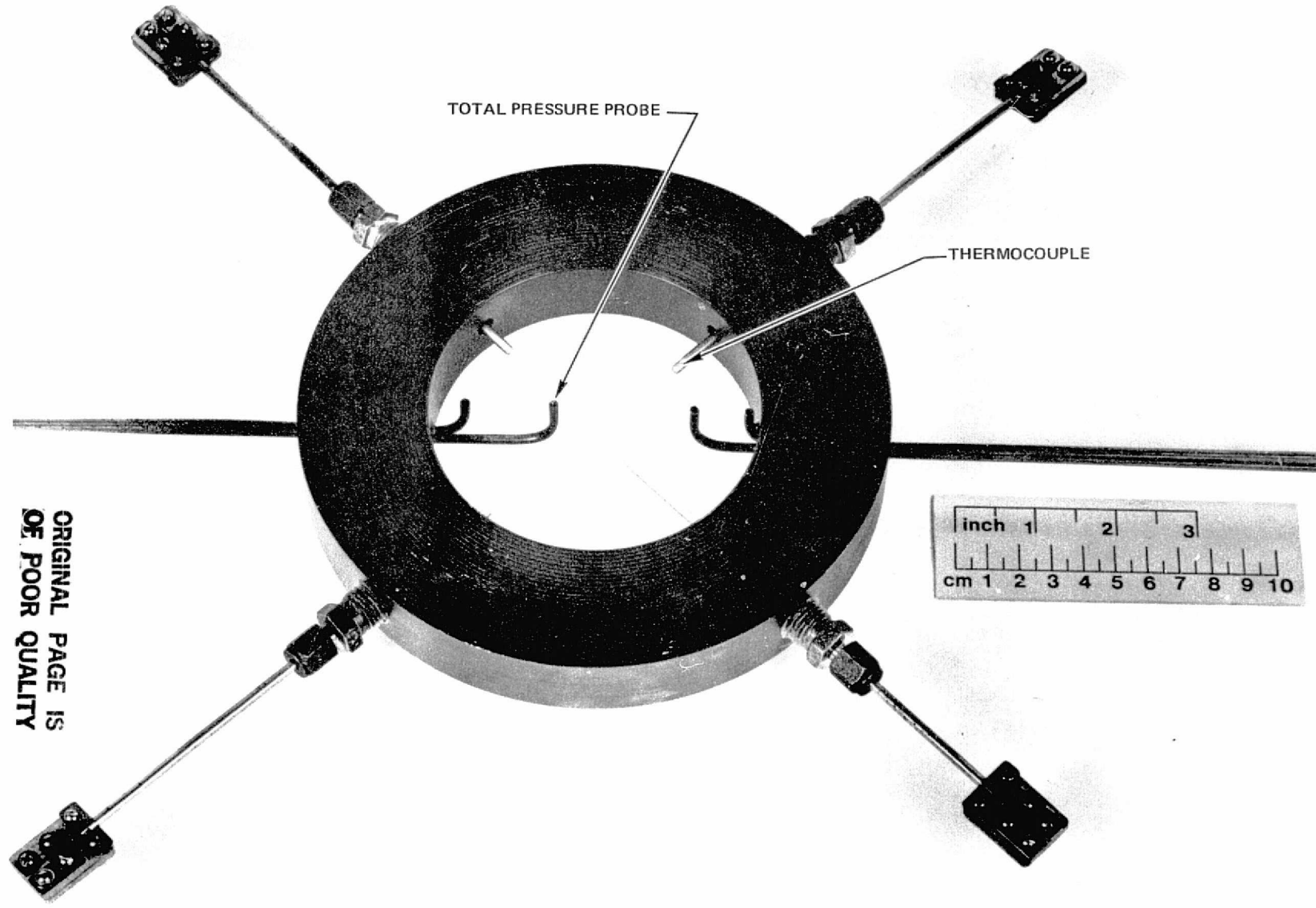


Fig. 39. Instrumentation Section—Fuel Injector Entrance Station.

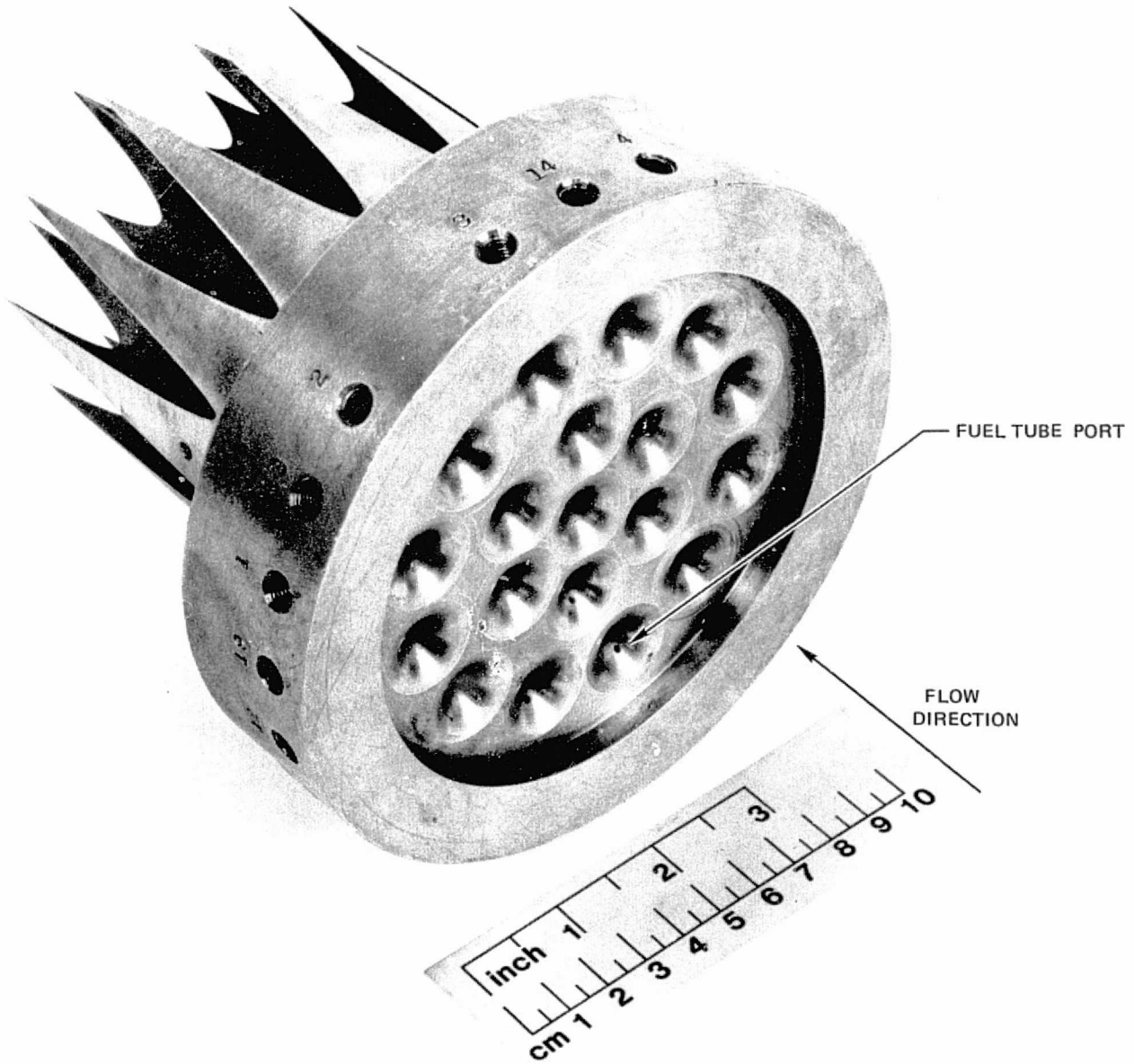


Fig. 40. Fuel Injector—Airflow Nozzle.

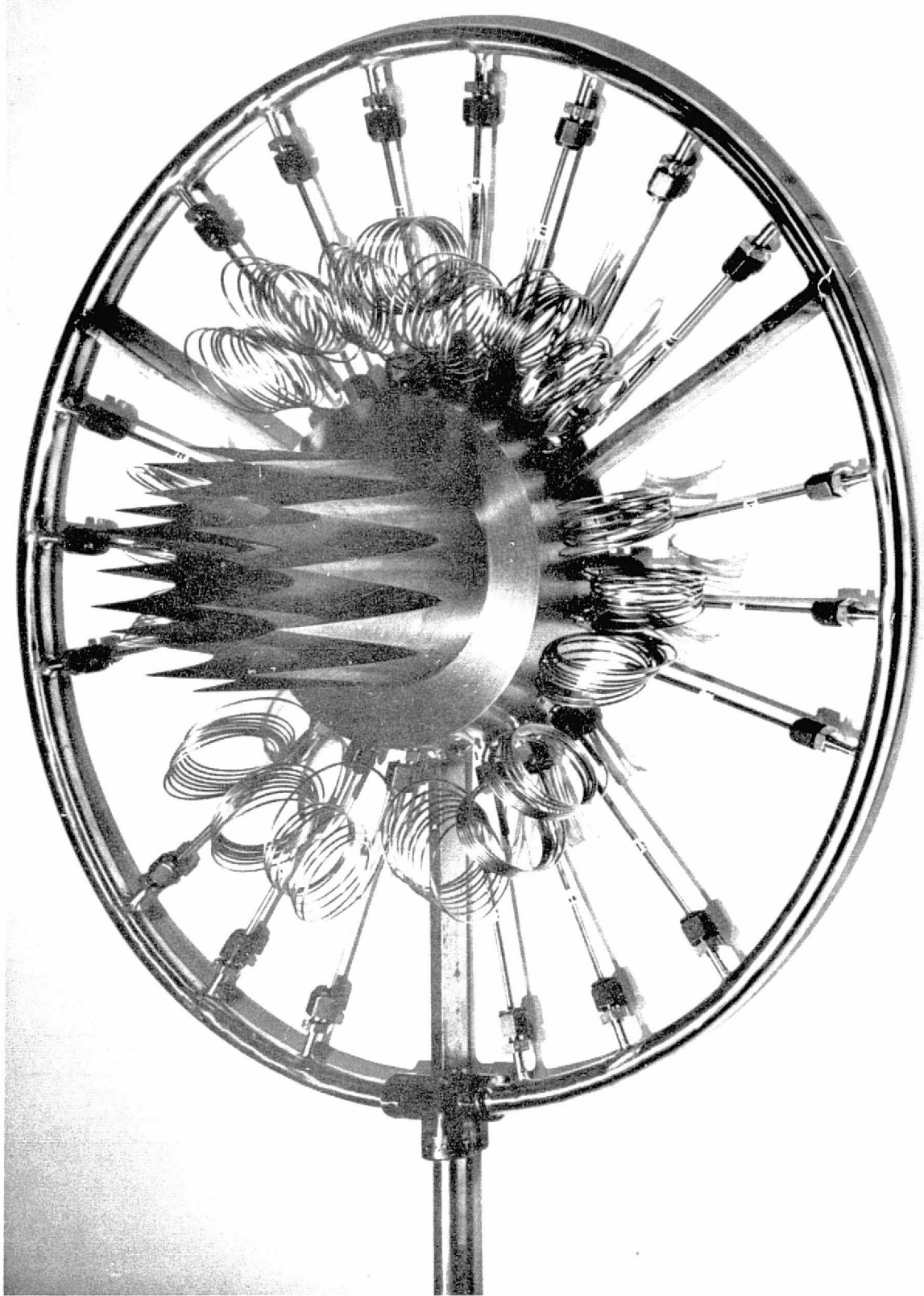


Fig. 41. Fuel Injector Assembly.

ORIGINAL PAGE IS
OF POOR QUALITY

79-01-305-5
RC78-174-C

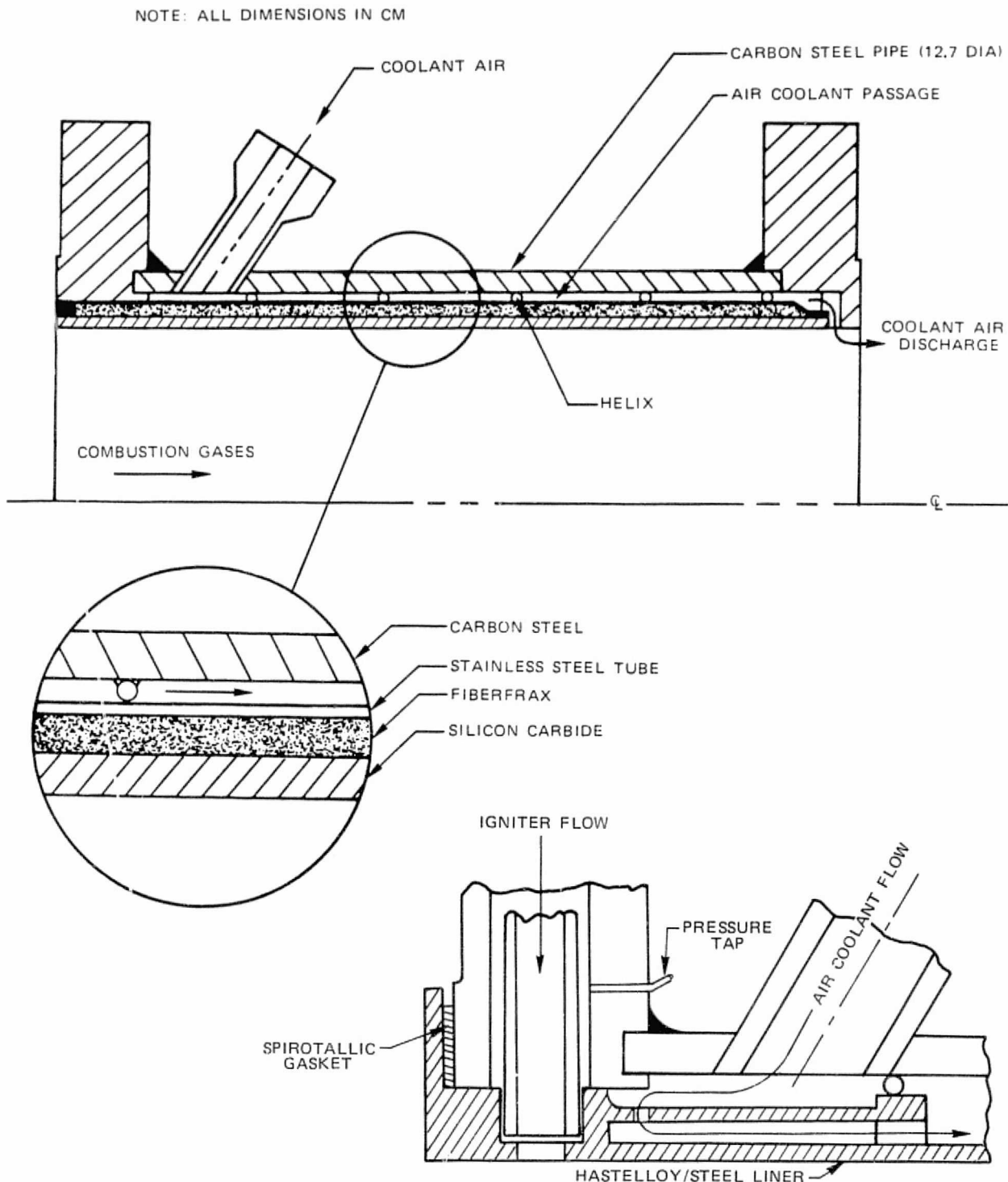


Fig. 42. Combustor Liner Configurations.

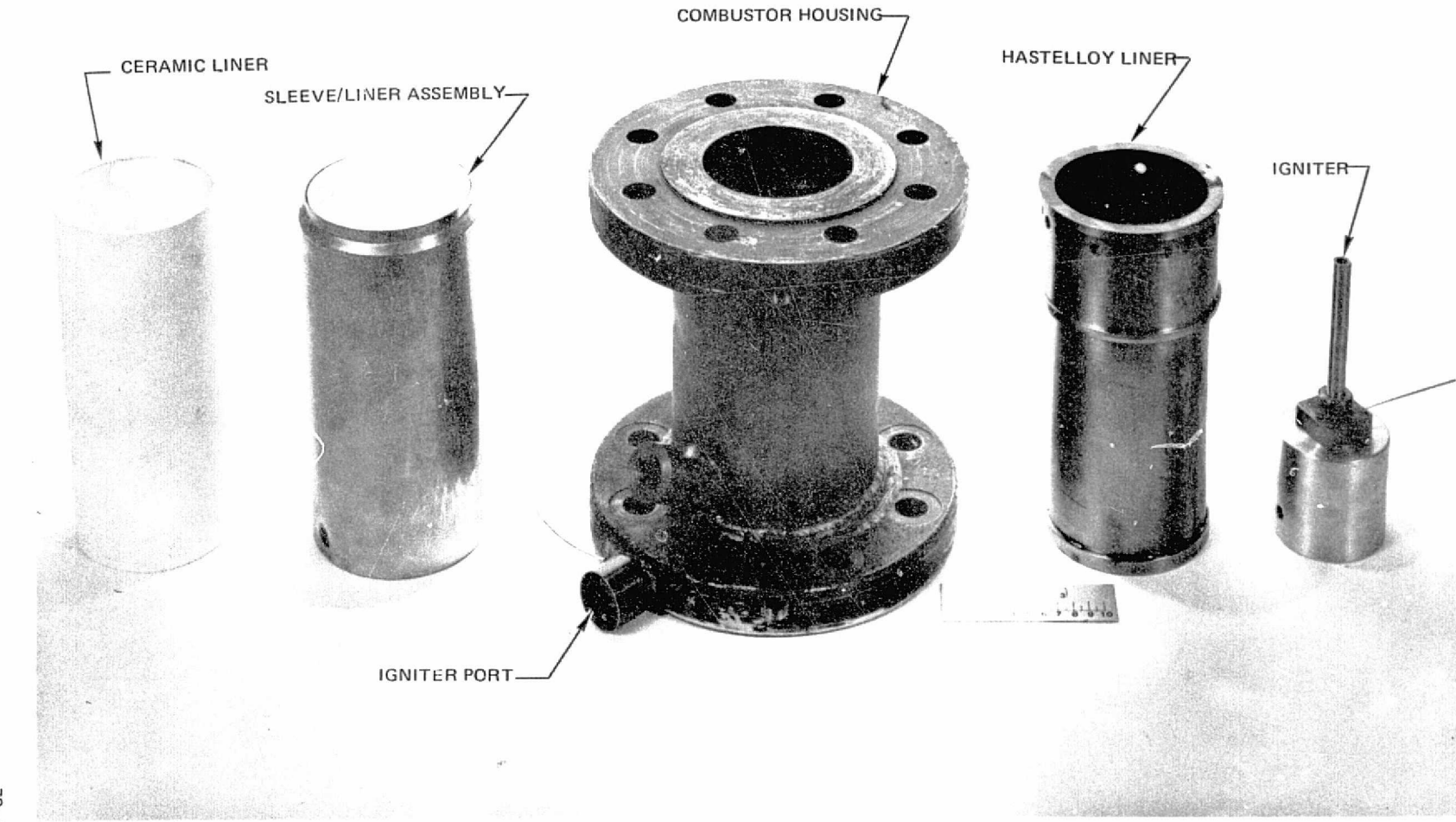


Figure 43. Combustor Assembly Components .

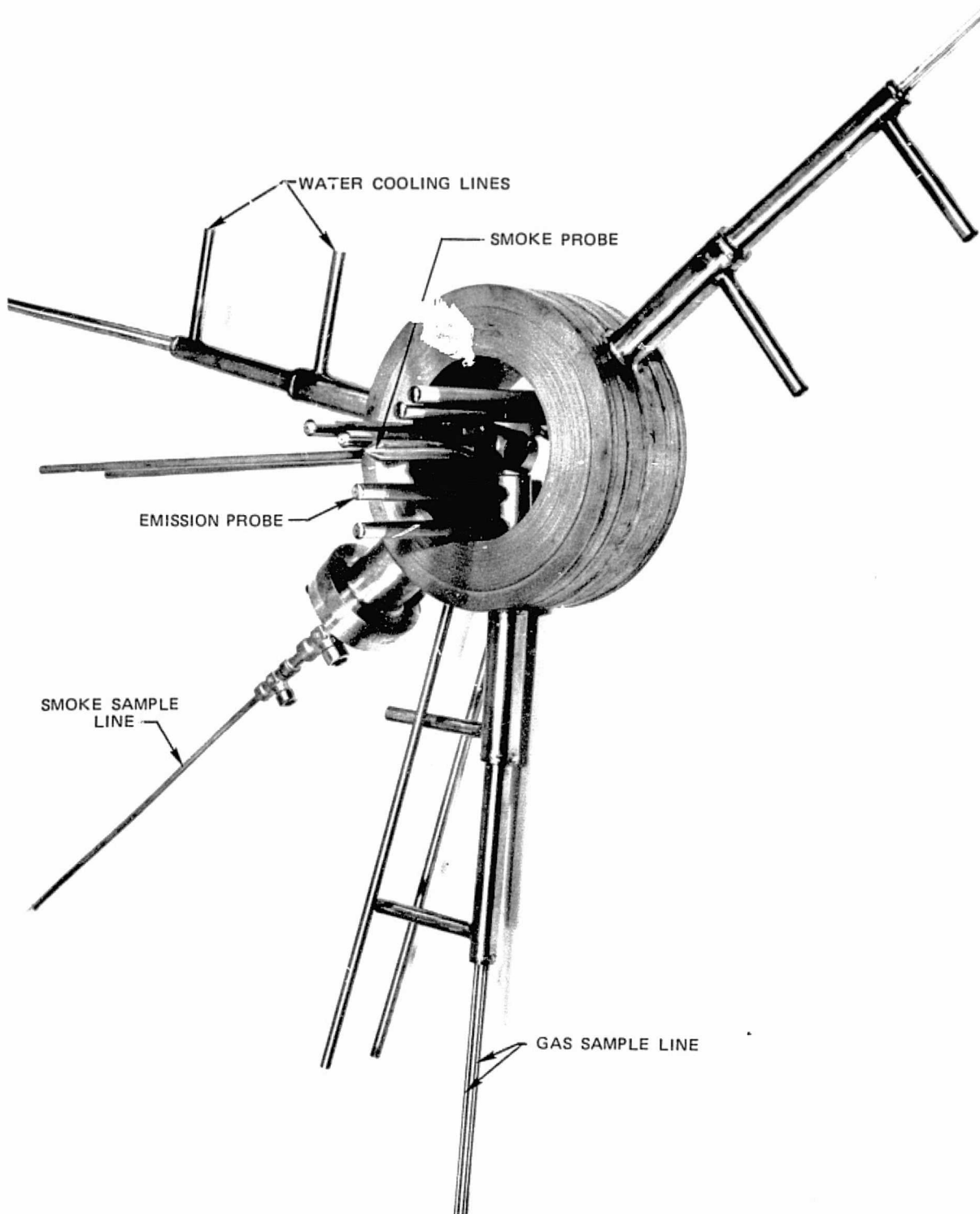


Fig. 44. Instrumentation Section—Combustor Exit Station

79-01-305-1
78-205-E

ORIGINAL PAGE IS
OF POOR QUALITY

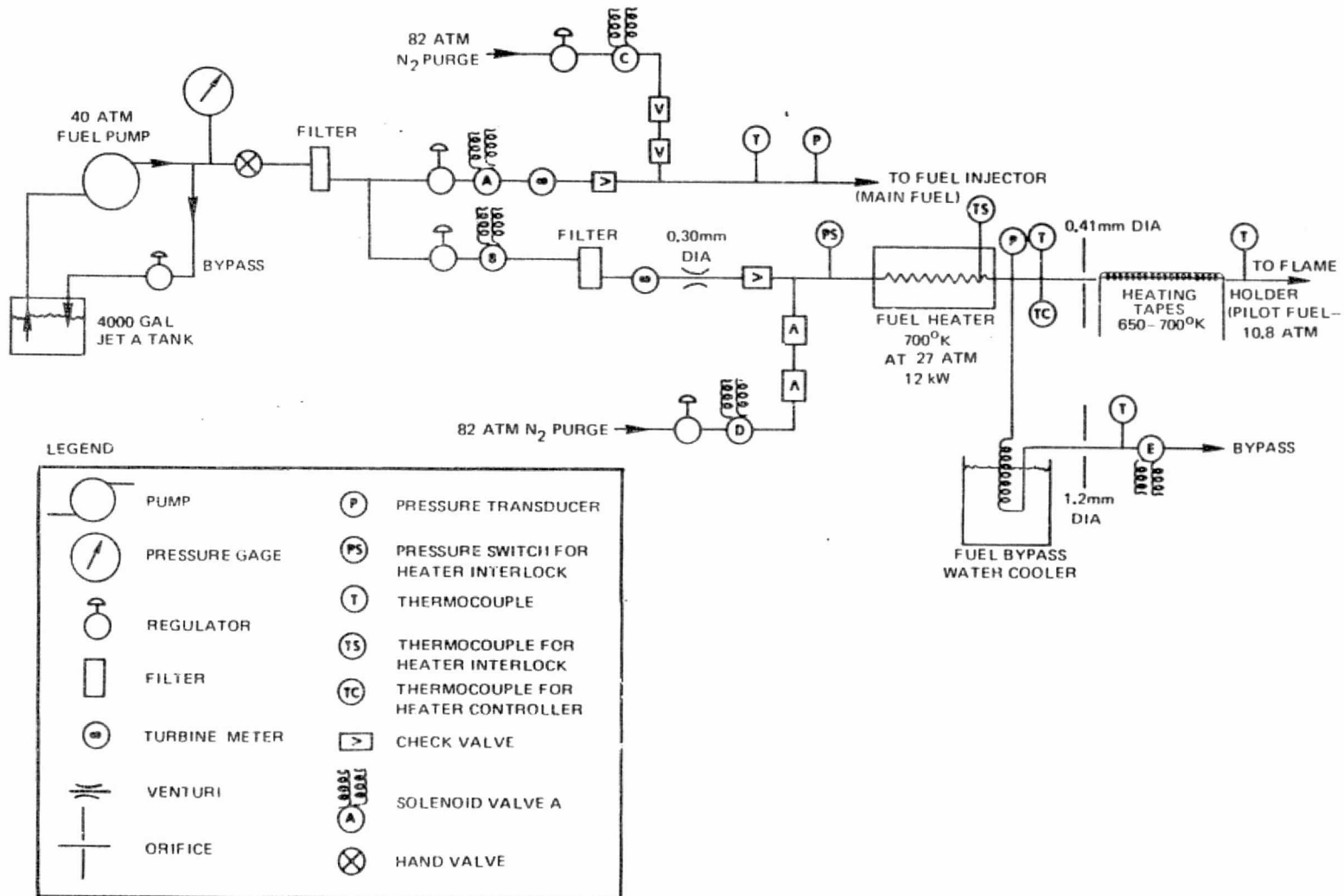
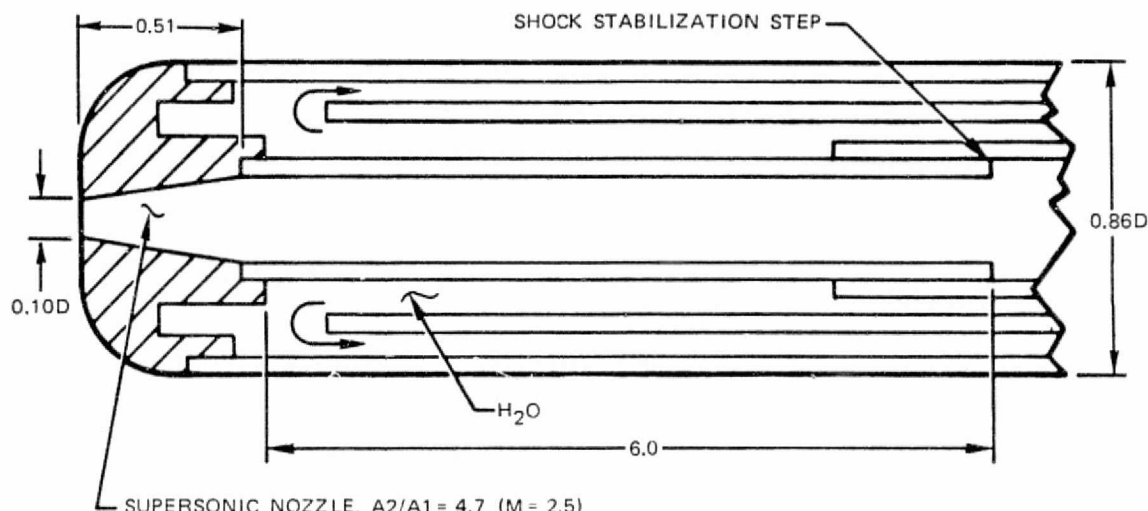


Fig. 45. Schematic Diagram of Fuel Supply System.



NOTE: ALL DIMENSIONS IN CM

Fig. 46. Emission-Probe Tip Construction.

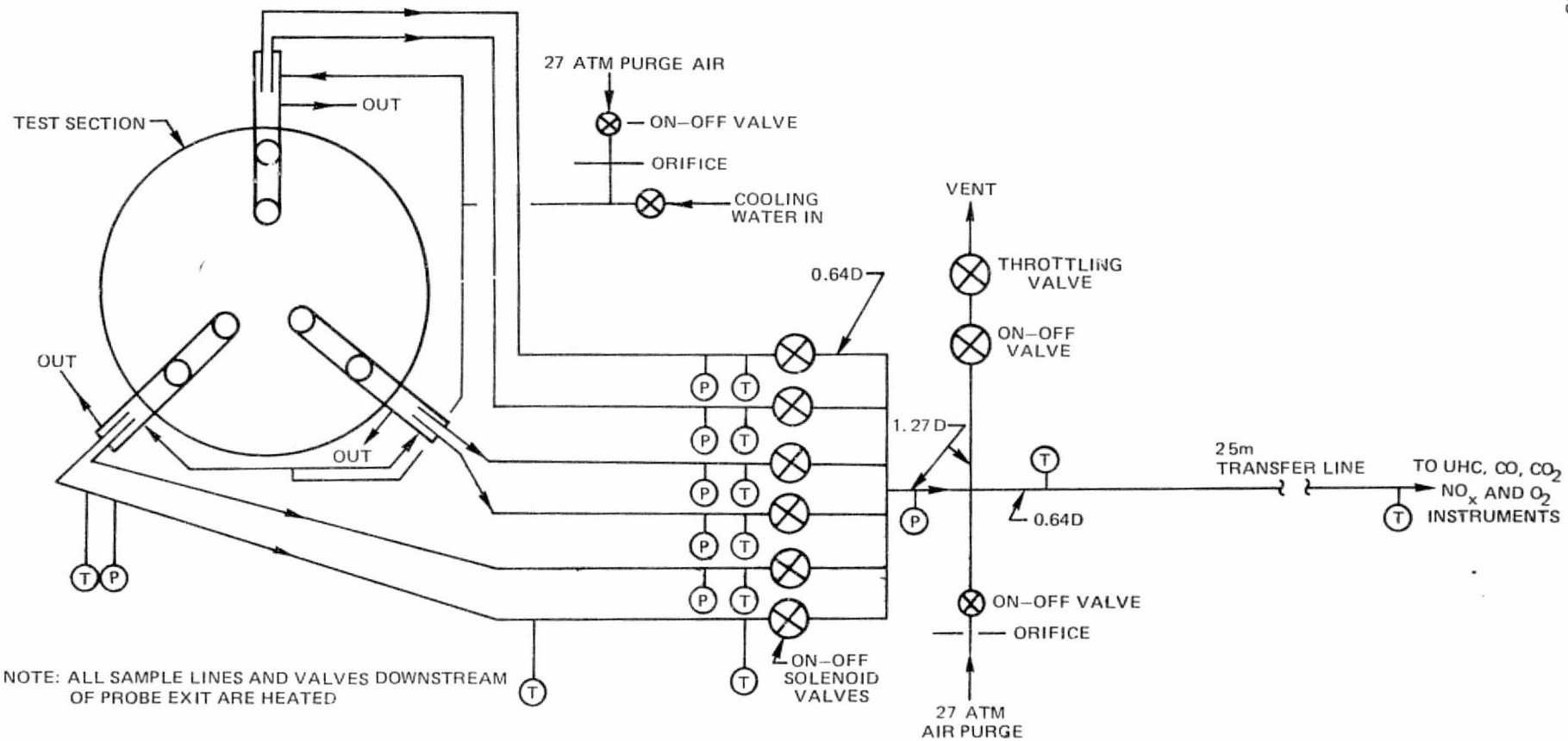


Figure 47. Six-Probe Emissions Rake Sample Transfer System

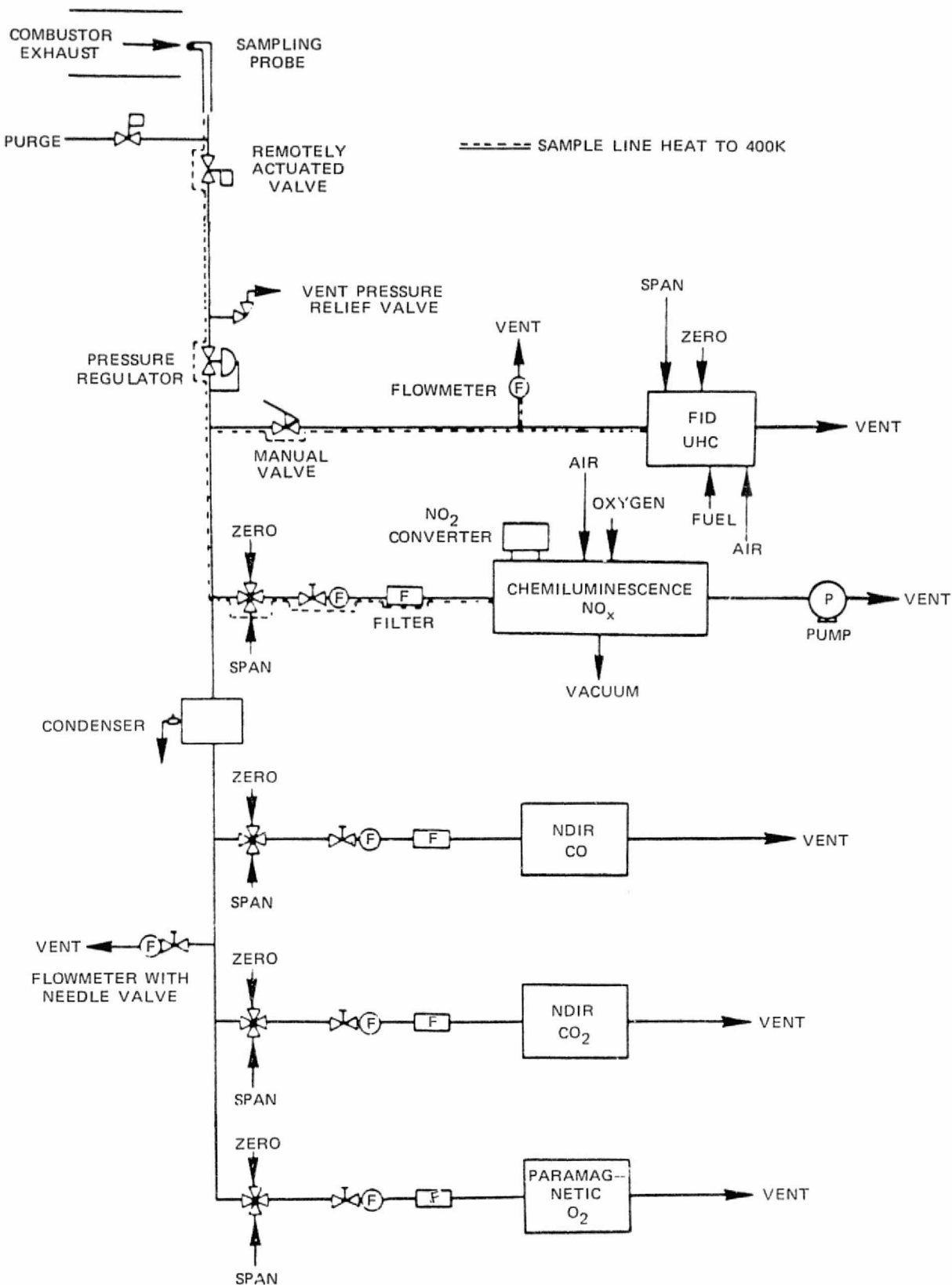


Fig. 48. Emission Sampling and Analysis System.

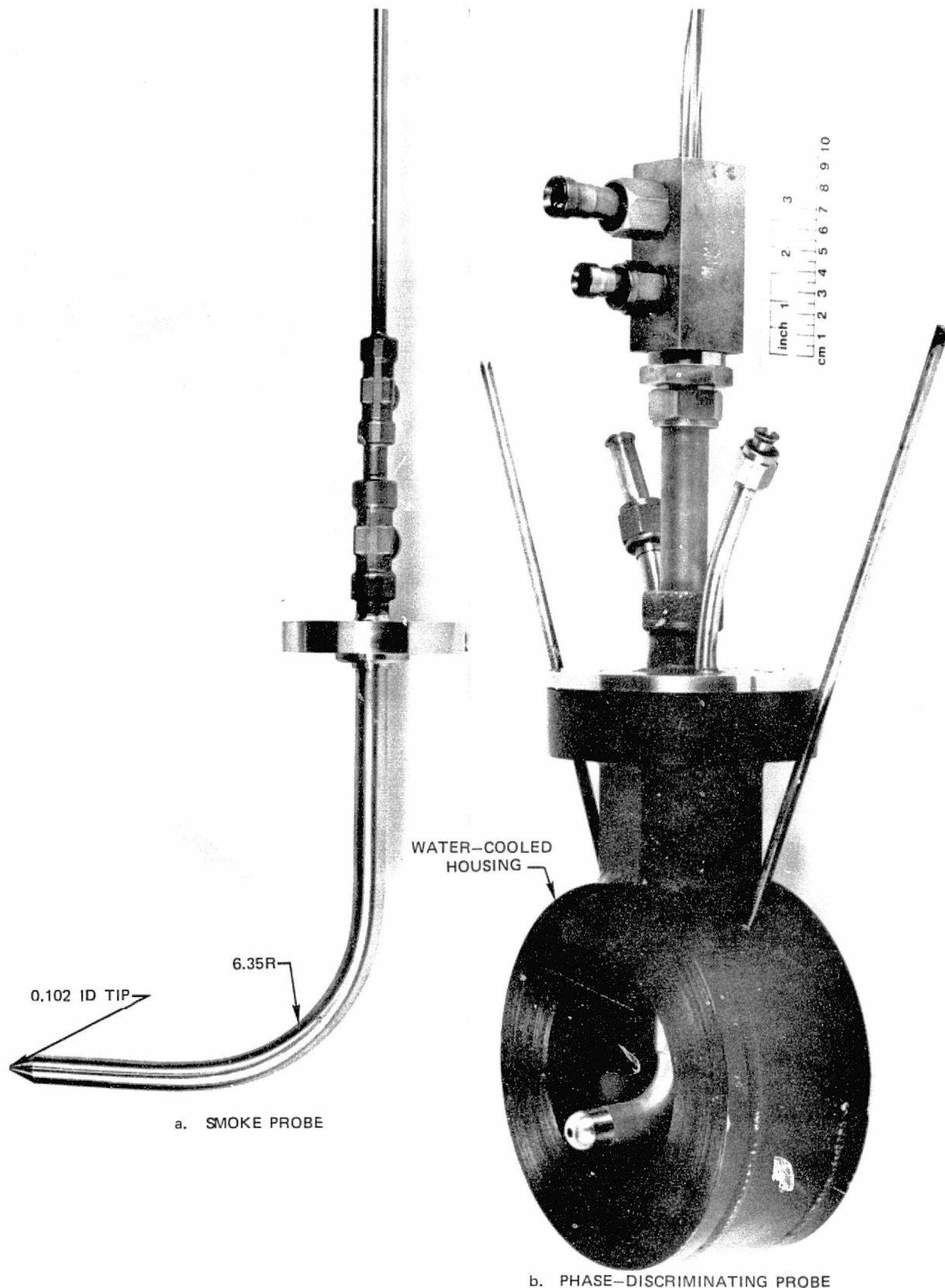
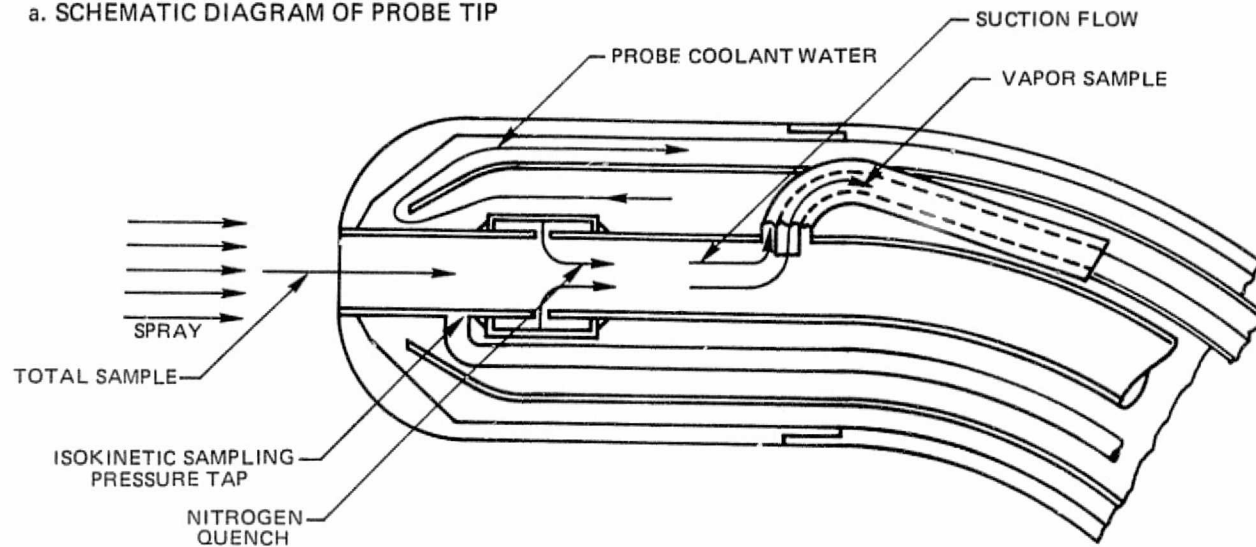


Fig. 49. Smoke and Phase-Discriminating Sampling Probes.

79-01-305-2
78-205-F
78-140-C

a. SCHEMATIC DIAGRAM OF PROBE TIP



b. GAS ANALYSIS SYSTEM

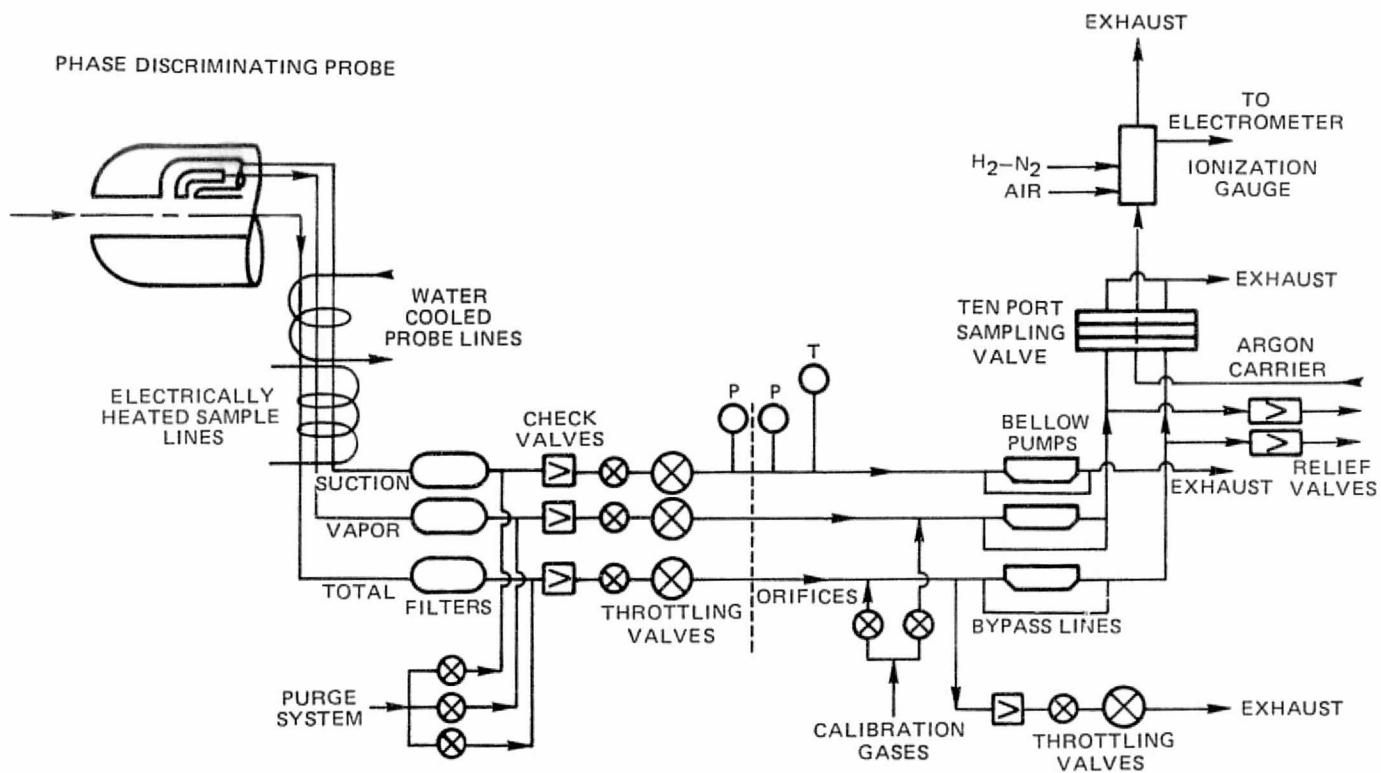


Figure 50 Phase-Discriminating Sampling System

ORIGINAL PAGE IS
DE POOR QUALITY

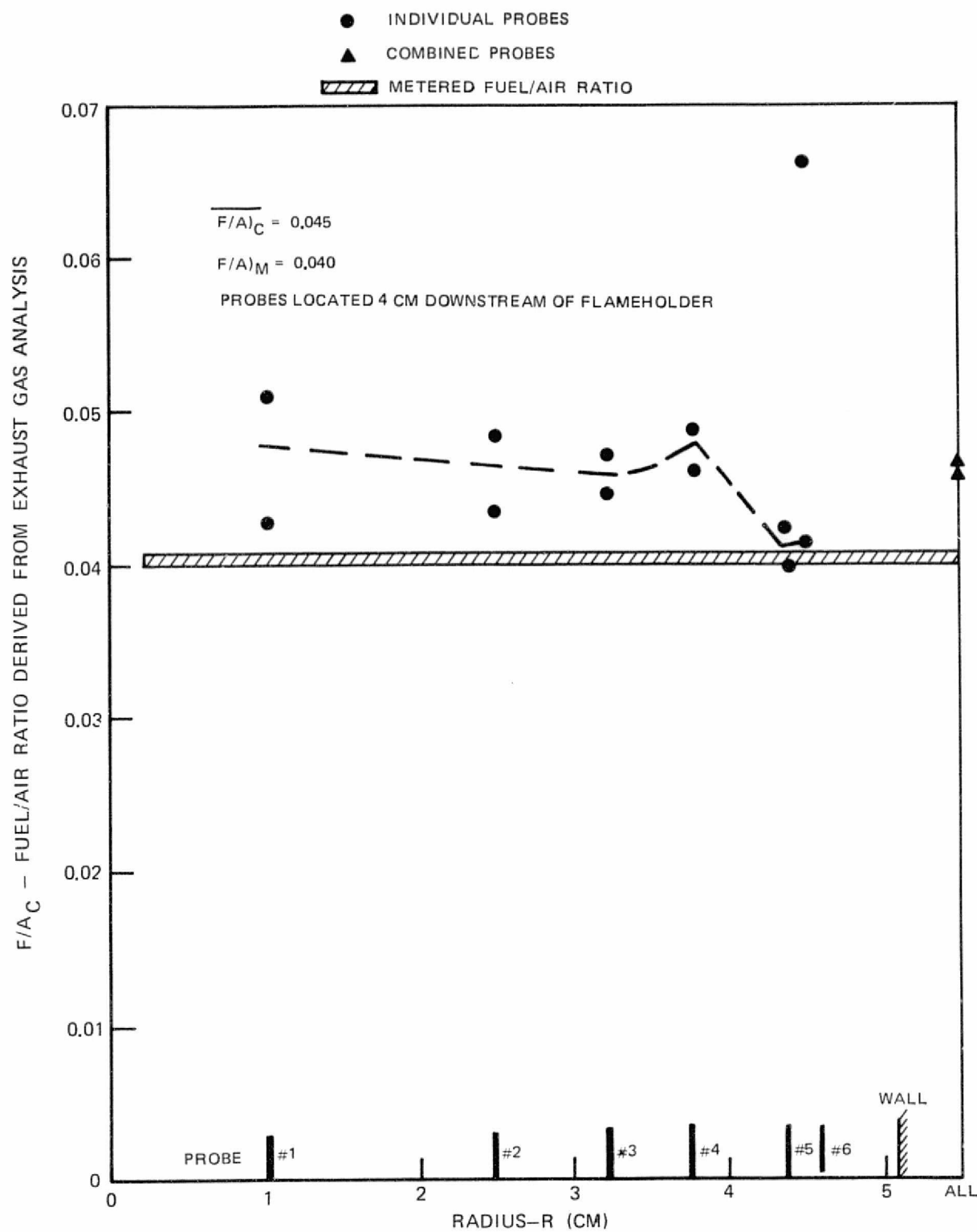


Figure 51. Fuel Profile Uniformity Test Results

ORIGINAL PAGE IS
OF POOR
QUALITY

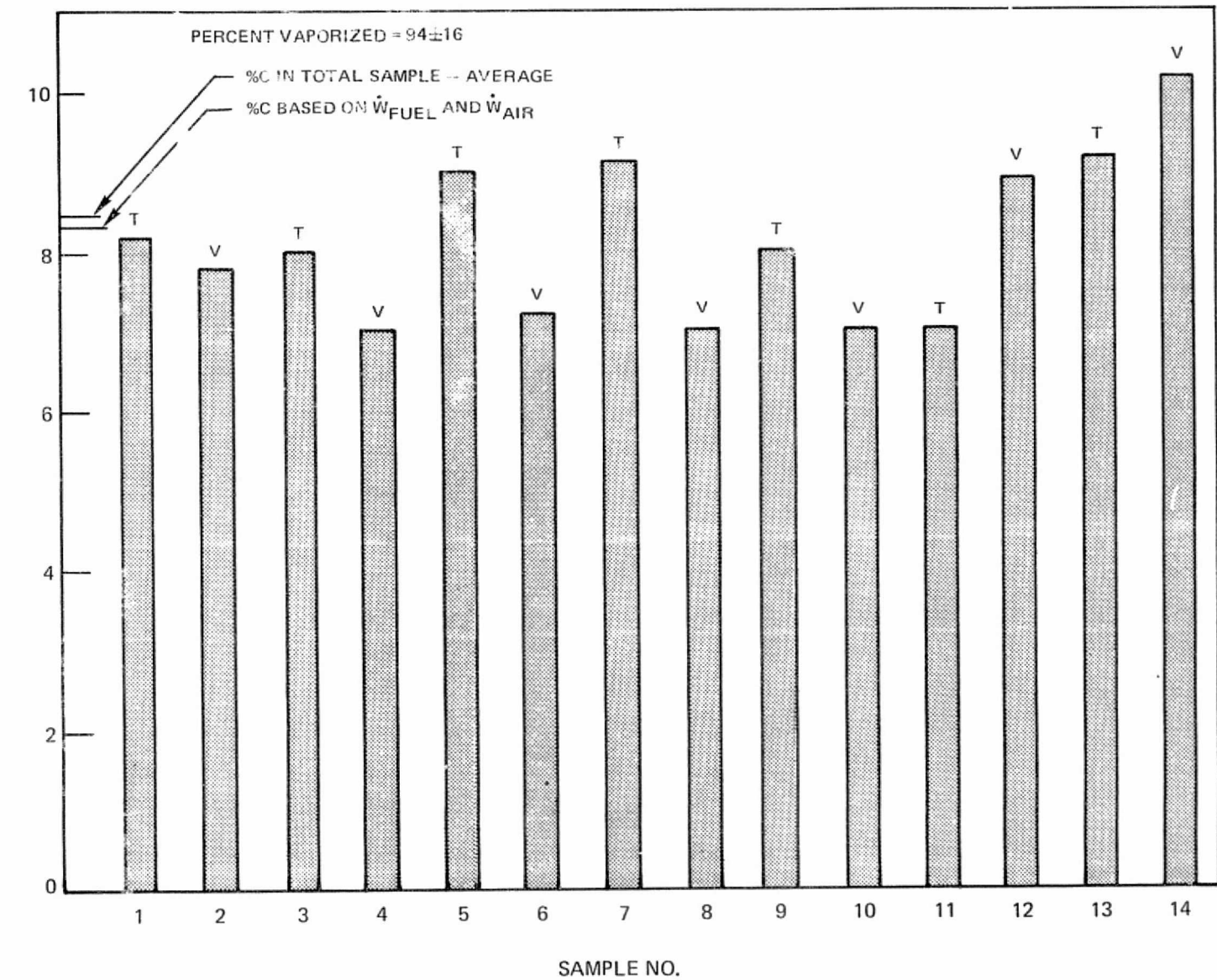


Figure 52. Fuel Vaporization Test Results – Survey 1

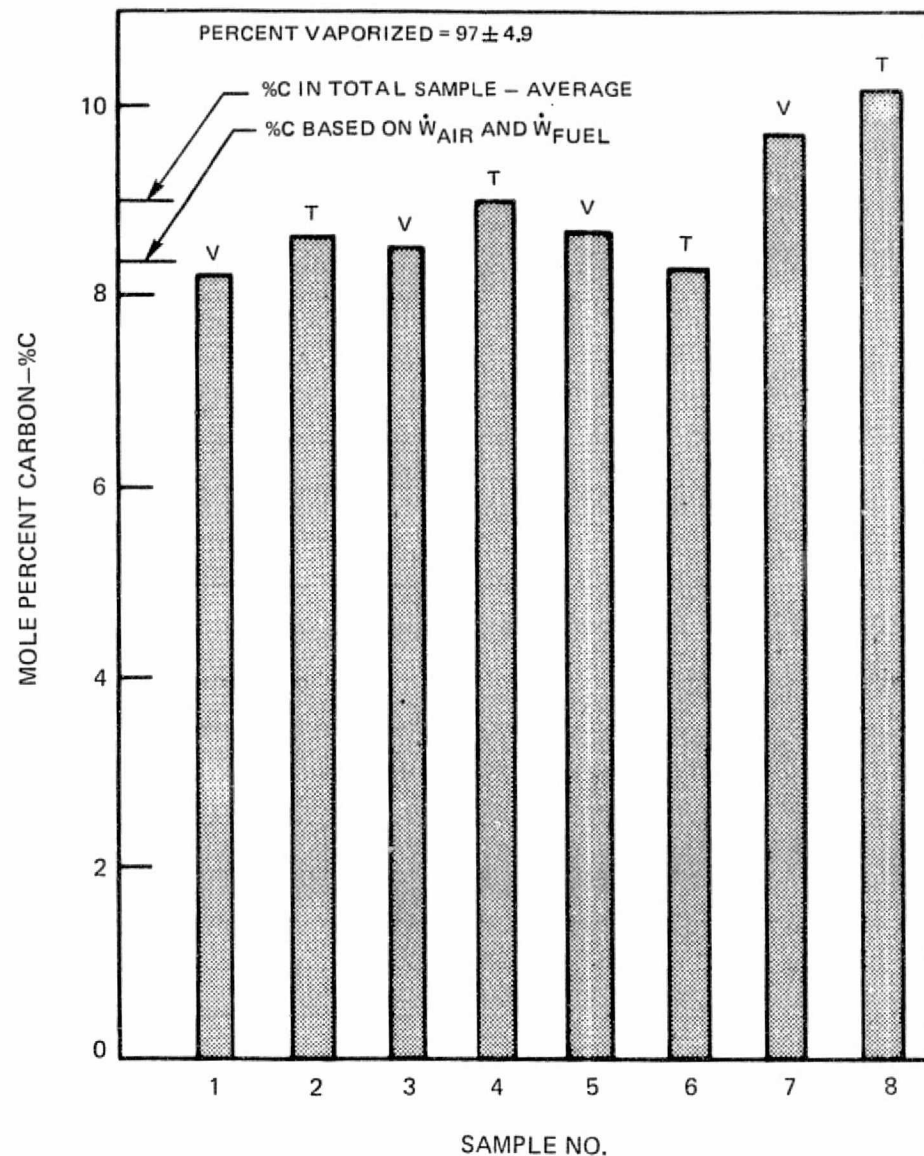
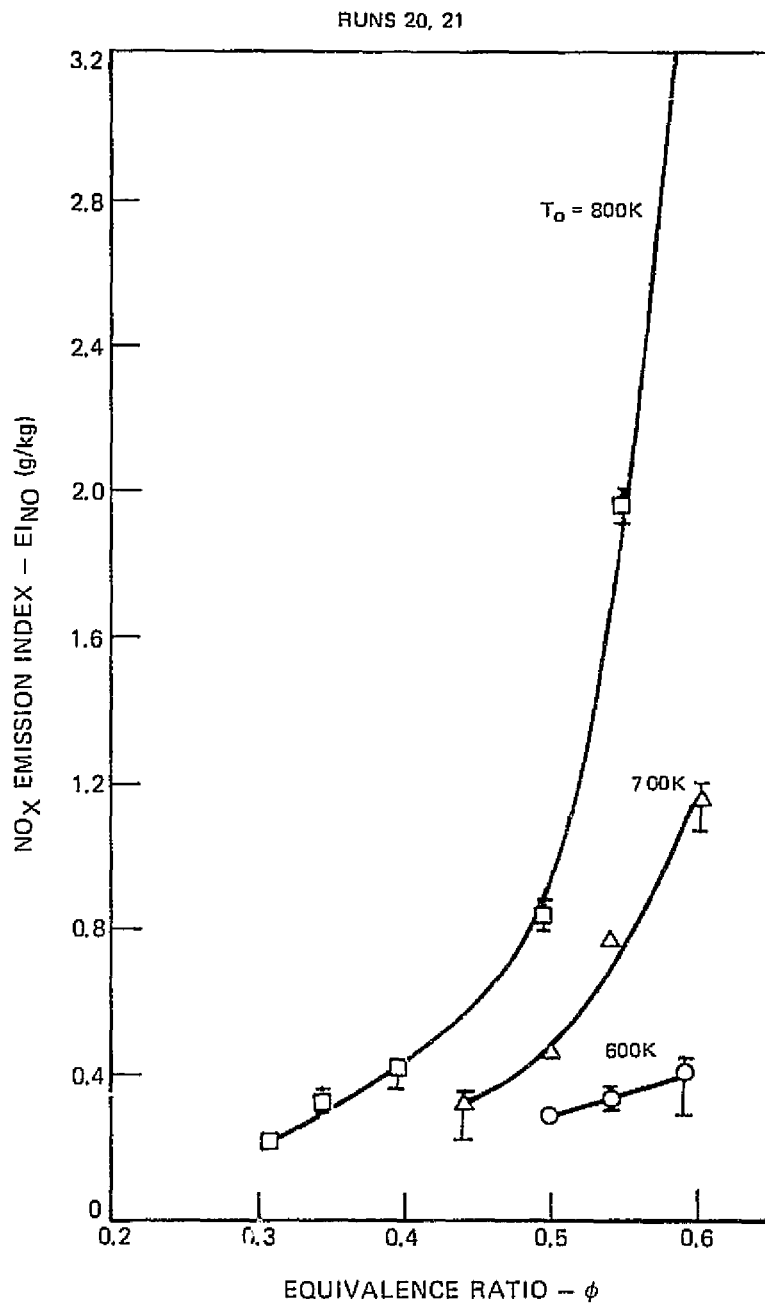


Figure 53. Fuel Vaporization Test Results — Survey 2

Figure 54. NO_x Emissions — Baseline Configuration

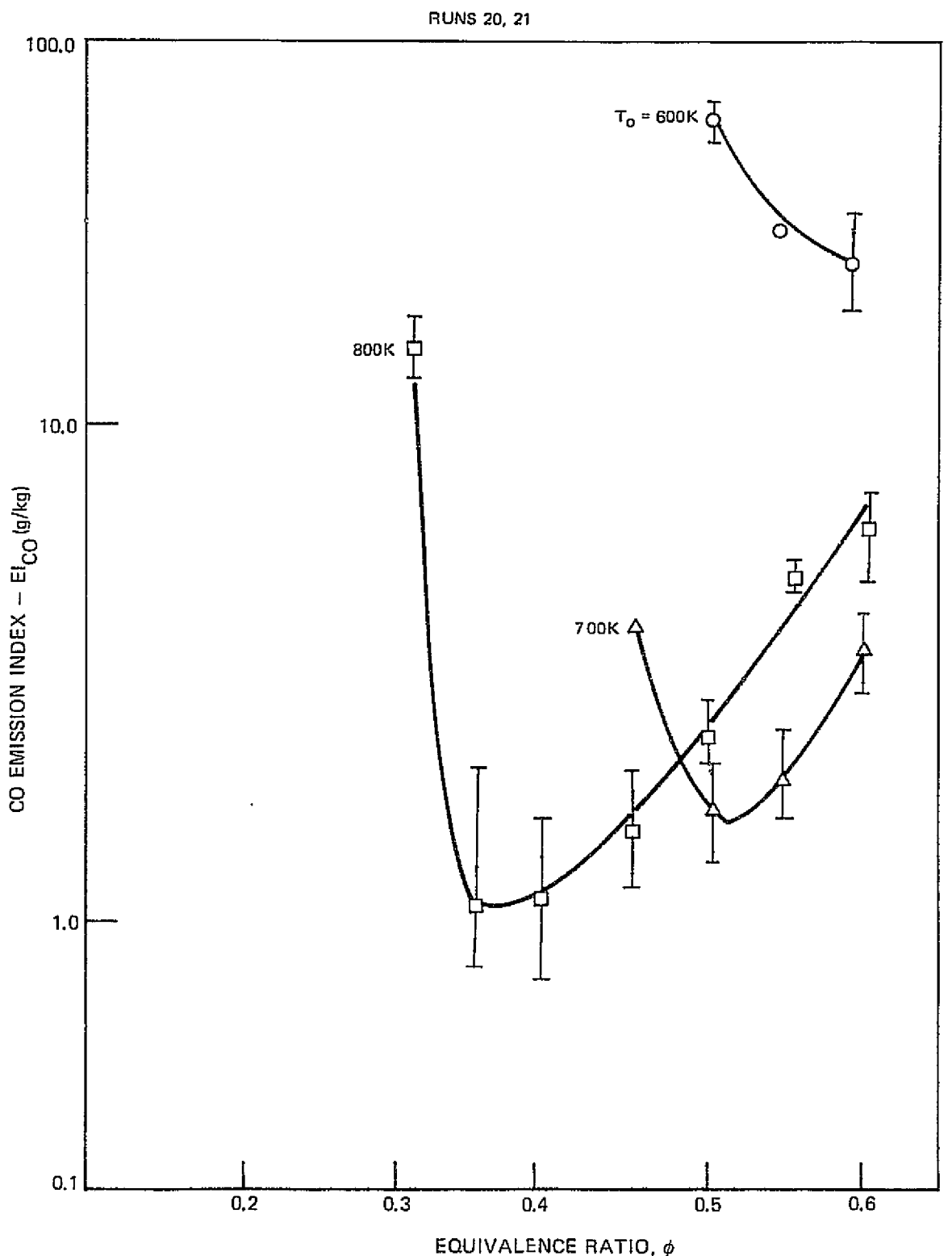


Figure 55. CO Emissions -- Baseline Configuration

ORIGINAL PAGE IS
OF POOR QUALITY

78-08-252-16

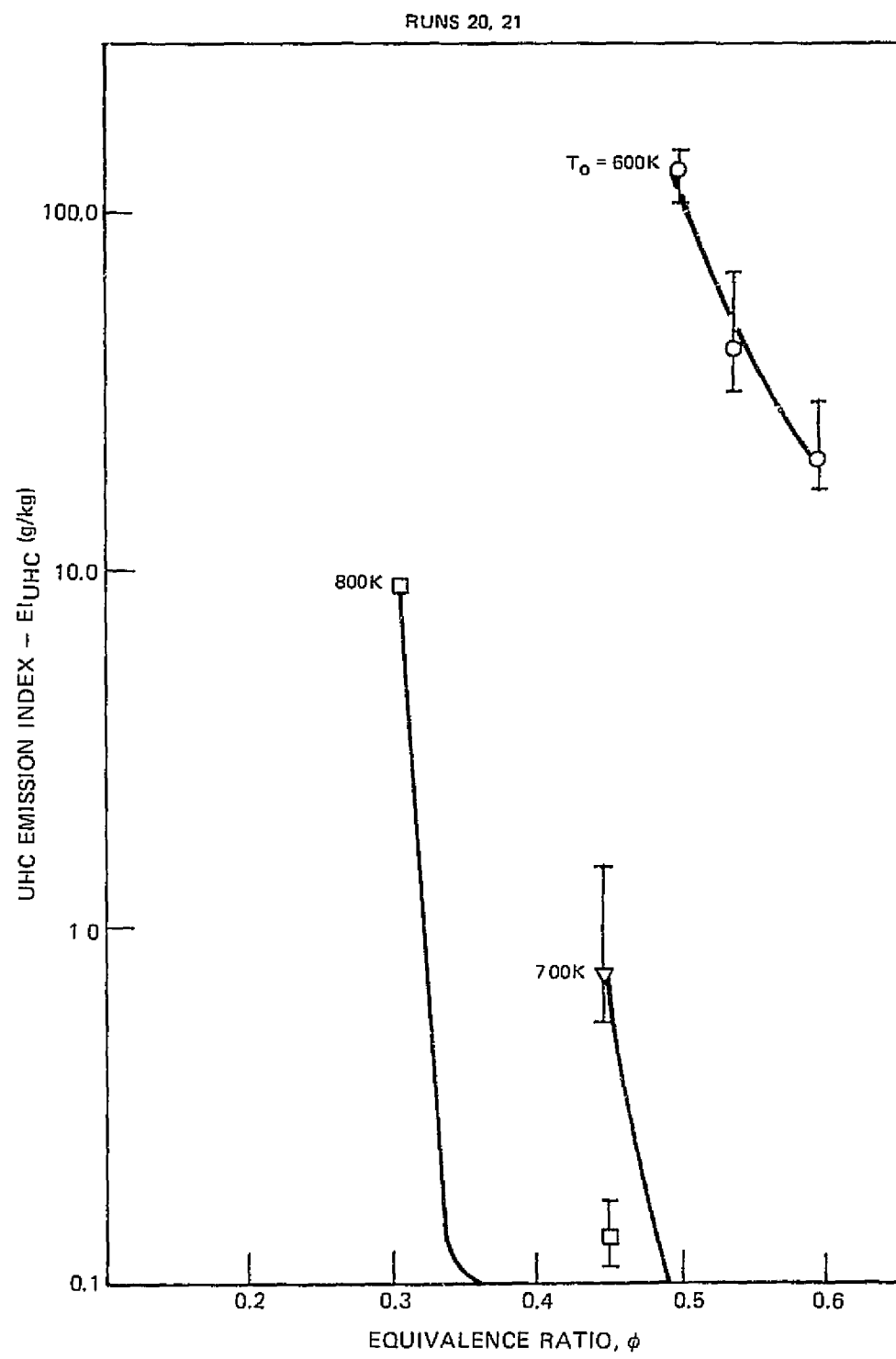


Figure 56. UHC Emissions — Baseline Configuration

ORIGINAL PAGE IS
OF POOR QUALITY

RUNS 20, 21

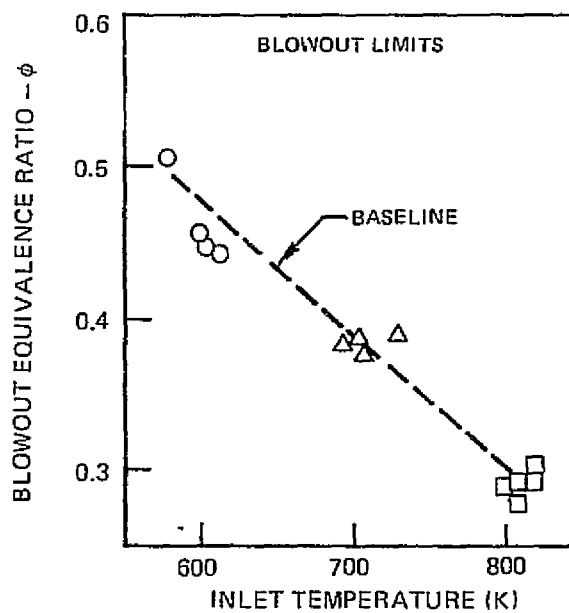
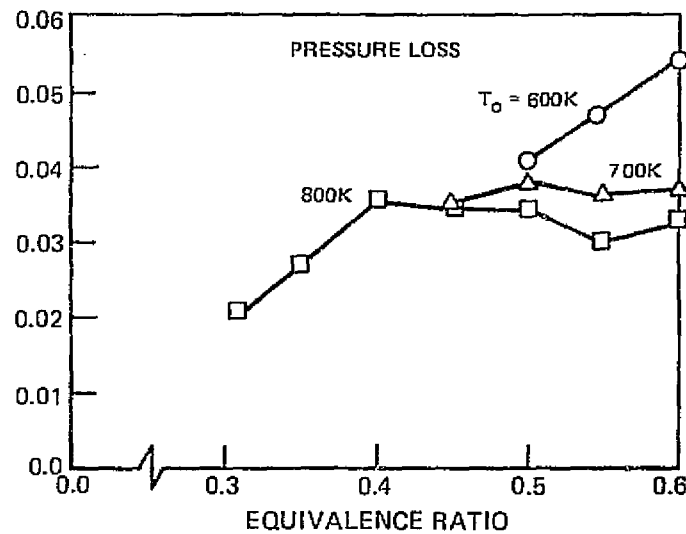
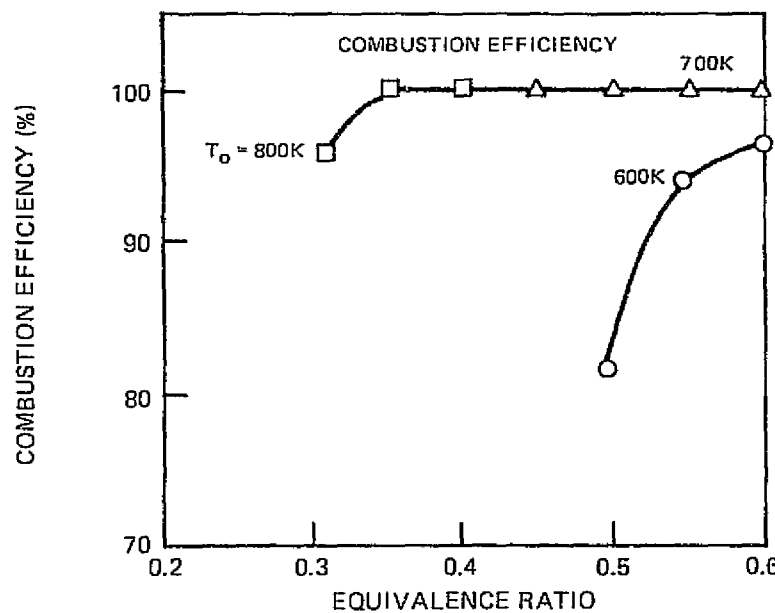
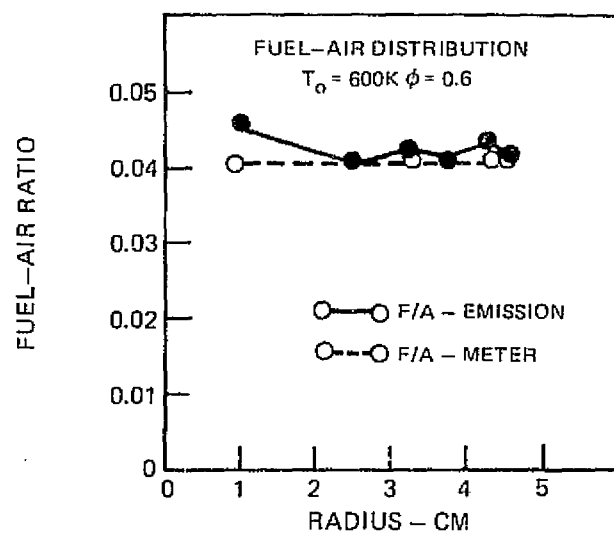


Figure 57. Combustor Performance - Baseline Configuration

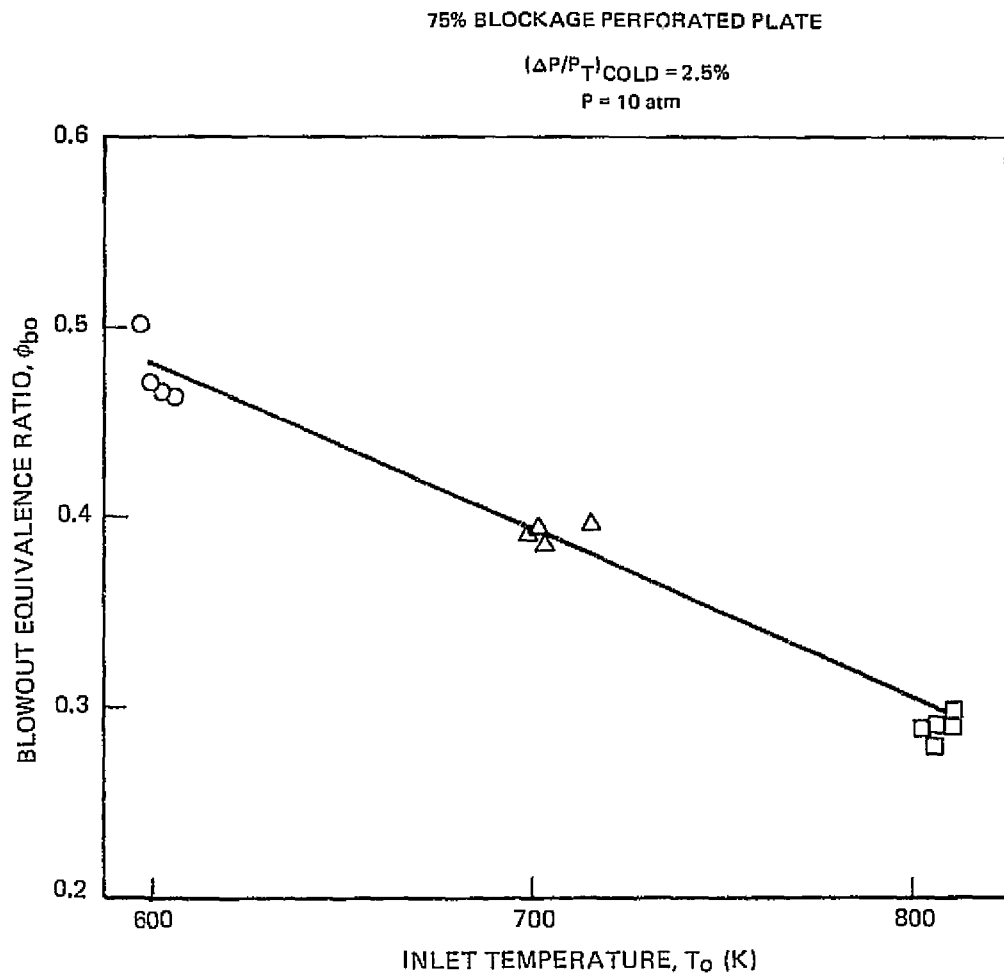


Figure 58. Baseline Flameholder Blowout Limits

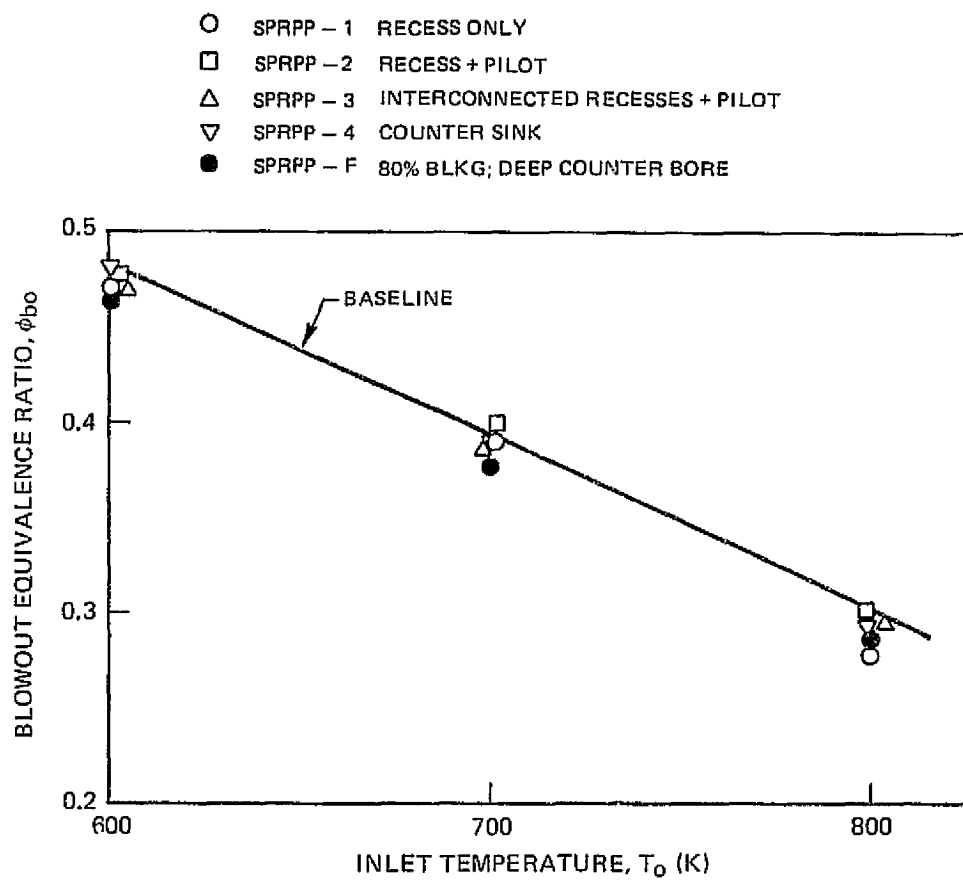
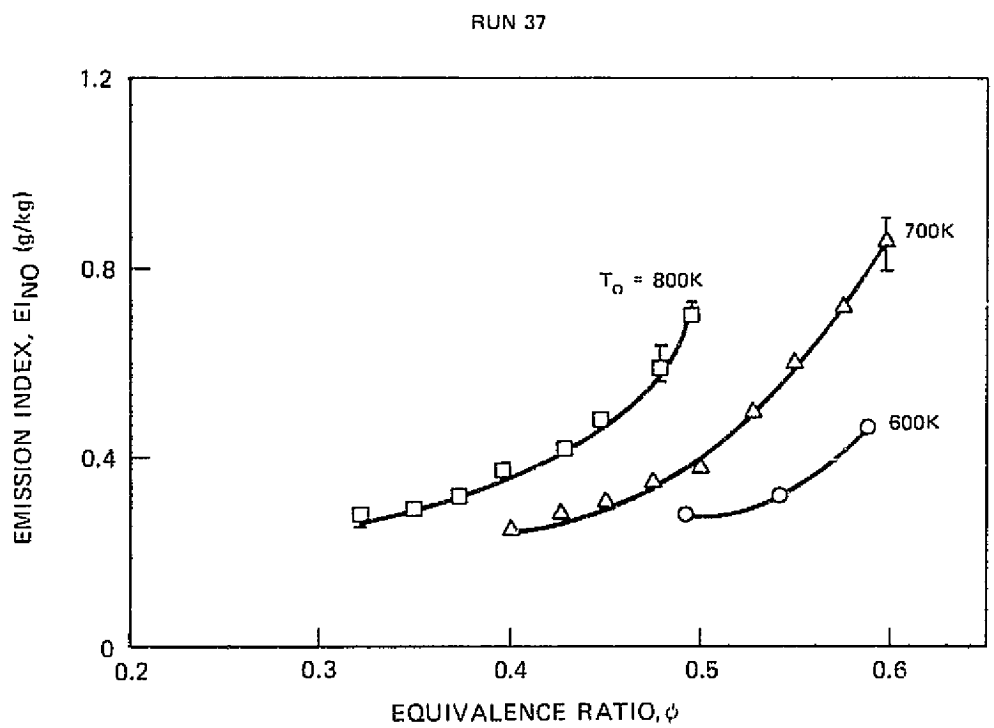


Figure 59. Lean Stability Limits, Self-Piloting Recessed Perforated Plate Series

ORIGINAL PAGE IS
OF POOR QUALITY

Figure 60. NO_x Emissions — Self Piloting Perforated Plate Final Design

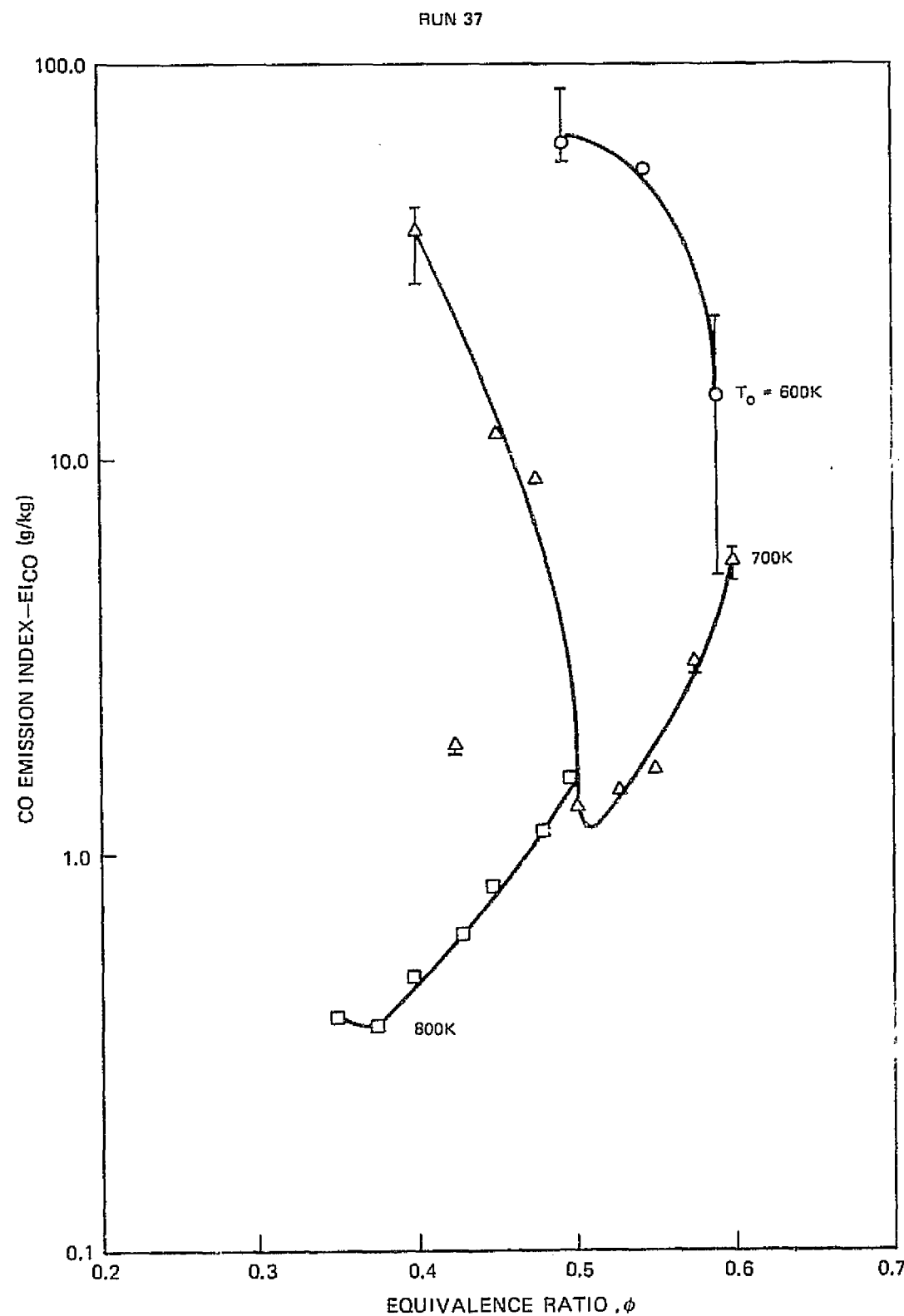


Figure 61. CO Emissions — Self Piloting Perforated Plate Final Design

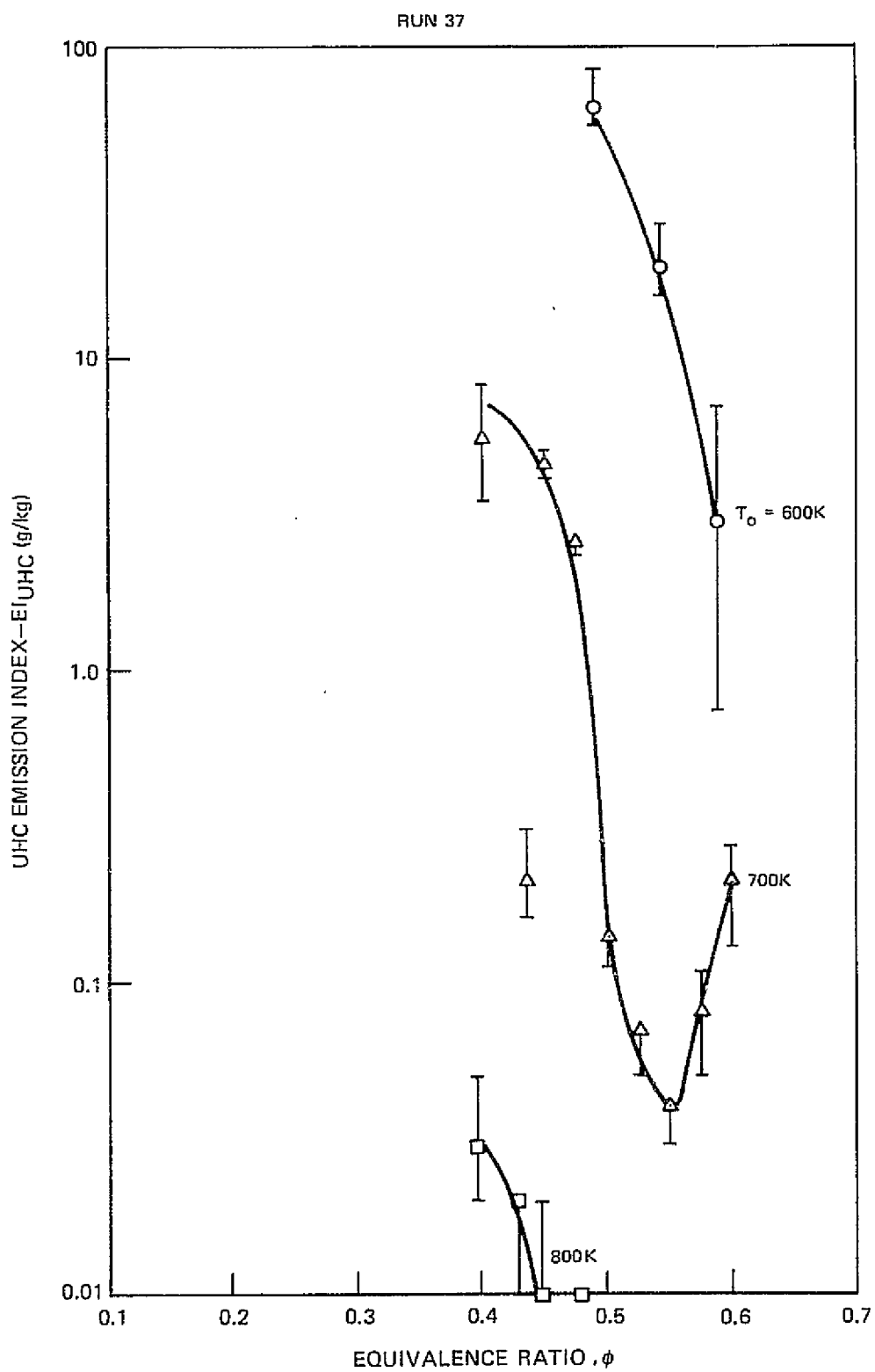


Figure 62. UHC Emissions — Self-Piloting Perforated Plate Final Design

ORIGINAL PAGE IS
OF POOR QUALITY

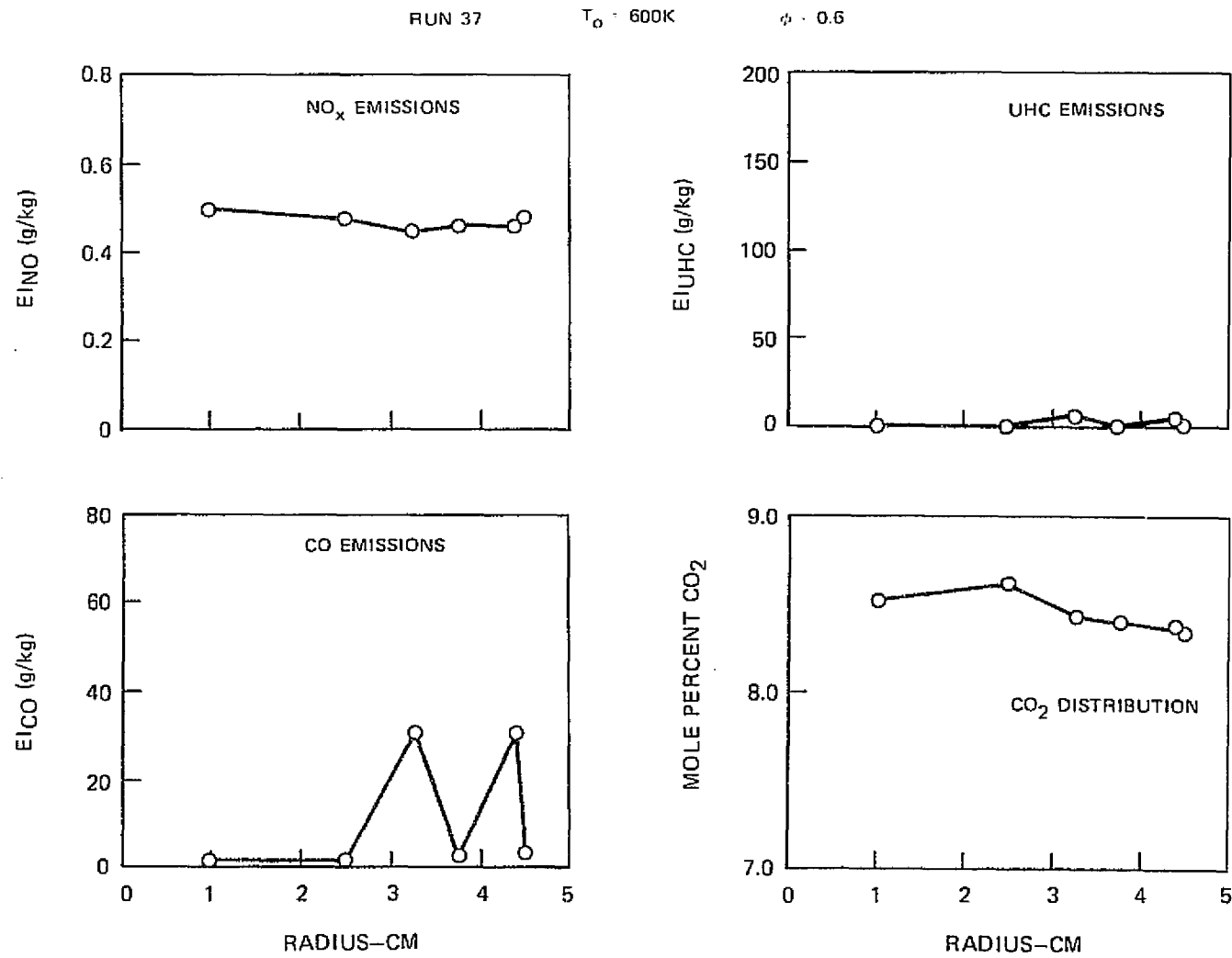


Figure 63. Emission Distribution - Self-Piloting Perforated Plate Final Design

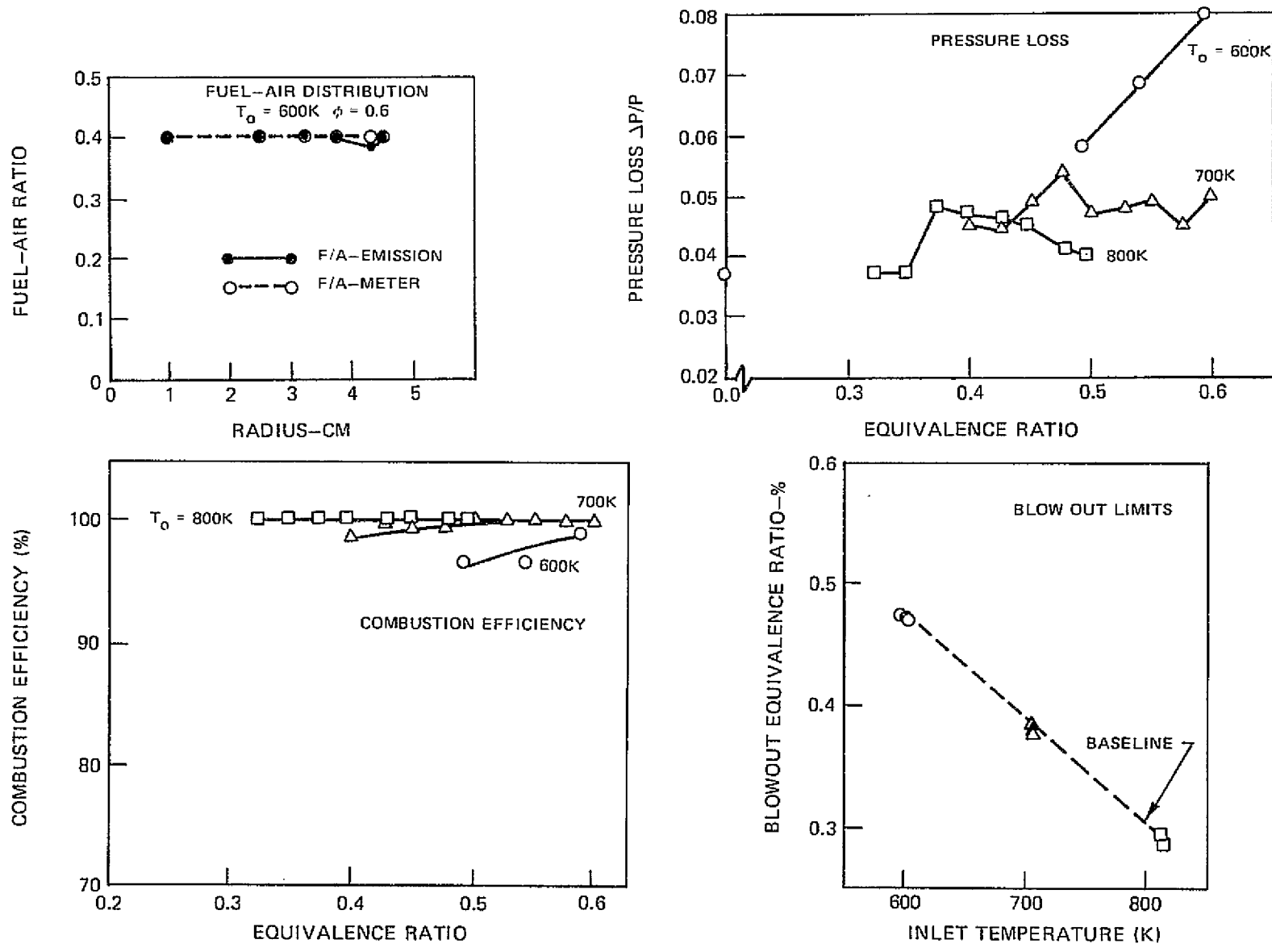


Figure 64. Combuster Performance — Self-Piloting Perforated Plate Final Design

ORIGINAL PAGE IS
OF POOR QUALITY

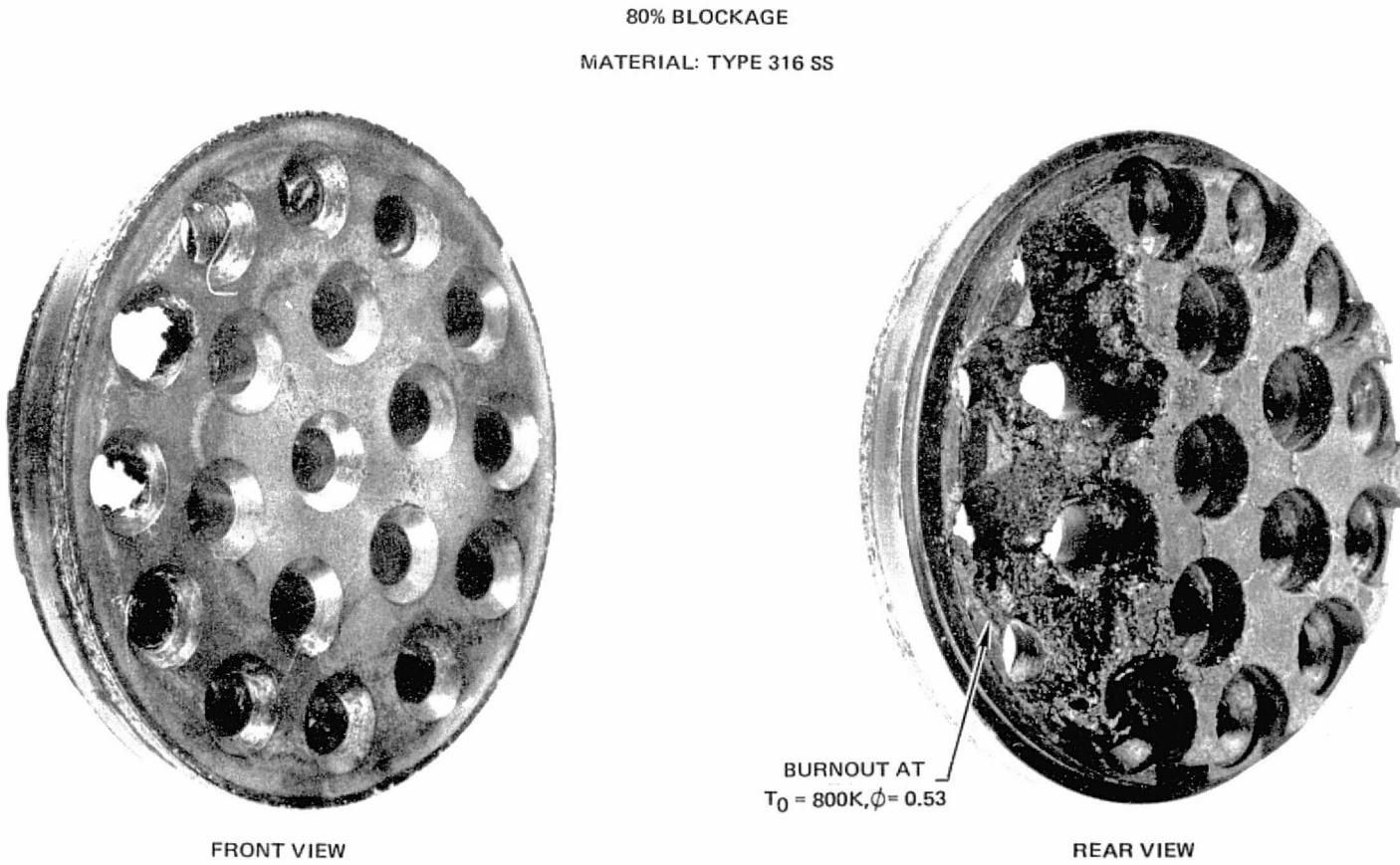


Figure 65. Post Test Condition of Self-Piloting Recessed Perforated Plate — Final Design

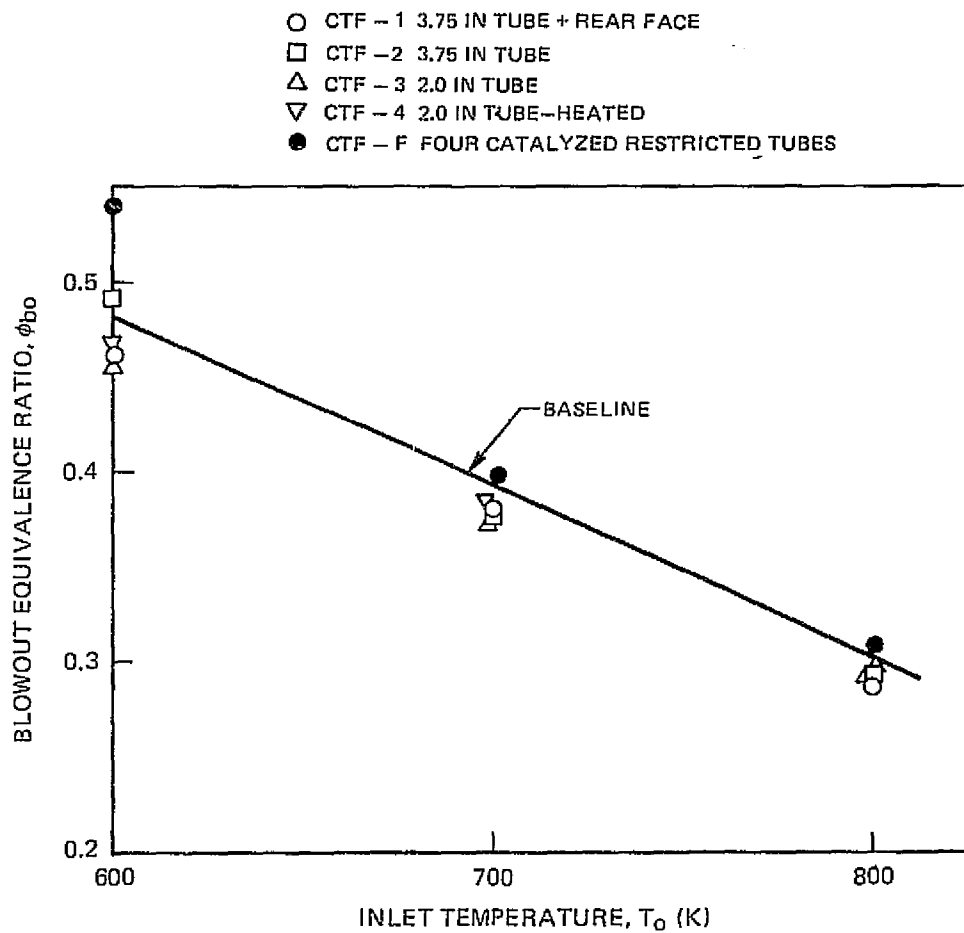
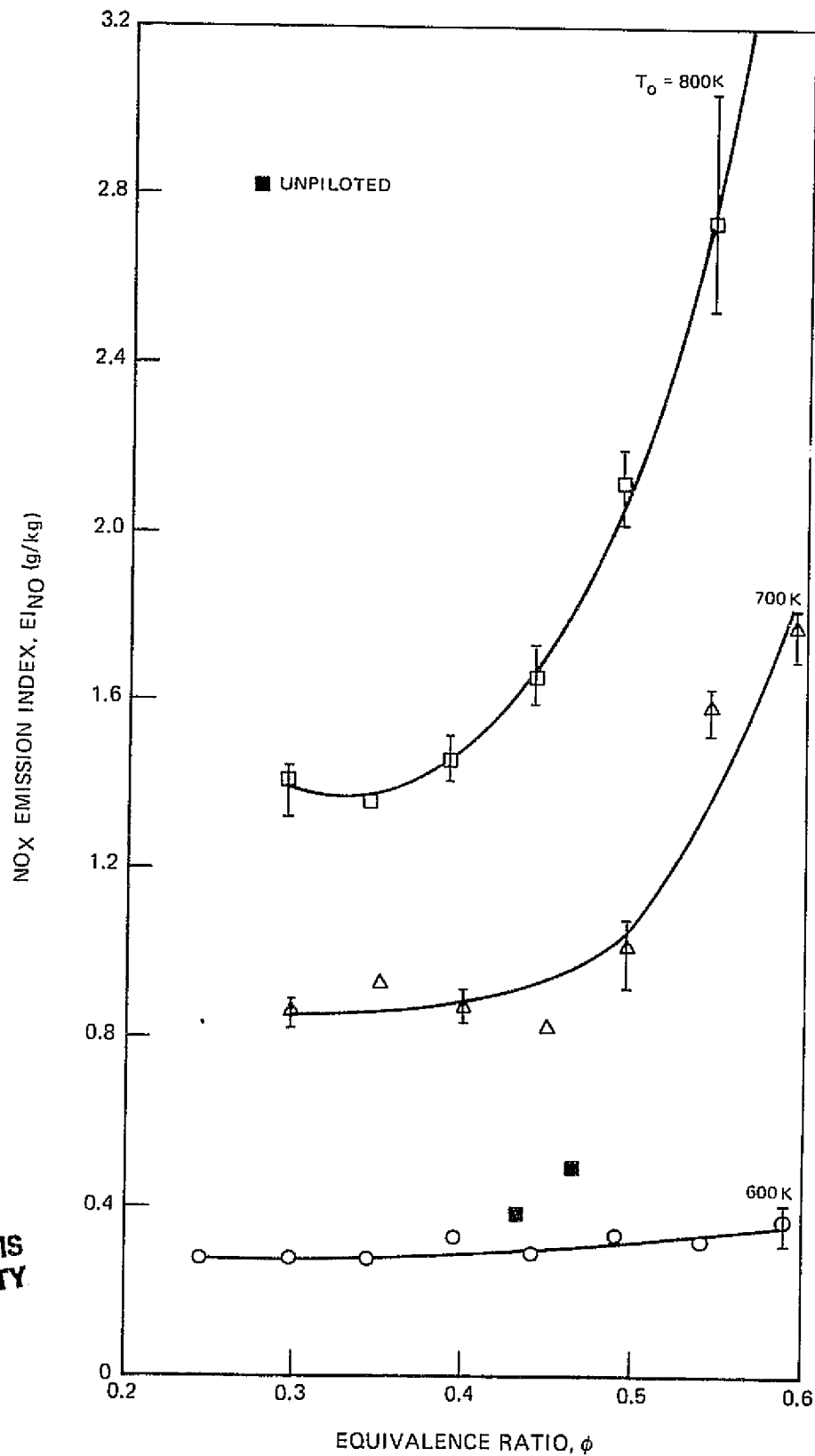


Figure 66 Lean Stability Limits, Catalyzed Tube Flameholder Series

RUN 35

Figure 67. NO_x Emissions — V-Gutter Flameholder — Configuration 1

RUN 35

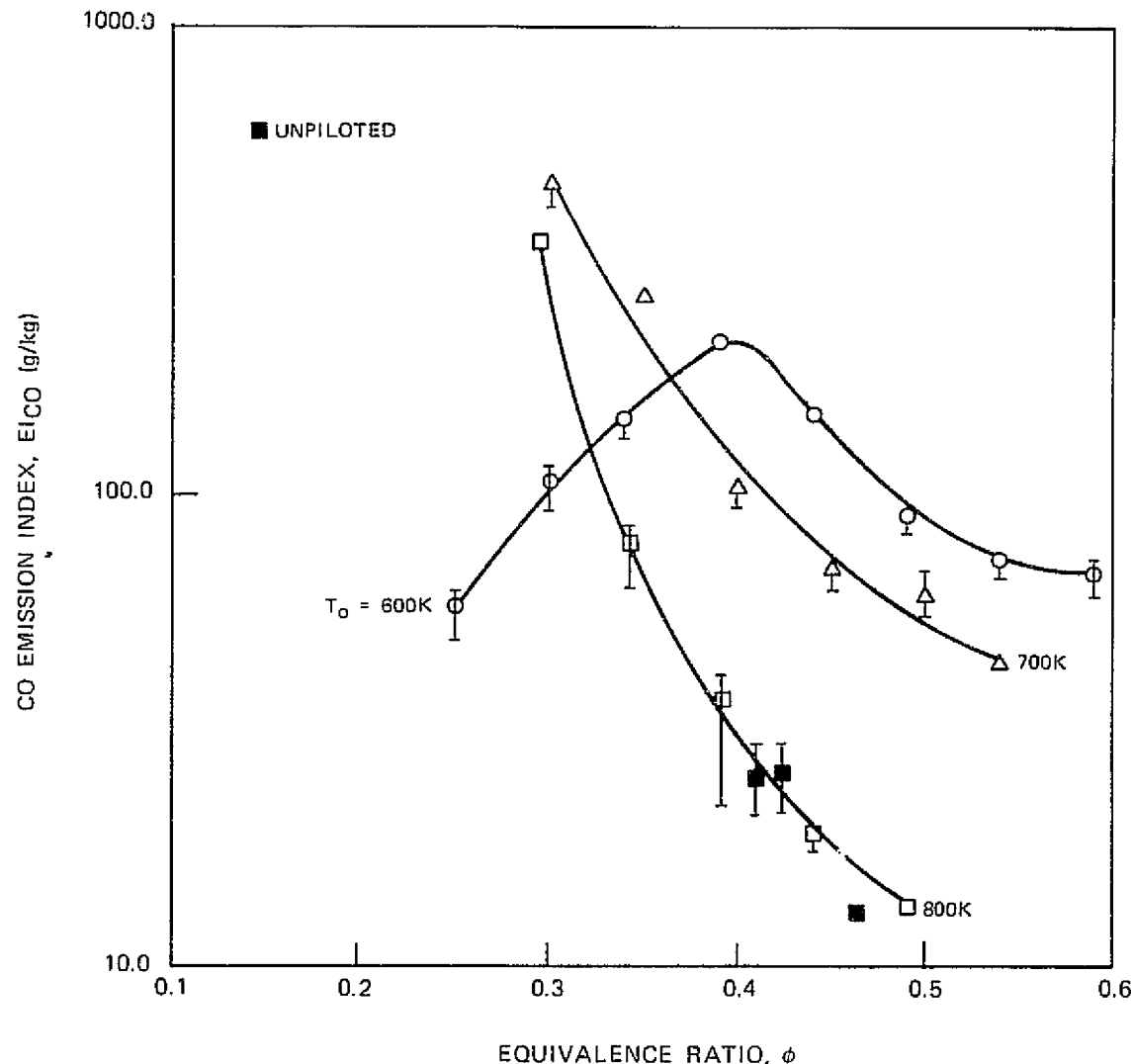


Figure 68. CO Emissions — V-Gutter Flameholder — Configuration 1

RUN 35

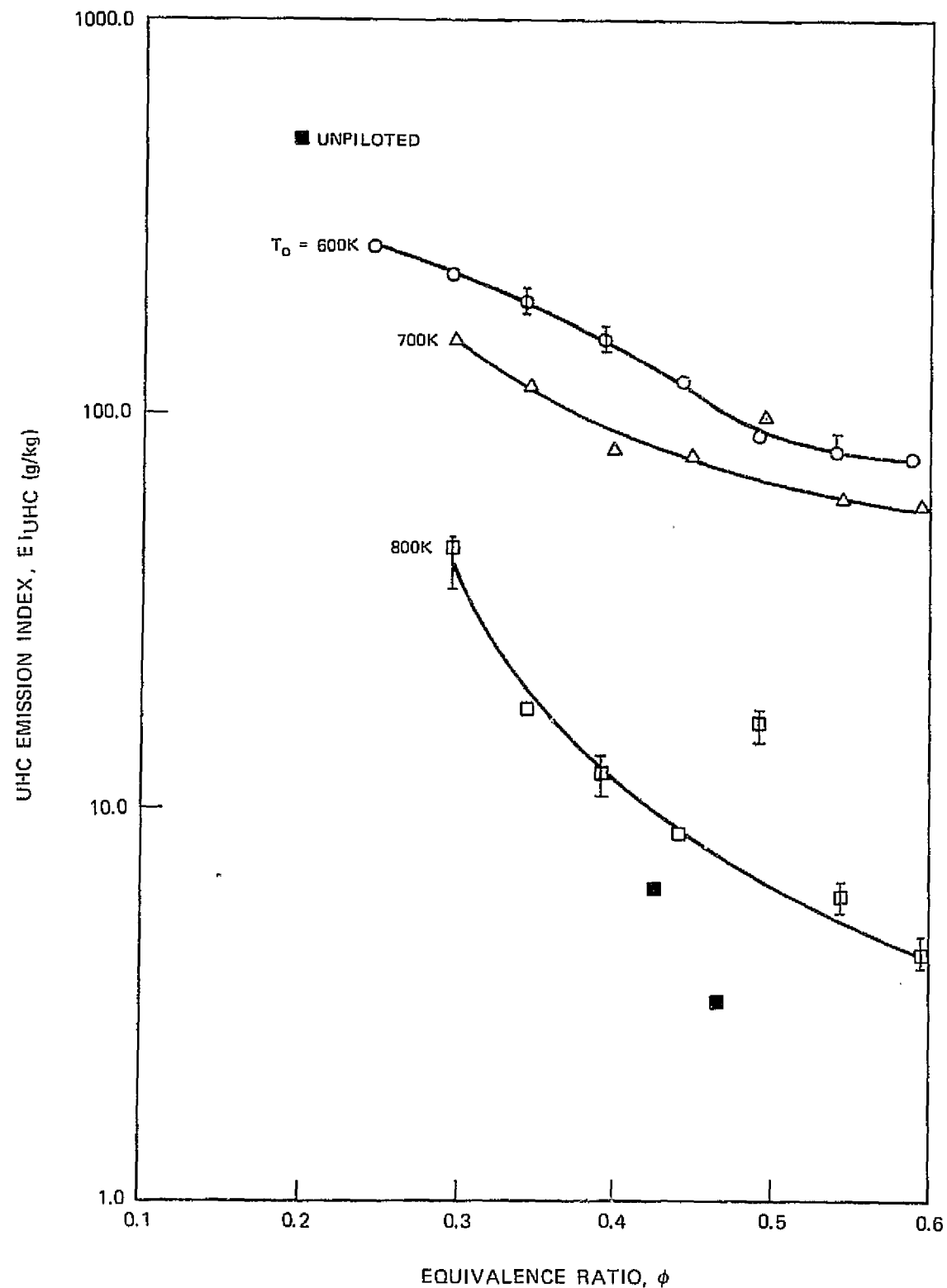


Figure 69. UHC Emissions — V-Gutter Flameholder — Configuration 1

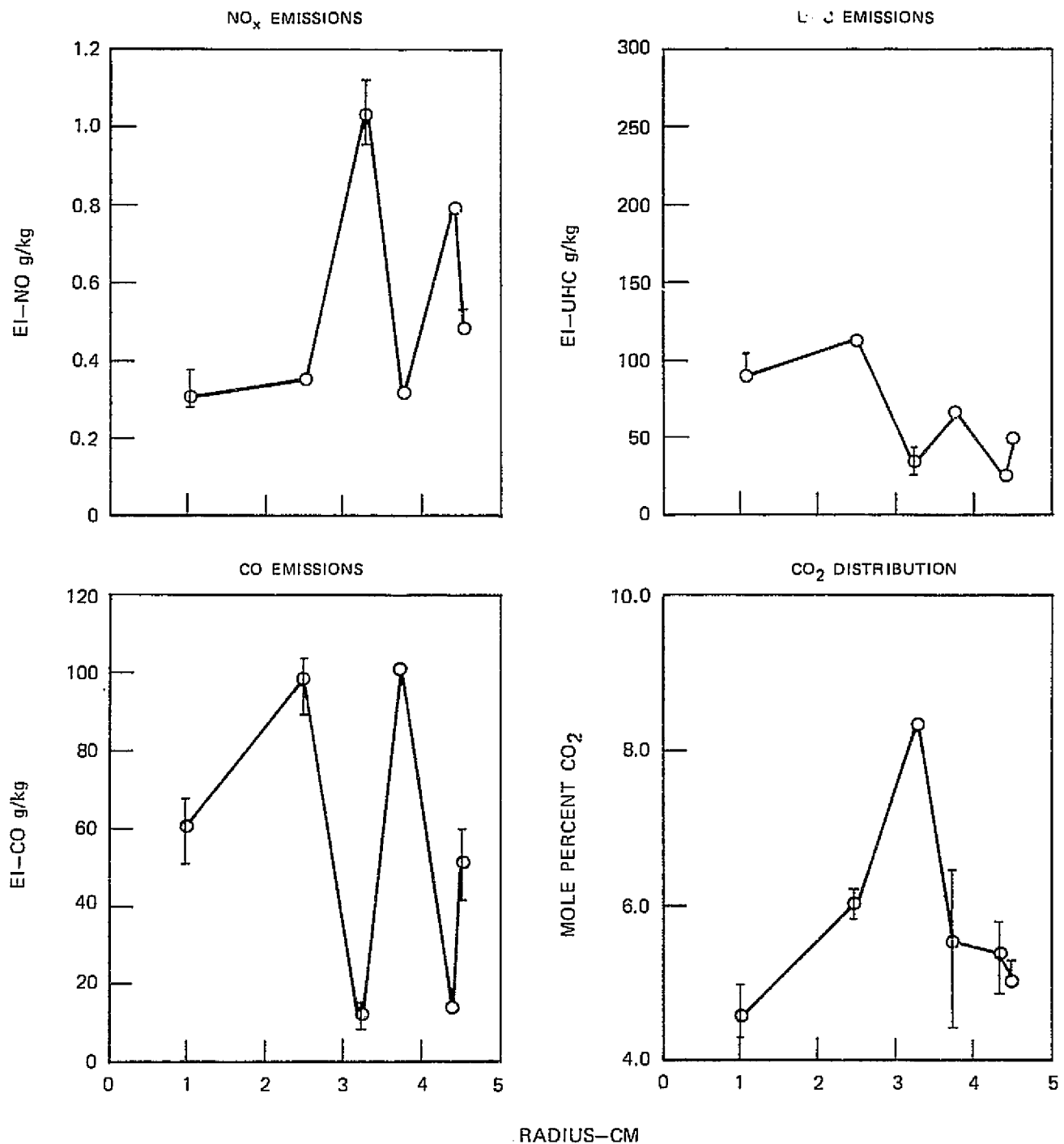
RUN 35 $T_0 = 600\text{K}$ $\phi = 0.6$ 

Figure 70. Emission Distribution — V-Gutter Flameholder — Configuration 1

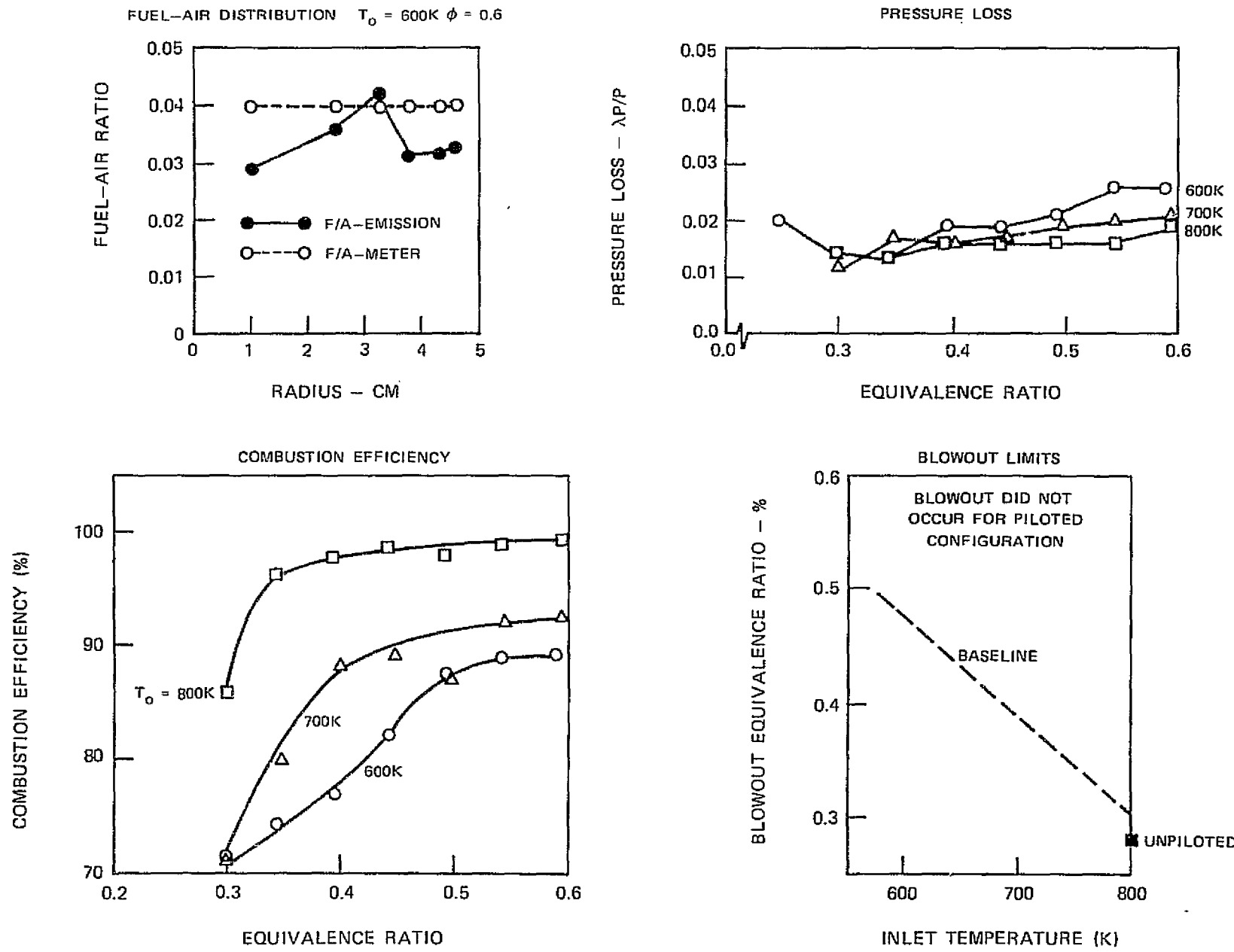
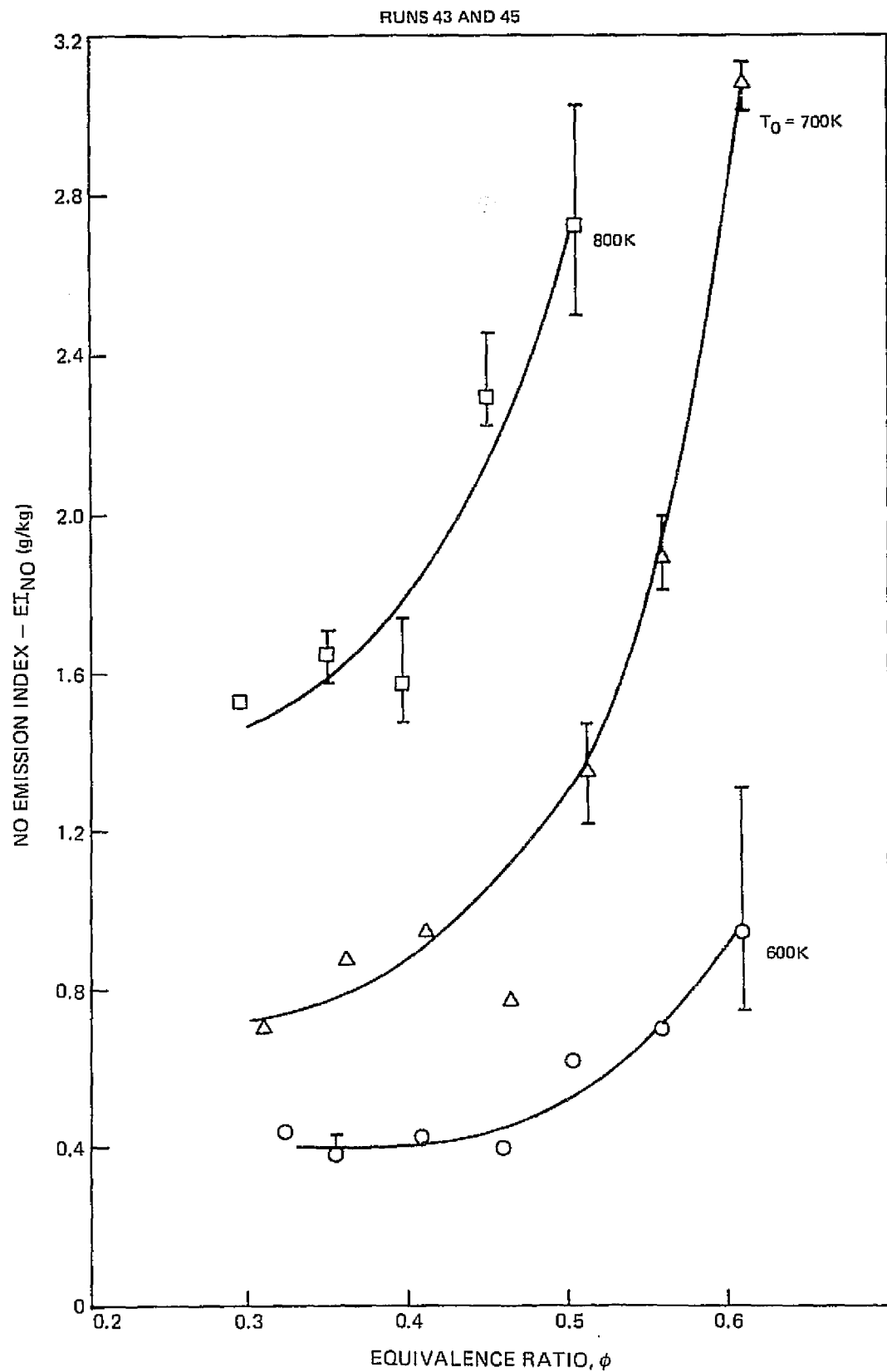


Figure 71. Combustor Performance - V-Gutter Flameholder - Configuration 1

Figure 72. NO_x Emissions — Piloted Flameholder — Configuration 4

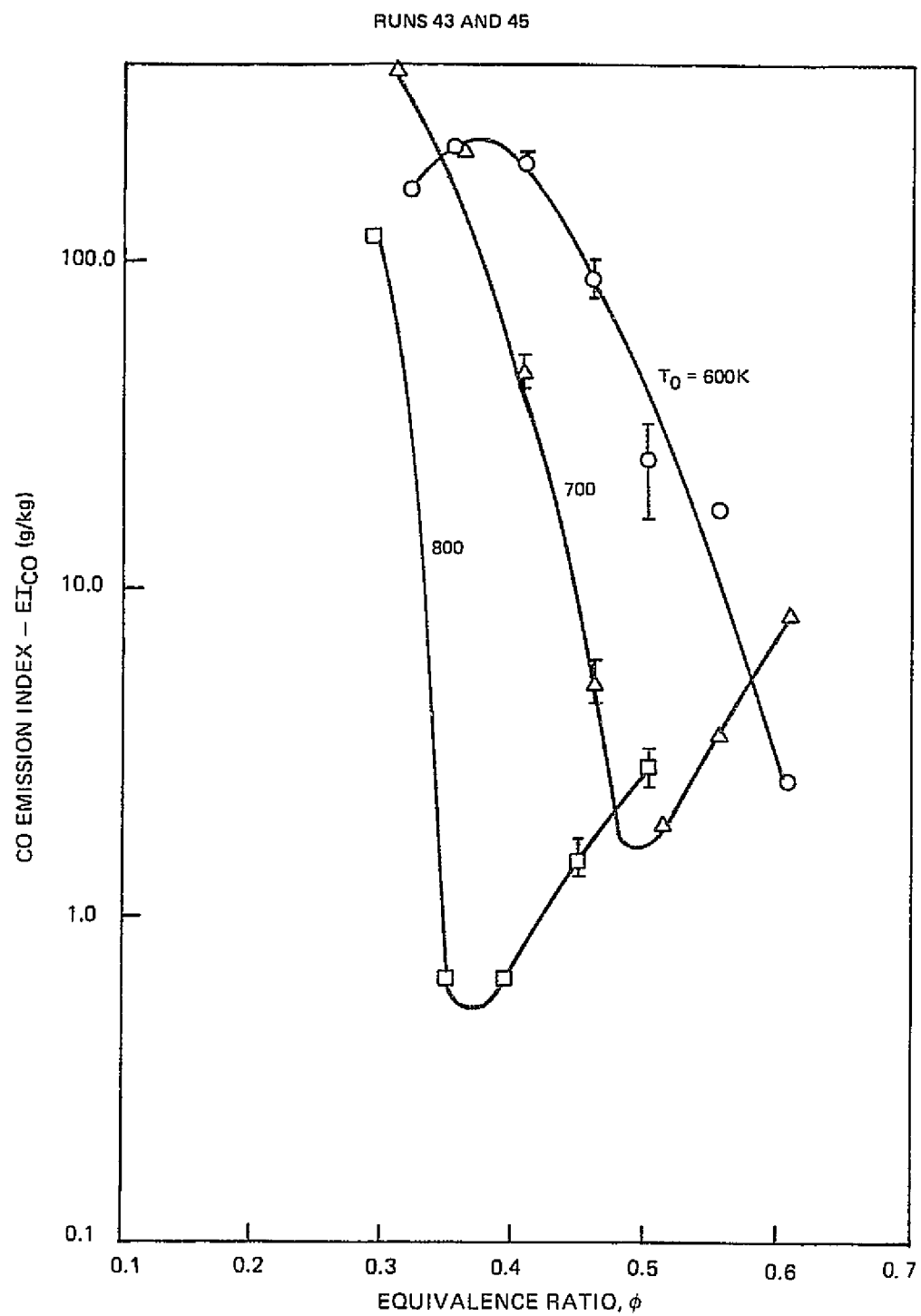


Figure 73. CO Emissions — Piloted Flameholder — Configuration 4

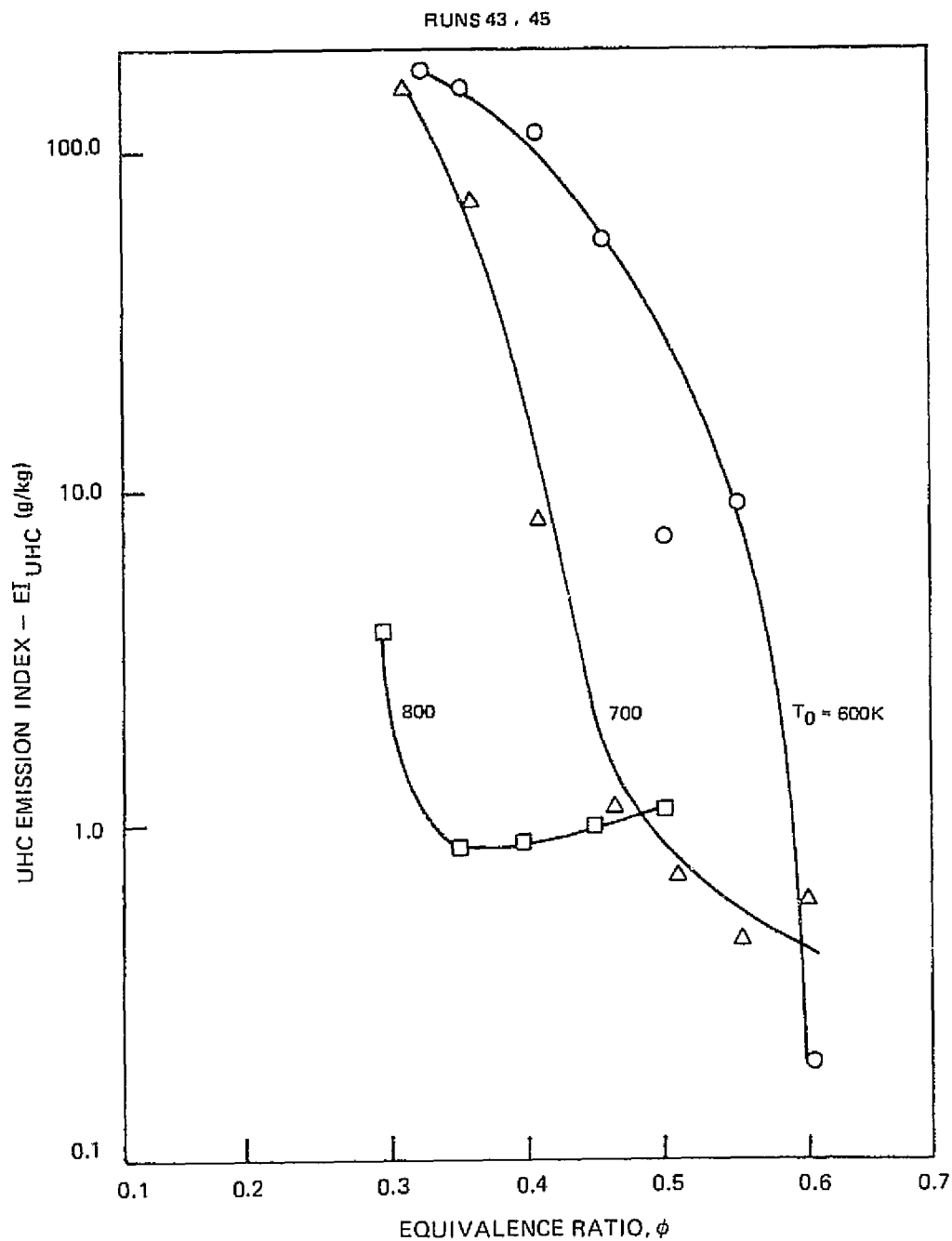


Figure 74. UHC Emissions — Piloted Flameholder — Configuration 4

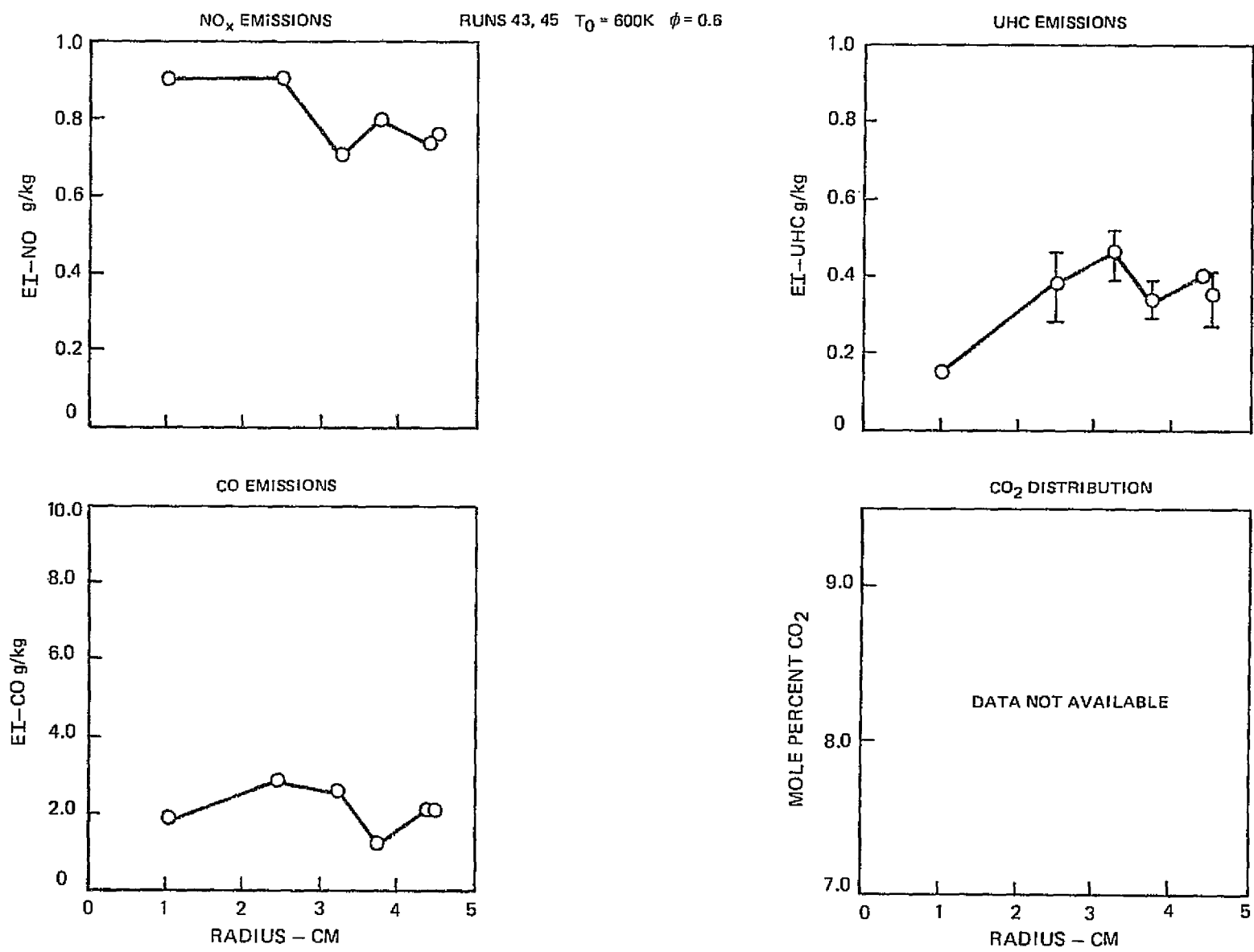


Figure 75. Emission Distribution — Piloted Flameholder — Configuration 4

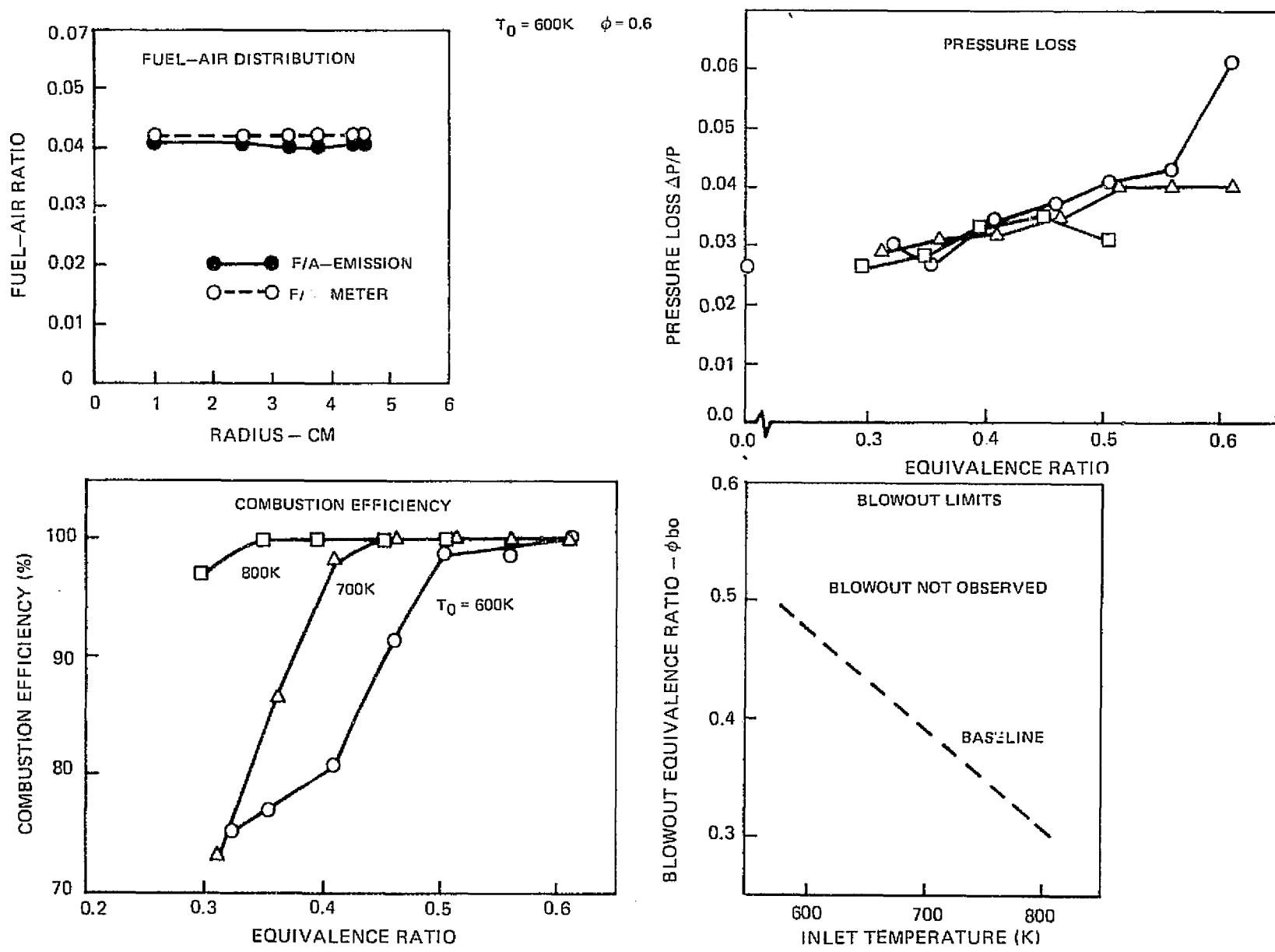


Figure 76. Combustor Performance — Piloted Flameholder — Configuration 4

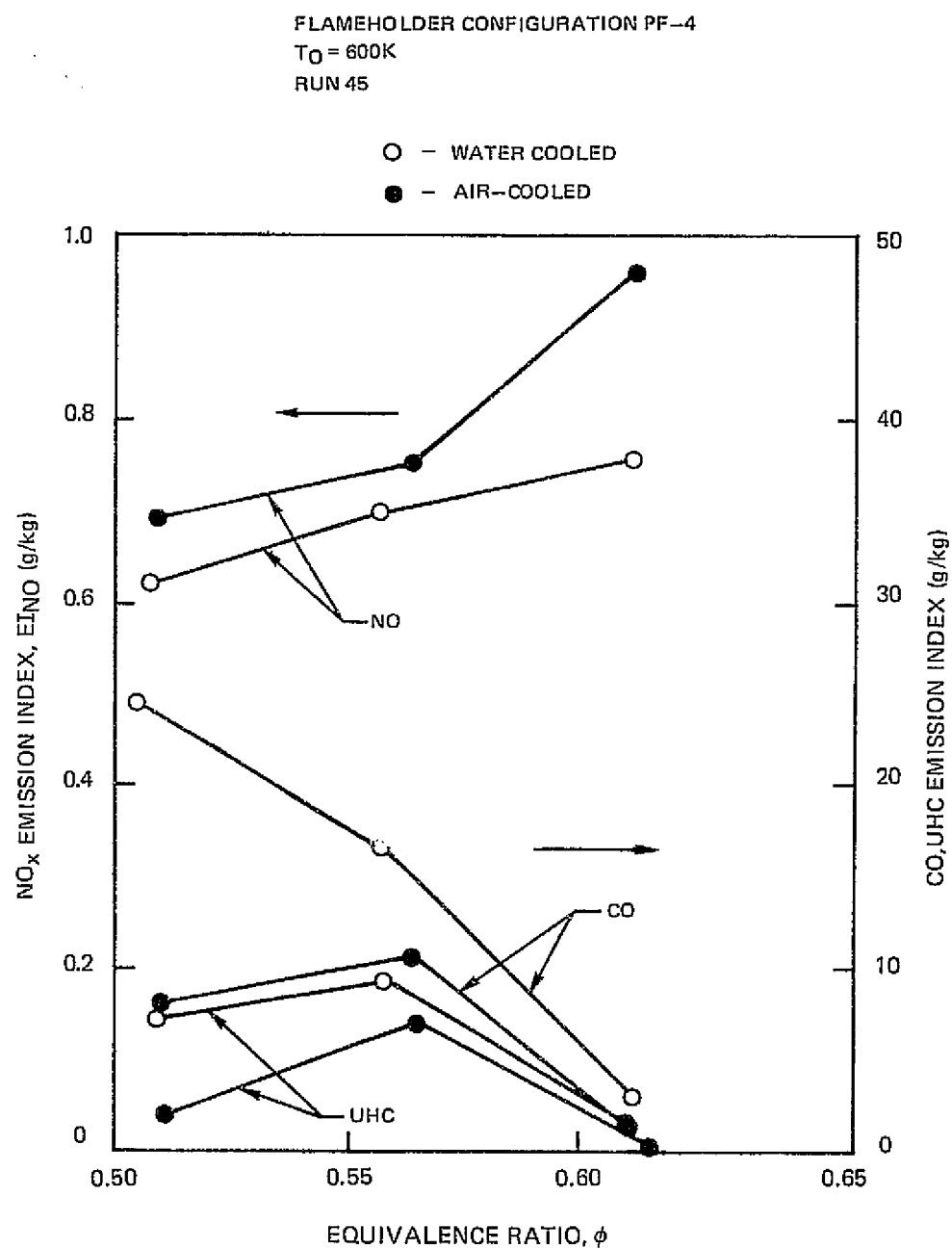


Figure 77 . Effect of Coolant Type on Emissions — Flameholder Configuration PF-4

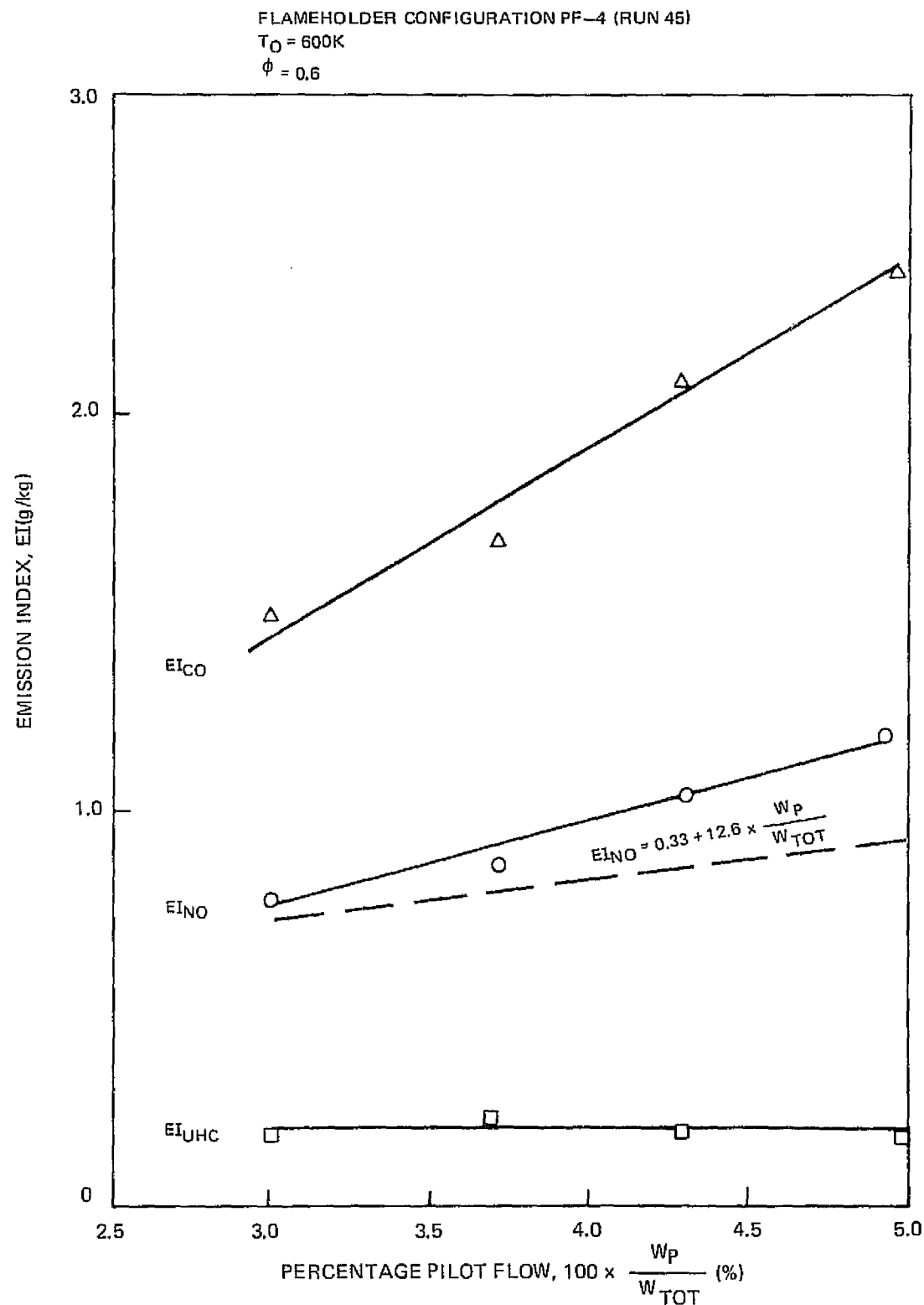


Figure 78. Effect of Pilot Fuel Flowrate on Emissions

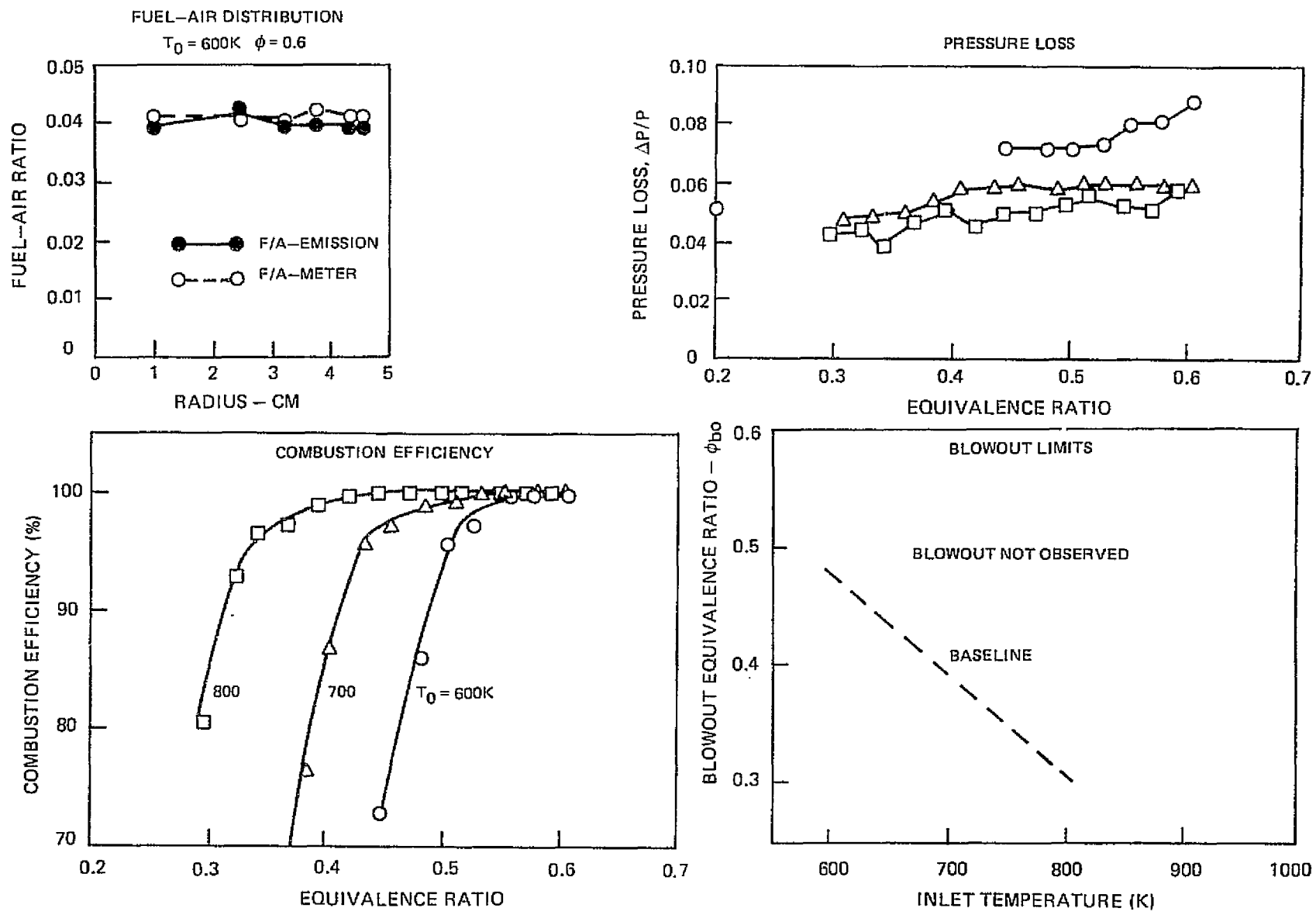
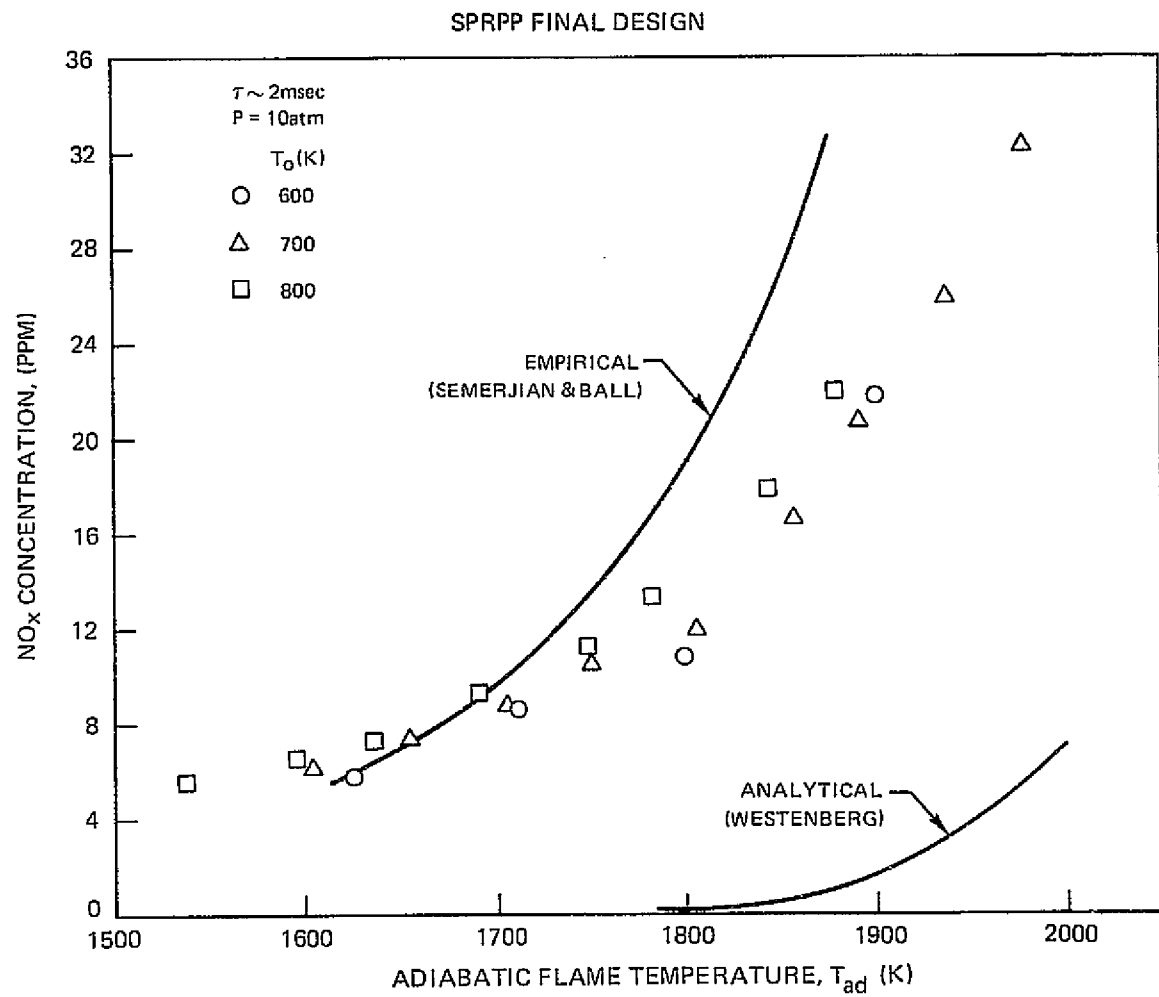


Figure 79. Combustor Performance — Piloted Flameholder — Final Design

Figure 80. Variation of NO_x Emissions with Flame Temperature

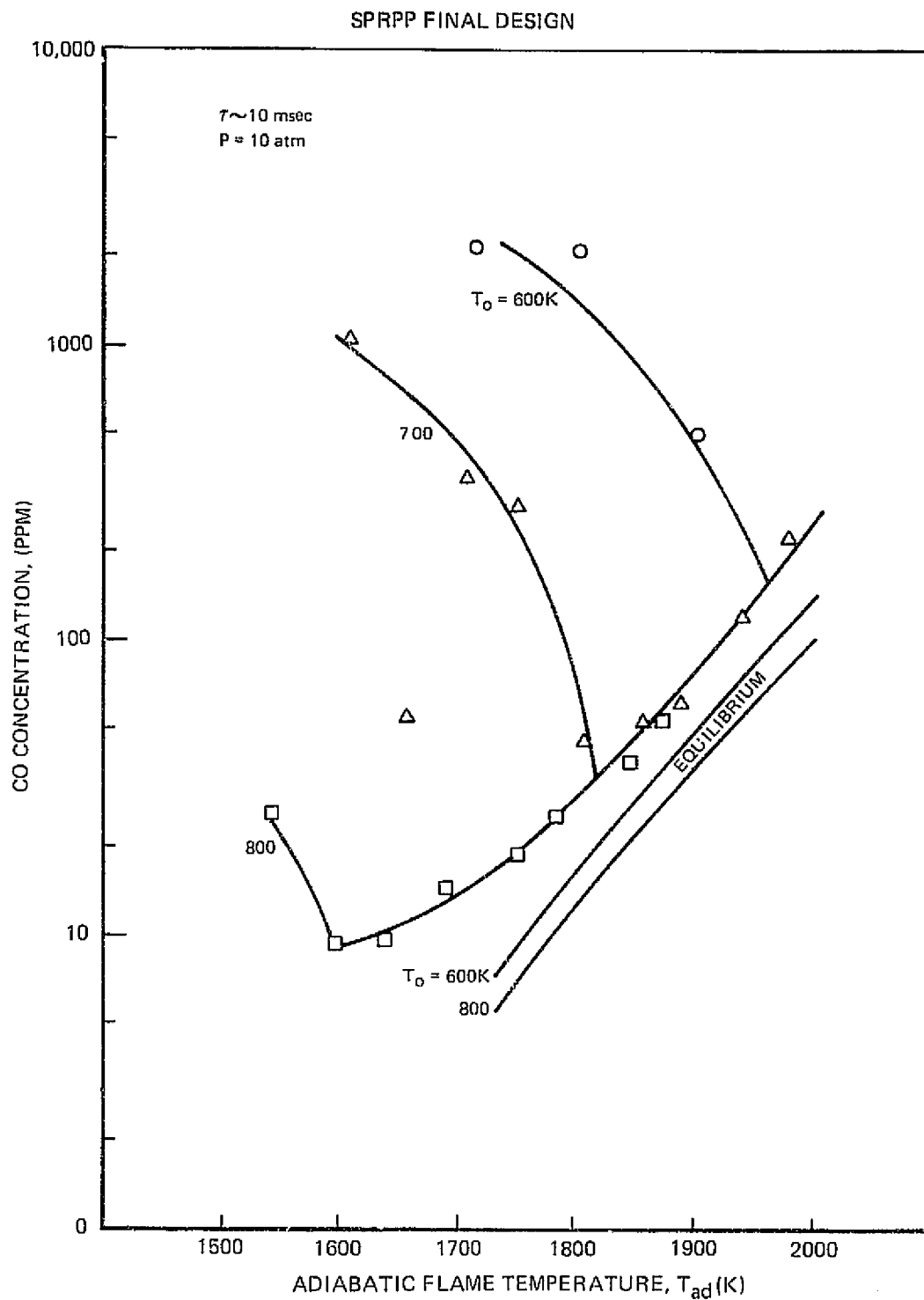


Figure 81. Variation of CO Emissions with Flame Temperature

ORIGINAL PAGE IS
OF POOR QUALITY

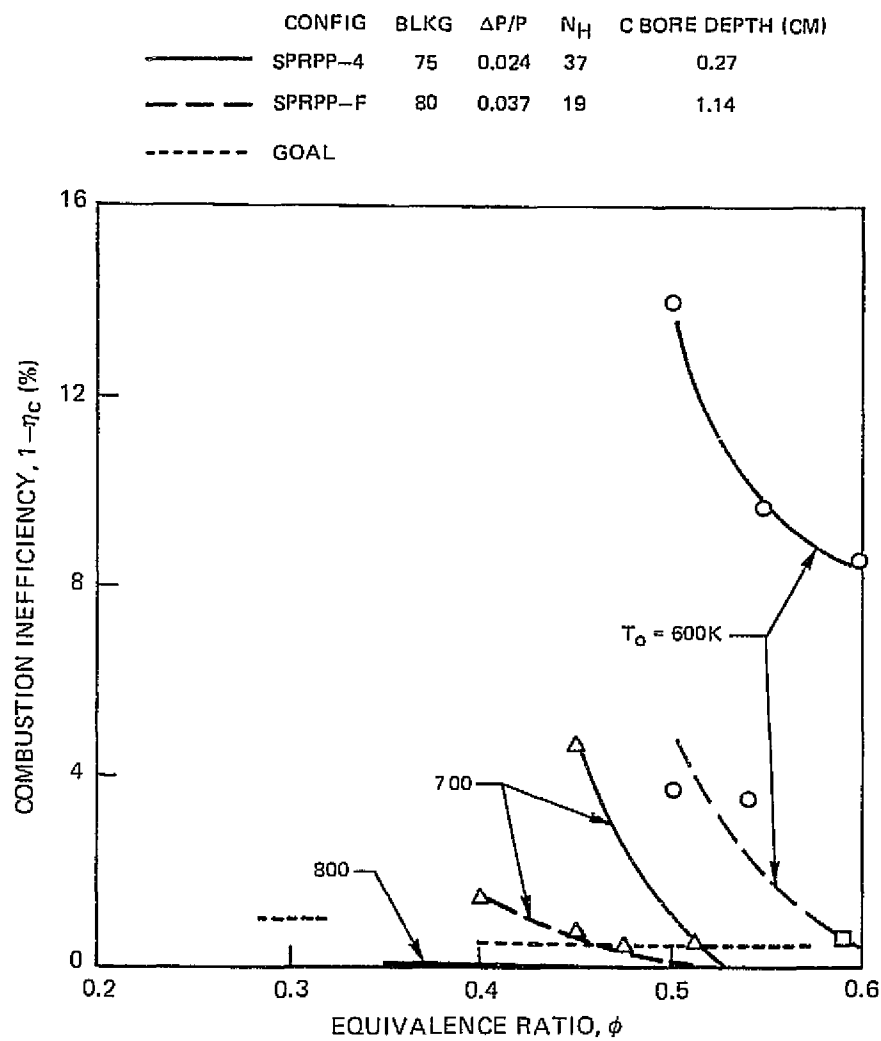


Figure 82. Effect of Flameholder Characteristics on Combustor Performance

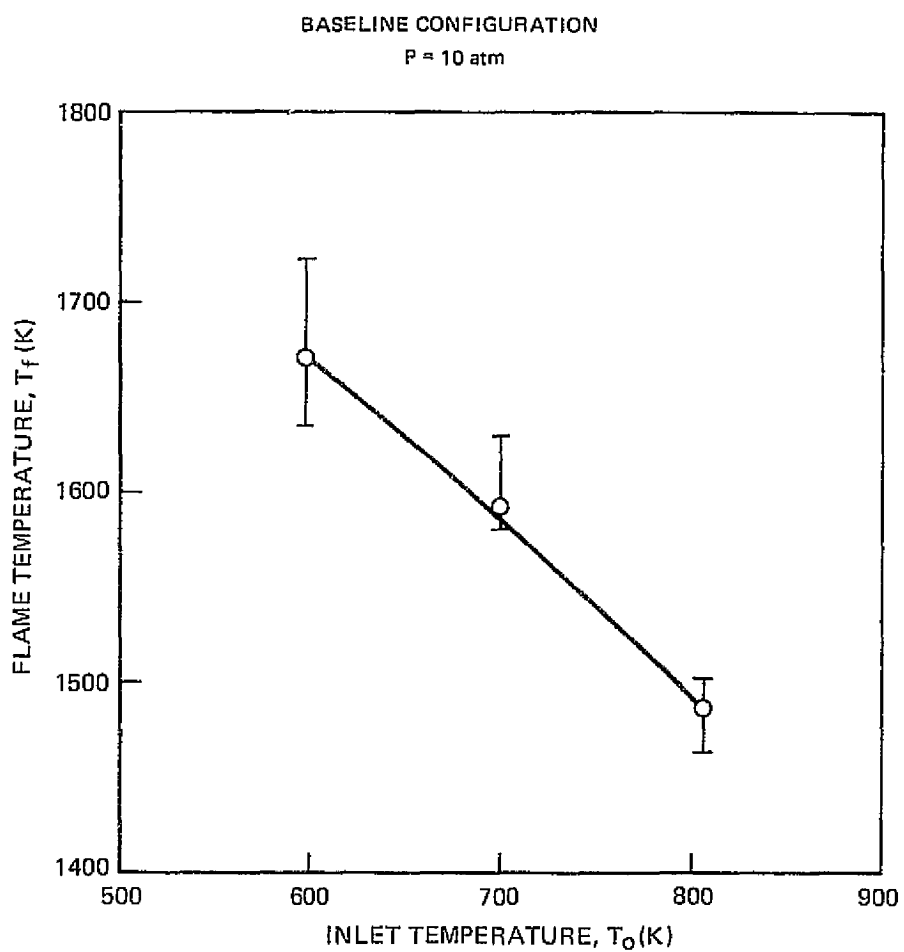


Figure 83. Variation of Blowout Flame Temperature with Inlet Temperature

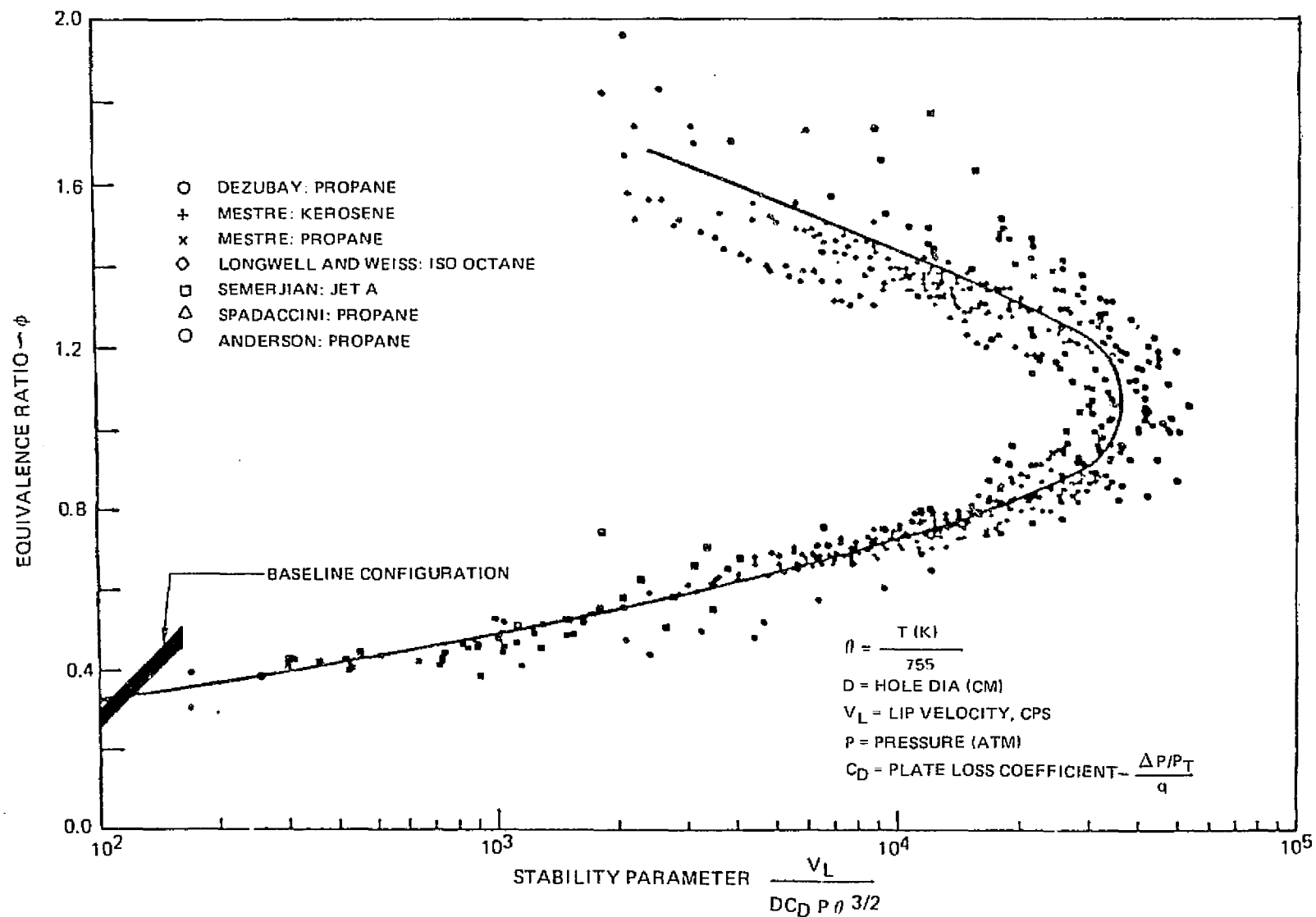


Figure 84. Perforated Plate Lean Stability Limit Data Correlation